Development of Plantar Strain Measurement to Characterise Diabetes-Related Foot Disease

Author:

Francesca Jade Sairally

Submitted in accordance with the requirements for the degree of

Doctor of Philosophy

University of Leeds

School of Mechanical Engineering

April 2026

Intellectual Property and Publication Statement

I confirm that the work submitted is my own and that appropriate credit has been given where reference has been made to the work of others.

This copy has been supplied on the understanding that it is copyright material and that no quotation from the thesis may be published without proper acknowledgement. The right of Francesca Jade Sairally to be identified as Author of this work has been asserted by Francesca Jade Sairally in accordance with the Copyright, Designs and Patents Act 1988.

In the publications listed below, the primary author conducted all experimental work, data analysis and preparation of the corresponding manuscript. All other authors contributed to proofing the articles prior to publication.

Francesca Sairally, Rory P. Turnbull, Heidi J. Siddle, David A. Russell, Claire Brockett, Peter R. Culmer. Development and Evaluation of a Novel 3D In-Shoe Plantar Strain Measurement System: STAMPS3D*, Proceedings of the Institution of Mechanical Engineers, Part H: Journal of Engineering in Medicine*, 239(5), pp.472-484, 2025.
Article DOI: https://doi.org/10.1177/09544119251330738

Francesca Sairally, David A. Russell, Heidi J. Siddle, Kate Chauhan, Daniele Trinca, Claire Brockett, Pete Culmer. Measuring Plantar Load with STAMPS3D: A Preliminary Study on the Impact of Contoured Orthoses, *Frontiers in Bioengineering and Biotechnology*, 13, p. 1648649, 2025.
Article DOI: https://doi.org/10.3389/fbioe.2025.1648649
Dataset DOI: https://doi.org/10.5518/1706

Francesca Sairally, David A. Russell, Heidi J. Siddle, Daniele Trinca, Claire Brockett, Peter R. Culmer. Measuring In-shoe Plantar Strain Outcomes in the Presence of Callus: A Preliminary Study Using the STAMPS3D Measurement System, *Journal of Foot and Ankle Research*, 19(2), p.e70169, 2026.
Article DOI: https://doi.org/10.1002/jfa2.70169
Dataset DOI: https://doi.org/10.5518/1820

Acknowledgements

I would like to express my deepest gratitude to my supervisory team – Professor Peter Culmer, Professor Claire Brockett, Professor Heidi Siddle and Mr David Russell. You have guided me through the steep learning curves of this PhD with patience, generosity and unwavering support. I am grateful not only for your academic mentorship, but also for the opportunities you gave me to develop across both engineering and clinical settings. More importantly, your understanding during times of personal difficulty made an enormous difference, and I will always appreciate the kindness you all showed me.

To my partner, friends and family: thank you for being my anchor. You have listened to every frustration, celebrated every small victory, and had patience when deadlines took priority. Your support has carried me through more than you know.

I also want to dedicate a special acknowledgment to Debbie, who I lost at the end of my first year. She championed me long before this PhD began and believed in me unfailingly. I know she would be incredibly proud of this moment – I wish she was here to see it, but I feel her cheering me on still.

Abstract

Diabetes-related foot ulceration is an increasingly prevalent issue in people with diabetes, placing substantial social and financial burden on individuals at risk and on healthcare services managing their care. Ulcer formation has been shown to be strongly influenced by mechanical loading, yet current assessment tools focus primarily on plantar pressure and overlook shear stress. This thesis aimed to develop a 3D Digital Image Correlation based in-shoe system (STAMPS3D), extending the previously developed 2D STAMPS system (a planar strain measurement approach that used Digital Image Correlation to assess plantar load at the plantar interface). By advancing this concept into three dimensions, the work enables measurement of plantar strain across non-planar surfaces to generate clinically relevant information related to ulcer risk.

The research was guided by five research questions, defined through an extensive literature review, which address both the technical feasibility of the system and its clinical relevance. Accordingly, key research topics included the evaluation of measurement performance, validation of the 3D DIC methodology, assessment of the system in clinically meaningful contexts, and incorporation of stakeholder perspectives to understand translational requirements. To address these questions, the project involved validation of the 3D system and proof-of-concept studies applying STAMPS3D to contoured orthoses and simulated callus. Stakeholder discussions informed the selection of these contexts and highlighted practical considerations for future development.

The results demonstrated the system's ability to capture plantar strain across both planar and non-planar surfaces, with outputs correlating with in-shoe pressure measurements captured using the Pedar system, a commercially available insole pressure device. The proof-of-concept studies showed that STAMPS3D can measure strain across complex contoured surfaces and is sensitive to localised changes introduced through simulated callus. Stakeholder insights aligned with these findings and identified further refinements needed to support clinical translation.

Overall, this thesis establishes the feasibility of a 3D strain-based in-shoe measurement system and provides the methodological foundation required for future clinical studies. The findings highlight the value of strain-based assessment for diabetes-related foot ulcer prevention and management and furthermore outline a clear pathway toward integrating STAMPS3D into future clinical pathways.

Table of Contents

List of Tables ..... **ix**
List of Figures ..... **x**
Abbreviations and Nomenclature ..... **xiv**
1 Introduction **1**
1.1 Research Aims **2**
1.2 Research Questions **2**
1.3 Research Objectives **3**
1.4 Thesis Overview **4**
1.5 Project Roadmap **5**
2 Literature Review **7**
2.1 Diabetes Mellitus **7**
2.1.1 Global and National Epidemiology 7
2.1.2 Types of Diabetes 8
2.1.3 Health Inequalities and Barriers to Care 9
2.1.4 Symptoms and Systemic Complications 9
2.2 Diabetes-Related Foot Disease **10**
2.2.1 Peripheral Arterial Disease and Diabetic Peripheral Neuropathy 10
2.2.2 Biomechanical Risk Factors 11
2.2.3 Tissue Breakdown and DFU Formation 11
2.2.4 DFU Location and Patterns 13
2.2.5 Ulcer Recurrence and Long-Term Risk 13
2.2.6 Social and Economic Costs 14
2.3 Patient Pathway **15**
2.3.1 From Diagnosis to Routine Care 16
2.3.2 Patient Self-Management 16
2.3.3 The Multidisciplinary Foot Care Team 18
2.3.4 Screening and Clinical Assessment Methods 19
2.3.5 Interventions and Offloading 21
2.3.6 Clinical Limitations of Current Clinical Approaches 24
2.4 Plantar Pressure and Shear Stresses **26**
2.4.1 Role in DFU Formation 26
2.4.2 Plantar Measurement Techniques and Devices 28
2.4.3 The STAMPS System 31

2.5 Digital Image Correlation 32
2.5.1 The Fundamentals of DIC 32
2.5.2 Speckle Pattern Design and Application 33
2.5.3 Camera Setup and Calibration 34
2.5.4 DIC procedure 35
2.5.5 DIC Software Packages 37
2.5.6 Parameter Selection and Validation Approaches 40
2.5.7 Barriers to Clinical Translation of the STAMPS System 42
2.6 Chapter Summary 43
3 Parameter Selection for Digital Image Correlation 44
3.1 Introduction 44
3.2 Methodology 45
3.2.1 DIC Software Selection 45
3.2.2 Examination of DIC Parameters 47
3.2.3 Methods Development 48
3.2.4 Final Methods 48
3.3 Results 52
3.4 Chapter Discussion 60
3.5 Chapter Conclusions 64
4 Development and Evaluation of a Novel 3D In-Shoe Plantar Strain Measurement System: STAMPS3D 65
4.1 Preface 66
4.2 Publication 66
4.3 Preliminary Work and Supporting Data 86
4.3.1 Stereo Camera Rig Development 86
4.3.2 Calibration 87
4.3.3 3D DIC Analysis 93
4.3.4 Experimental Methods 96
4.3.5 Case Study 99
4.4 Chapter Discussion 101
4.5 Chapter Conclusions 103
5 Engagement with Patients and Clinicians to Inform STAMPS3D Research and Development 104
5.1 Introduction 104
5.2 Methodology 104
5.2.1 Overall Approach and Objectives 104
5.2.2 PPIE Engagement 106

5.2.2.1 PPIE Groups 106
5.2.2.2 Session Format and Facilitation 106
5.2.2.3 Ethical Considerations 106
5.2.2.4 Funding and Resources 107
5.2.2.5 Reviewing and Summarising the Discussions 107
5.2.3 Clinical Stakeholder Engagement 108
5.3 Collective Review of Findings 108
5.3.1 Key Area 1: Awareness and Knowledge of DFUs 109
5.3.2 Key Area 2: Perceptions of Current Assessment Methods 110
5.3.3 Key Area 3: Acceptance and Attitudes Towards the STAMPS3D Tool 111
5.3.4 Summary of Clinical Stakeholder Feedback 116
5.4 Chapter Discussion 117
5.5 Chapter Conclusions 119
6 Measuring Plantar Load with STAMPS3D: A Preliminary Study on the Impact of Contoured Orthoses 121
6.1 Preface 122
6.2 Publication 122
6.3 Preliminary Work and Supporting Data 138
6.3.1 Mechanical Characterisation of Orthotic Insoles 139
6.3.2 Moulding STAMPS to 3D Contours 146
6.3.3 Preliminary Testing of STAMPS Across Contoured Surfaces 148
6.4 Chapter Discussion 150
6.5 Chapter Conclusions 152
7 Measuring In-Shoe Plantar Strain Outcomes in the Presence of Callus: A Preliminary Study using the STAMPS3D Measurement System 153
7.1 Preface 154
7.2 Publication 154
7.3 Preliminary Work and Supporting Data 169
7.3.1 Design Requirements for a Simulated Callus 170
7.3.2 Preliminary Tests of Early Callus Simulation 172
7.3.3 Mould Development 173
7.3.4 Material Selection 174
7.3.5 Preliminary Strain Assessments in the Presence of Callus 176

7.4 Chapter Discussion 178
7.5 Chapter Conclusions 179
8 Discussion and Conclusions 180
8.1 Review of Thesis Chapters and Research Objectives 180
8.2 Discussion 183
8.2.1 Technical Development of STAMPS3D 184
8.2.2 Shear-Related Measurement Capability of STAMPS3D 187
8.2.3 Clinical Translation of the STAMPS3D System 188
8.2.4 Clinical Applications and Impact of STAMPS3D 189
8.3 Future Work 192
8.3.1 Alternative Materials for the STAMPS Insole 193
8.3.2 Automation of STAMPS3D Post-Processing 194
8.3.3 Larger Cohort Studies Involving Healthy and Diabetes Individuals 194
8.3.4 Automated Risk Classification 195
8.4 Concluding Remarks 196
List of References 197
Appendix A 210
A.1 STLE Conference Poster 210
A.2 Supplementary Computational Results 211
A.3 Supplementary Experimental Results 219
A.4 Ncorr vs GOM Strain Data 222
Appendix B 224
B.1 BioMedEng24 Conference Poster 224
B.2 STAMPS3D Protocol Document 225
B.3 Independent Validation Calculations 238
Appendix C 240
C.1 Discussion Group Questions 240
C.2 PPIE Activity Research Articles 242
Appendix D 245
D.1 Mechanical Tests – 'Piano key' Stiffness Measurements 245
D.2 Mechanical Tests – Insole Stiffness Measurements 246

List of Tables

Table 2.3.1: Foot care activities advised for patient's self-management of foot health [28,52–54]. 17

Table 2.3.2: Characteristics corresponding to low, moderate and high risk of DFU development addressed by NICE [49]. 20

Table 2.3.3: Description of debridement techniques used on DFUs [59,79]. 22

Table 2.4.1: A summary of advantages and disadvantages of pressure measurement techniques including platform systems and in-shoe sensors [109,110]. 29

Table 2.5.1: Summary of available DIC software packages [134–136]. 38

Table 3.2.1: Initial sample of DIC parameters testing using computational and experimental methods. 48

Table 4.2.1: Average RMS error ± standard deviation corresponding to sphere fit applied to DIC and 3D scan data for both planar and non-planar samples. ... 79

Table 4.2.2: Summary of average peak strain ± standard deviation using DIC, showing the effect of shear distance on the components of peak strain (%). 79

Table 4.2.3: Average peak S_{MAG} ± standard deviation captured using 2D and 3D DIC methods across anatomical regions of the foot for deformed samples and corresponding. 81

Table 4.3.1: Summary of outputs from calibration trials. 90

Table 4.3.2: Comparison of baseline components and stereo angle using DIC calibration, motion capture and hand measurements. 92

Table 4.3.3: RBM translation vectors produced when insole placement is shifted between images. 95

Table 4.3.4: Average peak S_{MAG} captured using 2D and 3D DIC methods across anatomical regions of the foot for undeformed samples. 100

Table 6.2.1: Regional median peak S_{MAG} for each condition and PPP across all participants, with interquartile range (IQR) reported in brackets. 132

Table 6.3.1: Summary of the insole thickness, stiffness conditions and anatomical regions tested during the preliminary work. 143

Table 7.2.1: Peak S_{MAG} and PPP reported for each condition and anatomical region of the foot, with median and IQR used to summarised data across all five participants. 164

Table 7.3.1: Final design requirements for the simulated callus model. 172

List of Figures

Figure 1.5.1: Visual roadmap for this PhD project, demonstrating the progression and cohesion of each element of work. 6

Figure 2.2.1: Key contributing factors to DFU formation, including neuropathic, vascular, biomechanical and external influences (information summarised from [24], [34]). 12

Figure 2.3.1: Overview of the patient pathway for diabetes-related foot care, illustrating the parallel clinical and self-management processes from diabetes diagnosis through to ulcer formation, treatment and outcomes (summarised from [28], [49], [50]). The figure highlights the cyclical nature of the pathway, with healing and recurrence feeding back into earlier stages of care. 15

Figure 2.4.1: Schematics of custom shear and pressure platforms a) and in-shoe sensors b), demonstrating spatial resolution in contrast to DIC [112], [114]. . 30

Figure 2.5.1: Examples of speckle patterns used for DIC analysis, with differing characteristics such as size, density and variation. 34

Figure 2.5.2: Schematic representation of subset size and step-size during DIC analysis. 35

Figure 2.5.3: Schematic of displacement calculation during DIC analysis. 36

Figure 2.5.4: Illustration of a strain window used for local least-squares strain estimation in DIC post-processing. 37

Figure 3.2.1: Overview of the wider STAMPS tool-chain, illustrating the full workflow from insole fabrication to anatomically masked quantitative strain outputs. .. 47

Figure 3.2.2: Strain map for a fixed set of DIC parameters with row of data including peak strain highlighted in red (left). Computational ‘benchmark’ (black) aligned with a DIC output corresponding to a fixed set of DIC parameters (red), used to calculated peak and RMS error (right). 50

Figure 3.2.3: Silicone samples with applied speckle pattern (left). Speckled sample set up in Instron clamps (right). 51

Figure 3.3.1: Representative strain map for a single parameter combination (subset radius, subset spacing, strain radius) = (13, 1, 5) at 5% strain. 52

Figure 3.3.2: Magnitude of peak error corresponding to computational strain of 5% (left column) and 50% (right column) for different DIC parameter combinations, involving subset radius, subset spacing and strain radius. 54

Figure 3.3.3: Root-mean-squared error corresponding to computational strain of 5% (left column) and 50% (right column) for different DIC parameter combinations, involving subset radius, subset spacing and strain radius. 55

Figure 3.3.4: Representative strain maps for 5 and 40% strain with the parameters (15, 1, 5). A smaller 10 mm ROI is highlighted in which average peak strain error was calculated. 56

Figure 3.3.5: Absolute peak error averaged across three samples at 5 and 40% with error bars demonstrating standard deviation of error across the region of interest for each parameter combination. 58

Figure 3.3.6: Absolute peak error across 5–40% strain for the best and worst parameter combinations identified at each strain level, together with a fixed setting (17,4,5). 59

Figure 3.3.7: Average computational time for DIC analysis to be completed for subset radius = 10, 20 and 30 and subset spacing = 3, 6 and 9. 60

Figure 4.1.1: Graphical abstract for the paper: Development and Evaluation of a Novel 3D In-Shoe Plantar Strain Measurement System: STAMPS3D. 65

Figure 4.2.1: DIC camera rig setup, consisting of 2D and 3D configurations. 70

Figure 4.2.2: DIC analysis process including image acquisition, DIC parameters selection, spatial resolution and deformation measures demonstrated across two overlapping subsets. 72

Figure 4.2.3: STAMPS3D procedure including, pre-collection preparation, data collection and analysis. 74

Figure 4.2.4: Method setup corresponding to a) indentation tests performed at 2 mm on planar (top) and non-planar samples (bottom) to validate simple geometry of deformations and global surfaces with expected radius of curvature (ERC) = 10, 15 and 40 mm and b) shear tests performed at distances 0, 1 and 2 mm after an initial 2 mm indentation. 76

Figure 4.2.5: Examples of sphere fits applied to a) planar samples, b) global surface of non-planar samples (excluding data points corresponding to local deformation) and c) local deformation of non-planar samples (excluding data points which fall outside the deformation). 77

Figure 4.2.6: Average estimated radius of curvature for a) planar samples with local deformations using 10 and 15 mm radius indenters, b) non-planar samples with local deformations using 15 mm radius indenter and global surface with 40 mm radius, c) non-planar samples undeformed to measure global surface alone and d) peak strain measures for varying shear distances of 0, 1 and 2 mm. (Error bars +/- 95% confidence interval). 78

Figure 4.2.7: Demonstration of raw data masking and summary of results comparing 2D and 3D methods: a) Comparison of average peak S_{MAG} for deformed samples walked on for ten steps at a self-selected speed. b) Upper 10% percentile threshold of global strain measures showing differences in data distribution. c) Examples of highlighted upper 10% S_{MAG} across anatomical regions of the foot. (Error bars +/- 95% confidence interval). 82

Figure 4.3.1: Schematic demonstrating the camera setup, with the translation vector T and stereo angle, $\boldsymbol{\theta y}$, derived from the rotation matrix R. 89

Figure 4.3.2: Images showing a. the Qualisys motion capture setup and b. the stereo DIC rig with fluorescent markers used to define camera positions. Markers were placed on the rig to enable calculation of translation components and stereo angle for comparison with calibration outputs. 92

Figure 4.3.3: Conceptual illustration showing the 2D points and triangulation from the master camera image, and how these are mapped to their reconstructed 3D positions following stereo matching between cameras. 94

Figure 5.3.1: Word cloud generated from group summaries, illustrating the most frequently used terms across clinician and patient discussions. 109

Figure 5.3.2: Graphic summary of clinician perspectives on DFU assessment and STAMPS3D. 113

Figure 5.3.3: Graphic summary of patient perspectives on DFU assessment and STAMPS3D. 114

Figure 5.3.4: Graphic summary of common themes across clinician and patient groups. 115

Figure 5.3.5: Key areas identified by clinicians as priorities for enabling implementation of the STAMPS system. 117

Figure 6.2.1: Overview of methods, STAMPS3D and post-processing of 3D strain data. 128

Figure 6.2.2: Representative strain maps for S_{MAG} across each participant and condition, with absolute plots demonstrating strain brackets: 0-2.5% (blue), 2.5-5% (green), 5-7.5% (yellow), 7.5-10% (magenta) and > 10 (red). 131

Figure 6.2.3: Boxplot demonstrating regional distribution of peak S_{MAG} across all participants for the low stiffness, high stiffness and STAMPS conditions. Red lines above boxplots represent significance ($P < 0.05$) between the corresponding conditions based on median measures. For detail regional breakdowns, see section 2.2 of the Supplementary Material. 133

Figure 6.2.4: Scatter plot demonstrating the correlation between peak S_{MAG} and PPP across all participants. Points included are an average across three repeats for each region and participant. 134

Figure 6.3.1: Illustration of the iterative development process carried out prior to the final proof-of-concept study presented in Section 6.2. 138

Figure 6.3.2: Stress-strain curves for all 17 test samples (1-5 and intermediate variants), showing a single representative repeat for each. 140

Figure 6.3.3: Average Young's Modulus for each test sample, calculated between 10-20% strain. Error bars represent variability across the three repeats. 141

Figure 6.3.4: Illustration of regions on the custom orthoses that underwent compression testing. 142

Figure 6.3.5: Young's Modulus values for a) 3 mm and b) 6 mm orthotic insoles tested at the hallux, forefoot, midfoot and heel. Results are shown for low, medium, high and (where applicable) medium + spot materials. Error bars represent the 95% confidence interval across three repeats. 144

Figure 6.3.6: Combined stiffness of 3 mm and 6 mm orthotic insoles with a 5 mm STAMPS layer, tested at the hallux and forefoot. Results are shown for low, medium, high and (where applicable) medium + spot materials. Error bars represent the 95% confidence interval across three repeats. 146

Figure 6.3.7: Illustration of 3D printed mould and STAMPS insoles moulded to the orthoses. 147

Figure 6.3.8: Demonstration of the vacuum bag moulding approach (a), with initial attempts showing surface cracking and remaining excess material (b). 148

Figure 6.3.9: Example strain maps from preliminary testing, with contoured insoles showing pronounced lateral edge effects, illustrated by the upper 10% of strain values highlighted in red, compared to flat STAMPS insole demonstrating. 149

Figure 7.1.1: Graphical abstract for the paper: Measuring In-Shoe Plantar Strain Outcomes in the Presence of Callus: A Preliminary Study using the STAMPS3D Measurement System. 153

Figure 7.2.1: Schematic illustrating components of the multi-layer silicone callus samples, adhered to the MTH and heel regions of participants feet. 158

Figure 7.2.2: Process used to calculate the median strain fluctuation metric across participants for each region and test condition. The x-axis on the cross-section plots represents the distance along the extracted cross-section and is shown at the same scale as the strain maps. 160

Figure 7.2.3: Representative examples of plantar strain and pressure distribution maps for both callus and control conditions across five healthy participants.162

Figure 7.2.4: A summary of median strain fluctuation measured across horizontal (left) and vertical (right) cross-sections across the MTH and heel regions for both callus and control conditions. 165

Figure 7.2.5: Scatter plot demonstrating the correlation between peak S_{MAG} and PPP across all participants for callus and control conditions. 166

Figure 7.3.1: Illustration of the development process carried out prior to the final proof-of-concept study presented in Section 7.2.....170

Figure 7.3.2: Demonstration of initial simulated callus samples, using a blister plaster, metal washer and sandpaper, adhered to the 1st MTH and heel.....172

Figure 7.3.3: Strain response to the initial exploratory callus simulation: The strain map illustrates localised changes in strain at the 1st metatarsal head and heel when the sample was applied, with corresponding cross-sections revealing distinct differences in strain distribution between callus and control conditions. The bar chart provides a summary of average strain at the central sample sites, confirming a measurable increase in strain in the surrogate condition (Error bars = +/- STD). 173

Figure 7.3.4: Examples of silicone samples produced during the early development, including plain silicone sample cast using Ecoflex 00-30 and those with embedded materials. 175

Figure 7.3.5: Illustration of strain pattern produced in the presence of Ecoflex 00-30 samples at the 1st MTH and heel regions in comparison tests without. Altered strain behaviour seen at local sites, displaying ‘strain rings’ and corresponding strain variation in cross-sections. 177

Figure 8.2.1: TRLs (adapted from UKRI definitions) with corresponding stages of STAMPS3D development, illustrating how the work presented in this thesis progressed the system from proof-of-concept toward validation in relevant environments [196]. 186

Figure 8.2.2: Updated overview of the patient pathway for diabetes-related foot care (adapted from Chapter 2), with foot icons indicating points at which the STAMPS3D system could potentially be implemented and the work needed to enable this. 192

Abbreviations and Nomenclature

Abbreviations

DFU Diabetic Foot Ulcer

STAMPS STrain Analysis and Mapping of the Plantar Surface

DIC Digital Image Correlation

PPIE Patient and Public Involvement and Engagement

IDF International Diabetes Federation

MODY Maturity-Onset Diabetes of the Young

PAD Peripheral Arterial Disease

DPN Diabetic Peripheral Neuropathy

NICE National Institute for Health and Care Excellence

MDT Multidisciplinary Team

IWGDF International Working Group on the Diabetic Foot

IDSA Infectious Diseases Society

SINBAD Site, Ischaemia, Neuropathy, Bacterial Infection, Area and Depth

WIfI Wound, Ischaemia, Foot Infection

TCC Total Contact Casting

RA Rheumatoid Arthritis

RMS Root-Mean-Squared

ROI Region of Interest

ERC Expected Radius of Curvature

RPE Reprojection Error

RBM Rigid Body Motion

MTH Metatarsal Head

FOV Field of View

RRI Responsible Research and Innovation

AREA Anticipate, Reflect, Engage and Act

EPSRC Engineering and Physical Sciences Research Council

LDLS Leeds Diabetic Limb Salvage

NIHR National Institute for Health and Care Research

BRC Biomedical Research Centre

EVA Ethylene Vinyl Acetate

PPP Peak Plantar Pressure

CV Coefficients of Variation

IQR Interquartile Range

RMdSE Root Median Squared Error

TRL Technology Readiness Level

Nomenclature

S_X X-Component of Strain

S_Y Y-Component of Strain

S_Z Z-Component of Strain

S_{MAG} Magnitude of Strain

S_{AP} Anterior-Posterior Axial Strain

S_{ML} Medial-Lateral Axial Strain

S_P Pressure Axial Strain

Chapter 1

Introduction

Diabetes mellitus is one of the most pressing global health challenges, with its complications placing a substantial burden on both the individuals it affects and healthcare services. Among these, diabetic foot ulceration (DFU) is particularly devastating, contributing to reduced quality of life, increased risk of infection and amputation, and significant healthcare costs. The development of DFUs is multifactorial, driven by factors such as neuropathy (peripheral nerve damage resulting in loss of sensation), peripheral arterial disease (poor circulation), among others, which results in abnormal foot biomechanics and mechanical loading of the foot. Mechanical loading of the plantar surface of the foot has long been recognised as a critical contributor to DFU formation. Traditionally, research and clinical practice have focused on plantar pressure (vertical component of plantar load) as the primary mechanical risk factor, with elevated peak pressures linked to ulcer formation and recurrence. However, there is growing recognition that shear stresses (horizontal component of plantar load) that arise at the foot-surface interface also play a pivotal role in tissue breakdown. Despite this, the use of shear loading information in clinical practice to guide risk assessment and management has not yet been possible due to limited development of technology capable of capturing such measures. Consequently, treatment pathways remain pressure-focused with a lack of shear stress addressed, potentially affecting patient outcomes and our understanding on the contribution of shear stress in DFU formation.

Current commercial in-shoe measurement technologies, such as Pedar, provide valuable information on plantar pressure but are limited by their focus on pressure, sensor-based design and relatively low spatial resolution. These constraints mean that clinically important shear stresses cannot be captured, despite emerging understanding of shear contributions in ulcer formation. This gap has driven research in measurement technologies to determine plantar loading for clinical use, including the development of the Strain Analysis and Mapping of the Plantar Surface (STAMPS) system. The 2D STAMPS system, developed within the University of Leeds research group through doctoral work by Crossland and Jones, is an image-based technique that uses Digital Image Correlation (DIC) to quantify cumulative plantar strain. A speckled pattern applied

to the surface of a plastically deformable insole enables deformation to be tracked across repeated walking steps, with images captured before and after gait. While the 2D STAMPS system demonstrated that the cumulative strain measured using DIC reflects the combined effect of normal pressure and tangential shear stress, providing a surrogate measure of plantar loading patterns, limitations related to its restriction to planar measurement and challenges in clinical translation highlight the need for further advancement. Extending this approach into three dimensions enables the ability to capture 3D measures *and* on 3D non-planar surfaces, typical of clinical applications such as contoured orthoses. This offers the potential to capture a more complete picture of plantar loading, integrating both pressure and shear in a clinically relevant manner. A 3D system could provide greater insights into the mechanisms of ulcer formation, improve risk stratification, and inform more effective prevention and management strategies.

1.1 Research Aims

The aim of this project is to develop a 3D DIC based in-shoe system capable of measuring pressure and shear on non-planar surfaces, with the intention of generating clinically relevant information to support DFU prevention and management.

1.2 Research Questions

This thesis is guided by the following research questions, which arise directly from the limitations of existing approaches and the emerging recognition of shear as an influential component of plantar loading in DFU formation:

RQ1. Measurement feasibility – Can a 3D DIC based in-shoe measurement system reliably capture both pressure and shear components of plantar loading during gait?

RQ2. Stakeholder perspectives – How do stakeholders perceive the potential applications of STAMPS3D, and in what contexts do they see the greatest value?

RQ3. Clinical relevance – Do 3D plantar strain maps provide additional insights into DFU risk compared to conventional pressure-only measures?

RQ4. System validation – How does the performance of the 3D system compare to established tools in terms of accuracy, repeatability and usability?

RQ5. Translation potential – What are the practical considerations for integrating 3D plantar strain measurement into clinical risk assessment and management pathways?

1.3 Research Objectives

To address these questions, the project is structured around the following objectives:

1. Develop appropriate open-source DIC workflow using DIC software to provide a foundation for subsequent 3D analysis.
2. Develop and implement a novel 3D DIC based in-shoe measurement system for plantar load, validating the system against established measurement devices under controlled experimental conditions.
3. Engage clinicians and patients through discussion groups to explore perceptions of STAMPS3D, identifying potential applications for DFU prevention and management strategies.
4. Conduct proof-of-concept experiments to assess feasibility of capturing plantar load data across contoured surfaces and local regions of varying surface stiffness.
5. Develop summary metrics for clinical use derived from measures of plantar shear loading.
6. Identify methodological and practical limitations of STAMPS3D and propose potential solutions to support future clinical translation.

1.4 Thesis Overview

This thesis comprises eight chapters, including this introductory chapter, which outlines the research aims and objectives, content from three published papers and additional appendices. The aim and objectives have been addressed across chapters 3-7. Details of the content for each chapter are included below.

Chapter 2: Literature Review

Chapter 2 provides a critical review of the literature underpinning this project. Details of diabetes and related foot complications, examination of mechanical and clinical risk factors and evaluation of current pathways, tools and innovations, highlighting the gaps that motivate this research.

Chapter 3: Parameter Selection for Digital Image Correlation

Chapter 3 details the selection of suitable DIC parameters for open-source software, comparing performance between Ncorr and the previously used GOM to establish a robust methodological foundation for the following 3D DIC analysis.

Chapter 4: Development and Evaluation of a Novel 3D In-Shoe Plantar Strain Measurement System: STAMPS3D

Chapter 4 presents the development, calibration and validation of the STAMPS3D system, demonstrating its capability to capture plantar load while comparing against an established pressure measurement device. Details of this work contribute to the first published paper associated with this project.

Francesca Sairally, Rory P. Turnbull, Heidi J. Siddle, David A. Russell, Claire Brockett, Peter R. Culmer. Development and Evaluation of a Novel 3D In-Shoe Plantar Strain Measurement System: STAMPS3D*, Proceedings of the Institution of Mechanical Engineers, Part H: Journal of Engineering in Medicine*, 239(5), pp.472-484, 2025.

Chapter 5: Engagement with Patients and Clinicians to Inform STAMPS3D Research and Development

Chapter 5 reports on patient and public involvement and engagement (PPIE) discussion groups, summarising clinician and patient perspectives of STAMPS3D and identifying potential applications in prevention and management strategies.

Chapter 6: Measuring Plantar Load with STAMPS3D: A Preliminary Study on the Impact of Contoured Orthoses

Chapter 6 describes experiments assessing the feasibility of STAMPS3D in capturing plantar load measurements across contoured surfaces such as orthoses. Measurements across orthoses of varying stiffness were used, comparing against flat conditions in addition to in-shoe pressure data, exploring its potential to guide and evaluate effectiveness of management strategies. Details of this work contribute to the second published paper involving a proof-of-concept study associated with this project.

Francesca Sairally, David A. Russell, Heidi J. Siddle, Kate Chauhan, Daniele Trinca, Claire Brockett, Pete Culmer. Measuring Plantar Load with STAMPS3D: A Preliminary Study on the Impact of Contoured Orthoses, *Frontiers in Bioengineering and Biotechnology*, 13, p. 1648649, 2025.

Chapter 7: Measuring In-Shoe Plantar Strain Outcomes in the Presence of Callus: A Preliminary Study using the STAMPS3D Measurement System

Chapter 7 investigates the sensitivity of STAMPS3D to localised plantar deformations through simulated callus formation, comparing with Pedar measurements and highlighting the potential of strain-based measures for DFU prevention. Details of this work contribute to the final published proof-of-concept study associated with this project.

Francesca Sairally, David A. Russell, Heidi J. Siddle, Daniele Trinca, Claire Brockett, Peter R. Culmer. Measuring In-shoe Plantar Strain Outcomes in the Presence of Callus: A Preliminary Study Using the STAMPS3D Measurement System, *Journal of Foot and Ankle Research*, 19(2), p.e70169, 2026.

Chapter 8: Discussion and Conclusions

The final chapter synthesises findings across all of the chapters, reflecting on methodology development, clinical relevance and limitations, outlining future directions for STAMPS3D and translation into DFU prevention and management.

1.5 Project Roadmap

To help navigate through the thesis, Figure 1.5.1 provides a visual summary of my ‘PhD story’. It demonstrates the progression of work across the project, from methodological foundations to clinical applications and highlights how each chapter contributes to the overarching aim. The figure acts as a roadmap that will be referred to at the start of each chapter, emphasising its place within the broader narrative of the thesis.

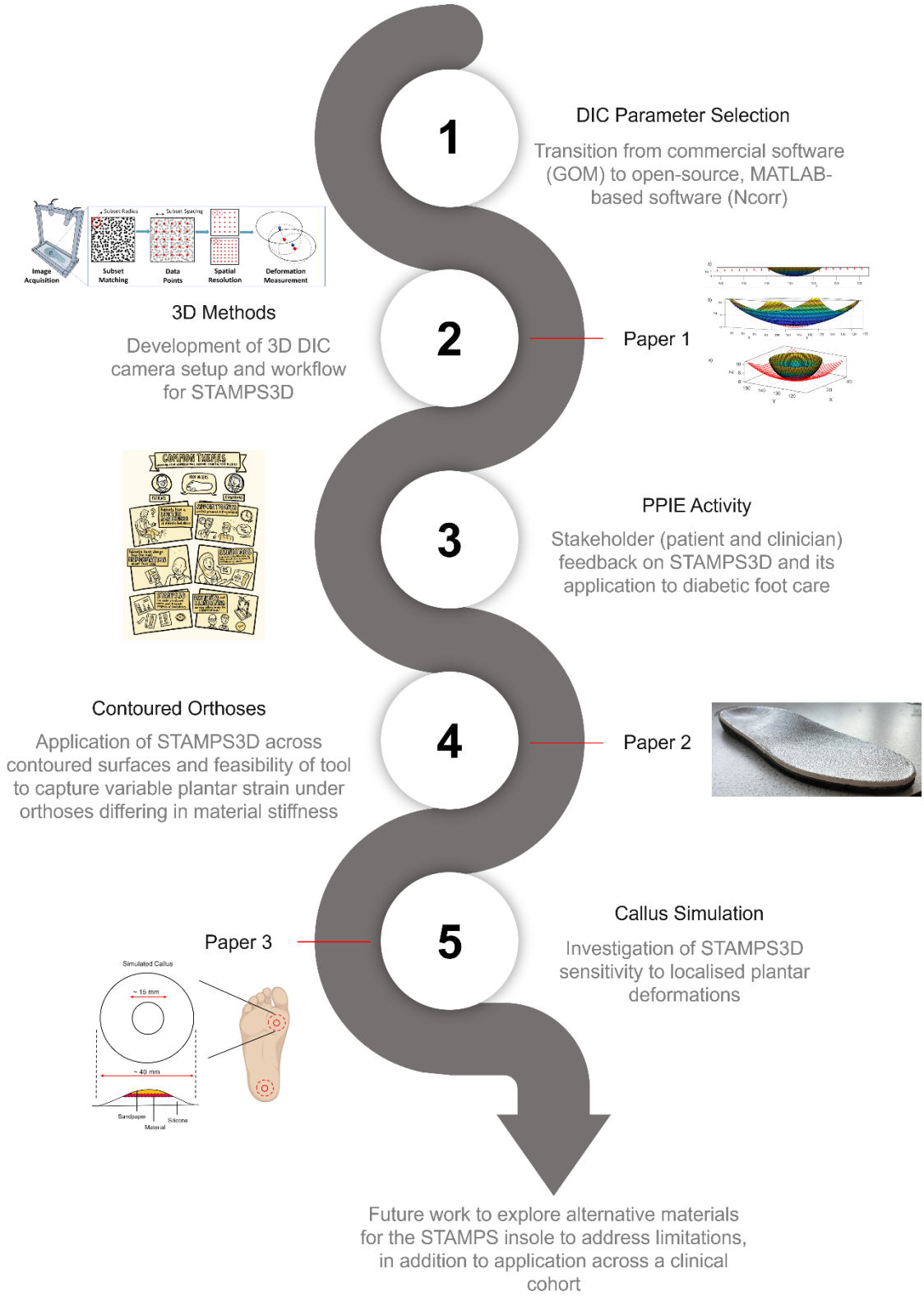


Figure 1.5.1: *Visual roadmap for this PhD project, demonstrating the progression and cohesion of each element of work.*

Chapter 2

Literature Review

This literature review includes the background on diabetes, its global impact and the associated complications, which affect the foot. The mechanisms that drive diabetes-related foot ulcer formation will be expanded on before giving an overview of the typical patient pathway, highlighting current screening practices and their limitations. This chapter also evaluates the roles of plantar pressure and shear in DFU formation and reviews existing measurement technologies, including strain-based approaches such as STAMPS. Finally, the principles of Digital Image Correlation are introduced, highlighting how they underpin the STAMPS approach and the practical considerations that currently limit its clinical translation.

2.1 Diabetes Mellitus

Diabetes mellitus represents one of the most significant global health challenges of the 21st century, with its rising prevalence placing increasing pressure on healthcare services and contributing to substantial morbidity, mortality and financial burden. Understanding the broader implications of diabetes is essential for giving context to the development of diabetes-related foot complications and the need for improved risk identification and management strategies. This section outlines the epidemiological background of diabetes mellitus, its clinical characteristics and the systemic complications most relevant to the foot.

2.1.1 Global and National Epidemiology

Recent global estimates highlight the rapidly growing prevalence of diabetes. In 2021, approximately 529 million people were living with the condition worldwide, with projections suggesting a rise to 1.31 billion by 2050 [1]. Of these, roughly 96% are attributed to Type 2 diabetes, reflecting the influence of risk factors such as obesity, physical inactivity and diet. Prevalence is found consistently higher in men than women, with further increases found with age, peaking between 75-79 years [1]. Data from the International Diabetes Federation (IDF) reinforces these findings. In 2024, an estimated 589 million adults between the ages of 20-79 were living with diabetes, representing

11.1% of the global population [2]. In addition to this, 252 million adults are thought to be living with undiagnosed diabetes, highlighting significant gaps in early detection. Diabetes also imposes a substantial financial burden, with global health expenditure exceeding USD 1 trillion in 2024, accounting for 12% of total health spending [2].

Within the UK, the prevalence follows global trends. Diabetes UK estimated that 5.8 million people are currently living with diabetes, with Type 2 diabetes contributing to approximately 90% of these cases [3]. The financial impact is also significant, with diabetes costing the NHS roughly £10.7 billion annually.

2.1.2 Types of Diabetes

Diabetes is a complex metabolic disorder characterised by uncontrolled blood glucose levels resulting from insufficient insulin secretion, resistance to insulin action or a combination of both [4], [5]. Although several forms of diabetes exist, the most common categories are Type 1, Type 2 and gestational diabetes [5]. Other less common presentations include monogenic disorders such as Maturity-Onset Diabetes of the Young (MODY), neonatal diabetes, and secondary diabetes resulting from pancreatic disease, endocrinopathies, infections or medication use [4], [5], [6].

Type 1 diabetes is caused by destruction of pancreatic β-cells due to an autoimmune response, leading to reduced or absent insulin secretion [7]. Consequently, individuals with this form of diabetes are dependent on insulin use for survival. Type 1 diabetes most commonly presents in childhood or adolescence, with incidence peaking between 10 and 14 years of age, although it has been found to occur in adulthood [5], [7].

Type 2 diabetes, the most prevalent form, is characterised by insulin resistance combined with insufficient β-cell response to rising insulin demands [5], [8]. Its development is strongly influenced by genetic, metabolic and lifestyle factors, including obesity, physical inactivity and dietary patterns [8]. Type 2 diabetes often has a gradual onset and many individuals remain asymptomatic for years, contributing to delayed diagnosis and increased risk of complications [6].

Despite the differing types of diabetes, all forms carry the potential for microvascular, macrovascular and neuropathic complications, the severity of which is linked to the degree and duration of hyperglycaemia [4]. These complications underpin many of the mechanisms relevant to diabetes-related foot disease and are explored in the subsequent sections.

2.1.3 Health Inequalities and Barriers to Care

The burden of diabetes varies in distribution across populations. Globally, the condition is most prevalent in low- and middle-income countries, where access to screening, education and long-term management is often limited [2]. Sex differences are also evident, with an estimated 9.8 million more men than women living with diabetes in 2024.

In the UK, ethnic disparities are found, with individuals of Asian, Black African and Black Caribbean heritage being 2-4 times more likely to develop Type 2 diabetes than white populations [3]. Socioeconomic deprivation further compounds risk, influencing both the likelihood of developing diabetes and the severity of its complications. These inequalities underscore the need for accessible, effective risk-assessment strategies that can be applied across diverse clinical and community settings.

In addition to these inequalities, behavioural and educational factors also influence how people engage with diabetes prevention and management. Patients' knowledge, attitudes, beliefs and cultural or linguistic backgrounds strongly shape their ability to understand and manage their condition, with limited health literacy consistently associated with poorer engagement in self-management behaviours [9]. These challenges are compounded by socioeconomic pressures, personal life demands, comorbidities and limited social support, all of which can restrict opportunities to adopt lifestyle changes or attend routine health checks [10]. Together, these factors contribute to delayed diagnosis, which reinforce existing inequalities in access to timely and effective care.

2.1.4 Symptoms and Systemic Complications

Symptoms and complications of the various forms of diabetes come from excess glucose remaining in the bloodstream. Common early symptoms include excessive thirst, frequent urination, fatigue, blurred vision, unintended weight loss, slow-healing wounds and recurrent infections [11]. These reflect the body's attempt to manage persistently elevated glucose levels and often precede the development of long-term complications.

Chronic complications of diabetes are traditionally categorised as microvascular or macrovascular. Microvascular complications include diabetic neuropathy, nephropathy and retinopathy, all of which result from progressive damage to small blood vessels that supply the nerves, kidneys and retinal tissue [12], [13]. Neuropathy is particularly relevant to lower-limb risk. Peripheral neuropathy affects up to one third of people with diabetes and leads to sensory loss, altered proprioception, impaired protective responses in feet and motor changes that can alter foot mechanics through intrinsic muscle wasting [14]. Retinopathy and nephropathy similarly reflect microvascular damage, contributing to visual impairment and progressive renal dysfunction [15], [16].

Macrovascular complications involve damage to larger vessels, including narrowing and reduced blood flow, which contributes to cardiovascular disease and peripheral arterial disease (PAD) [17], [18]. PAD reduces blood flow to the lower limbs, impairing oxygen delivery and the capacity for wound healing. When combined with neuropathy, PAD substantially increases the risk of ulceration, infection and amputation.

Beyond vascular and neurological complications, diabetes also disrupts immune function and inflammatory responses, contributing to delayed wound healing and increased susceptibility to infection [18]. These systemic effects collectively create a high-risk environment in the lower limb, where loss of protective sensation, compromised blood flow and reduced healing capacity overlap, increasing overall vulnerability to injury. These mechanisms contribute to the development of diabetes-related foot complications. The following section explores how neuropathy, vascular disease and biomechanical factors interact to drive the onset and progression of diabetic foot pathology.

2.2 Diabetes-Related Foot Disease

Understanding how the described mechanisms interact is essential for identifying individuals at risk of developing a DFU and informing preventative strategies. The following subsections outline the key contributors to diabetes-related foot pathology and the pathways leading to ulcer formation.

2.2.1 Peripheral Arterial Disease and Diabetic Peripheral Neuropathy

Diabetic peripheral neuropathy (DPN) and PAD are key mechanisms that lead to diabetes-related foot complications. DPN is associated with the decline of sensory, motor and autonomic lower-limb function [19]. Sensory neuropathy reduces the ability to detect pain, pressure and temperature, leading to trauma going unnoticed and prolonged exposure to harmful mechanical loads [20], [21]. Motor neuropathy contributes to intrinsic muscle wasting, altering foot stability and motor control [20], while autonomic neuropathy further compromises skin integrity by reducing sweat production, resulting in dry, fissured skin that is more vulnerable to breakdown [19].

PAD reflects progressive narrowing of the major arteries supplying the lower limb, leading to reduced blood flow, impaired oxygen delivery and lowered capacity for tissue repair. In diabetes, the associated metabolic changes drive the progression of PAD, contributing to further structural and functional alterations to arteries [22], [23]. In individuals with diabetes, PAD often presents more distally and progresses more rapidly than in non-diabetes populations. When PAD and DPN coexist, ischaemia amplifies the effects of neuropathy, increasing the risk of ulceration, delayed healing and lower-extremity amputation [24].

2.2.2 Biomechanical Risk Factors

The biomechanical consequences of diabetes arise largely from the effects of neuropathy and metabolic tissue changes. Motor neuropathy contributes to structural deformities and bony prominences such as claw toes, hammer toes and prominent metatarsal heads, which create local regions of elevated pressure [20]. Glycation of collagen within the tendons, ligaments and plantar soft tissues increases the stiffness of these tissues and reduces the foot's ability to dissipate mechanical loads [25]. Limited joint mobility, particularly at the ankle and the metatarsophalangeal joints, further restricts normal gait mechanics.

Decreased sensation can lead to a lack of response to sensory stimuli and failure to protect against damage caused by deformity [20], [24]. As a result, individuals may continue to load high pressure areas without awareness, leading to repetitive trauma. Altered gait patterns, driven by deformity and sensory impairment, redistribute plantar pressures in ways that increase vulnerability to tissue breakdown.

These biomechanical alterations set the stage for the mechanical pathways that lead to callus formation, tissue stress and ultimately ulceration, which are explored in the following subsection.

2.2.3 Tissue Breakdown and DFU Formation

The development of a DFU typically occurs from the complex cumulative effect of mechanical, neurological and vascular factors (summarised in Figure 2.2.1). DFUs can be categorised as neuropathic, ischaemic or neuro-ischaemic, with neuro-ischaemic ulcers accounting for up to 50% of cases [26], [27]. In neuro-ischaemic feet, reduced blood flow limits tissue resilience and wound healing capacity, meaning that even modest loads can cause breakdown.

A key initiating factor is the presence of bony prominences, which create local areas of elevated stress during gait. In these regions, localised high pressures arise and cannot be effectively dissipated due to increased stiffness of plantar soft tissues [25]. This stiffness is driven in part by glycation-related changes to soft tissues, which reduces their capacity to deform and absorb load. Simultaneously, the high mechanical stresses can lead to plantar callus formation (a dermatological response to repetitive pressure and shear), resulting in localised thickening of the skin [28]. While often asymptomatic and protective in healthy individuals, callus can become pathological when pain arises or when mechanical stress is concentrated between the callus, underlying soft tissue and prominent bone [29], [30]. In people with diabetes, particularly those with sensory neuropathy, this stress may go unnoticed due to sensory impairment and a lack of

protective responses [20], [24]. As callus thickens, it further increases plantar stiffness and amplifies local pressures, creating a self-reinforcing cycle of mechanical overload.

Repetitive trauma beneath callused areas can cause subdermal haemorrhage, inflammation and eventual skin breakdown. Hence, callus is recognised as a predictive marker for DFU formation [29], [31]. Ischaemia present in PAD amplifies these effects, slowing healing and increasing the risk of ulceration [24], [32]. Impaired immune responses and altered inflammatory pathways in diabetes further hinder the healing process, increasing susceptibility to infection [33].

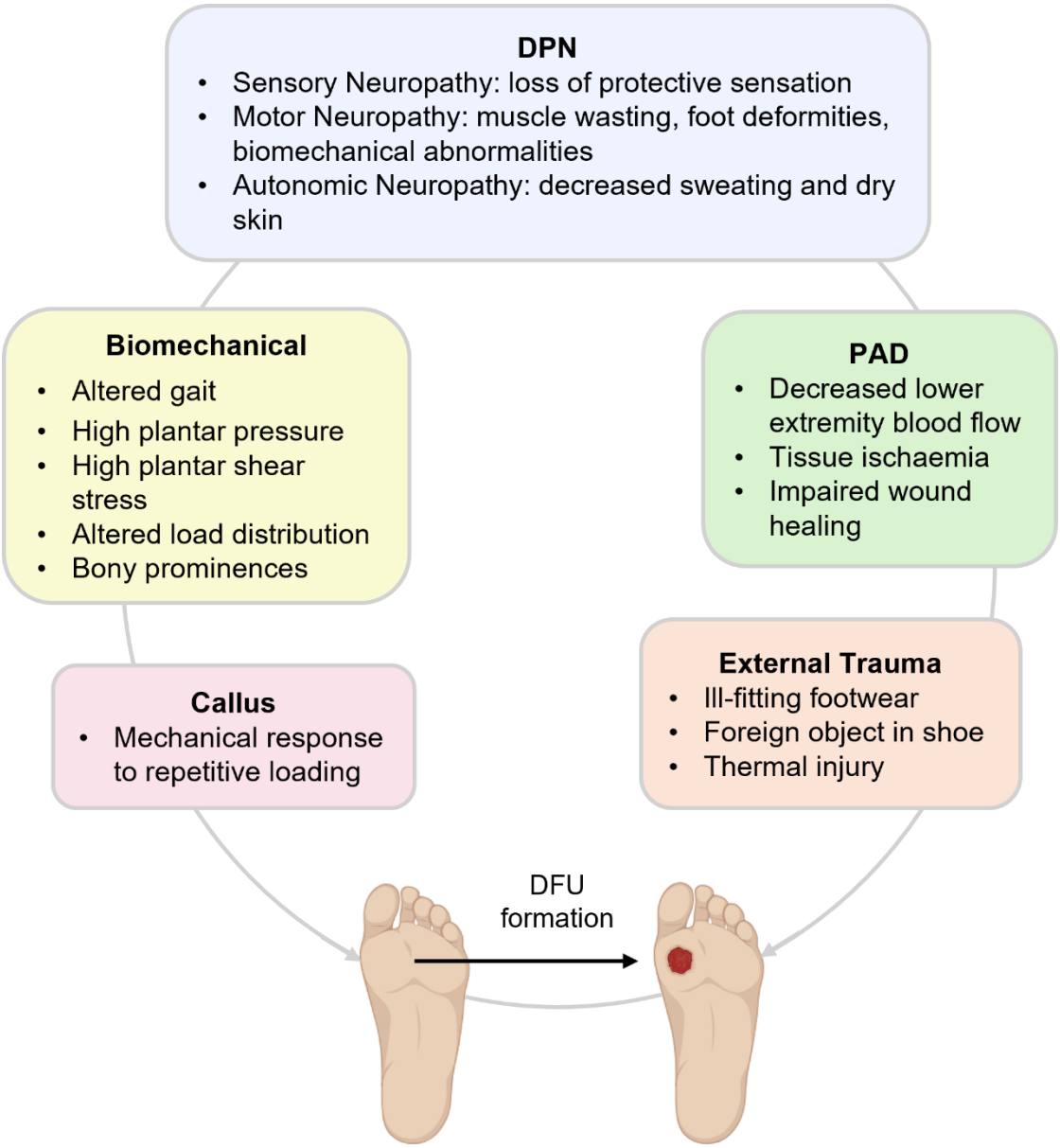


Figure 2.2.1: *Key contributing factors to DFU formation, including neuropathic, vascular, biomechanical and external influences (information summarised from [24], [34]).*

2.2.4 DFU Location and Patterns

The anatomical distribution of DFUs reflects the underlying loading patterns and vascular supply of the foot. As such, the different forms of DFUs demonstrate characteristic location patterns [26].

Neuropathic ulcers most frequently occur on the plantar surface at sites exposed to repetitive high stress. These include the metatarsal heads and heel, where bony prominences, structural deformity and altered gait mechanics concentrate loads [26], [35]. Limited joint mobility, particularly at the first metatarsophalangeal and subtalar joints, further alters weight-bearing patterns and increases forefoot loading [36]. Ischaemic ulcers, by contrast, tend to be found on the tips of the toes, lateral aspects of the foot or other distal sites vulnerable to trauma and poor healing [26]. Lastly, neuro-ischaemic ulcers display a mixed pattern, occurring both on plantar surfaces and at distal sites, with one study reporting that 51.8% of neuro-ischaemic ulcers were located in these regions [37]. This reflects the combined influence of mechanical loading, loss of sensation and impaired blood flow.

Epidemiological studies consistently show that the majority of DFUs occur in the forefoot. In a large cohort, 77.8% of ulcers were located in the forefoot, 11.9% in the midfoot and 10.3% in the hindfoot [38]. Other studies report that more than 75% of all ulcers occur in the toes and forefoot region [37]. Although DFUs are classically associated with the plantar aspect of the foot, non-plantar ulcers are also common. In the Eurodiale study, 52% of ulcers were non-plantar, with dorsal or interdigital toe ulcers representing the most frequent site (32%) [39].

Patterns of recurrence mirror these loading distributions. In one study, 84% of re-ulcerations occurred on the same foot and over one third recurred at the same anatomical site, demonstrating the persistent nature of biomechanical risk factors [40].

2.2.5 Ulcer Recurrence and Long-Term Risk

Studies suggest that patients with diabetes have a lifetime risk of developing a DFU of up to 34% [41]. Of those who develop DFUs, fewer than half of the cases successfully heal by 12 weeks and those with DPN will fail to heal if interventions such as offloading are not implemented [42]. Approximately 50% of patients with neuropathy and foot ulcers also have PAD, increasing the risk of poor wound healing, gangrene and lower-limb amputation, with up to 85% of lower amputations in people with diabetes being the result of non-healing DFUs [28], [43]. Even in patients who have achieved improvements or DFU resolution, recurrence is common, with approximately 40% of patients experiencing a re-ulceration within one year, 65% within 5 years and 90% with ten years [41].

Persistent neuropathy, structural deformity and altered loading patterns remain after ulcer closure, meaning that the underlying risk factors are rarely fully resolved. PAD further prolongs the healing times and increases the likelihood of complications such as infection and amputation.

2.2.6 Social and Economic Costs

DFUs are associated with substantial financial pressures on healthcare services and significant social burdens for patients. They often require prolonged treatment, frequent hospitalisation and multidisciplinary care, contributing to high medical costs. Quality of life is markedly reduced due to pain, immobility and psychological distress. In the UK, NHS England is estimated to spend up to £1 billion annually on foot ulceration and diabetes-related amputation, based on 2014-2015 spending [44].

The financial burden also extends beyond healthcare systems. Patients frequently experience indirect costs related to loss of employment, reduced productivity, travel to appointments and the need for long term assistance or home adaptations. In low- and middle-income countries, DFU management costs may represent several years of income, with limited access to specialist care contributing to poorer outcomes [45]. These financial pressures are compounded by social inequalities mentioned in Section 2.1.3, with disadvantaged populations experiencing higher rates of ulceration, amputation and mortality.

DFUs are also associated with high mortality burden. Reported five-year mortality rates after DFU presentation range widely in the literature from around 30% in DFU cohorts to over 60% in older or more comorbid populations [34], [46], [47]. Such variation potentially reflects differences in ulcer severity, presence of PAD, renal disease and other comorbidities. Mortality is even higher following amputation, with diabetes-related major amputations carrying a five-year mortality exceeding 70% [34], [41]. Long-term outcomes are similarly poor; the ten-year risk of death of a person with a history of DFU is approximately twice that of a person with diabetes who has never ulcerated [41].

The COVID-19 pandemic further exacerbated these challenges by disrupting routine care, reducing access to podiatry and vascular services and increasing incidence of late presentations [48]. These disruptions disproportionately affected individuals in resource-limited settings, further widening global disparities in DFU outcomes.

Taken together, this section has shown that diabetes-related foot disease is not a minor complication but a serious, high-risk condition with profound clinical and societal consequences. DFUs arise from a combination of mechanical, neurological and vascular factors, that once present, carry high rates of recurrence, amputation and mortality. The

scale of the economic burden and the social cost underline the urgency of effective prevention, early detection and timely access to specialist care.

2.3 Patient Pathway

Given the substantial burden associated with diabetes-related foot complications, care is organised through a structured patient pathway that supports early detection, ongoing monitoring and specialist management from the point of diagnosis onwards. This section outlines the typical patient pathway, integrating self-management, routine clinical review, multidisciplinary care, screening and targeted intervention. A summary of the patient pathway has been illustrated in Figure 2.3.1.

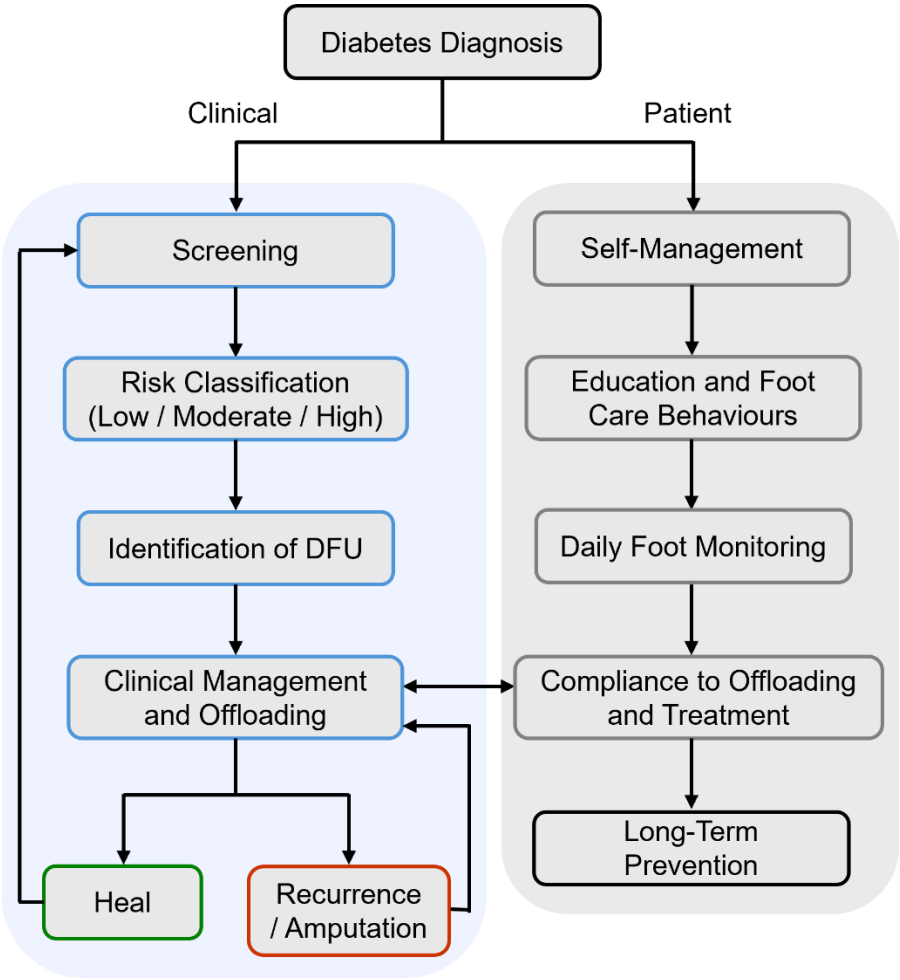


Figure 2.3.1: *Overview of the patient pathway for diabetes-related foot care, illustrating the parallel clinical and self-management processes from diabetes diagnosis through to ulcer formation, treatment and outcomes (summarised from [28], [49], [50]). The figure highlights the cyclical nature of the pathway, with healing and recurrence feeding back into earlier stages of care.*

2.3.1 From Diagnosis to Routine Care

A patient's journey begins at the point of diabetes diagnosis. At this stage, the patient is made aware of what the condition is and receives education on lifestyle modification, complication prevention and long-term self-management. From this point onwards, the assessment and management of foot health is a continuous component of diabetes care.

Routine care forms the foundation of DFU prevention. In the UK, the National Institute for Health and Care Excellence (NICE) recommends that all individuals with diabetes receive at least one foot assessment per year, with more frequent reviews for those at moderate or high risk [49]. These annual checks aim to identify early signs of neuropathy, PAD, structural deformity or skin changes that may predispose to ulceration. As such, early detection of these features enables clinicians to monitor changes in a patient's condition over time and therefore focus on early intervention to prevent DFU formation. Typical components of the review include [28], [49]:

- Inspection of skin, nails and callus
- Assessment of foot deformity and footwear
- Sensory testing (e.g., 10 g monofilament)
- Vibration perception testing (e.g., tuning fork)
- Vascular assessment (e.g., pedal pulses, Doppler)
- Evaluation of previous ulcer history or amputation
- Assessment of risk factors such as glycaemic control and smoking status

The purpose of routine care is not only to detect emerging risk factors but also to reinforce patient education, encourage engagement with self-management behaviours and ensure timely referral to specialist services when needed.

2.3.2 Patient Self-Management

Self-management is a core component of DFU prevention and runs in parallel with routine clinical care. It requires the patient to be personally engaged in daily activities involved in foot care such as foot checks and appropriate footwear choices [51]. These behaviours allow individuals to monitor changes or progression of their own foot condition between clinical appointments and to identify early signs of deterioration.

Daily foot care activities recommended for people with diabetes are summarised in Table 2.3.1, including washing and drying the feet, moisturising appropriately, inspecting the skin daily, trimming toenails safely, wearing suitable socks and footwear, avoiding barefoot walking and checking shoes for foreign objects before use. These practices aim to reduce the risk of trauma, maintain skin integrity and detect early signs of ulceration.

Table 2.3.1: *Foot care activities advised for patient's self-management of foot health [28], [52], [53], [54].*

	Foot Care Activities
1	Keep feet clean, washing everyday with warm soapy water but avoid soaking
2	Ensure feet and between the toes are dry
3	Keep feet moisturised, avoiding between the toes
4	Check feet daily for any cuts, sores or changes to skin
5	Trim toenails regularly, ensuring they are not too short
6	Wear clean and suitably sized socks
7	Keep your feet warm and dry
8	Wear appropriate style and sized shoes
9	Do not walk barefoot
10	Examine shoes for anything that might rub or damage skin before putting them on
11	Remain active to encourage blood circulation and mobility
12	Maintain foot temperature, avoiding extreme cold or heat

Following the guided foot care activities is an important element of preventing DFU formation from a self-management perspective. As a result, patient compliance to a daily routine integrating the described foot care activities is crucial and therefore the patients are relied on to mitigate the risk. However, many factors can limit a patient's ability to carry out these tasks effectively. Barriers to effective self-management may include reduced mobility, visual impairment, comorbidities, limited health literacy, low social support or psychological distress, all of which can contribute to poor compliance [51].

Recent literature highlights that self-management is not a single behaviour but a multi-step process. Costa et al. describe a progression from awareness to motivation, to capability and finally to consistent practice, emphasising that patients often require support at each stage before they can reliably perform daily foot care independently [50]. This aligns with findings from Untari et al., who reported that knowledge gaps remain a major barrier to effective self-care, particularly in settings where health literacy or access

to education is limited [55]. Their study found that many patients demonstrated moderate to low levels of foot self-care knowledge and did not fully meet recommended practices. Key areas requiring improved patient understanding included ulcer development and prevention, glucose control, appropriate footwear, daily inspection techniques and recognising early signs of skin breakdown.

Digital tools and remote monitoring technologies are increasingly being explored to support self-management. Smartphone applications, educational platforms and temperature-monitoring devices may help patients detect early changes and engage more consistently with foot care routines [56]. Pouwer et al. note that digital health technologies can enhance patient involvement and improve coordination between patients, caregivers and clinicians [57]. However, they also highlight challenges related to usability, cost, alignment with patient goals and integration into existing healthcare systems. These considerations demonstrate the need for digital tools that are accessible, intuitive and tailored for patient needs.

Overall, effective self-management requires not only patient motivation and capability but also adequate education, accessible resources and ongoing clinical support. Strengthening these elements may improve compliance, reduce ulcer incidence and support long-term foot health in people with diabetes.

2.3.3 The Multidisciplinary Foot Care Team

Alongside patient-led self-management, the clinical management of diabetic foot health relies heavily on the coordinated input of a multidisciplinary team (MDT). The complexity of DFU development, arising from interacting metabolic, vascular, neurological and biomechanical factors mentioned in the previous sections, means that no single clinician can address all aspects of prevention or treatment [58], [59]. Instead, effective care requires integrated expertise spanning metabolic control, vascular assessment, wound management, infection control, pressure redistribution and patient education [49], [60].

The composition of an MDT varies across healthcare systems, but the NICE NG19 guidelines specify that MDTs should collectively provide expertise in diabetology, podiatry, diabetes specialist nursing, vascular and orthopaedic surgery, microbiology, interventional radiology, biomechanics and orthoses, casting and wound care, with access to rehabilitation, psychological and nutritional support [49]. This collaborative structure ensures that each area is addressed simultaneously.

Evidence strongly supports the effectiveness of multidisciplinary care. Numerous studies and systemic reviews demonstrate that MDTs reduce major amputation rates, shorten healing times and improve survival [60], [61], [62], [63]. For example, Krishnan et al. reported a major amputation rate of 4.7% among patients treated by an MDT compared

with 21.7% in those without multidisciplinary input, alongside a substantial reduction in in-hospital mortality [62], [64].

National guidance reflects this, with NICE and The International Working Group on the Diabetic Foot (IWGDF) recommending that individuals with active foot ulceration receive same-day referral to an MDT, emphasising the importance of rapid coordinated intervention [28], [49]. Early involvement of an MDT has also been associated with improved compliance to offloading, more timely vascular assessment and more consistent monitoring of infection, all of which contribute to ulceration prevention, management of active disease, reduction of risk of recurrence and amputation and overall better clinical outcomes [41], [60].

2.3.4 Screening and Clinical Assessment Methods

Screening is another central component of diabetic foot care that runs alongside patient self-management and routine clinical review. Its primary purpose is to identify individuals at risk of developing a DFU and guide the frequency of follow-up and the need for intervention. Studies suggest that a number of factors influence an individual's risk including sex, glycaemic control, structural foot abnormalities, DPN, PAD, smoking status and duration of diabetes [32], [65], [66]. These factors often accumulate over time, meaning that risk can increase as the condition progresses.

Clinical Assessment Tools

Current clinical practice relies on a combination of medical history, visual inspection and simple bedside tests to identify risk factors outlined in Table 2.3.2. The Inlow 60-second Diabetic Foot Screening Tool, updated in line with IWGDF guidance, provides a structured checklist covering skin integrity, deformity, sensation and vascular status [67]. Woodbury et al. describe a simplified version suitable for low- and middle-income settings, emphasising feasibility and rapid assessment [68]. This tool involves a compiled list of checks that need to be performed by a healthcare professional including medical history, identification of superficial and structural foot features/deformities as well as sensation, linking to presence of neuropathy. As each of the elements of the screening tool are performed for each foot, the number of characteristics is recorded and totalled, using this to determine whether the patient has a positive screen and thus at high risk. In the UK, the NHS "Ask-Inspect-Examine" form structures screening into three steps, focusing on history, visual inspection and neurological/vascular examination [69].

Other clinical assessment tools mentioned in the literature include the Ipswich touch test, VibraTip and Neuropad, through the palpation of tissues, applied vibrations and colour changes related to the presence of normal sweating. Each are used to test a patient's perception of feeling, indicating the presence of diabetic neuropathy [64]. These tools

are widely used because they are quick, inexpensive and practical in routine clinical settings.

An additional challenge within clinical assessments relates to the detection of early signs of foot disease in people with darker skin tones. Subtle changes such as erythema, inflammation or early tissue damage may be less visible or present differently, increasing the risk of delayed recognition and progression to more severe ulceration [70]. This issue is widely acknowledged in diabetic foot care, with reports emphasising that traditional visual cues used in lighter skin may not reliably translate across diverse skin tones [71], [72]. Recent initiatives, including adapted skin-tone assessment tools and guidance from organisations such as Diabetes Africa and Wounds International, aim to support clinicians in recognising early pathology more consistently across different skin types [73], [74]. These developments highlight the need for more inclusive assessment frameworks to ensure appropriate and timely identification of risk in all patient groups.

Risk Classification Systems

The outcome of screening is typically expressed through a risk classification system. In the UK, NICE guidance stratifies patients into low, moderate or high risk, or identifies active foot disease, based on combinations of neuropathy, PAD, deformity, callus, previous ulceration or amputation [49]. The characteristics corresponding to each risk category are summarised in Table 2.3.2.

Table 2.3.2: *Characteristics corresponding to low, moderate and high risk of DFU development addressed by NICE [49].*

Type of Risk	Characteristics
Low	No signs of risk factors except callus formation
Moderate	Neuropathy (or) Non-critical limb ischaemia (or) Foot deformity (or) Skin changes (not including callus)
High	Neuropathy and non-critical limb ischaemia (or) Neuropathy and presence of callus/foot deformity (or)

	Non-critical limb ischaemia and presence of callus/foot deformity (or) History of DFU or amputation (or) Currently on renal replacement therapy

Internationally, the IWGDF 2023 guidelines provide a similar risk-based structure and recommend follow-up intervals ranging from annually (low risk) to every 1-3 months (high risk) [28]. These frameworks help determine the urgency of referral, the need for offloading or vascular assessment and the intensity of patient education.

Ulcer Severity Classification

For individuals with active ulcers, several classification systems are used to standardise assessment and guide management. The IWGDF/Infectious Diseases Society (IDSA) infection severity scale grades ulcers from uninfected (Grade 1) to severe infection with systemic involvement (Grade 4), helping clinicians determine the urgency of patient hospitalisation and surgical intervention [26], [75]. The SINBAD score evaluates site, ischaemia, neuropathy, bacterial infection, area and depth, producing a 0-6 score that correlates with healing and amputation risk [26], [76]. The WIfI (Wound, Ischaemia, foot Infection) system assigns scores 0-3 for each category and groups them into stages predicting 1-year amputation risk and the need for revascularisation [26], [77].

These systems support decision-making within MDTs and help standardise communication across services, while considering individual patient risk factors and comorbidities.

2.3.5 Interventions and Offloading

Once a patient's DFU risk has been identified, the appropriate form of intervention must be implemented. Individuals classified as low risk typically continue with self-management and routine annual review, whereas those at moderate or high risk require more frequent clinical assessments, enhanced education and, where necessary, targeted treatment for foot-related complications [49]. The IWGDF prevention guidance summarises this stratified approach, outlining tailored advice for each risk category and noting that patients at high risk may be eligible for prescribed insoles or specialist footwear to redistribute plantar pressures [28]. Despite preventative efforts, DFUs may still develop. When an ulcer is identified, clinical assessment focuses on determining the presence of infection, evaluating vascular status and establishing the most appropriate management pathway [78].

Wound care is another component of DFU management and includes infection control, appropriate dressings and the use of debridement to remove necrotic or non-viable tissue and promote healing [59], [64]. Debridement may be performed using surgical, mechanical, enzymatic or biological methods, each with specific advantages and limitations (Table 2.3.3).

Table 2.3.3: *Description of debridement techniques used on DFUs [59], [79]*.

Debridement Approach	Description
Surgical	Performed using a sharp blade to manually separate non-viable tissue from the healthy tissue Complications may include bleeding and issues related to anaesthesia
Mechanical	Application of a wet dressing to the wound and left to dry before removal, mechanically pulling away non-viable tissue that has become embedded within the applied dressing Non-selective approach, which may also remove viable tissue
Autolytic	Uses the body's own immune cells and wound moisture, together with moisture-retentive dressings, to facilitate softening and breakdown of non-viable tissue Cannot be used on infected wounds unless paired with another debridement method
Enzymatic	Application of topical agents containing enzymes that result in the breakdown of non-viable tissue Slower method
Biological	Implementation of maggot therapy, whereby the maggots digest the non-viable tissue revealing the healthy tissue Possible discomfort from maggots moving across the surface of the wound

The plantar soft tissues act as natural shock absorbers, distributing ground reaction forces across the foot during load-bearing activities [21]. These forces occur in both the vertical and horizontal planes and are referred to as plantar pressure and plantar shear stress, respectively. In individuals at risk of DFU development, or in those with an existing ulcer, abnormal magnitudes of these forces can arise [60]. This often results from altered or uneven distribution of loads caused by diabetes-related tissue changes, as described previously. An important element of DFU wound care therefore involves alleviating these excessive forces in order to encourage healing and reduce the risk of recurrence [60], [80]. Offloading techniques are used to achieve this by redistributing load away from high-risk or ulcerated areas, thereby reducing plantar pressures across the foot [64]. This includes the use of either removable or non-removable devices such as total contact casting (TCC), short and knee length walker boots, custom footwear/orthotics as well as surgical offloading options [59], [60], [81]. Consistent with this, the IWGDF offloading guidance recommends non-removable knee-high devices as the preferred first line option for plantar DFUs [28]. TCC has been described as the ‘Gold standard’ offloading approach, with peak pressures in the forefoot reported to be reduced by up to 87% [60], [80]. This, as well as other non-removable devices, are agreed among the literature to be more effective in promoting healing. In comparison to previously conventional treatments such as bed rest, the described offloading techniques allow patients to continue with their daily activities, reducing the need for bed rest and improving overall quality of life [82]. Even among the non-removable devices available, differences in effectiveness have been described, with knee-high walkers capable of reducing plantar pressures greater than short walkers [83]. This is due to the longer device being able to absorb a larger portion of the load on the lower extremity of the patient. However, patients do not always tolerate the use of non-removable devices, meaning that removable walkers and custom shoes are often used instead [83]. Regardless of the method of offloading applied, compliance remains a major challenge. Similar to foot-care routines, compliance with offloading is influenced by biological, psychological and social factors, including but not exclusive to age, gender, education and surrounding support [81]. Hence given that offloading is accepted as a key element of DFU management, emphasis on compliance to these approaches in addition to foot care routines is necessary in the prevention and treatment of DFUs.

Callus management also represents an important aspect of DFU prevention. Callus formation is widely recognised as a marker of elevated mechanical stress, arising from repetitive vertical and shear forces at prominent plantar sites [29]. In people with diabetic neuropathy, callus is considered highly predictive of ulceration. Murray et al. reported an eleven-fold increase in ulcer risk at callus sites compared with non-callused areas, and relative risk of 56.8 at locations with a history of previous ulceration [84], [85]. This contrasts with elevated plantar pressure alone, which carried a lower, but still significant,

relative risk of 4.7 compared with areas without high pressure, highlighting that factors beyond vertical pressure, such as shear forces implicated in callus formation, may contribute to the higher ulcer risk at these sites. Although callus may initially form as a protective response, its progressive thickening concentrates plantar stresses and can contribute to tissue breakdown and eventual ulcer formation [29], [41]. Scalpel debridement is therefore routinely used to reduce localised pressure and interrupt its progression. Studies in cohorts with diabetes and neuropathy consistently demonstrate significant reductions in peak plantar pressure following callus debridement, typically by up to 30% [86], [87], [88]. When callus removal is combined with orthotic or offloading interventions, an additional reduction of peak pressures by 24% has been reported [88]. This contrasts with findings in rheumatoid arthritis (RA) populations, where debridement was reported to reduce pain but not significantly alter pressure distribution [31], [89]. This likely reflects differences in sensory response rather than differences in callus itself. For example, individuals with intact sensation (as in RA) subconsciously offload painful areas, whereas those with diabetes and neuropathy lack protective sensation and therefore continue to load callused regions in the same way before and after debridement. Similarly, callus debridement in a healthy cohort showed no significant difference in peak pressure, yet significantly elevated pressure was reported at the participant's callus sites compared to those without any callus [30].

Through clinical management and treatment, the objective is to prevent the development of DFUs or heal those that occur. However, as mentioned previously, a large proportion of healed DFUs recur and often lead to amputation [43], [60]. Although the typical patient pathway is often presented as a sequence of stages, progression is not necessarily linear. Patients may move back and forth between stages as their risk status changes, an ulcer heals, or recurrence develops (as demonstrated in Figure 2.3.1). Therefore, this reinforces the importance of preventing initial ulcer formation wherever possible, both to reduce the substantial social and economic burden of diabetes-related foot disease and to support patients remaining outside the more complex stages of the 'patient journey'.

2.3.6 Clinical Limitations of Current Clinical Approaches

Despite the range of screening tools, clinical assessments and management strategies available, a range of limitations remain within current approaches to diabetic foot care. These limitations affect the accuracy of risk identification, the timeliness of intervention and the effectiveness of treatment, contributing to the persistent burden of DFUs.

Most screening tools rely heavily on clinician judgement, visual inspection and simple bedside tests. As a result, assessments can be subjective and show variable reliability. Tools such as the Inlow 60-second screen [67], the Woodbury simplified tool [68], the NHS Ask-Inspect-Examine form [69] and neuropathy tests including the Ipswich Touch

Test, VibraTip and Neuropad [64] are practical and low-cost but they lack sensitivity for early tissue damage and do not quantify biomechanical loading. Consequently, individuals at rising risk may not be identified until structural or sensory changes are already established.

Current clinical guidance focuses primarily on plantar pressure, with little or no assessment of plantar shear stress, despite growing evidence that shear plays a significant role in ulcer formation and recurrence [43], [90]. This means that important contributors to tissue breakdown remain unmeasured, limiting the ability to tailor intervention such as offloading or footwear modification.

Risk classification systems outlined by NICE and IWGDF guidelines stratify patients based on clinical features including neuropathy, PAD, deformity, callus and ulcer history [32], [65], [66]. However, these systems do not provide insight into *why* a patient is at risk or indicate which specific intervention would be most effective for an individual. As a result, management often follows broad categories rather than personalised risk profiles. In addition to this, routine screening in primary care rarely includes biomechanical assessment or measurement of plantar pressure due to time and cost constraints, meaning that key contributors to tissue breakdown remain unassessed. Ulcer severity systems such as SINBAD, WIfI and the IWGDF/IDSA infection scale, support standardised documentation and audits, but they are applied only once an ulcer has already developed. Consequently, they do not contribute to primary prevention and offer limited insight into the biomechanical or behavioural factors that may have contributed to ulcer formation.

Finally, although offloading is key to DFU healing, its effectiveness is constrained by patient compliance. Non-removable devices such as TCC are most effective but are often poorly tolerated, leading clinicians to prescribe removable alternatives that are less effective when not worn consistently [83].

These challenges limit the real-world effectiveness of preventative and management strategies put in place for patients either at risk of developing a DFU or with an existing DFU. As such, there is a need to develop techniques that are clinically applicable, tolerable by patients and acceptable to clinicians, while also integrating new research to improve the effectiveness and success of DFU risk screening and offloading of DFUs. Reflecting these gaps, a priority list was developed for research around diabetes-related foot health. This is in association with the James Lind Alliance and was developed jointly by patients and healthcare professionals. The priority list consisted of questions related to the following: prevention of DFUs and further amputations; referral delays; outcome improvements where infection is present; blood flow and risk assessment improvements; recurrence prevention; factors that affect healing time; and education surrounding

diabetes-related foot complications [91]. Out of the 10 research priorities, 6 of the priorities involved prevention which could be achieved through improved measurement techniques used towards screening, in addition to improved compliance to self-management behaviours, education on complications associated with different levels of risk of developing an ulcer.

2.4 Plantar Pressure and Shear Stresses

Mechanical forces acting on the plantar surface of the foot play a fundamental role in the development of diabetes-related foot complications. Pressure and shear forces arise in several biological and clinical contexts, including the plantar surface of the foot during gait, the development of pressure injuries from prolonged loading on support surfaces and the mechanical behaviour of vascular tissues under blood flow [92], [93], [94]. During standing and walking, the foot is exposed to a combination of vertical forces (plantar pressure) and horizontal forces (applied shear forces), generated through interactions between the foot, footwear and the supporting surface. Plantar pressure refers to the perpendicular force applied over a given area, whereas shear describes the applied tangential forces acting parallel to the skin, typically in the anterior-posterior or medial-lateral directions [95]. Together, these forces contribute to the plantar loads experienced during gait.

In people with diabetes, neuropathy, tissue stiffness, deformity and altered gait patterns can lead to abnormal magnitudes or distributions of pressure and shear [24], [96]. These altered loading patterns increase localised mechanical stress and contribute to the development of callus, tissue breakdown and ulceration. As a result, understanding the mechanical environment of the foot, and the relative contributions of pressure and shear, is essential for explaining DFU formation and for developing objective methods to identify patients at increased risk.

2.4.1 Role in DFU Formation

Within the literature, there are varying opinions on the extent to which plantar pressure and shear stress contribute to DFU formation. Until recently, plantar pressure has been considered to be the primary mechanical driver of ulceration, which led to the development of assessment tools strictly relying on pressure and the identification of high pressure regions on the plantar surface [97]. The risk of ulceration has been described to increase six-fold where peak barefoot plantar pressures exceed 650 kPa, comparatively to those below this threshold [98], [99]. In addition to this, the IWGDF recommends in-shoe peak pressures of less than 200 kPa to reduce risk of ulceration [28]. Increased peak pressures have also been observed in those with two or more foot

deformities and are generally higher in patients with diabetes, particularly those with active or previous ulceration [96], [98].

Although increased risk of ulceration has been associated with regions of high plantar pressure, little correlation between peak pressure and the formation of DFUs has been definitively found [100]. For example, Veves et al., concluded that high plantar pressures were good indicators of ulceration, especially in patients with neuropathy, however only 38% of ulcers were found to develop at peak pressure regions [101]. Furthermore, ulceration has been observed at pressure levels considered to be un-problematic in individuals without diabetes [102]. These findings have prompted increasing attention toward the role of plantar shear stress in DFU formation.

Recent research has examined whether peak pressure and peak shear occur at the same anatomical locations and at the same time during gait, with evidence suggesting that they often do not. Studies using custom built platforms that capture pressure and shear have shown that peak pressure and peak shear coincide at the same location in only around 50% of cases, with poor repeatability across trials [100], [102]. These systems typically use discrete sensor arrays to capture local barefoot forces, which limits spatial resolution and contributes to variability in reported shear measurements. Perry et al. reported plantar pressure magnitudes consistently higher than shear forces, with peak shear of ~33 kPa vs peak pressure of ~189 kPa [102]. However, shear loading occurs more frequently during gait due to alternating anterior–posterior and medial–lateral shear directions from initial contact to push-off [43]. This repeated tangential loading is thought to contribute to cumulative tissue stress, particularly in feet with diabetes where increased tissue stiffness, deformity and reduced protective sensation increase vulnerability to mechanical loading. While these findings support the contribution of shear to plantar tissue breakdown, the link between plantar shear forces and ulcer formation remains an emerging and not yet definitively established relationship.

Shear stress has been recognised as a contributor to both superficial and deeper tissue injury, including the formation of callus, which itself is a known precursor to ulceration [103]. In people with diabetes, neuropathy and foot deformities often lead to elevated plantar pressures, while diabetes-related changes in soft tissue properties further exacerbate vulnerability to mechanical stress. Studies consistently report significantly increased stiffness in plantar tissues of those with diabetes compared to healthy participants, although findings regarding tissue thickness are mixed [104], [105], [106]. These inconsistencies have been linked to factors such as age, neuropathy severity or foot health characteristics such as callus [104], [107]. Both increased stiffness and altered thickness reduce the shock-absorbing capacity of plantar tissues, impairing their ability to distribute pressure and shear during gait. Consequently, it is expected that the

combined effect of reduced tissue cushioning and elevated mechanical loading is likely to contribute to tissue break down and DFU formation [104].

Therefore, assessing peak pressure or shear in isolation may be insufficient for identifying individuals at risk of ulceration. Considering both forces together may provide a more comprehensive understanding of mechanical risk, particularly for ulcers that develop at locations not predicted by pressure alone [108]. However, the ability to evaluate these plantar forces in clinical or research settings depends heavily on the measurement technology available.

2.4.2 Plantar Measurement Techniques and Devices

Plantar loading can be assessed using a range of measurement techniques that vary in complexity, cost and clinical applicability. Low cost methods such as projection devices, microcapsules and podoscopes have been available in clinical settings and provide rapid, visual representations of plantar loading patterns [109]. These approaches generate ink- or light-based pressure maps that allow clinicians to identify regions of increased loading, however they do not enable quantification of the magnitudes of pressure and therefore only offer qualitative information.

Alternatively, pressure platforms and in-shoe sensor devices provide quantitative measurements of plantar pressure across the foot [110]. These systems enable both global and regional analysis of pressure distribution, including identification of peak pressure sites. Examples of commercial pressure measurement systems discussed among the literature include Novel Pedar, F-scan, medilogic WLAN insole, BioFoot, P-WALK, emed, MatSCAN, footscan, FlexiForce and ParoTec [97], [109], [110]. Pressure platforms are typically used for barefoot assessments, whereas in-shoe sensors capture loading the foot-shoe interface. Advantages and disadvantages of these systems are summarised in Table 2.4.1. Although pressure measurement is recommended by the IWGDF to guide offloading strategies [28], the cost, time requirements and technical expertise needed to operate these systems mean they are used predominately in research rather than routine clinical practice.

Table 2.4.1: *A summary of advantages and disadvantages of pressure measurement techniques including platform systems and in-shoe sensors [109], [110].*

Method	Advantages	Disadvantages
Platform systems	Can be used for static and dynamic analysis Easy to use since the platform itself is stationary	Altered gait due to steps needing to be aligned with plate Not easily portable Large space required
In-shoe sensors	Flexible Portable Direct measurement between foot and insole/shoe Representative of real pressures being subjected on the patient when walking	Spatial resolution limited due to the number of sensors

As highlighted in the previous subsection, plantar pressure alone is a poor indicator of DFU risk, and increasing attention has been directed toward the role of plantar shear stress. However, shear is considerably more challenging to measure. Recent developments have extended traditional pressure-based technologies to capture shear using magneto-resistors, piezoelectric transducers, strain gauges, capacitive sensors and optical fibre systems [95], [108]. Yavuz et al. developed a custom measurement platform consisting of 80 sensors (each with a sensing area of 1.27 x 1.27 cm) distributed to target the forefoot, meaning that the number of measurement points captured depends on the contact area of the foot [111], [112]. This corresponds to an approximate spatial sampling density of ~0.6 sensors/cm^2 across the forefoot region. Although this system demonstrated an increase in pressure and shear in patients with diabetes, limitations included spatial resolution, large device size and measurements restricted to barefoot conditions [111].

In-shoe shear measurement remains particularly difficult due to technical challenges, such as validation and calibration of such measurement systems [108]. Studies by Amemiya et al. and Lord and Hosein reported in-shoe measurement devices

incorporating shear-sensitive sensors embedded within insoles or attached directly to the plantar surface [113], [114]. Lord and Hosein incorporated three discrete sensors of 15.96 mm diameter positioned at the metatarsal heads and heel, providing only three measurement locations regardless of insole size and requiring multiple configurations of the insole to capture measurements across the entire forefoot [114]. This approximately equates to a spatial sampling density of ~0.5 sensors/cm^2, with only three discrete measurement points available per walk. These systems provide valuable insight into shear during gait but are constrained by the number of sensors, preventing full-surface mapping of plantar loads. Examples of these measurement techniques are demonstrated in Figure 2.4.1, highlighting the spatial resolution of these custom devices in contrast to alternative imaging-based approaches such as DIC. Unlike sensor-based systems, DIC allows the user to define the number of data points through software parameters, offering substantially higher spatial resolution. Further details on DIC are included in Section 2.5.

Despite ongoing innovation, there remains a lack of commercially available devices capable of capturing both pressure and shear in-shoe with sufficient resolution, portability and clinical practicality [108], [115]. As a result, most shear measurement technologies remain confined to research environments. Given that clinical risk screening still relies heavily on subjective assessment of medical history and physical examination (Section 2.3.4), there is a clear need for measurement techniques that are clinically feasible, cost-effective and capable of providing quantitative data relevant to DFU risk. Bridging the gap between research and clinically applicable technologies is therefore essential for improving the accuracy of risk identification and ultimately preventing DFU formation.

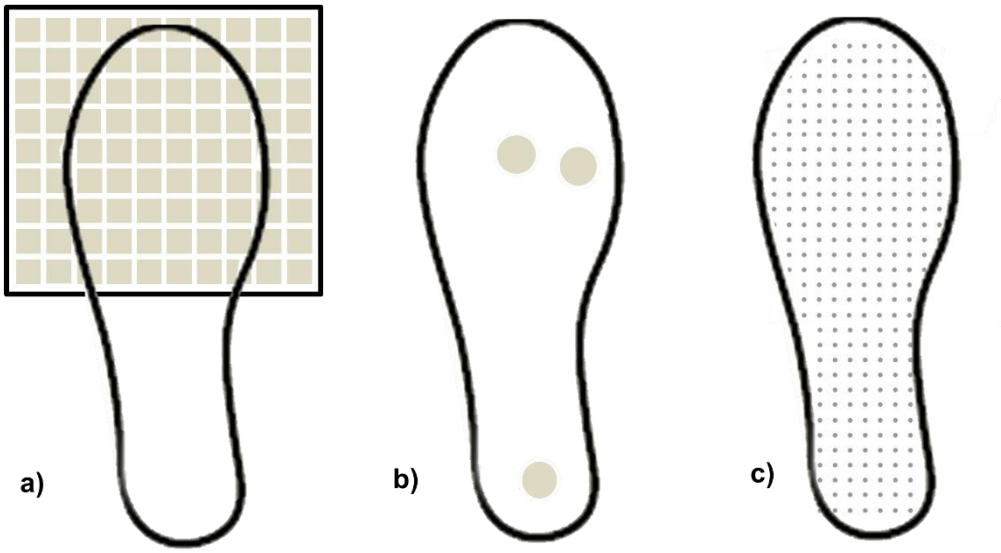


Figure 2.4.1: *Schematics of custom shear and pressure platforms a) and in-shoe sensors b), demonstrating spatial resolution in contrast to DIC [112], [114].*

2.4.3 The STAMPS System

Given the challenges of existing pressure and shear measurement technologies, strain has also been explored as an alternative way to represent combined plantar loading. In this context, strain describes the deformation of a surface under load and can be captured either instantaneously, using DIC to image the plantar surface during a single step [115], or cumulatively when deformation is captured across multiple steps in a deformable material [116]. Unlike sensor-based systems, strain-derived measures are not constrained by fixed sensor locations or sparse spatial sampling, offering the potential for high-resolution mapping of plantar load distribution across the entire foot.

Research at the University of Leeds has developed a novel strain-based measurement tool known as STAMPS [116]. The STAMPS tool uses a novel plastically deformable insole with a high-contrast speckle pattern, which undergoes permanent deformation during gait. DIC is then applied to pre- and post-loading images of the insoles to compute full-field strain maps across the entire plantar surface. The use of commercial DIC software (GOM Correlate) enables dense, user-defined spatial resolution, allowing detailed visualisation of strain patterns without the need of embedded sensors.

The STAMPS system offers several advantages over traditional pressure and shear devices. The plastically deformable insole is adaptable to the patient's foot shape, enabling personalised mapping of plantar loading. This approach is low-cost, requires minimal instrumentation and can be utilised in a wide range of research settings. Since strain reflects both pressure and shear, STAMPS has the potential to identify high-risk regions that may not be detected by pressure measurements alone. However, several limitations remain. The use of commercial DIC software introduces cost barriers that may restrict clinical use, and the system cannot capture real-time data due to the absence of embedded sensors. The plastically deformable material currently requires the use of a standardised wide boot rather than the patient's own footwear, and the 2D DIC approach captures strictly planar deformation, which may not fully represent the non-planar geometry of the foot.

Despite these limitations, feasibility studies have demonstrated the potential of STAMPS for characterising plantar loading. Initial research using 2D DIC has been validated across multiple studies, including a cohort of 18 healthy participants that established a range of 'normal' strain values [115], [116], [117]. These studies showed that STAMPS is sensitive to variations in plantar loading and capable of producing repeatable strain patterns. Importantly, earlier validation work demonstrated that the cumulative strain measured using DIC reflects the combined effect of normal pressure and tangential shear stress, with increased shear producing proportionally increased strain [116]. More recently, the system has been applied to a clinical cohort. Jones et al. reported that

participants with a recently healed DFU demonstrated elevated strain characteristics compared to a low-risk group [118], suggesting that strain-based measures may be capable of identifying individuals at increased risk of DFU.

By providing a high-resolution, clinically practical method for assessing plantar loading, STAMPS addresses key gaps in current measurement technologies. Its ability to capture integrated mechanical stresses, combined with its relative simplicity and adaptability, positions STAMPS as a promising tool for improving DFU risk identification and supporting future clinical pathways.

2.5 Digital Image Correlation

DIC is the core method used within the STAMPS system to quantify plantar strain. As such, this section introduces the principles of DIC and its application to plantar measurement.

2.5.1 The Fundamentals of DIC

DIC is a contact-free optical technique used to measure displacement and strain by analysing changes in images of a surface before and after deformation [119]. This method works by comparing a reference image with subsequent deformed images and tracking the movement of small, unique regions of the surface (known as subsets) across the image sequence. By quantifying how these subsets shift, DIC computes full-field displacement and strain maps across the material surface [115], [119].

DIC has been widely adopted across engineering and biomedical fields due to its versatility and ability to capture complex deformation patterns. Applications include aerospace and civil engineering, materials science, biomaterials and biomechanics, where DIC is used to evaluate the mechanical behaviour of components, structures and biological tissues under load [120]. The technique can be implemented in either two dimensions (2D DIC), which assumes a planar surface, or three dimensions (3D DIC), which uses stereo camera systems to capture out-of-plane deformation and is therefore suitable for curved or irregular geometries.

Successful implementation of DIC relies on several key factors, including the quality of the speckle pattern applied to the surface, the camera setup, lighting conditions and the overall imaging procedure. When these elements are optimised, DIC provides high-resolution, full-field strain measurements that are not achievable with traditional point-based sensors, making it particularly valuable for applications where spatial detail and non-contact measurement are essential.

2.5.2 Speckle Pattern Design and Application

During DIC analysis, displacement tracking is achieved by identifying and following small, unique regions across the surface of interest. To enable this, a speckle pattern is applied to the target surface prior to deformation. An effective speckle pattern should meet several criteria [121], [122]:

1. Stochasticity – the pattern should be random, ensuring each subset contains a unique set of speckles.
2. High contrast – sufficient variation in greyscale pixel intensity to allow robust correlation.
3. Isotropy – uniform appearance with no directional bias.
4. Adherence – the pattern must remain firmly attached to the surface and deform with it as a single body.

Since DIC relies on the ability to track these speckles accurately, the quality of the pattern directly influences the precision of displacement and strain measurements. As such, generating an appropriate speckle pattern is a critical preparatory step in the DIC workflow [122].

A variety of techniques can be used to create and achieve a high quality speckle pattern including, airbrushing, spray painting, compressed air methods and ink tattoo applications [122], [123]. Application parameters such as nozzle diameter, spray pressure and distance from the surface can be adjusted to control speckle size, density and distribution [123]. However, manual application methods may introduce inconsistencies, such as variation in speckle size or visible direction, which can compromise isotropy and reduce correlation accuracy.

To overcome these limitations, computationally generated speckle patterns have become favourable. These patterns can be rendered with user defined speckle size, density and randomness, ensuring optimal characteristics for the users intended application and setup. Once generated, the pattern can be printed and transferred to the sample surface using methods such as ink tattoo application, as implemented in the STAMPS study [116]. Open-source tools such as Correlated Solutions Speckle Generator and Glare provide accessible means of producing high-quality, customisable patterns [124]. Examples of speckle patterns with varying sizes and densities are shown in Figure 2.5.1.

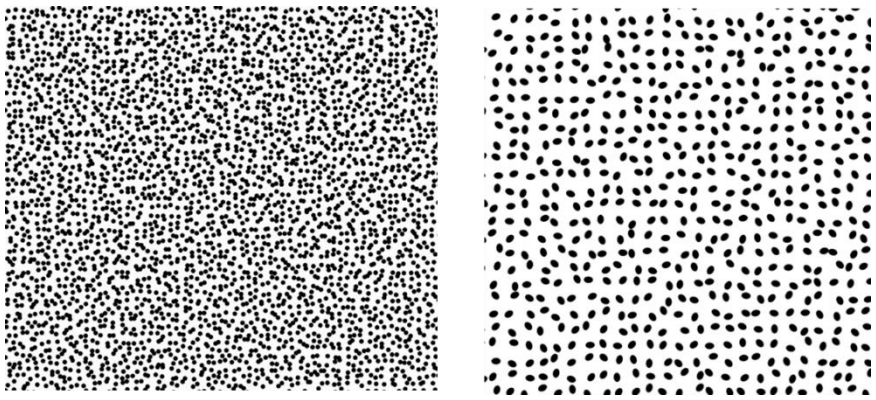


Figure 2.5.1: *Examples of speckle patterns used for DIC analysis, with differing characteristics such as size, density and variation.*

2.5.3 Camera Setup and Calibration

DIC can be implemented using either 2D or 3D configurations, each requiring different camera arrangements and calibration procedures [125]. In 2D DIC, images are captured using a single camera and deformation is calculated under the assumption that the surface is planar and that all motion occurs in-plane. In contrast, 3D DIC uses two or more synchronised cameras arranged in a stereo configuration to capture out-of-plane motion and reconstruct full 3D surface deformation [120], [125]. Depending on the experimental setup, images may be acquired either during deformation (dynamic testing) or before and after loading (quasi-static testing), resulting in multiple images from each camera.

For dynamic applications, synchronisation of stereo camera pairs is essential to ensure that images are captured simultaneously and to avoid errors caused by out-of-plane motion or timing discrepancies [125]. This requirement does not apply to 2D DIC, which relies on a single camera and is therefore simpler to implement, provided the surface remains flat and perpendicular to the camera throughout deformation.

Calibration is also necessary for both 2D and 3D methods, although the purpose and complexity differ. In 2D DIC, calibration is primarily used to scale the image and correct for lens distortion. In 3D DIC, calibration determines both the intrinsic and extrinsic parameters of the stereo system [126]. The intrinsic parameters describe the characteristics of each camera, including focal length, image centre and lens distortion. The extrinsic parameters define the spatial relationship between cameras, such as their relative positions, orientations and the stereo angle. Accurate calculation of these parameters is essential for reconstructing 3D coordinates and correcting positional errors, enabling precise measurement of out-of-plane deformation [120].

2.5.4 DIC procedure

Once an appropriate speckle pattern has been applied and adhered to the sample surface, DIC analysis can be performed. Images of the samples are captured in its undeformed state and again after deformation. Depending on the application, images may also be acquired during deformation, enabling dynamic tracking of displacement throughout loading. DIC then identifies and tracks small, unique regions of the speckle pattern between images to compute full-field displacement across the surface.

A key parameter is the subset size, which defines the number of speckles contained within each tracked region. Subsets must be large enough to be distinguished from other subsets, containing an adequate number of features for accurate matching of local regions [121], [127], [128]. The step-size determines the spacing between neighbouring data points and therefore controls the spatial resolution of the displacement and strain fields [126]. Each subset is associated with a single point, located at its centre, where the displacement is calculated. Adjacent subsets typically overlap because the step-size is smaller than the subset size, meaning the displacement grid is formed from a series of partially overlapping subsets. These parameters are illustrated schematically in Figure 2.5.2.

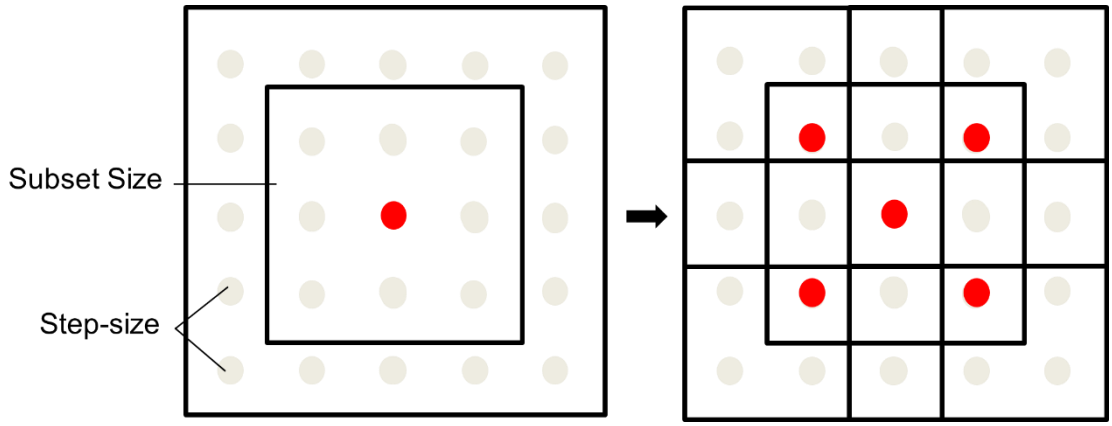


Figure 2.5.2: *Schematic representation of subset size and step-size during DIC analysis.*

Correlation begins with the placement of an initial ‘seed’ point, which is used to identify matching subsets between the undeformed and deformed images. A correlation coefficient quantifies the similarity between subsets, enabling the software to determine the most likely displacement vector for each data point [129]. Once the corresponding subsets have been identified and matched among the images, full-field displacement measurements are calculated (Figure 2.5.3).

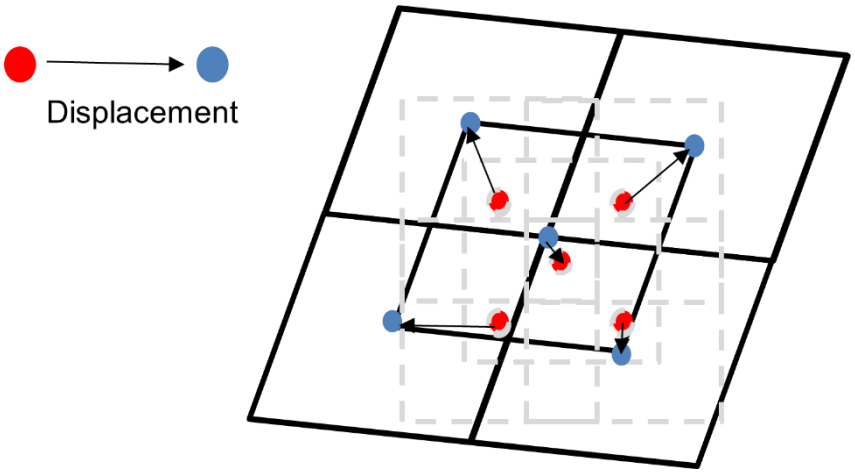


Figure 2.5.3: *Schematic of displacement calculation during DIC analysis.*

Strain is then derived from the displacement field. Although strain can be obtained mathematically by differentiating displacement, this approach is highly sensitive to noise, as differentiation amplifies small errors in the measurements [128], [130]. To mitigate this, displacement fields are often smoothed prior to differentiation [129]. However, smoothing introduces a trade-off. While it reduces noise, it can blur sharp strain gradients and reduce spatial resolution, potentially masking localised features of interest.

A number of alternative strain estimation methods are reported in the literature, to balance noise reduction with spatial fidelity. This includes the implementation of finite-element-based methods, both alone and in combination with generalised cross-validation algorithms as well as local least-square fitting methods [129], [131], [132], [133]. The latter uses a user-defined strain window, within which a least-squares approximation of the displacement field is computed to filter noise and produce more stable strain estimates [120], [129], [134]. Figure 2.5.4 illustrates how the strain window defines the defines the displacement date used for this fitting process.

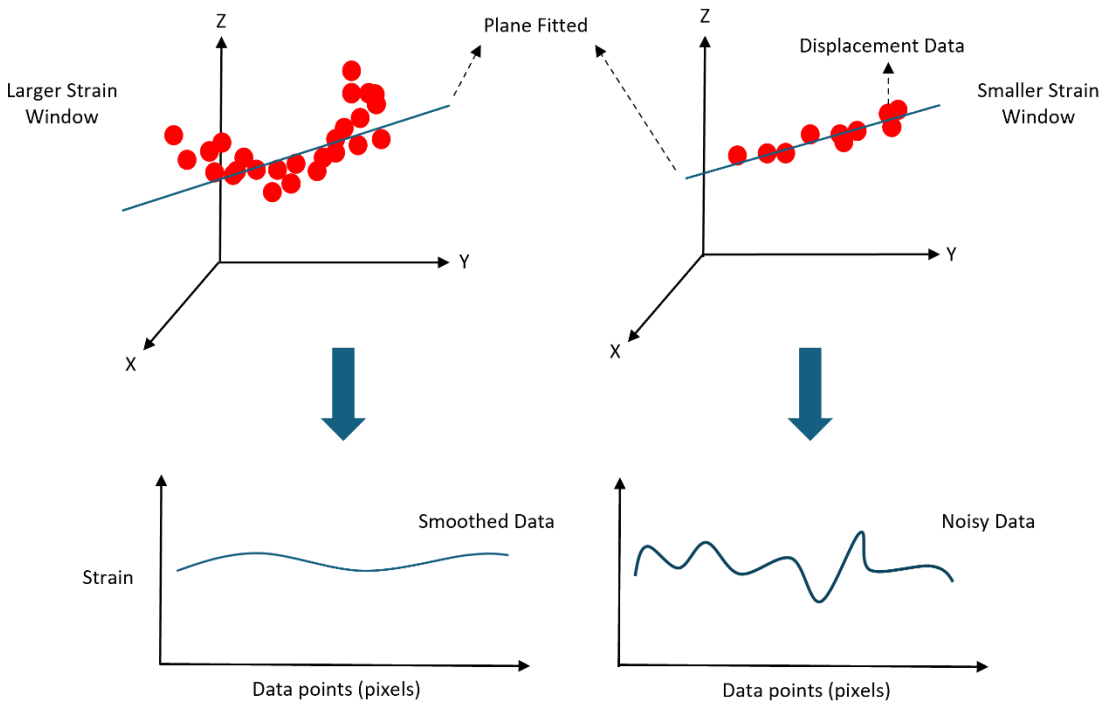


Figure 2.5.4: *Illustration of a strain window used for local least-squares strain estimation in DIC post-processing.*

2.5.5 DIC Software Packages

A wide range of commercial and open-source DIC software packages are available for evaluating 2D and 3D deformation. Table 2.5.1 summarises commonly used packages and their capabilities. Commercial software typically offers high computational performance, robust algorithms and integrated quality-control features, reflecting substantial financial investment in development. However, these packages are often costly and may be inaccessible in low-resource research environments. In addition, the underlying algorithms are usually proprietary limiting transparency and user understanding of the correlation process [134], [135].

In contrast, open-source DIC software provides free access to correlation tools developed within the research community. These packages are highly adaptable, often supported by active user forums and allow researchers to inspect or modify underlying algorithms [135]. This transparency can be advantageous for tailoring DIC parameters to specific applications. However, some open-source tools require additional licences for programming environments such as MATLAB or Python [136] and computational performance may be lower than that of commercial alternatives.

The choice between 2D and 3D DIC software is also influenced by cost and experimental requirements. Since 2D DIC only requires a single camera, it is considerably more

affordable than 3D DIC, which requires stereo or multi-camera setups [121]. Nevertheless, 3D DIC offers important advantages for biomechanical applications, with it capturing both planar and non-planar deformation and enables strain visualisation in axes corresponding to pressure and shear components of plantar load.

Among open-source packages, several support both 2D and 3D analysis, including DICe, YADICS, iCorrVision-3D, DuoDIC and MultiDIC. DuoDIC and MultiDIC extend the 2D MATLAB-based platform Ncorr to enable 3D reconstruction, with MultiDIC designed specifically for multi-camera stereo setups [137], [138].

Table 2.5.1: *Summary of available DIC software packages [134], [135], [136]*.

DIC Software	***Commercial/Open-source***	***2D/3D Capabilities***
Correlated solutions [139]	Commercial	2D, 3D
GOM [140]	Commercial	2D, 3D
MatchID [141]	Commercial	2D, 3D
LaVision [142]	Commercial	2D, 3D
CorreliSTC [143]	Commercial	3D
Dantec Dynamics [144]	Commercial	2D/3D
Image systems [145]	Commercial	2D/3D
DICe [146]	Open-source	2D/3D
py2DIC [147]	Open-source	2D
μDIC [148]	Open-source	2D
RealPi2dDIC [149]	Open-source	2D
ADIC2D [150]	Open-source	2D
YADICS [151]	Open-source	2D/3D
ALDIC [152]	Open-source	2D
iCorrVision-2D [134]	Open-source	2D
iCorrVision-3D [153]	Open-source	3D
Ncorr [130]	Open-source	2D
DuoDIC [137]	Open-source	3D
MultiDIC [138]	Open-source	3D

Open-Source Software: Ncorr and Its Extensions

Ncorr has been widely adopted as an open-source alternative to commercial software such as Correlated Solutions and LaVision [135]. It includes features such as a user-defined strain radius, enabling control over the strain window used for smoothing displacement fields. However, concerns have been raised regarding its computational efficiency, particularly for large datasets. Lunt et al. reported that Ncorr was 10-20 times slower than commercial software, with processing times of approximately 25 minutes compared to under 4 minutes for Correlated Solutions and LaVision [135]. Multithreading options within Ncorr can partially mitigate this limitation by utilising multiple processor cores [130].

Comparative studies have also examined accuracy differences between commercial and open-source software. Jorge et al. reported that commercial packages such as GOM produced lower strain errors and shorter computational processing times than open-source alternative, with maximum strain errors of 9.55% for GOM compared with 12.81% for Ncorr and 16.76% for DICe [154]. These discrepancies have been attributed to proprietary optimisation of subset shapes, integrated speckle-quality assessment tools and interface features that are typically supported by greater financial investment in commercial development [155]. Even so, open-source tools remain viable options due to their accessibility, transparency and adaptability.

Although commercial software often achieves lower error magnitudes, Ncorr has demonstrated acceptable strain accuracy for many experimental applications. Validation studies using simulated images and the SEM 2D DIC challenge reported strain errors on the order of 10^{-13} [130]. Experimental comparisons have shown Young's Modulus values within 5% of strain-gauge measurements [156] and strain differences of 4.7% relative to experimental outputs [157]. Overall, these findings indicate that Ncorr provides a flexible, transparent and cost-effective option for 2D DIC analysis.

3D DIC Software and Emerging Approaches

Although the number of 3D DIC packages is increasing, open-source options remain limited. DuoDIC and MultiDIC extend Ncorr's algorithm to 3D by incorporating stereo reconstruction. DuoDIC supports dual-camera setups, whereas MultiDIC accommodates multiple stereo pairs and offers flexibility in camera positioning without substantially increasing calibration time [138]. Verification tests reported displacement errors on the order of 10^{-3} for DuoDIC and 10^{-2} for MultiDIC, with strain errors for DuoDIC on the order of 10^{-4} [137], [138].

Challenges associated with multi-camera systems include complex calibration procedures and the need to merge data from multiple stereo pairs [138]. To reduce

equipment costs, several single-camera 3D DIC techniques have been proposed, using optical components such as bi-prisms, mirrors or fibre bundles to generate stereo image pairs [125], [158], [159].

Comparative studies of 3D open-source software remain limited. Pisonero et al. reported no statistically significant differences in mechanical properties calculated using MultiDIC compared with Ncorr, suggesting that MultiDIC provides comparable accuracy while enabling 3D measurement [160]. Given the shared algorithmic foundation between Ncorr, DuoDIC and MultiDIC, similar accuracy may be expected across these tools. For applications requiring non-planar deformation measurement at lower cost, DuoDIC may offer a practical compromise between 2D affordability and 3D capability.

iCorrVision-3D provides an alternative Python-based open-source platform structured into modules for image acquisition, calibration, correlation and post-processing. Reported errors include a relative error of 0.0012% when measuring cylinder diameter and close agreement with the commercial software MatchID [153]. However, the extensive parameter selection required during correlation may increase setup time compared with Ncorr-based tools.

Interpreting these error values requires consideration of the intended application, as there is no universally defined threshold for acceptable DIC error in clinical or biomechanical contexts. Rather than absolute accuracy, the key requirement is that measurement uncertainty remains small relative to the deformation magnitudes and spatial patterns of interest. For applications such as identifying regions of elevated plantar strain or comparing offloading interventions, strain errors in the range reported for open-source tools may be sufficient to detect clinically meaningful differences, even if they are higher than those achieved by commercial systems. Consequently, the suitability of a given DIC package depends not only on its error magnitude but also on its ability to provide consistent, interpretable outputs within the constraints of the intended experimental or clinical environment.

2.5.6 Parameter Selection and Validation Approaches

A crucial element of DIC analysis is the selection of appropriate DIC parameters including subset size and step-size and, for certain software packages, the strain radius. Although the literature offers varied recommendations, there are broad agreement that small to moderate parameter values generally provide a good balance between accuracy, precision and computational efficiency [161]. It is also important to note that optimal parameter choices can be software-specific: different DIC packages use different correlation algorithms, subset shapes and interpolation schemes, meaning that settings optimised for one software may not necessarily transfer to another.

The choice of subset size has a direct influence on correlation quality, spatial resolution and computational cost. Larger subsets generally improve correlation precision but increase processing time and may introduce error if they span regions with heterogeneous deformation [121]. Conversely, smaller subsets enhance spatial resolution and reduce smoothing but may contain too few features for reliable matching, leading to increased strain error [127], [162]. This occurs as subsets with insufficient speckle detail are more difficult to track accurately between images [121]. The DIC good practice guidelines further note that when speckle features fall within the optimal 3-5 pixel size range and the feature density is approximately 50%, subsets of around 15 x 15 pixels are typically required. However, larger features or less dense patterns would require increasing the subset size to ensure reliable correlation [126].

The step-size directly influences the density of displacement data and the spatial resolution of the resulting strain fields. Together with the subset size, it determines the spacing of subsets and the degree of overlap between adjacent subsets [163]. When the step size is smaller than the subset size, subsets overlap, increasing the number of data points and allowing measurements closer to the edges of the region of interest [161]. This improves spatial resolution but increases the associated computational load. The DIC Good practices guidelines recommend selecting a step-size between one-third and one-half of the subset size to ensure partial overlap and stable correlation [126]. The pixel resolution of the acquired images also influences achievable spatial resolution and measurement accuracy [127].

For software such as Ncorr, the strain radius (or strain window) is an additional parameter that controls the number of displacement points included in the local least-squares fitting used to compute strain. The Ncorr manual advises selecting the smallest radius that avoids visibly noisy strain fields [130], although this approach is subjective. The optimal strain radius depends on the deformation behaviour: larger radii are suitable for homogeneous deformation, whereas smaller radii are preferable for heterogeneous deformation to avoid excessive smoothing [128], [129, p. 200]. An oversized strain radius can over-smooth strain gradients by fitting a linear plane across too many displacement points, while a radius that is too small increases noise by relying on too few points [131]. In practice, the strain radius defines the neighbourhood of displacement data used for the local approximation, and its selection directly influences the balance between noise reduction and spatial fidelity. Although parameters are defined in pixel units, they can be converted to physical dimensions using the calibration scale.

Overall, the literature reflects a wide range of opinions on optimal DIC parameter selection, influenced by speckle quality, deformation characteristics, image resolution and software capabilities.

2.5.7 Barriers to Clinical Translation of the STAMPS System

Although the STAMPS system has demonstrated strong potential for quantifying plantar deformation, several barriers currently limit its translation from research environments into clinical practice. A major challenge relates to **practical implementation**. Traditional DIC setups often require controlled lighting, stable camera positioning, calibration procedures and high-quality speckle patterns, all of which are difficult to achieve consistently in busy clinical settings. Even simplified 2D systems can be sensitive to patient movement, variable footwear, and inconsistent surface preparation, reducing the reliability of measurements outside laboratory conditions.

A further barrier concerns computational and workflow demands. DIC typically involves substantial post-processing, parameter optimisation and data interpretation, which require technical expertise not routinely available in clinical teams. Processing times can be lengthy, particularly for open-source software, and the need for manual parameter tuning (e.g., subset size, step size, strain radius) limits the feasibility of rapid, point-of-care assessments.

There are also challenges related to clinical relevance and validation. While DIC can quantify detailed displacement and strain fields, these outputs do not yet map directly onto established clinical risk metrics for diabetic foot ulceration. The absence of validated thresholds, standardised protocols and evidence linking DIC-derived strain measures to ulcer outcomes restricts its adoption. Additionally, most existing studies have been conducted in controlled research settings, with limited evaluation of DIC performance in real-world clinical workflows.

Finally, cost and equipment burden remain obstacles. Although open-source software reduces financial barriers, multi-camera 3D systems, high-resolution imaging equipment and calibration tools can still be prohibitively expensive or impractical for routine clinical use.

Together, these barriers highlight the need for measurement approaches that are robust to clinical variability, computationally efficient, easy to implement and capable of producing clinically interpretable outputs. This motivates the exploration of simplified, open-source 2D and 3D DIC methods tailored for clinical translation.

2.6 Chapter Summary

Diabetic foot ulceration arises from the complex interaction of systemic, vascular, neurological and biomechanical factors, yet current clinical approaches rely heavily on subjective assessment and simple bedside tests. While routine screening, patient self-management and multidisciplinary care form the foundation of DFU prevention, these strategies do not quantify the mechanical loading patterns that drive tissue breakdown. Evidence increasingly shows that both plantar pressure and shear contribute to DFU formation, but existing measurement technologies are limited. Pressure systems are most commonly used but overlook shear, whereas shear-capable devices remain confined to research settings due to cost, complexity and poor clinical practicality.

Strain-based approaches offer a promising alternative to sensor-based systems by capturing the combined effects of pressure and shear. The STAMPS system demonstrates the feasibility of using DIC to generate high-resolution strain maps across the plantar surface, but its reliance on commercial software and controlled laboratory conditions restricts wider adoption. Although open-source DIC tools such as Ncorr and DuoDIC provide accessible alternatives, their clinical applicability remains constrained by workflow demands, parameter sensitivity and the absence of validated clinical thresholds.

In conclusion, the literature highlights a clear gap: there is currently no clinically practical, affordable and high-resolution method for quantifying plantar strain in a way that supports DFU risk identification. This gap motivates the work presented in the following chapters, which explore the development and evaluation of open-source 3D DIC-based approaches tailored for clinical translation.

Chapter 3

Parameter Selection for Digital Image Correlation

This chapter consists of initial work undertaken to explore alternative 2D DIC software frameworks and to develop objective methods for the selection of appropriate DIC parameters. Some of the described work was presented at the 2023 STLE Tribological Conference (California, USA), see Appendix A.1 for the corresponding poster.

In Chapter 2, the literature review highlighted that the process for determining DIC parameters can often be subjective, with users required to balance parameter size while considering spatial resolution, subset distinguishability, computational load, and noise/smoothing effects. Since these choices can introduce variation in the estimated strain outputs, in addition to different DIC software packages offer varying parameter options/settings, particularly between those that are commercial or open source, a systematic and transferrable approach for assessing parameter performance is necessary.

Within the context of this project, establishing such an approach has clinical relevance with objective parameter selection enabling a set of suitable DIC parameters to be determined. These can then be given to clinicians, streamlining clinical workflows and improving the accuracy of strain-based screening of risk for DFU formation. This chapter therefore develops computational and experimental approaches to quantify the influence of DIC parameters on the accuracy of strain measurements and computational load, addressing Objective 1 of this project (development of open-source 2D DIC workflow).

3.1 Introduction

DIC is widely used to quantify deformation and strain, however its accuracy depends heavily on the selection of several interdependent parameters. Subset radius, subset spacing (commonly referred to as ‘step-size’ in the DIC literature, as described in Section 2.5) and strain radius each influence noise, smoothing, spatial resolution and computational time, but the literature provides limited objective guidance on how to select these parameters for a given application. This results in the DIC process relying on

subjective judgement or software defaults, which can introduce error into strain measurements.

For applications such as strain-based screening for DFU risk, the reliability of the measured strain fields is critical, where inconsistent parameter choices could undermine the clinical utility of the method. Ensuring robust and reproducible DIC settings is therefore essential for future translation of STAMPS, where a streamlined workflow should minimise the need for users to manually tune parameters.

This chapter therefore aims to develop an objective, reproducible method for selecting DIC parameters appropriate for the speckle pattern, camera setup and deformation characteristics relevant to this project. Computational and experimental methods are used to quantify the effect of parameter choices on strain error and computational load, providing a basis for parameter selection and supporting the translational potential of DIC in clinical settings.

3.2 Methodology

3.2.1 DIC Software Selection

The selection of a DIC software was based on the following set of requirements, which reflect the needs of this project:

1. Open-source framework: Enabling future integration within a semi-automated tool-chain, transparency of DIC calculations and full control over parameter settings.
2. Extensibility: Compatibility with 3D DIC workflows, supporting future work on the applicability to non-planar surfaces.
3. Interoperability: Ability to export displacement and strain field data for post-processing and integration with MATLAB-based analysis.

As outlined in the literature review (Section 2.5.5), several commercial and open-source DIC tools are available, each offering different trade-offs in accuracy, usability and flexibility. These requirements were based on the limitations of commercial software such as GOM Correlate, primarily due to its ‘black box’ nature, lack of high-fidelity export of strain fields and inability to be easily placed within an automated software tool-chain as a result.

Among open-source alternatives, iCorrVision-2D and its 3D extensions represent a viable Python-based option, offering transparency and extensibility [134]. However, although a user manual is available, the documentation focuses primarily on describing the parameters rather than guiding their selection, making it difficult to determine the appropriate correlation settings in practice. This increases the risk of inconsistent

analysis and makes it less suitable for iterative parameter selection work. Its Python-based environment also limits interoperability with MATLAB, reducing its suitability for a workflow that relies heavily on MATLAB-based post-processing.

Ncorr, an open-source MATLAB-based 2D DIC package, met these requirements. Its MATLAB integration directly satisfies the interoperability requirement, enabling seamless post-processing, early visualisation and incorporation into the wider STAMPS tool-chain. Figure 3.2.1 illustrates the STAMPS tool-chain, outlining the complete workflow from insole fabrication through to quantitative strain outputs. The process begins with preparation of the plastically deformable insole and application of the speckle pattern, completed at least 24 hours before use. Data capture starts with acquisition of a pre-deformation image, followed by a controlled walking trial and subsequent post-deformation imaging. These images are processed using DIC to generate displacement and strain fields, which are then imported into MATLAB for masking, strain-map generation and extraction of quantitative metrics using a custom post-processing script. This workflow underpins both the 2D and 3D STAMPS systems and provides the structure within which the MATLAB post-processing pipeline operates. Ncorr's open-source structure provides full transparency of the DIC calculations and complete control over parameter settings, addressing the need for methodological clarity during parameter optimisation. Although Ncorr is not the highest accuracy option reported in the literature, its performance is consistent with other open-source tools and within the error ranges reported across validation studies. Jorge et al addressed this, comparing the errors of GOM and Ncorr, finding maximum strain errors of 9.55% and 12.81% respectively [154]. Other studies reported errors between DIC and experimental outputs of up to 5%, with the authors finding errors on the order of 10^{-13} when carrying out validation [130], [156]. Crucially, Ncorr's documentation, community support and compatibility with DuoDIC (its 3D extension) satisfy the extensibility requirement, enable a coherent transition to 3D DIC workflows explored in Chapter 4.

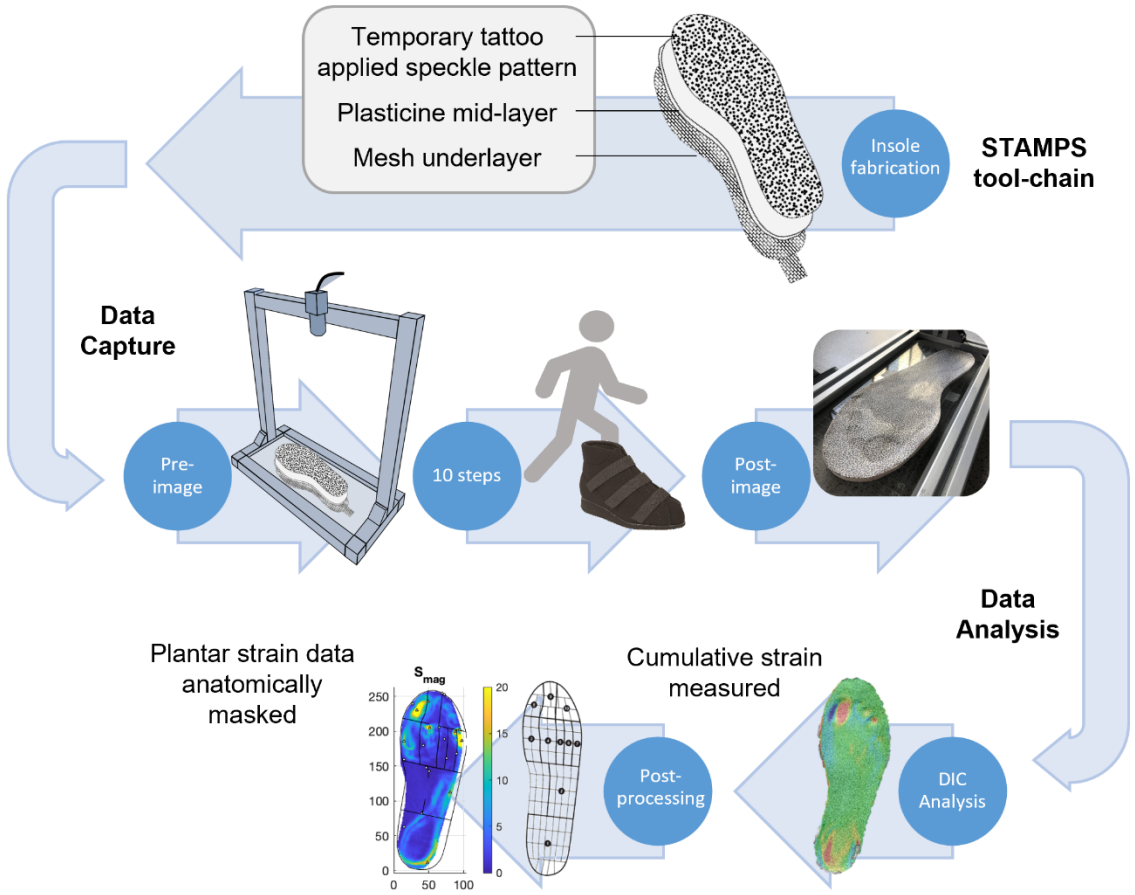


Figure 3.2.1: *Overview of the wider STAMPS tool-chain, illustrating the full workflow from insole fabrication to anatomically masked quantitative strain outputs.*

3.2.2 Examination of DIC Parameters

Three parameters were examined, each described in more detail in the literature review (Section 2.5.4):

- Subset radius: the size of the subsets that are used to distinguish regions of a speckle pattern.
- Subset spacing: the distance between data points placed across an image, in which displacement measurements are taken.
- Strain radius: the size of the subsets in which the local region of displacement measurements is included in a local least-square fitting approximation, interpreted as a linear plane.

Each of these parameters directly influence spatial resolution, noise and smoothing behaviour, with chosen parameter values also being interconnected with speckle pattern and camera setup. Their effects were quantified using both computational and experimental approaches, with 2D DIC analysis performed in Ncorr for all the parameter combinations tests. By comparing DIC derived strain fields against a ground-truth, in

which the strain profile is known, the influences of each parameter on measurement error could be systematically assessed.

3.2.3 Methods Development

Preliminary work explored several approaches for identifying suitable DIC parameters. Initial iterations involved adjusting parameter combinations using pre-existing insole images and visually assessing dropout in the resulting strain maps. This was followed by a second approach using locally applied numerical transformations to replicate deformation of an insole after a person has worn the insole and test parameter sensitivity under controlled conditions. However, a key limitation of this approach was a lack of a known strain for the transformation applied, limiting its ability to objectively evaluate parameter performance. These exploratory stages highlighted the need for a more rigorous and quantifiable approach, which informed the development of computational methods described in the next section.

3.2.4 Final Methods

A final set of computational and experimental methods were established to assess the suitability of DIC parameters. The respective effects on strain output for a set of DIC parameter combinations for each method were compared and used to determine the final DIC parameters.

DIC parameters were refined during preliminary computational tests (Table 3.2.1), based on a comparison between measured and expected strain. These parameters were chosen to act as a starting point for the final computational and experimental tests.

Table 3.2.1: *Initial sample of DIC parameters testing using computational and experimental methods.*

DIC Parameter	Parameter Value (pixel)
Subset Radius	13, 15, 17, 19
Subset Spacing	1, 2, 3, 4
Strain Radius	5, 10, 15

Final parameter selection followed an iterative evaluation process. Parameter combinations were assessed using criteria including strain error, spatial resolution, computational load and alignment with DIC parameter recommendations in the literature. These criteria were applied consistently across the computational methods, experimental methods and computational load assessment described below, allowing

identification of parameter values that performed reliably across deformation ranges and were suitable for clinical workflows.

Computational Methods

Computational benchmarking was performed using the open-source software Glare, which can generate defined speckle patterns and apply both linear and non-linear numerical transformations. The speckle pattern was matched to that used on the STAMPS insoles (density = 65%, variation = 75%, and size = 0.8mm / 4.5 pixels).

A non-linear transformation was chosen to replicate deformation profile of an insole, defined by Equation (1). When plotted, the function produces a 'bell-shaped' curve with a peak strain of a = 0.5 (50% strain), which was used as the 'benchmark' for parameter iterations. Strain magnitudes were chosen to match those representative of plantar strains reported in the STAMPS study, which ranged between 2-59% [116]. Therefore, speckle patterns were generated with peak strains ranging from 5-50% in 5% increments, corresponding to a = 0.05 to 0.5.

$$\varepsilon_{xx} = aexp(-\frac{(x-x_0)^2}{c^2}), \text{ where } a = 0.5,\ x_0 = 150 \text{ and } c = 20. \quad (1)$$

Once the DIC analysis were performed for each of the parameter combinations, peak and root-mean-squared (RMS) errors were calculated relative to the computational benchmark. This was to quantify the deviation between the DIC derived and benchmark strain profiles. Peak error was calculated by taking the absolute difference between the measured and expected strain. Figure 3.2.2 illustrates this, where the black line represents the 'benchmark' and the red line represents a DIC output for a fixed DIC parameter combination, corresponding to a row of data containing the peak strain in the strain map.

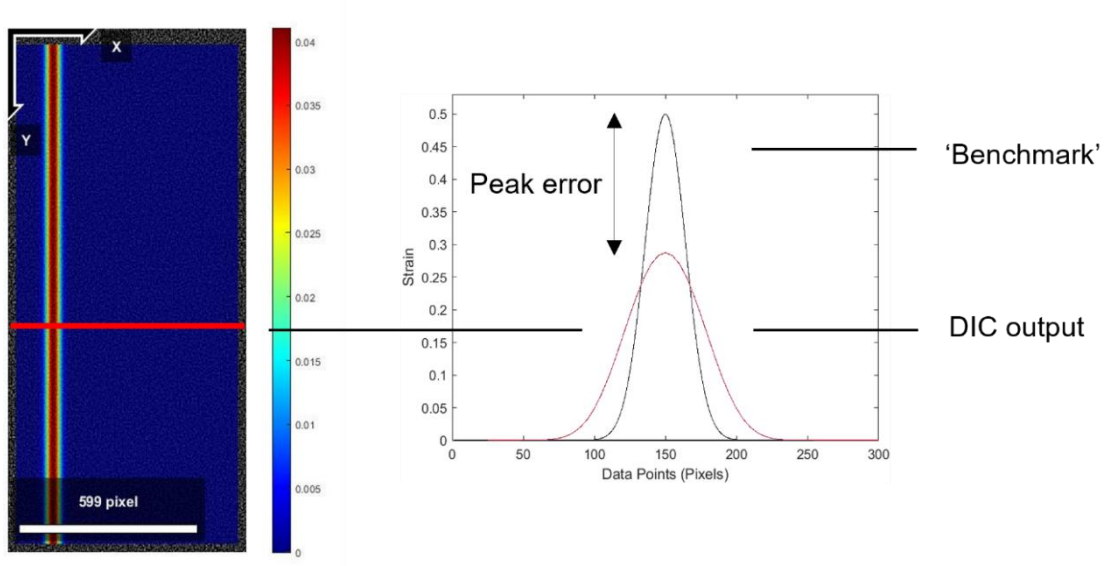


Figure 3.2.2: *Strain map for a fixed set of DIC parameters with row of data including peak strain highlighted in red (left). Computational 'benchmark' (black) aligned with a DIC output corresponding to a fixed set of DIC parameters (red), used to calculated peak and RMS error (right).*

Experimental Methods

To complement the computational work, experimental validation was performed using silicone samples. A commercial white silicone sheet of 2 mm thickness was used. As the aim of this experiment was to assess DIC measurement behaviour rather than material properties, a generic silicone with uniform elastic deformation and good optical contrast was sufficient. The silicone sheet was cut into samples with dimensions 20 x 100 mm such that there was a sufficient surface for speckle tracking. Temporary tattoo sheets were used to coat the silicone samples, matching the speckle pattern used in the computational methods and STAMPS fabrication procedure. Samples were strained from 5-50% in 5% increments using an Instron. As only pre- and post-deformation images were required for DIC analysis, no continuous loading rate was specified. As such, the sample was held briefly at each target strain while images were acquired. A custom camera rig was designed with a single camera positioned planar to the sample surface, matching the setup of the camera rig used in the STAMPS study (see Chapter 4, Section 4.2 for full setup description).

The same DIC parameter combinations were tested. For each combination, the magnitude of error across the region of interest (ROI) was computed, with the mean and standard deviation used to characterise accuracy and variability across repeats. A 10 mm central ROI was selected to ensure analysis of the most uniform region of the specimen, as edge effects and sample geometry produced non-uniform deformation near the

boundaries. The number of strain measurements is relative to the size of the ROI and selected subset spacing. See Figure 3.2.3 for the speckled silicone samples and Instron setup.

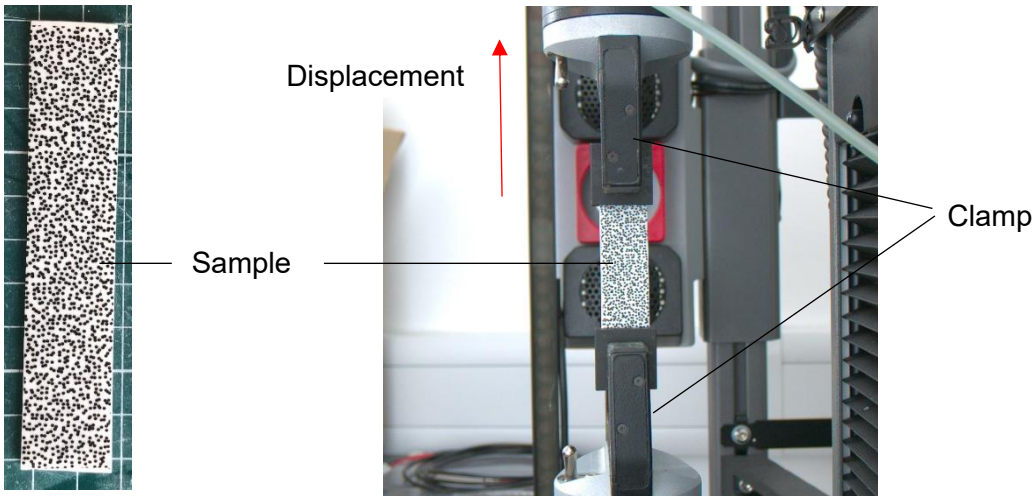


Figure 3.2.3: *Silicone samples with applied speckle pattern (left). Speckled sample set up in Instron clamps (right).*

Computational Load Assessment

The computational time for DIC analysis to be performed was also considered to see the effect of the DIC parameters on the time taken to perform an analysis. The computational time was outputted automatically in the MATLAB window once seed placement and DIC analysis steps were completed within the software. These were averaged across three trials for each parameter combination. For this, subset radius = 10, 20, 30 and subset spacing = 3, 6, 9 were chosen to show their effects on computational time across a larger range of values than used for the parameter iterations of both the computational and experimental components of work. Note that the effect of strain radius on the computational time was not included as this was unaffected by changing this parameter.

Once the final parameter combination was determined, pre-existing data from the case study portion of the 2D STAMPS publication [116], were re-analysed in Ncorr to ensure consistency with the optimised DIC workflow. These data had previously been processed in GOM Correlate using different parameters. Significance was defined as $p < 0.05$ using paired t-tests to assess whether the regional strain values obtained from the Ncorr re-analysis differed significantly from the original GOM outputs.

3.3 Results

Computational Results

For the computational analysis, four plots were generated for each subset radius (13, 15, 17, 19), reporting peak error and RMS error across all combinations of subset spacing and strain radius. This was repeated for each of the strains from 5-50%. A representative strain map for a single parameter combination is presented in Figure 3.3.1. Representative results for 5% and 50% strain, corresponding to low and high plantar strain, for peak error and RMS error are also shown in Figure 3.3.2 and Figure 3.3.3 respectively, with other cases provided in Appendix A.2.

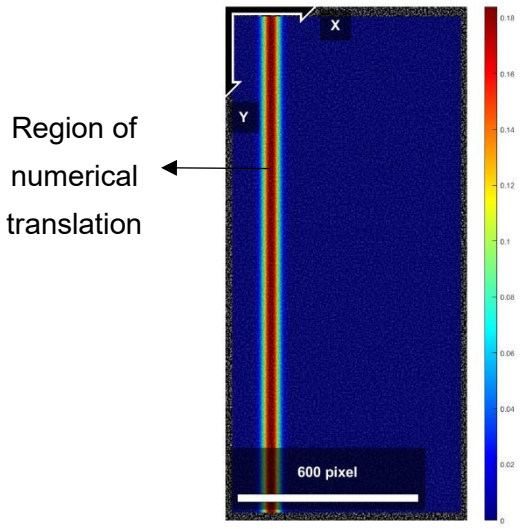


Figure 3.3.1: *Representative strain map for a single parameter combination (subset radius, subset spacing, strain radius) = (13, 1, 5) at 5% strain.*

Across all strain levels tested, the same general pattern was observed. Peak error and RMS error increased with increasing strain radius and increased further as subset spacing was increased. This pattern was consistent across subset radii and was also evident for intermediate strain levels (10–45%), where a gradual increase in overall error magnitude was found as strain increased.

Figure 3.3.2 illustrates this behaviour for peak error. For clarify, parameter combinations are denoted as (subset radius, subset spacing, strain radius). At 5% strain, peak error values were similar across subset radii, ranging from approximately 0.005 for (13, 1, 5) to 0.031 for (19, 4, 15). At 50% strain, the same trend was present but with substantially larger magnitudes. Several parameter combinations deviated from the expected pattern, including (13, 1, 5), (15, 2, 5), (15, 4, 10) and (15, 4, 15), with the greatest inconsistencies occurring for subset radius = 15. The lowest peak error at 50% strain was 0.002 for (15, 2, 5), while the highest was 0.400 for (15, 4, 15).

A similar relationship is shown for RMS error in Figure 3.3.3. At 5% strain, RMS error ranged from 0.001 for (13, 1, 5) to 0.006 for (19, 4, 15). At 50% strain, the same pattern persisted, although it was less pronounced for strain radius = 5, where RMS error values were slightly higher than expected. The lowest RMS error at 50% strain was 0.011 for (13, 2, 5), and the highest was 0.056 for (19, 4, 15).

Although the lowest and highest values are presented here, Figure 3.3.2 and Figure 3.3.3 show that several parameter combinations produced similar levels of error, particularly at lower strain levels.

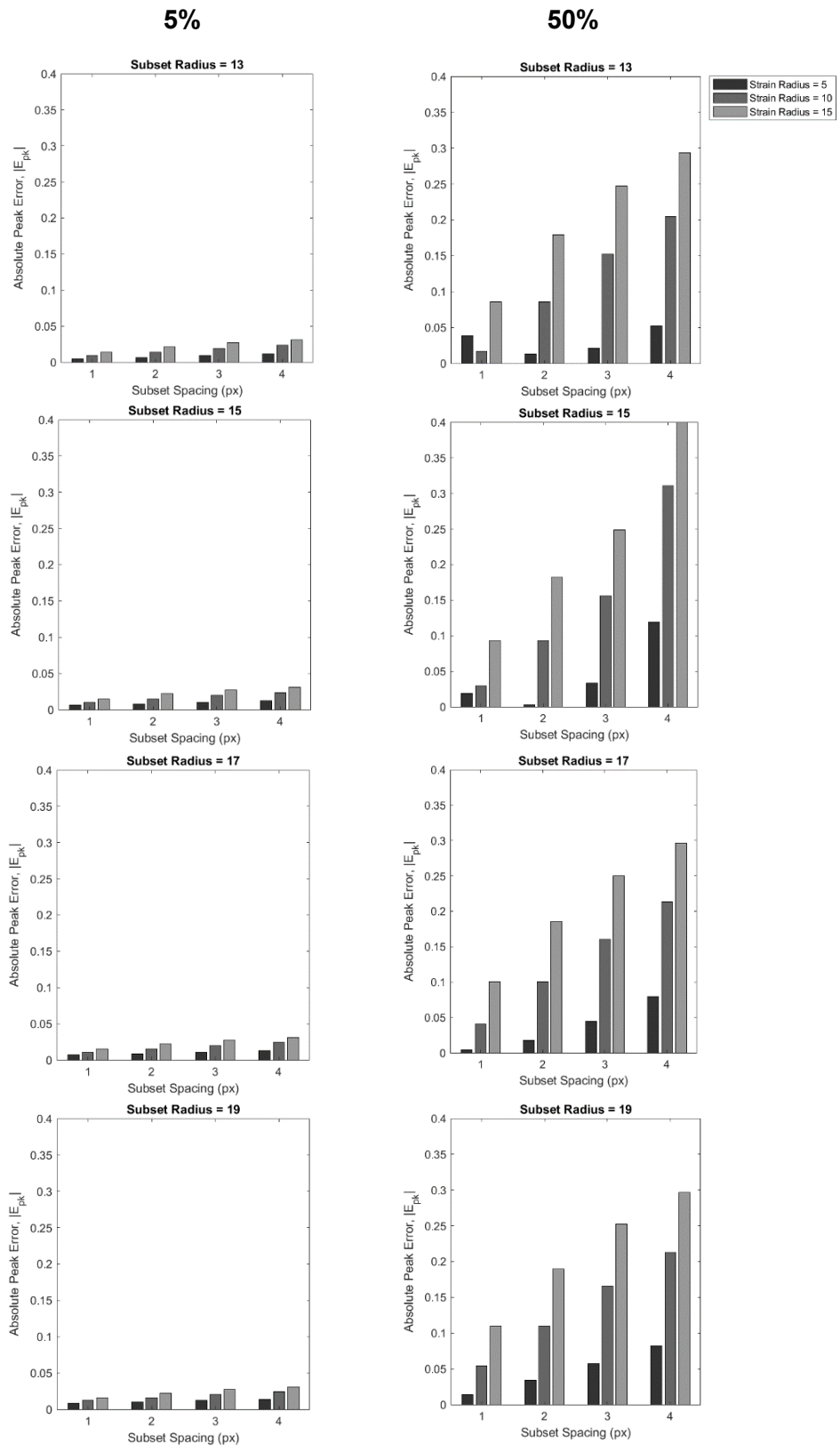


Figure 3.3.2: *Magnitude of peak error corresponding to computational strain of 5% (left column) and 50% (right column) for different DIC parameter combinations, involving subset radius, subset spacing and strain radius.*

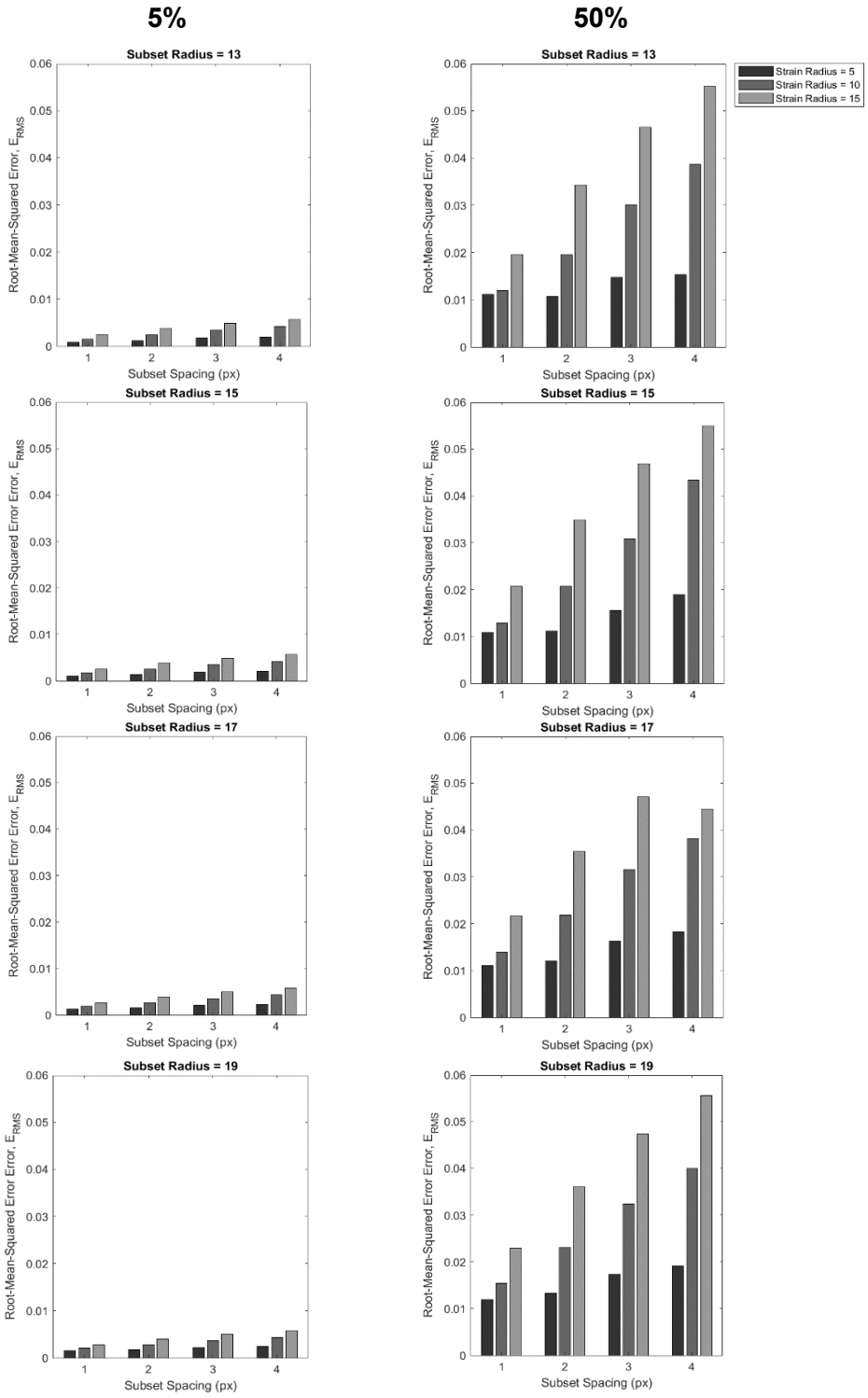


Figure 3.3.3: *Root-mean-squared error corresponding to computational strain of 5% (left column) and 50% (right column) for different DIC parameter combinations, involving subset radius, subset spacing and strain radius.*

Experimental Results

For the experimental analysis, four average error plots were generated for each strain from 5-40%. Representative strain maps and error plots for 5 and 40% strain are shown in Figure 3.3.4 and Figure 3.3.5. Note that only strains up to 40% are reported due to tracking issues that prevented successful DIC analysis at 50%.

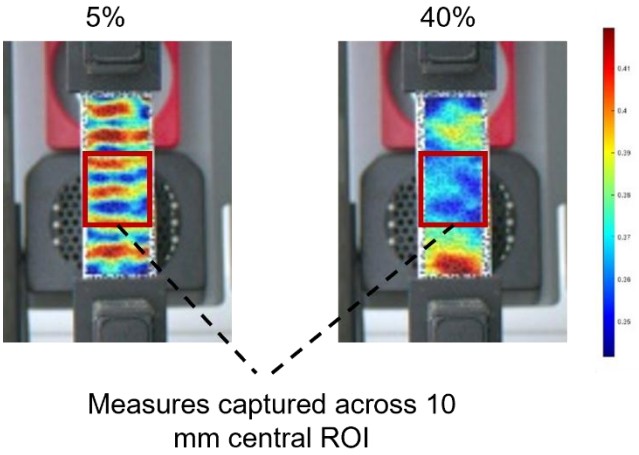


Figure 3.3.4: *Representative strain maps for 5 and 40% strain with the parameters (15, 1, 5). A smaller 10 mm ROI is highlighted in which average peak strain error was calculated.*

At 5% strain, the peak strain error was small in magnitude and the pattern across parameter combinations was more variable (Figure 3.3.5). At this low deformation level, the true strain is small relative to measurement noise, so differences between subset spacing and strain radius are less consistent. Errors ranged from approximately 0.001 to 0.012 across the combinations tested. In contrast, at 40% strain, the overall magnitude of error increased (approximately 0.016 to 0.023), but the pattern across parameters became more consistent, with peak error values tending to level out. Subset radius had a relatively small influence at both strain levels, consistent with the computational findings. The lack of strong parameter dependence may reflect the uniform strain field applied experimentally, in contrast to the heterogeneous computational field.

Across the intermediate strain levels (10–35%), the same behaviour was observed, with a gradual increase in error magnitude and a progressive levelling of peak error across parameter combinations. These additional results are provided in Appendix A.3.

To assess whether ROI selection influenced the measured strain, the mean, standard deviation, median, minimum and maximum strain were calculated for both the 10 mm central ROI and the larger full-width ROI. This comparison was performed using the parameter combination (17, 4, 5) at 20% strain to illustrate the effect of including non-uniform edge regions on the resulting strain measures. The smaller ROI produced

a mean strain of 0.1759 with a very low standard deviation (0.0007), and a narrow min–max range (0.1706–0.1812), indicating a highly uniform strain field within the central region. In contrast, the larger ROI yielded a higher mean strain (0.1813) but more than double the variability (STD = 0.0017) and a much wider min–max range (0.1544–0.2042), reflecting the inclusion of non-uniform edge regions. These findings support the use of the reduced ROI for subsequent analysis, as it provides a more stable and representative measure of strain.

Having established that ROI selection did not substantially alter the overall conclusions, the next step was to examine how parameter sensitivity varied across the full strain range. To complement the strain-specific bar charts (Figure 3.3.5), absolute peak error was evaluated for the parameter combinations yielding the lowest and highest errors at each strain level, together with a representative fixed setting (17, 4, 5). This provides an overview of how DIC performance changes with increasing deformation and whether certain parameter combinations consistently outperform others across the 5–40% strain range.

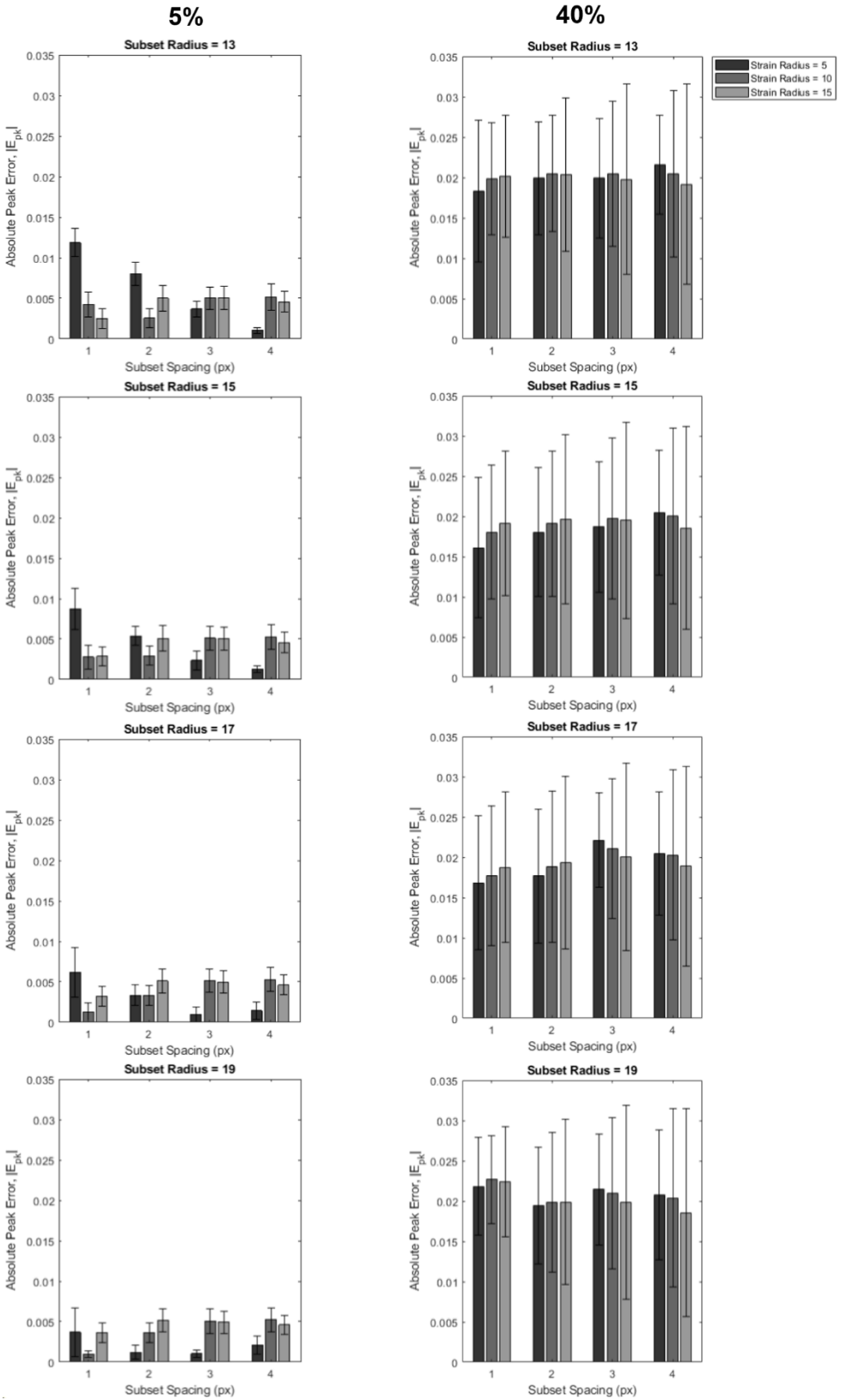


Figure 3.3.5: Absolute peak error averaged across three samples *at 5 and 40% with error bars demonstrating standard deviation of error across the region of interest for each parameter combination.*

Figure 3.3.6 shows the absolute peak error as a function of strain for the three parameter categories. The optimal and worst settings vary with strain, demonstrating that no single parameter combination is universally optimal. The fixed setting performs consistently between the two extremes, illustrating the compromise involved in selecting a single set of parameters for experimental use.

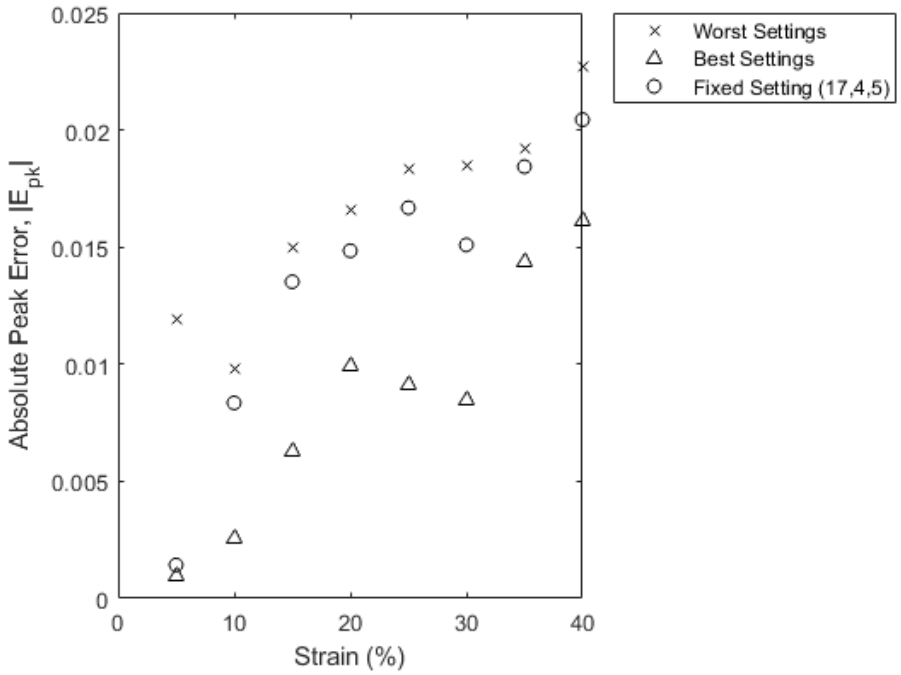


Figure 3.3.6: *Absolute peak error across 5–40% strain for the best and worst parameter combinations identified at each strain level, together with a fixed setting (17,4,5).*

Computational Load Results

Figure 3.3.7 demonstrates the effect of subset radius and subset spacing on computational time to complete DIC analysis. The average processing time increased with larger subset radii and decreased subset spacing. This can be seen for the parameter combination (10, 9, -). This indicates that parameter combinations involving a small subset radius and larger subset spacing are more computationally efficient. Note that differences in time may also vary depending on the device used for DIC analysis and the resolution of the images.

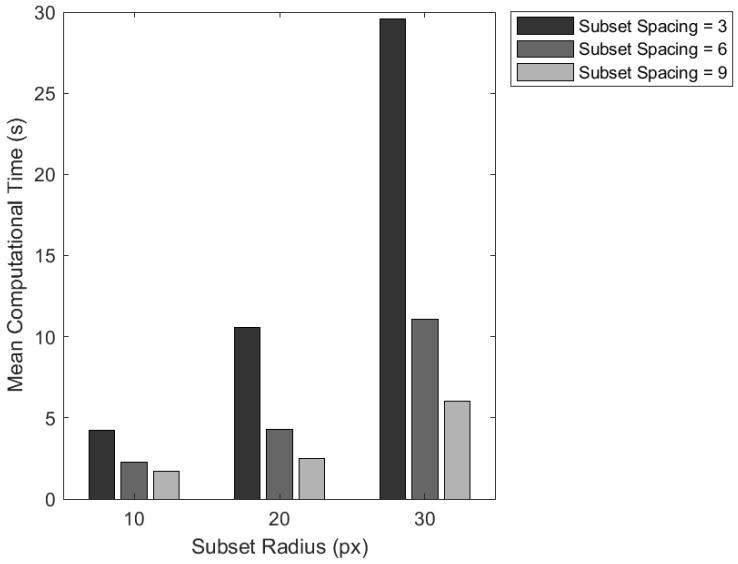


Figure 3.3.7: *Average computational time for DIC analysis to be completed for subset radius = 10, 20 and 30 and subset spacing = 3, 6 and 9.*

Final Parameter Selection and Validation

Based on the combined computational and experimental findings, in addition to alignment with general DIC parameter-selection guidelines, a final parameter set was selected for subsequent analysis: subset radius = 17 pixels, subset spacing = 8 pixels, and strain radius = 5 pixels. This combination provided an appropriate balance between spatial resolution, noise minimisation and computational efficiency.

To validate this selection, the final parameter combination was applied to the STAMPS case-study dataset [116], comparing against measures produced by GOM Correlate and alternative parameter combinations. Regional strain values were found to be consistent with the original findings. Paired t-tests showed no significant differences between the Ncorr and GOM values for any region except the hallux region in P03 ($p < 0.05$). A full summary of the original GOM outputs is provided in Appendix A.4 for reference.

3.4 Chapter Discussion

This chapter focused on establishing an objective and reproducible approach for selecting DIC parameters, in relation to the camera setup and defined speckle pattern of the STAMPS methodology. The work combined computational and experimental methods, aiming to quantify how parameter choices influence strain accuracy and computational load, as well as to find a configuration that is appropriate for clinical translation. The following discussion interprets these findings in the context of DIC parameter selection, and the chapter aims, evaluates the strengths and limitations of the approach and considers the implications for future development of STAMPS.

The computational analysis demonstrated a clear trend of increasing peak error as subset spacing and strain radius were increased, consistent with established DIC guidance favouring smaller parameter values. Reducing subset spacing increases the number of correlation points and therefore enhances spatial resolution, while a smaller strain radius limits the number of displacement measurements contributing to the least-squares fit, reducing smoothing effects and preserving local strain features. These trends were broadly consistent across all subset radii, although some differences from this were observed at 50% strain, suggesting that subset radius has a greater influence under larger deformations. The magnitude of error increased progressively as the numerically transformed speckle patterns were strained from 5% to 50%, likely reflecting both the amplification of correlation error with deformation and limitations inherent to the measurement technique. Since the error measure was taken as an absolute magnitude, it does not distinguish between under- and overestimation. However, inspection of the strain outputs indicated that strains of 5–30% were consistently underestimated, whereas both under- and overestimations occurred at 35–50%. This behaviour may explain the less uniform trends observed at higher strains. RMS error showed similar patterns, although its interpretability is limited in this context, as plantar strain data do not form smooth, continuous curves, reducing the usefulness of RMS error as a comparative metric in relation to the wider context of this work.

The experimental analysis showed that the averaged peak strain error increased progressively with applied deformation, with low-strain conditions (5%) producing small but more variable errors, and higher strains (40%) producing larger but more consistent error patterns across parameter combinations. Visual inspection of the representative strain maps supports this behaviour. At 5% strain, the central ROI displayed banded or locally heterogeneous strain despite the applied deformation being uniform (Figure 3.3.4), reflecting the dominance of measurement noise when the true strain is small. This explains the greater variability observed in the averaged strain error across parameter combinations at low strain. In contrast, the 40% condition produced a more spatially uniform strain field within the ROI, resulting in more stable error values (Figure 3.3.4). This behaviour is consistent with the computational findings and may reflect the combined effect of measurement noise at low strains and amplification of correlation error at higher deformations. It is worth noting that although absolute error was observed to increase with strain magnitude (~0.005 at 5% strain and ~0.02 at 40% strain), the relative error decreased (~0.1 vs ~0.05), indicating proportionally greater stability at higher strains and supporting the requirement for the device to perform reliably across both low and high strain levels. Subset radius appeared to only have a minor influence on error magnitude, consistent with the relatively uniform strain field applied in the central region of the sample, which reduces the sensitivity to local smoothing effects. The ROI selected also influenced the stability of the strain estimates, with the smaller central ROI

producing lower variability and a narrower strain range, whereas the larger ROI involved non-uniform edge regions and therefore exhibited a wider spread of strain values. This supported the use of a reduced ROI for subsequent analysis, as it provided a more representative measure of the underlying deformation. Examination of parameter sensitivity across the full strain range tested (5-40%) confirmed that no single parameter combination resulted in a consistently low error, with the best and worst settings varying with strain level. The fixed configuration (17, 4, 5) performed consistently between these extremes, illustrating the compromise required when selecting a single parameter set for experimental use.

The computational load analysis showed that processing time increased with larger subset radii and decreased subset spacing, reflecting the greater number of correlation calculations required under these settings. Smaller subset spacing increases the number of correlation points, while larger subset radii expand the area over which each point must be matched, both of which increase the computational demand. Conversely, combinations involving a small subset radius and larger spacing were markedly more efficient, consistent with the reduced number of correlation operations required. These findings highlight the practical trade-off between accuracy and processing time. Although a smaller spacing and larger radius may improve stability in some contexts, they impose a significant computational burden that may be impractical for routine or clinical use. While processing times will vary with hardware performance and image resolution, the relative trends observed here are likely to remain fairly consistent across systems.

The final parameter set (subset radius = 17, subset spacing = 8, strain radius = 5) was selected by combining the trends observed across the computational, experimental and computational load analyses with established guidelines for DIC parameter selection. Although smaller subset spacing values produced lower error in the computational benchmarking, a spacing of 8 pixels provided a balance between spatial resolution, noise behaviour and computational load. This spacing provided the sampling density required for stable correlation and for capturing plantar strain without amplifying noise or creating excessive processing time when analysing full insoles, appropriate for clinical workflows. The selected spacing also aligns with DIC guidelines suggesting a value of approximately 1/3 to 1/2 of the subset radius [126], providing further support for its suitability within this configuration. The chosen subset radius of 17 pixels reflected a similar balance, providing adequate distinguishability without the substantial increase in processing time associated with larger radii. A strain radius of 5 pixels was selected to prevent over-smoothing, while being large enough to minimise noisy, unstable estimates. Importantly, the strain-dependent error behaviour observed in both the computational and experimental analyses meant that no single parameter combination was optimal across the full deformation range. Given that healthy individuals typically exhibit low

plantar strains, whereas those at risk of ulceration may present with substantially higher strains, the selected parameters needed to perform reliably across both contexts. The chosen configuration attempted to achieve this balance, by balancing the different factors discussed. Validation against strain measures calculated using GOM Correlate showed no meaningful differences, supporting the suitability of the selected parameters for subsequent plantar strain analysis and for integration into a streamlined clinical workflow.

Several limitations should be acknowledged when interpreting these findings. The computational benchmarking was based on numerically transformed speckle patterns, meaning that repeated DIC runs would produce identical deformation fields and as such, repeat variability could not be assessed within this element of work. In the experimental work, the shape of the sample introduced non-uniform edge regions, meaning the applied strain field was not perfectly uniform and may have influenced the sensitivity of certain parameter combinations. Differences in strain-field characteristics between the computational (heterogeneous) and experimental (nominally uniform) tests also mean that the two datasets cannot be directly compared in magnitude, instead only based on trends. The preliminary testing phase narrowed the parameter combinations taken forward into the computational and experimental analyses, but this was based solely on numerical error and did not yet incorporate other considerations such as computational load, spatial resolution or guidelines. As a result, some parameter combinations, including larger subset spacing values that were ultimately selected, were not assessed in the main testing stages. The findings from this chapter are also specific to the speckle pattern, imaging resolution and camera setup used in this study, and optimal parameters may differ for other configurations or sample geometries. Finally, although the final parameter set was selected using quantitative trends, some degree of subjectivity remains due to the need to balance accuracy, spatial resolution and computational load across different strain levels. This reflects the inherently multi-factorial nature of DIC parameter selection, though the approach taken here provides a more structured and numerically justified basis than reliance on general guidelines alone.

The selected parameters enabled the development of a semi-automated plantar strain measurement workflow using an open-source DIC tool fully compatible with MATLAB, enabling integrated post-processing and efficient analysis within the STAMPS framework. This creates a clear pathway for future development of the system into a 3D strain measurement platform in which Ncorr underpins the 3D DIC software DuoDIC. The methodological insights gained here therefore offer a strong starting point for extending STAMPS into 3D, where more representative plantar strain fields can be captured. Although exploring parameter selection specifically for a 3D DIC system falls outside the scope of this project, the fact that DuoDIC is built on the same Ncorr

framework provides greater confidence that the set of parameters established here will be transferable to the next stage of development.

3.5 Chapter Conclusions

This chapter established a rigorous and evidence-based approach for selecting DIC parameters suitable for plantar strain analysis within the STAMPS workflow. By combining computational benchmarking, experimental testing and computational load analysis with published recommendations, a balanced parameter set (17, 8, 5) was identified that offers reliable performance across the strain levels relevant to both healthy and at-risk feet. This removes the need for a subjective approach and supports a streamlined, open-source workflow that integrates directly with MATLAB, meeting the interoperability and transparency requirements defined in Section 3.2.1. The approach developed here also provides transferable methodology for others seeking to identify suitable DIC parameters for their own setups, ensuring that measurement accuracy is not compromised for subjective choices. Although optimisation for 3D DIC lies beyond the scope of this chapter, the shared Ncorr foundation underpinning DuoDIC provides a natural platform for extending the STAMPS system toward 3D plantar strain analysis, which is explored in Chapter 4.

Chapter 4

Development and Evaluation of a Novel 3D In-Shoe Plantar Strain Measurement System: STAMPS3D

The work reported in Section 4.2 of this chapter has been published as:

Francesca Sairally, Rory P. Turnbull, Heidi J. Siddle, David A. Russell, Claire Brockett, Peter R. Culmer. *Proceedings of the Institution of Mechanical Engineers, Part H: Journal of Engineering in Medicine*, 239(5), pp. 472-484. (2025)

The graphical abstract for this chapter is shown in Figure 4.1.1, with the corresponding journal article available online at: https://doi.org/10.1177/09544119251330738.

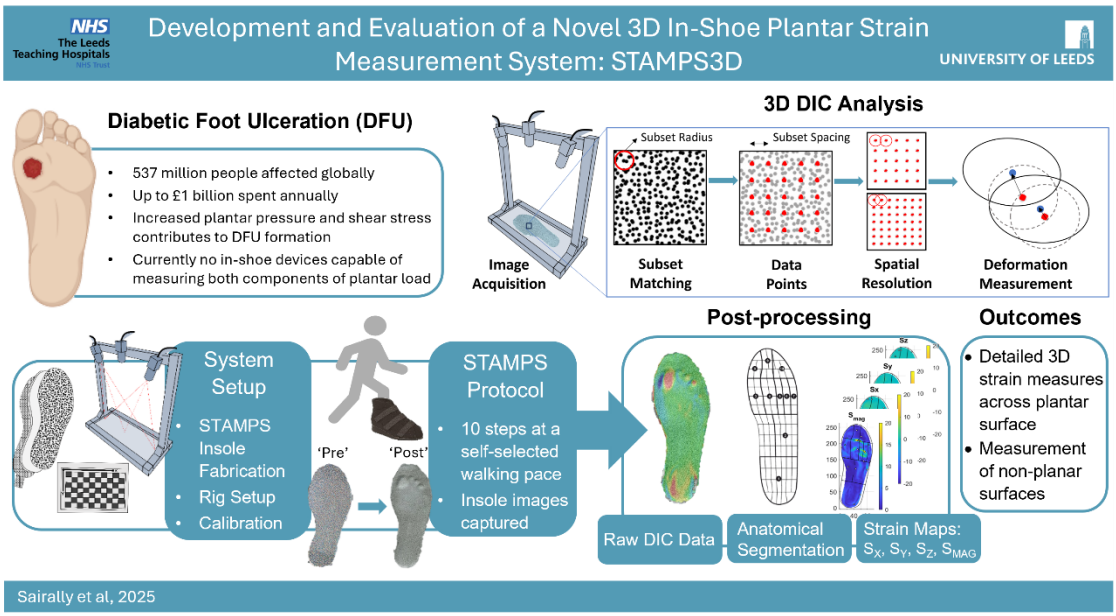


Figure 4.1.1: *Graphical abstract for the paper: Development and Evaluation of a Novel 3D In-Shoe Plantar Strain Measurement System: STAMPS3D.*

4.1 Preface

This chapter concerns the development, validation and application of 3D DIC methods to enhance the STAMPS tool. The work reported in Section 4.2 was published as 'Development and Evaluation of a Novel In-Shoe Plantar Strain Measurement System: STAMPS3D' and addresses Objective 2 (development and implementation of a 3D DIC based in-shoe measurement system) of this project. This chapter demonstrates how experimental rig design, calibration and preliminary testing informed the methodological structure that underpins subsequent investigations described in the later chapters.

As first author, my contribution to the paper included the design and performance of the experimental procedure, the development of calibration and validation procedures and the analysis, interpretation of data and writing the manuscript. A section on Preliminary Work and Supporting Data is included following the publication (Section 4.3). This additional content details the iterative development of the camera rig, calibration against an independent motion capture system and preliminary shear and indentation tests that shaped the final experimental design. These sections provide insight into how the workflow was refined and how methodological challenges were addressed.

A summary of this work was also disseminated at the BioMedEng24 conference, where findings were presented in a poster format (Appendix B.1). This dissemination highlights the broader impact of the study and its relevance to the biomechanics community. In addition to this, a protocol document was developed to support future use of the STAMPS3D tool. This resource outlines the fabrication process, calibration steps, 3D DIC analysis workflow and post-processing procedures (Appendix B.2).

4.2 Publication

The following publication presents three experimental components: indentation testing, shear distance testing and a single participant case study. To support interpretation within the thesis, each component corresponds to a brief research question that clarifies the purpose of the work and the expected contribution of each test:

- Can 3D DIC accurately capture deformation and global surface geometry on both planar and non-planar samples, when compared against benchmark 3D scans?
- Does increasing shear distance produce corresponding increases in strain measures, demonstrating that STAMPS3D captures the combined effects of pressure and shear loading?
- Do plantar strain patterns measured using 3D DIC differ from those measured using 2D DIC when applied to a single participant during gait?

Abstract

The formation of diabetic foot ulcers (DFU) is consequential of peripheral neuropathy, peripheral arterial disease and foot deformity, leading to altered foot biomechanics and plantar loads. Plantar load comprises of normal pressure and shear stress, however, there are currently no in-shoe devices capable of measuring both components. The STrain Analysis and Mapping of the Plantar Surface (STAMPS) system, developed at the University of Leeds, utilises Digital Image Correlation (DIC) to measure the strain captured by a plastically deformable insole, as a method to understand plantar load during gait. A 2D DIC software was used to capture cumulative plantar strain and displacement pointwise data, however this method was limited to the analysis of planar surfaces. To address this, 3D instrumentation and DIC methods have been developed and implemented into the STAMPS3D system, used as a tool to capture data that is representative of the non-planar nature of plantar surfaces of the foot. A case-study is used to demonstrate how STAMPS3D can measure multi-dimensional strain, bringing potential to improve clinical screening of DFU risk.

Introduction

Diabetes is a globally prevalent chronic condition, with numbers expected to reach 537 million and 783 million by 2030 and 2045 respectively [164]. Of those with diabetes, up to 25% will go on to develop a diabetic foot ulcer (DFU), with a 40% recurrence rate at 1 year in those that heal [32], [60]. Consequently, diabetic foot care has been estimated to cost nearly £1 billion annually based on NHS England spending from 2014/15 [44]. To address the social and financial costs associated, the James Lind Alliance identified the top 10 diabetic foot research priorities. From this set of priorities, six of the ten included ‘prevention’ highlighting its importance in diabetic foot care [91]. DFU formation is driven by diabetic peripheral neuropathy (DPN) and soft tissue changes, resulting in structural foot deformities and increased plantar load within these regions [165]. Unfortunately, in the presence of neuropathy, there is a loss of the protective pain sensation which contributes to soft tissue damage due to repetitive high or abnormal stresses going unnoticed.

Plantar load comprises of pressure and tangential shear stress. Plantar pressure is the force acting perpendicular to the surface, whereas shear stress acts parallel to the surface with anterior/posterior and medial/lateral components [95]. Previously, increased plantar pressure has been identified as a risk factor for DFU development. In regions where peak plantar pressure exceed 650 kPa, risk of ulceration has been described to increase by 6-fold, in contrast to areas below that pressure threshold [98]. Additionally, plantar pressure has been found to be greater in those with diabetes and more so in those with DFUs present [96]. However, the correlation between peak pressure and DFU

formation is not definitive, as shown by Veves et al., where although it was concluded that high plantar pressures were good indicators of ulceration (especially in the presence of neuropathy) only 38% of ulcers were identified at peak pressure locations [101]. It has also been found that ulceration occurs at pressures that would be otherwise considered normal in people without diabetes, suggesting that other factors may contribute to DFU formation [102]. Yavuz et al. found that there are two cycles of shear in contrast to pressure during a single step, due to stresses that arise in opposing directions during contact and push-off phases of gait [43]. This suggests that shear may have a greater effect on plantar tissues, resulting in an increased risk of tissue damage and DFU formation under repetitive or elevated shear forces in contrast to the effects described under peak pressures.[1] Although it has been suggested that pressure and shear may be influential in DFU formation, plantar shear is still poorly understood due to measures being difficult to capture. In addition to this, measurement technology is often limited to research conditions due to associated cost, time and expertise required for use [115].

Currently, there are no commercial measurement systems capable of capturing both plantar pressure and shear. A custom measurement platform consisting of 80 sensors has been developed in a research setting and is capable of measuring both components of plantar load [111], [112]. However, this method is limited to barefoot conditions and therefore is not representative of in-shoe stresses that may arise during gait, as well as device size impeding clinical usage. In-shoe measurement devices for shear have also been described with sensors either being directly attached to the plantar surface of the foot or imbedded in an insole worn by an individual [113], [114], [166]. In these cases, the spatial resolution is restricted by the number of sensors and therefore unable to capture data across the entirety of the plantar surface. In addition to this, sensors attached directly to the foot may disrupt natural gait patterns compared to those integrated within a wearable insole. Hence, the development of a wearable device capable of capturing in-shoe plantar load is necessary, ensuring that the limitations described are addressed.

At the University of Leeds, the STrain Analysis and Mapping of the Plantar Surface (STAMPS) system has been developed [116]. This approach involves a plastically deformable insole, which utilises 2D Digital Image Correlation (DIC) to capture cumulative plantar strain across a period of gait. Consequently, real-time strain data is not captured, however this compromise enables higher spatial resolution of the data and mapping across the plantar surface. DIC is an optical technique which uses an applied speckle pattern to track local regions between deformed and undeformed images, which are used to calculate displacement and strain. Further technical details on the

[1] Although shear has been suggested as a potential contributor to DFU formation, current evidence remains preliminary and does not establish shear as a definitive risk factor.

development and validation of STAMPS are presented in prior work [116]. The STAMPS system has been successful in capturing plantar strain data in a healthy cohort, identifying a range of normal values across 18 healthy participants [117]. Although the system was successful in capturing plantar strain data, the 2D nature limits its application to planar surfaces, which are not representative of the surface of the foot where DFU formation occurs. Hence, this paper investigates the implementation of 3D DIC methods to better represent the non-planar nature of the plantar surfaces of a foot, by capturing 3D strain measures. In doing so, improved accuracy of strain data indicative of plantar shear is expected to guide clinical screening procedures by providing quantitative measures to identify DFU risk, enabling appropriate management and aid in prevention.

This paper presents our work to extend STAMPS to a 3D measurement system (STAMPS3D) capable of measuring non-planar surfaces and capturing 3D strain data at the plantar interface. In System Development we present the development of the STAMPS3D approach, Experimental Evaluation of STAMPS3D details the experimental validation methods before a final Case Study with a single healthy participant demonstrating the differences between 2D and 3D methods. This is concluded with a discussion considering any associated limitations and future prospects for the described 3D methods.

System Development

System Requirements

The aim of this work is to progress the 2D DIC methods incorporated with the STAMPS system to instead harness open-source 3D DIC software and thus improve fidelity of measurement. The use of open-source software provides a cost-effective approach which enables future integration into semi-automated data analysis, and that can be readily adapted to stakeholder needs. Adopting this 3D DIC approach also requires development of stereo-camera instrumentation. The STAMPS3D system will then be capable of capturing data from both non-planar deformations and surfaces. The resulting 3D strain measures will then fully describe the x, y and z components of the strain tensors, providing an improved method in contrast to 2D DIC measures.

3D Digital Image Correlation (DIC)

STAMPS3D uses a combination of open-source toolboxes; 2D DIC is performed using ‘Ncorr’ (v1.2.2) which is then used by the ‘DuoDIC’ toolbox to form a 3D representation. Ncorr and DuoDIC are MATLAB (Mathworks, USA) based software. The main stages involved in 3D DIC, as implemented in DuoDIC, are: 1) Stereo Camera Calibration, 2) 2D DIC Analysis (using Ncorr), 3) 3D Reconstruction and 4) Post-processing. These are illustrated in the Case Study provided in Section 4.

This section now describes implementation of the 3D DIC technique, detailing configuration of the stereo imaging system, calibration of the system, selection of DIC parameters and finally the process of conducting and analysing the 3D DIC measures.

Stereo Imaging Rig Design

A custom imaging rig was built to provide a consistent method of imaging insoles of various sizes before and after deformation. Both 2D and 3D camera setups were integrated to enable both DIC methods for comparative tests (Figure 4.2.1). Three high resolution USB cameras (Basler, Germany, A2A 1920-160UCBAS) paired with camera lenses (Basler, Germany, C23-08245M-P) with a fixed focal length of 8 mm were used to capture images with a resolution of 1920x1200. The system is powered and run through a high-performance laptop. For the 2D setup, a single camera is required and fixed central to the top of the rig frame, perpendicular to the base surface and at a height ensuring the entire base plate was within the field of view. For the 3D setup, two cameras acting as a single stereo camera pair were attached to the rig, aligned to the height of the single central camera (Figure 4.2.1, Left). Additional camera units can be used within this framework if occlusion of the 3D surface occurs, however two cameras were selected based on preliminary work which showed this configuration was appropriate in this context. Following established recommendations on good practice in DIC measurement for camera lenses used with a focal length of 8-12 mm [126], a stereo angle of 35° was chosen to ensure that entire base plate was within each camera field of view, such that the speckled insoles were fully visible and focused across the whole insole (Figure 4.2.1, Right).

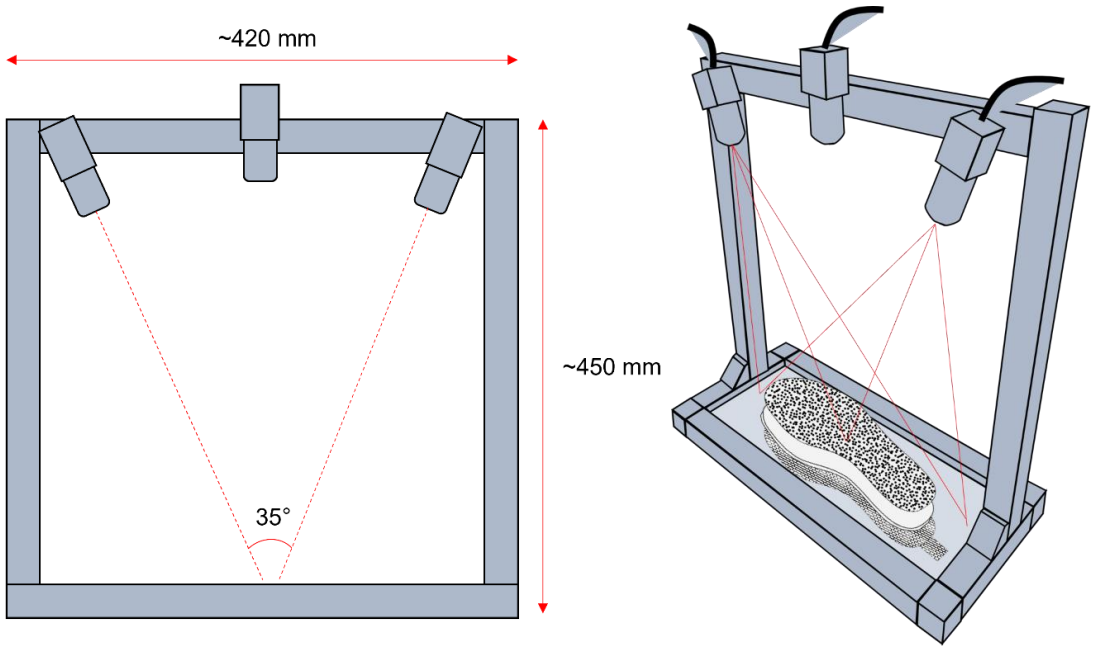


Figure 4.2.1: *DIC camera rig setup, consisting of 2D and 3D configurations.*

Calibration Procedure

Calibration of the DIC system is an important aspect to determine camera parameters and the 3D configuration of the stereo camera pair. Using a rigid camera rig ensures that calibration is only necessary once, remaining unchanged unless the camera system is adjusted. A calibration procedure workflow has been developed to ensure each step is fulfilled to achieve accurate measures of the intrinsic and extrinsic parameters, which define the camera properties (focal length, optical centre and lens distortion) and relative positioning of the cameras in space (rotation matrix and translation vector) respectively.

Pre-calibration involved initialisation of cameras and lighting to prevent over-exposure or glare. Image acquisition was performed using a 15x15 mm checkboard calibration target, in which 66 image pairs were captured in a synchronised manner [126], such that images from each camera only differ in terms of their respective perspectives. The image pairs captured consist of rotation and translation of the calibration target about the x, y and z axes such that the entire field of view was imaged. Each of the images were quality checked prior to performing calibration to remove any images that were unfocused or with glare. The MATLAB computer vision toolbox was used to calibrate the 3D system. Assessment of the calibration outputs (camera extrinsic parameters, reprojection error (RPE) and image rectification) was performed. Independent validation of the camera extrinsics was performed using a Qualisys motion capture kit. Calibration images were included such that they each have RPE < 1 [167], with the average RPE ≤ 0.5 to ensure accuracy. Lastly, the image rectification provided within the MATLAB window was assessed to ensure the images corresponding to each camera were correctly row aligned. The successful calibration file was then used during 3D reconstruction, where any lens distortion was removed from each of the speckled images automatically. This is unlike DIC software, in which lens distortion must be removed manually from each of the images using a MATLAB script.

DIC Parameter Selection

The second step of STAMPS3D involves performing initial 2D DIC analysis. For this, the appropriate DIC parameters, including subset radius and subset spacing, was selected. The subset radius is a defined region consisting of a speckled pattern based on the diameter chosen. The speckles that fall within this radius are then used to match regions between the undeformed and deformed images across the insole. The subset spacing is the number of pixels defined between the datapoints, where measurements are captured. Each of these datapoints are located at the centre of a different subset, therefore overlap of subsets can be found where the subset spacing is less than the subset radius. The subset spacing chosen effects the spatial resolution of the data collected, where a smaller spacing results in a greater number of data points placed

across the sample and therefore increasing the spatial resolution, demonstrated in Figure 4.2.2.

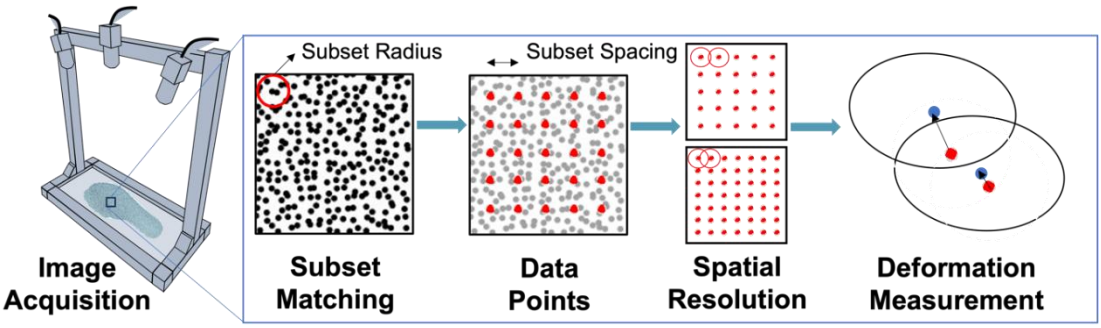


Figure 4.2.2: *DIC analysis process including image acquisition, DIC parameters selection, spatial resolution and deformation measures demonstrated across two overlapping subsets.*

The recommendations on DIC parameter selection vary among the literature and are often subjective. Supplementary work to the 3D methods was performed to determine appropriate DIC parameters using an objective approach, ensuring that spatial resolution, subset distinguishability and computational processing time were considered. DuoDIC is a 3D extension of the 2D DIC software Ncorr, utilising it for step two where 2D DIC analysis is performed. Hence, the DIC parameters determined in the supplementary work were also used for this application. A subset radius of 17 pixels and subset spacing of 8 pixels were selected. The 2D DIC analysis was performed for the images corresponding to each camera in the stereo pair, producing a set of 2D image points where the associated 2D measures are located.

3D DIC Analysis

The calculated set of 2D image points are used with the calibration file to reconstruct 3D image points. The final step involves the calculation of displacement and 3D sample deformations. The DuoDIC software also enables the removal of rigid body motion (RBM) from measures to account for misalignment of a given sample between imaging pre- and post-deformation, mitigating any mis-alignment of insoles between imaging phases.

Segmentation and Post-Processing

An analysis process was developed (Mathworks, USA) to process and provide visualisation of the computed deformation data. Firstly, the normal strains S_X, S_Y and S_Z were extracted from the Green-Lagrangian strain tensor as calculated from the 3D DIC analysis. The corresponding strain map is segmented corresponding to ten anatomical regions of the foot according to a masking protocol employed by the commercial plantar analysis software (PEDAR INC., Novel GmbH, Munich, Germany): Heel, midfoot, 1st

Metatarsal Head (MTH), 2nd MTH, 3rd MTH, 4th MTH, 5th MTH, hallux, second toe, toes 3-5. Based on the insole shape and size, the mask is scaled and adjusted to fit the individual plantar data. Strain data is allocated into each of the corresponding regions. Anatomically, the normal strains can be interpreted as the mediolateral axis (S_{ML}), anteroposterior axis (S_{AP}), pressure axis (S_P) and strain magnitude (S_{MAG}). The upper 10% S_{MAG} measures are highlighted to identify the global strain distribution about the localised peak strain measures.

STAMPS3D Insole Fabrication

The STAMPS insole has a multi-layer structure, with a 5 mm mid-layer made of industrial plasticine to enable plastic deformation, which can be cut to measure a range of shoe sizes and shapes [116]. A high-contrast speckle pattern is printed onto temporary tattoo paper using a commercial inkjet printer and adhered to the surface of the plasticine mid-layer using the water-activated sheet backing. The speckled pattern is generated using a commercial pattern generator (Correlated Solutions Inc.) defined with 65% speckle density, 0.8 mm speckle diameter and 75% pattern variation. Figure 4.2.3 outlines the steps involved in the insole fabrication, calibration, data capture and analysis for STAMPS3D.

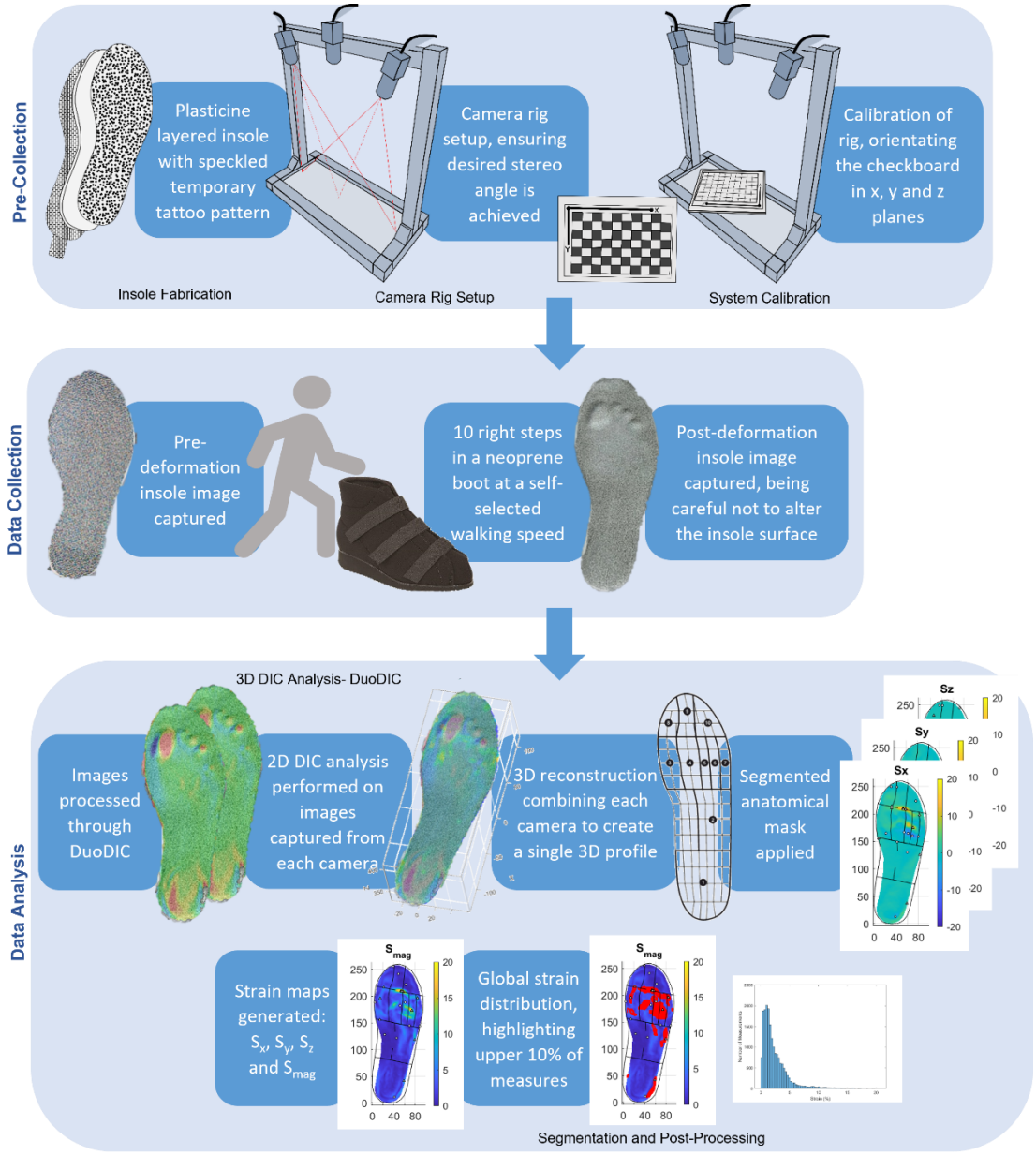


Figure 4.2.3: *STAMPS3D procedure including, pre-collection preparation, data collection and analysis.*

Experimental Evaluation of STAMPS3D

Experimental testing was performed to validate the STAMPS3D system as a measurement technique. The tests aimed to first validate 3D deformation measurements on both planar and non-planar samples, comparing deformations and global surfaces of non-planar samples measured using 3D DIC (DuoDIC) against 3D scans (Artec 3D, USA), which were taken to be the benchmark. The second aim was to validate the shear measures captured using 3D DIC.

Methods

Testing was performed through indentation and shear tests using a universal load tester (Instron, 5943) and a custom multi-axis load tester (Thorlabs, NJ, USA), respectively. Speckled plastically deformable samples (50 x 50 mm) were made, consistent with the fabrication of the STAMPS3D insoles. For the planar case, a custom fixture was 3D printed (Form 3, FormLabs) to act as a supportive backing and prevent any unwanted warping during testing. For the non-planar case, samples were moulded into a 3D printed hemi-spherical surface with an inner diameter of 80 mm. Hemi-spherical indenters were 3D printed with diameters 20 and 30 mm. Indenter sizes were selected to test a range of deformations reflective of anatomical regions of the foot, such as the metatarsal heads, together with overlying soft tissue. An initial pre-load of 0.01 N was applied. Samples were then indented at a depth of 2 mm. Five repeats of each indenter size were performed (n = 15). Stereo images were captured for each test, pre- and post-deformation, and were used for 3D DIC analysis. 3D scans of samples were taken post-deformation. A custom script was developed to post-process the data and apply a sphere fit to either the local deformation or global surface of non-planar samples. From this an estimated radius of curvature was calculated with the corresponding root-mean-squared (RMS) error. The mean RMS error and standard deviation across the five samples were collected. These measures were compared against the 3D scan data, with percentage error for estimated radius of curvature and RMS error calculated.

For the shear tests, planar samples were fabricated as described above. Each sample was held in a custom 3D-printed fixture, which could be attached to the Thorlabs multi-axial stage, securing samples and ensuring shear occurred in a single axis. The 20 mm hemispherical indenter was used to indent the samples to a depth of 2 mm, followed by shear distances of 0, 1 and 2 mm. With five repeats for each test performed (n = 15).

The test methods for each setup are demonstrated in Figure 4.2.4.

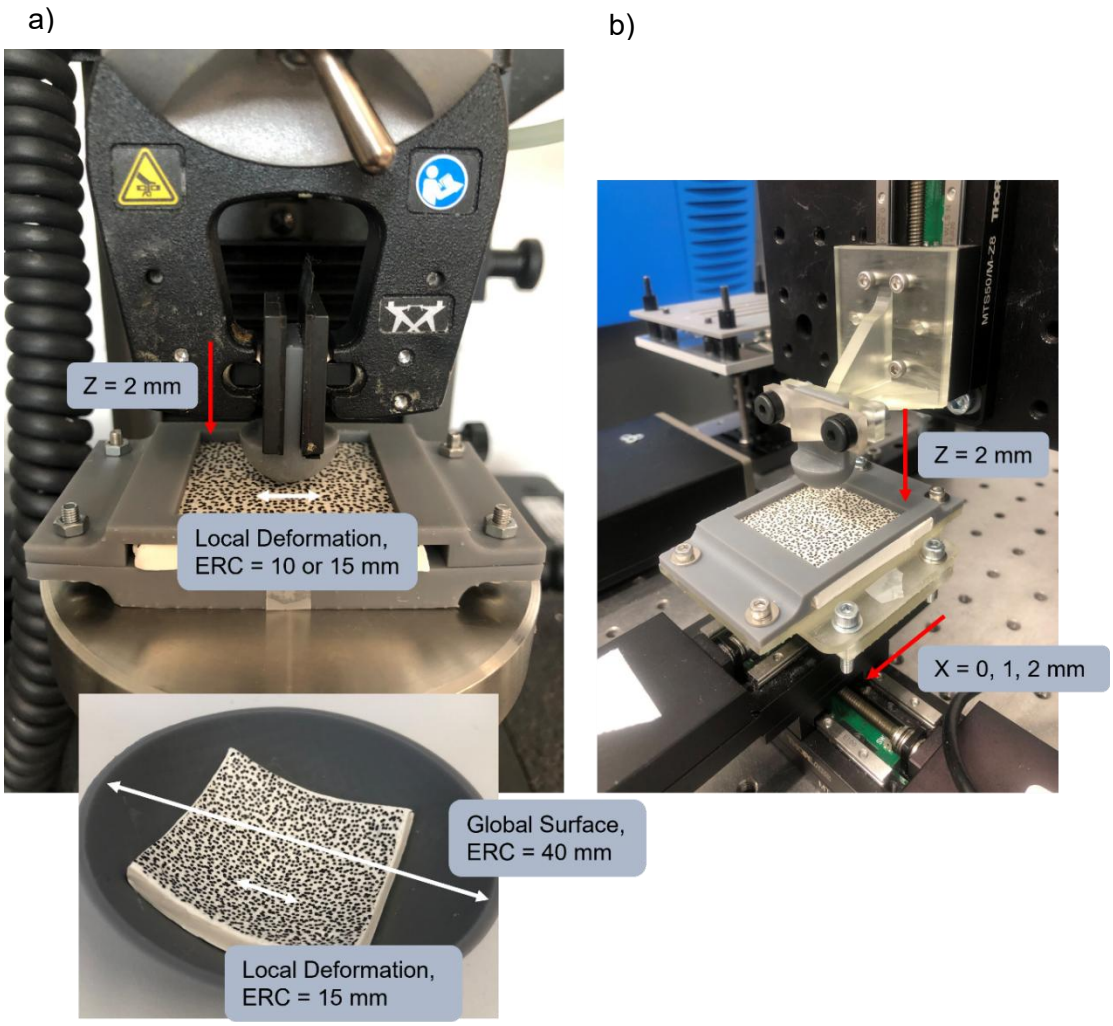


Figure 4.2.4: *Method setup corresponding to a) indentation tests performed at 2 mm on planar (top) and non-planar samples (bottom) to validate simple geometry of deformations and global surfaces with expected radius of curvature (ERC) = 10, 15 and 40 mm and b) shear tests performed at distances 0, 1 and 2 mm after an initial 2 mm indentation.*

Results

All tests described were successfully performed and analysed using 3D DIC. The first set of tests set out to validate simple geometry deformations. Sphere fits were applied as exemplified in Figure 4.2.5. Figure 4.2.6 (a-c) compares the estimated radius of curvature corresponding to each indenter and global surface measured using either 3D DIC or a commercial 3D scanner. Figure 4.2.6 (d) presents peak strain components S_X, S_Y, S_Z and S_{MAG} reported for shear distances 0, 1 and 2 mm. Table 4.2.1 and Table 4.2.2 report all the measures corresponding to those summarised in Figure 4.2.6, respectively.

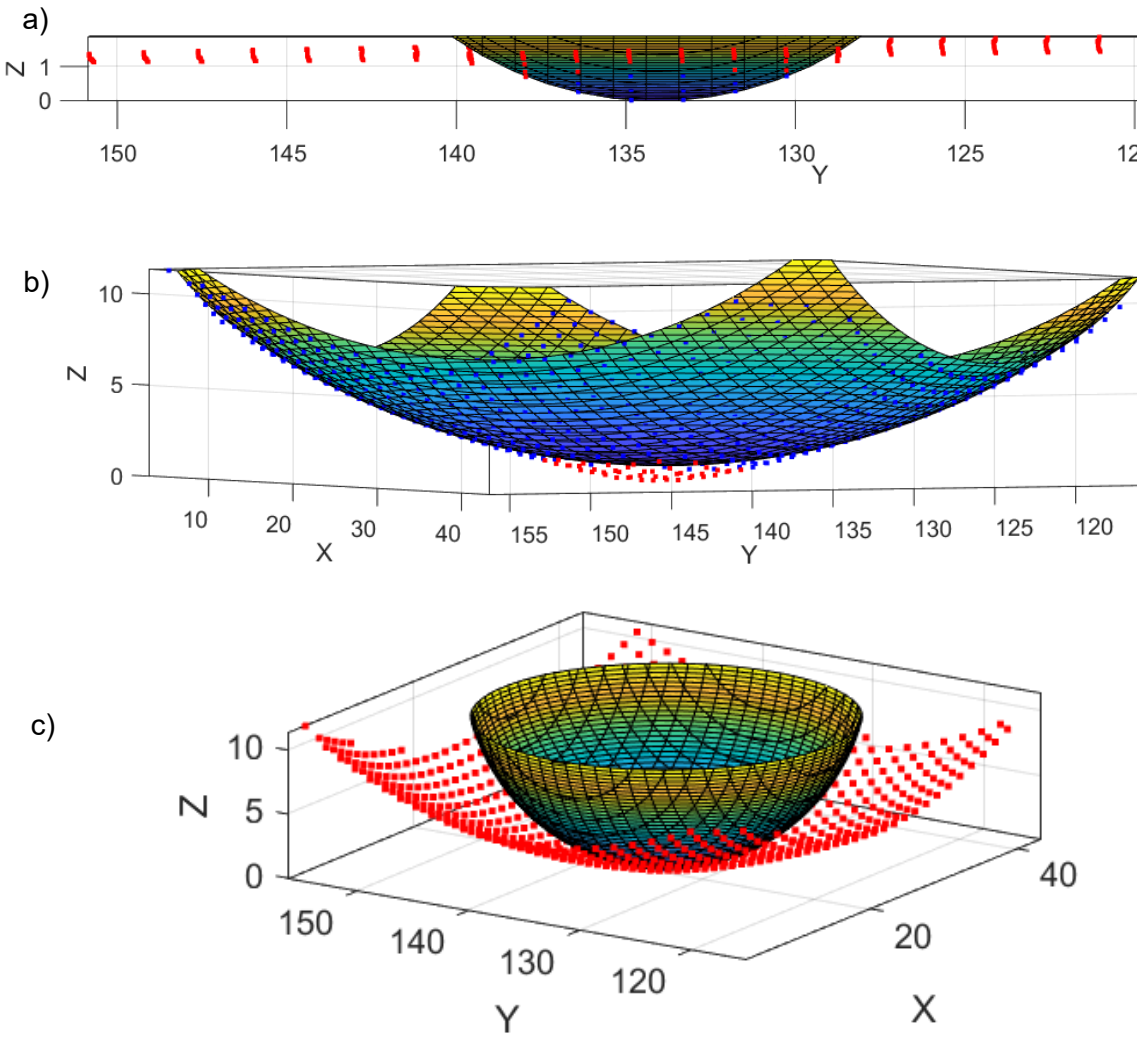


Figure 4.2.5: *Examples of sphere fits applied to a) planar samples, b) global surface of non-planar samples (excluding data points corresponding to local deformation) and c) local deformation of non-planar samples (excluding data points which fall outside the deformation).*

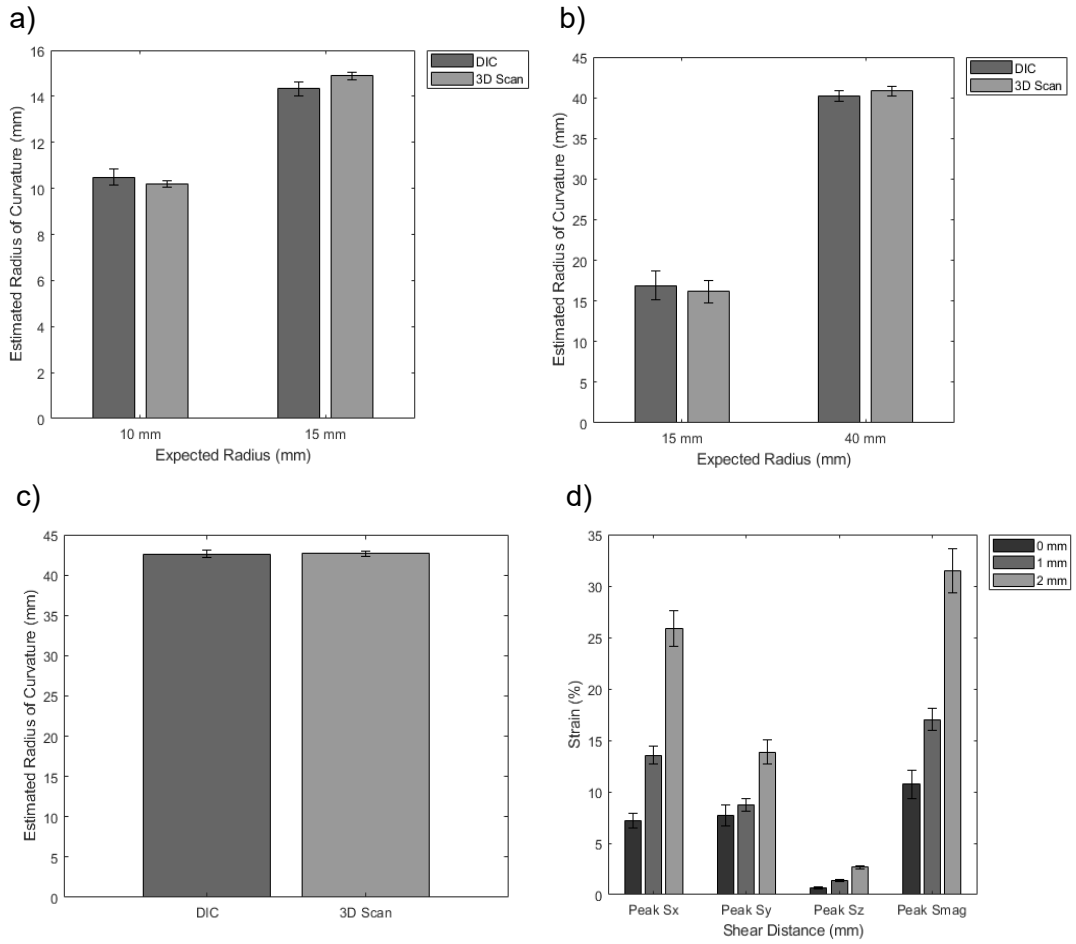


Figure 4.2.6: *Average estimated radius of curvature for a) planar samples with local deformations using 10 and 15 mm radius indenters, b) non-planar samples with local deformations using 15 mm radius indenter and global surface with 40 mm radius, c) non-planar samples undeformed to measure global surface alone and d) peak strain measures for varying shear distances of 0, 1 and 2 mm. (Error bars +/- 95% confidence interval).*

The results show that the estimated radius of curvature corresponding to both local deformations and global geometry for the data captured using 3D DIC, closely align to the data captured using the 3D scanner (Figure 4.2.6). The average error across the three test configurations ranged between 0-5% where DIC measures were compared to the benchmark 3D scans. The average RMS error for sphere fits applied to data analysed using 3D DIC were slightly lower than those of the 3D scans across each test configuration, in the range of 0.003-0.081 and 0.018-0.140 respectively (Table 4.2.1). Statistical significance between the DIC and 3D scan sphere fits were assessed using a paired t-test, where a significant result was determined if $P < 0.05$. Significant differences were determined for planar samples indented using 15 mm radius indenter and non-planar (deformed) samples for the 40 mm global surface ($P = 0.02$ and $P = 0.002$).

Table 4.2.1: *Average RMS error ± standard deviation corresponding to sphere fit applied to DIC and 3D scan data for both planar and non-planar samples.*

Sample	***Expected Radius (mm)***	***DIC Sphere Fit RMS error***	***3D Scan Sphere Fit RMS error***
Planar	10	0.015 ± 0.003	0.033 ± 0.003
Planar	15	0.008 ± 0.001	0.032 ± 0.005
Global	15	0.003 ± 0.001	0.018 ± 0.003
Global	40	0.081 ± 0.013	0.140 ± 0.019
Global (undeformed)	40	0.060 ± 0.007	0.096 ± 0.009

Table 4.2.2: *Summary of average peak strain ± standard deviation using DIC, showing the effect of shear distance on the components of peak strain (%).*

Peak Strain Measures (%)	***Shear Distance (mm)***		
	0	1	2
Peak S_X	7.169 ± 0.799	13.540 ± 0.985	25.850 ± 1.708
Peak S_Y	7.718 ± 1.140	8.750 ± 0.675	13.875 ± 1.276
Peak S_Z	0.706 ± 0.124	1.395 ± 0.097	2.665 ± 0.132
Peak S_{MAG}	10.720 ± 1.526	17.027 ± 1.233	31.478 ± 2.131

The results also show an increase in strain as shear distance was increased from 0 to 2 mm and was consistent across each of the peak measures S_X, S_Y, S_Z and S_{MAG} (Figure 4.2.6 (d) and Table 4.2.2). For shear distance = 0 mm peak S_X and S_Y were not found to be significantly different ($P > 0.05$), however statistical differences were found as shear distance was increased. The peak S_X measure were found to be larger at shear distances 1 and 2 mm compared to peak S_Y ($P = 0.002$ and $P = 0.0002$ respectively) and peak S_Z ($P = 0.00001$ and $P = 0.000009$ respectively) which was expected due to the shear being applied in the x-axis. The peak S_{MAG} measures were larger than the other measures reported due to the cumulative effect of the x, y and z components of strain. These results

were expected based on the experimental work reported in the previous STAMPS paper [116].

Case Study

A case study was conducted to compare the use of 3D DIC methods in STAMPS3D with a 2D DIC approach, evaluated through use of the system with a healthy participant.

Methods

Ethical approval was obtained from the University of Leeds Ethics Committee to conduct the case study (EPS FREC 2024-1462-1817). Eligibility included the participant being aged >18 years, capable of walking for 50 metres unaided, and not diagnosed with diabetes or foot health conditions. Prior to assessment, the participant read the participant information sheet and provided written consent.

A STAMPS insole and supportive neoprene boot (Ninewells Boot, Chaneco inc.) was selected based on the participant shoe size. A pre-deformation image of the STAMPS insole was taken using both the 2D and 3D camera setups of the rig. This was then inserted into the corresponding boot, with a similarly sized insole placed into the opposite foot to minimise any alterations in gait due to depth differences. The participant was asked to walk 20 steps, ensuring that ten steps were taken with each foot at a normal walking speed of their choice. The insole was removed and a 'deformed' image was taken again with both the 2D and 3D camera setups. Three repeats were taken. Both global and anatomical regions of the foot for measures of S_{ML}, S_{AP}, S_P and S_{MAG} were captured, in which S_P was only calculated using 3D methods. Two measures of S_{MAG} were also calculated using 3D methods, corresponding to those calculated using x, y and z components or x and y alone. S_{MAG} calculated using 2D methods corresponds to the latter. This post-processing analysis was performed using the custom processing described previously. Anatomical regions of the foot were segmented using a mask containing ten regions: Heel, midfoot, 1st metatarsal head (MTH), 2nd MTH, 3rd MTH, 4th MTH, 5th MTH, hallux, second toe, toes 3-5.

Results

The regional peak S_{MAG} calculated using 2D and 3D DIC methods are reported in Table 4.2.3. Figure 4.2.7 demonstrates the masking of raw data and summarises the peak S_{MAG} data across anatomical regions for both 2D and 3D methods from Table 4.2.3, in addition to the percentile data highlighted in the corresponding strain maps.

Table 4.2.3: *Average peak S_{MAG} ± standard deviation captured using 2D and 3D DIC methods across anatomical regions of the foot for deformed samples and corresponding.*

	2D	***3D***	***3D***
Region	Peak S_{MAG} (x,y) (%)	Peak S_{MAG} (x,y) (%)	Peak S_{MAG} (x,y,z) (%)
Global	21.72 ± 1.08	61.44 ± 9.33	78.47 ± 18.82
Hallux	19.59 ± 0.81	32.56 ± 1.28	36.60 ± 1.41
2nd Toe	8.96 ± 1.00	12.99 ± 1.68	15.03 ± 2.27
Toes 3-5	6.08 ± 1.94	12.78 ± 4.64	15.05 ± 5.35
MH1	8.85 ± 2.03	12.02 ± 6.13	14.03 ± 6.03
MH2	15.82 ± 4.79	44.91 ± 19.44	50.25 ± 27.20
MH3	5.97 ± 2.93	9.82 ± 5.22	11.33 ± 6.74
MH4	8.24 ± 1.38	17.78 ± 3.61	24.21 ± 3.56
MH5	18.07 ± 0.94	47.62 ± 2.35	67.30 ± 3.17
Midfoot (Lateral)	8.14 ± 0.49	12.24 ± 1.45	14.25 ± 1.53
Midfoot (Medial)	3.39 ± 4.49	3.52 ± 17.52	4.04 ± 19.57
Heel	9.52 ± 0.10	15.28 ± 0.57	17.59 ± 0.67

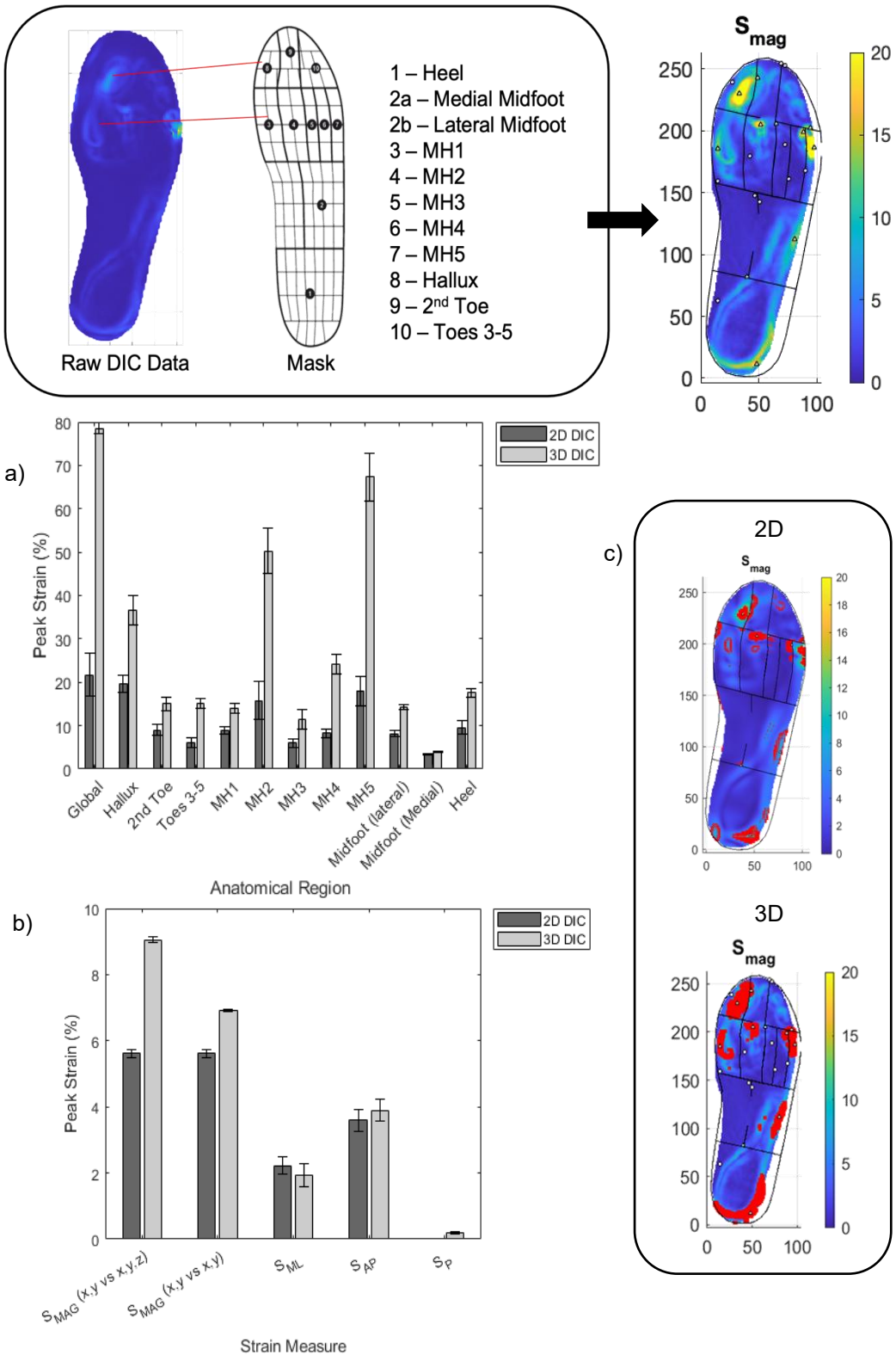


Figure 4.2.7: *Demonstration of raw data masking and summary of results comparing 2D and 3D methods: a) Comparison of average peak S_{MAG} for deformed samples walked on for ten steps at a self-selected speed. b) Upper 10% percentile threshold of global strain measures showing differences in data distribution. c) Examples of highlighted upper 10% S_{MAG} across anatomical regions of the foot. (Error bars +/- 95% confidence interval).*

Figure 4.2.7 (a) compares the average peak S_{MAG} (x,y vs x,y,z) computed using 2D and 3D DIC methods across the same samples after being worn for ten steps, reported in Table 4.2.3. The results show that across the anatomical plantar regions, similar patterns arise for both 2D and 3D methods. However, the strains produced using 3D DIC are larger than those calculated using 2D DIC. Statistically significant differences were found for all anatomical regions except at the 2nd toe, MH3, MH5 and medial midfoot ($P < 0.05$).

The upper 10% percentile of global strain measures were also recorded to assess strain distribution across anatomical regions of the plantar surface of the foot. The upper 10% threshold for 2D and 3D DIC methods for each strain measure is reported in Figure 4.2.7 (b), with S_{MAG} measures highlighted in red across the strain maps in Figure 4.2.7 (c). The results show that the upper 10% threshold for S_{MP} and S_{AP} were similar for 2D and 3D methods. Differences were found between the two methods for S_{MAG} (x,y vs x,y,z) and S_{MAG} (x,y vs x,y), with 3D methods resulting in larger threshold measures in both cases. The strain maps from Figure 4.2.7 (c) show larger regions highlighted for the 3D methods due to increased magnitude shown in Figure 4.2.7 (a). Increased detail of anatomical regions of the foot can also be seen in Figure 4.2.7 (c), where 3D methods have been used, unlike the 2D strain map, which appears to have a smoother surface.

Discussion

The development of a low-cost measurement system capable of measuring in-shoe plantar shear and plantar pressure has been reported, with STAMPS3D building on previous work to capture 3D plantar measurements. The total setup cost for the system is < £1000 with ongoing consumable costs of approximately £2.50 per insole. This makes STAMPS3D an affordable proposition which differs from other plantar measurement devices (e.g. Pedar, Novel) with potential to be used in low resource settings. The system weighs ca. 2 kilograms, with compact dimensions (see Figure 4.2.1), making it portable and easy to transport between clinical settings. The previous STAMPS study demonstrated that the strain measured using DIC resulted from normal pressure and tangential shear stress, where increased levels of the latter resulted in increased strain measures [116]. Therefore, this presented a measurement technique capable of capturing in-shoe strain measures indicative of plantar pressure and plantar shear, where other techniques offer strictly pressure measurements, capture un-shod conditions or limited data resolution [109], [111], [112], [113], [114]. However, the utilisation of 2D DIC methods means that measures are limited to a single plane and, therefore, may not accurately capture data from non-planar surfaces, such as plantar surfaces of the foot. This work reports validation of the adapted 3D measurement system (STAMPS3D), which utilises 3D DIC together with the previously reported STAMPS insole. The development of a low-cost 3D system aims to improve the accuracy of plantar load

measurement at the foot-surface interface to guide risk identification and thus prevent DFU formation.

The results of the geometry tests showed that 3D DIC accurately measures deformations, with comparable accuracy to measurements from a commercial 3D scanner. Errors corresponding to the estimated radius of curvature reported between the two methods were 0-5%. The average RMS error, reported in Table 4.2.1, were slightly lower for the sphere fits applied to the DIC data compared to those of the 3D scans across each test configuration. This showed that for each test, the fitted spheres were closely matched to the selected data for either the local deformations or global surfaces. Differences in the radius of curvature estimation and sphere fit RMS errors may be due to the initial manual cropping of sample meshes from the 3D scanned data, which is necessary to select the specific data corresponding to the local deformations or global surface. Although two indenters of diameters 10 and 15 mm were used, indentation depths tested were limited to 2 mm. Preliminary tests showed that depths less than 2 mm resulted in inaccurate measures due to small deformations, including too few data points once processed using DIC or the 3D scanner. For depths greater than 2 mm, sample warping occurred. It is believed to occur due to full contact across samples not being present, as would be the case when participants wear STAMPS insoles.

Shear tests showed results that agreed with the UMT tests performed in the STAMPS study. The results showed that as shear distance was increased, the measured strain using 3D DIC increased. This was consistent for the magnitude of strain and each of the x, y and z strain components. For shear distance = 0 mm, peak S_X and S_Y were not found to be significantly different to each other with average strains 7.71 and 7.17%. These measures were expected due to the spread/shearing of material around the indenter in both the x- and y-directions, as deformation occurs at a single point in the z-direction. As shear distance was increased to 1 and 2 mm, an increase in all components of strain was found, however this was greatest for the x component. This was found since shearing of the samples were performed in the x-direction. The strains measured for S_Y and S_Z were lower than that seen of S_X, particularly for S_Z due to deformation occurring in that direction during initial indentation. However, the combined effect of each component can be seen for the peak magnitude of strain, S_{MAG}. For these tests, normal force was not set as a control and so the results may represent the effect on strain as shear distance and normal force were increased together.

The STAMPS3D system was successfully used to measure plantar strain in the single-participant study, involving ten steps at a self-selected walking pace, following established protocol outlined in the STAMPS2D study [116]. This study involves a small sample size to only demonstrate the application of STAMPS3D in contrast to 2D DIC methods rather than providing strain data representative of the population. Therefore,

broader conclusions can not be made based on this data. Similar patterns could be seen from Figure 4.2.7 (a) across each anatomical region for both 2D and 3D methods. However, 3D measures were larger overall due to the additional z component captured. Statistical differences were found for the regions, Global, Hallux, Toes 3-5, MH1, MH2, MH4, Midfoot (Lateral) and Heel. The remaining regions reporting no significance may be due to reduced contact between the foot and the insole (e.g. medial midfoot) or positional error during the data masking. The upper 10% percentile of strains across all anatomical regions were also reported to consider the data distribution across the foot, alternatively to using a single peak value as an indicator of high-strain regions. Figure 4.2.7 (b) summarises the upper 10% percentile threshold of global strain measures, comparing the difference between 2D and 3D methods. No significant difference was found between 2D and 3D methods for S_{ML} and S_{AP}, which suggests comparable distribution characteristics regardless of method used. Peak measures of S_{ML} and S_{AP} were significantly larger when 3D DIC was performed, highlighting that 3D measures are more complete since the distribution of data is comparable to 2D data, whilst also providing larger peak strain measures that are more representative of the non-planar surface of the foot. The upper 10% percentile threshold for both S_{MAG} measures were significantly increased where 3D methods were used. This is due to larger peak measures and the additional S_P component, as mentioned previously.

This system allows for adaptations based on user requirements unlike other insole measurement devices available which often have set sizes. The base of the rig is designed such that it can accommodate insole sizes up to a UK size 14 and insole shapes can be easily adapted to fit individuals with wider feet. In a healthy study consisting of 18 participants it was reported that no statistically significant relationship was found between S_{MAG}, peak plantar pressure and the individuals weight [117]. Therefore design changes to the system would not be needed and has the potential to be used across the wider population. In the current system, no modifications are required for participant use, however future work looks to use the STAMPS3D system on a diabetic cohort with varying degrees of DFU. Data collection can also be completed within 10-15 minutes making the system suitable for clinical application, fitting within patient appointment slots. Limitations of the STAMPS system have been previously reported [116]. Although this work demonstrates the system's ability to capture non-planar data, the STAMPS insoles themselves are planar. Future work will evaluate STAMPS3D using non-planar STAMPS insoles to enable full plantar contact. This will involve moulding the planar STAMPS insoles to the surface of contoured (non-planar) orthotic insoles to identify whether changes in insole characteristics such as stiffness, thickness or regions of variable stiffness prescribed to individuals, result in altered plantar strain measured. This could be useful to indicate the interaction between the plantar

surface of the foot and contoured orthoses used to manage callus and high-risk areas for DFU formation.

Conclusions

This study demonstrated that 3D DIC can accurately measure deformations on planar and non-planar surfaces, comparable to a commercial 3D scanner. The relationship between strain measured using DIC and shear have been shown, aligning with a previous study that validated a 2D system. This work provides evidence that STAMPS3D can capture relevant information and characterise plantar strain. The use of 3D DIC in the case study showed similar distribution patterns to that of the 2D system, and an overall increase in strain was measured due to being able to capture the z component of the strain tensor. Overall, using 3D DIC techniques here provides a higher fidelity measurement to assess in-shoe plantar loads, and provides for inclusion of non-planar insole surfaces typical of clinical situations related to diabetic foot ulceration.

4.3 Preliminary Work and Supporting Data

This section presents the supplementary material that supports and extends the published work in Section 4.2. While the paper reports the main findings, the research process involved developmental steps that were critical in shaping the final experimental design. These include the iterative construction of the camera rig, calibration against an independent motion capture system, preliminary shear and indentation tests and the refinement of experimental methods. A case study is also provided to demonstrate the application of the workflow. Together, these elements show how any methodological challenges were addressed and how the workflow was progressively refined, offering a more complete picture of the research process than could be included within the publication.

4.3.1 Stereo Camera Rig Development

A stereo camera rig was constructed to enable capture of image pairs used for 3D DIC analysis. The 3D system comprised of two USB cameras (Basler, Germany, A2A 1920-160UCBAS) (2.3 MP, 1920 x 1200 pixel resolution, 3.45 μm pixel size, 160 frames per second), each fitted with a lens with fixed focal length of 8 mm (Basler, Germany, C23-08245M-P) (5 MP resolution). The compact nature of the cameras enabled mounting to the rig using custom laser-cut acrylic brackets (51 x 29 x 5 mm), which were designed to allow fine adjustment of camera positioning and stereo angle.

The rig itself measured approximately 420 x 190 mm at the base, with a height of 450 mm and had an incorporated laser-etched base plate with a 10 x 10 mm grid (Figure 4.2.1). Both single-camera and stereo configurations were trialled on the same rig, since

the single camera was previously set up for STAMPS using 2D DIC analysis. Initial positioning of the stereo camera pair on the side arms produced a larger stereo angle but restricted the field of view (FOV) and introduced sharp image angles. Alternatively, mounting the cameras closer together on the top bar reduced the stereo angle but improved sample visibility and focus. Iterative adjustments were therefore undertaken to balance these trade-offs (Figure 4.2.1 of publication).

Calibration was performed after each adjustment to quantify the effective stereo angle and assess image clarity across the FOV. A stereo angle of approximately 35° was selected based on established DIC guidance for short focal length lenses, and the iterative adjustments ensured that this recommended configuration was achieved in practice. The final setup ensured full sample visibility from both perspectives, adequate depth-of-field, and compliances with established DIC good practice guidelines [126].

4.3.2 Calibration

Calibration was performed iteratively alongside adjustments to the stereo rig, providing quantitative feedback that guided the refinement of the final camera configuration. Following the rig setup described in Section 4.3.1, calibration trials were used both to establish a reproducible workflow and to validate the stereo angle achieved. This process ensured that each design modification was supported by accurate geometric measurements before the camera setup was finalised.

Calibration Workflow

A 15 x 15 mm checkboard grid was used as the calibration target, with at least 20 images required and typically more than 50 acquired to ensure robustness. Images were captured with varied orientations and translations across the FOV, including rotations around both horizontal and vertical axes. Exposure times were limited to ~25 ms to reduce motion blur, and care was taken to fill the entire FOV of each camera. Blurred images or those affected by glare were rejected, as calibration accuracy depends strongly on image quality and variation of orientation [126].

The calibration workflow was formalised as follows:

1. Warm cameras to operating temperature.
2. Adjust lighting or rig positioning to eliminate glare.
3. Acquire ~60 synchronised image pairs with varied orientations (rotations in x and y planes, translations across the field of view, flat and raised target positions, and 90° rotations).
4. Assess image quality and reject blurred or glare-affected images.
5. Calibration processing and assessment

a. 50 ≥ accepted images in total.
b. Camera extrinsic parameters: relative camera positioning and stereo angle.
c. Reprojection Error (RPE): average RPE < 0.5 pixel with all included images having RPE < 1 pixel.
d. Image rectification: check camera images are row aligned correctly.

6. Repeat if calibration does not meet criteria.
7. Save calibration file.

Calibration Outputs

The calibration process produces both extrinsic and intrinsic parameters (see Section 2.5.3 of the literature review for further details). The extrinsic parameters comprised the rotation matrix (3 x 3 matrix) and translation vector (1 x 3 vector), describing the relative position of one camera to another. The stereo angle is derived from the rotation matrix, ***R***, which describes the relative orientation between the two cameras. Rotation about the X and Z axes is expected to be minimal, while the Y component corresponds to the stereo angle. Each rotation angle is calculated using Equation (1), based on elements of ***R***.

$$\theta_x = \tan^{-1}\left(\frac{r(3,2)}{r(3,3)}\right),$$
$$\theta_y = -\sin^{-1}(r(3,1)), \qquad where\ R = \begin{bmatrix} r(1,1) & r(1,2) & r(1,3) \\ r(2,1) & r(2,2) & r(2,3) \\ r(3,1) & r(3,2) & r(3,3) \end{bmatrix} \tag{1}$$
$$\theta_z = \tan^{-1}\left(\frac{r(2,1)}{r(1,1)}\right),$$

The stereo rig is defined with respect to a ‘master’ and ‘slave’ relationship between the cameras, in which the master camera is assigned to the origin (0,0,0). The translation vector, $\boldsymbol{T} = [t_x, t_y, t_z]$, is calculated based on the relative displacement of the slave camera with respect to the master, defining t_x as the baseline of the system. Figure 4.3.1 demonstrates the stereo camera configuration, highlighting the translation vector and stereo angle derived from the rotation matrix. This schematic demonstrates how the calibration outputs relate to the physical geometry of the rig and the equations used to compute the camera orientation.

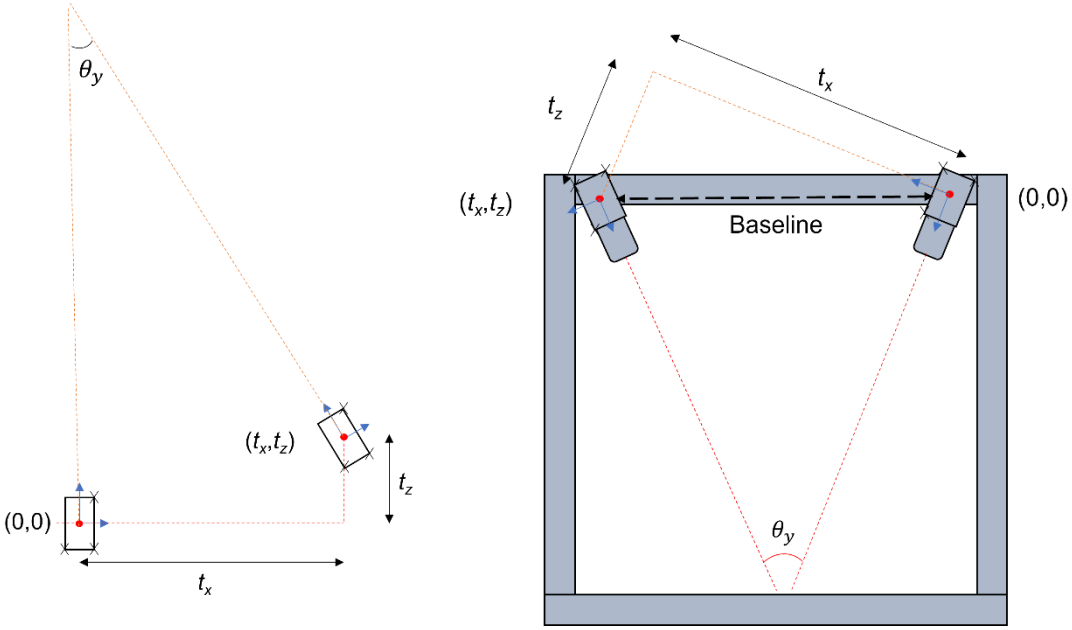


Figure 4.3.1: *Schematic demonstrating the camera setup, with the translation vector T and stereo angle, θ_y, derived from the rotation matrix R.*

The intrinsic parameters provide information about the cameras themselves and include the focal length, principal point coordinates, skew coefficient, and lens distortion coefficients. Focal lengths were consistent with the expected values based on the 8 mm lenses and 3.45 μm pixel size, while the principal point was located near the image centre (960 x 600 pixel). Lens distortion coefficients (radial and tangential) were close to zero and used during DIC analysis for integrated removal of distortion from images. Calibration outputs were saved as intrinsic matrices, distortion coefficients and extrinsic parameters for both cameras.

A series of calibration trials were conducted using the MATLAB stereo camera calibrator app to refine the workflow and assess reproducibility. Across ten tests, acquisition parameters were varied (exposure time, acquisition duration, board orientations). Early trials frequently resulted in high reprojection rates, particularly when motion blur or glare was present. Subsequent refinements, including static acquisition with increased board orientations and careful lighting control, resulted in reduced rejection rates and improved RPE.

Table 4.3.1 summarises the calibration outputs from each of the trials.

Table 4.3.1: *Summary of outputs from calibration trials.*

Calibration Trial	Rejected/Acquired Images	Average RPE (pixel)	t_x (mm)	t_y (mm)	t_z (mm)	Stereo Angle (°)
1	101/137	-	-	-	-	-
2	1/120	0.27	259.61	3.16	74.33	35.73
3	0/130	0.34	259.02	3.33	75.79	36.12
4	0/79	0.36	256.98	4.18	81.62	35.97
5	7/118	0.57	255.30	2.07	83.91	37.30
6	0/60	0.40	258.41	1.67	77.95	35.49
7	0/72	0.38	256.31	1.56	83.55	37.01
8	2/53	0.36	257.22	0.84	79.02	35.06
9	0/57	0.39	257.57	1.20	78.89	34.90
10	0/68	0.36	257.42	0.78	78.98	35.10

The final calibration achieved an average RPE of 0.36 pixel, well within the recommended threshold of <1 pixel. Outliers with RPE >1 pixel were excluded, although individual images with slightly higher error were occasionally retained to preserve orientation variation. The translation values were consistent with approximate hand measurements, with t_x = 257 mm and t_z = 79 mm, corresponding to a baseline of ~269 mm. t_y was close to zero, confirming alignment of the rig arms following adjustment. These values were then independently validated using a motion capture system described in the next section, to provide confidence in the stereo angle measurement.

Independent Validation

Independent validation of extrinsic parameters was performed using a Qualisys motion capture system. The aim of this work was to validate the stereo angle produced by camera-based calibration using an external measurement system with its own coordinate frame. This provided independent confirmation of the stereo geometry during the developmental phase of the STAMPS3D system, rather than establishing a process that must be repeated each time the camera rig is used. Two infrared cameras and one

visible camera were positioned such that each of their FOV overlapped and had visibility of the camera rig (Figure 4.3.2 (a)). Calibration of the motion capture system was achieved using a standard L-plate and wand, with 6 mm diameter markers placed on the front face of each DIC camera in addition to the side arms and base plate of the rig (Figure 4.3.2 (b)).

The marker coordinates were used to calculate the baseline components (t_x, t_z) and stereo angle. These calculations were performed using a custom application that converted pixel coordinates to real-world distances based on the calibrated motion capture system. This involved 3D marker geometry, where the respective marker positions in the calibrated global coordinate frame were used to derive the translation components, baseline and stereo angle. Full calculations can be found in Appendix B.3. Across three trials, the motion capture outputs were consistent, with t_x = 282 mm, t_z = 90.8 mm and stereo angle = 34.6° (Table 4.3.2). These values closely matched independent measures taken with a measuring tape, which estimated the baseline at ~305 mm. While t_x and t_z from the motion capture were slightly larger than those obtained through DIC calibration (t_x = 258 mm, t_z = 79 mm), the stereo angle showed strong agreement across both methods. The component differences are likely due to marker placement inaccuracies and reference frame mismatch and therefore do not negate the validity of the DIC calibration.

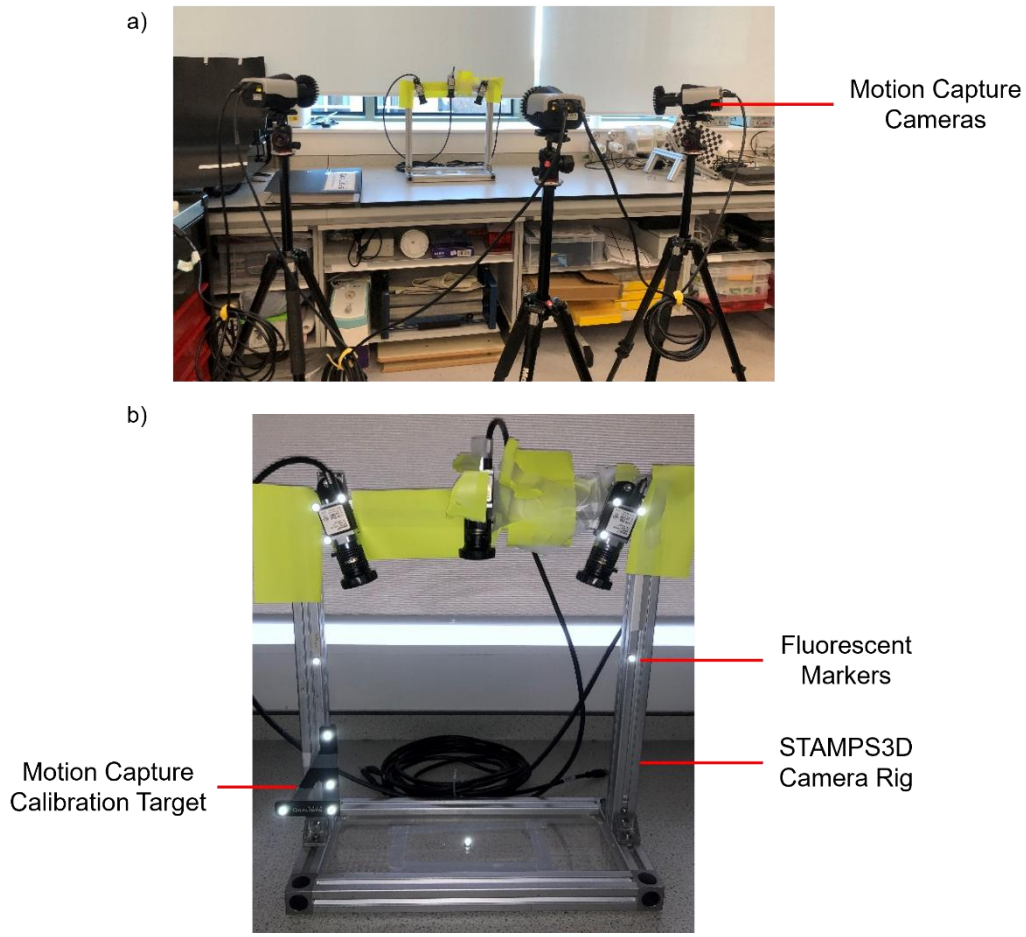


Figure 4.3.2: *Images showing a. the Qualisys motion capture setup and b. the stereo DIC rig with fluorescent markers used to define camera positions. Markers were placed on the rig to enable calculation of translation components and stereo angle for comparison with calibration outputs.*

Table 4.3.2: *Comparison of baseline components and stereo angle using DIC calibration, motion capture and hand measurements.*

Method	**Baseline**	**t_x (mm)**	**t_z (mm)**	**Stereo Angle (°)**	**Notes**
DIC Calibration	268.87	257.8	78.8	35.7	From extrinsic parameters
Motion Capture	296.25	282.0	90.8	34.6	From marker coordinates
Hand Measurement	~305	~290	~95	-	Using measuring tape

In summary, this work validated that the stereo angle produced by camera-based calibration was accurate when compared with an external motion capture system, confirming a stereo angle of approximately 35°, consistent with recommended practice for short focal lenses. This validation was performed during system development to confirm the stereo geometry externally. Since the cameras are fixed to the rig using custom brackets, the stereo angle does not change between tests. The repeatable component of the workflow is therefore the calibration procedure itself, which ensures stable camera positioning and reliable geometric accuracy for subsequent 3D DIC analysis.

4.3.3 3D DIC Analysis

Once the stereo camera setup was calibrated, image acquisition of samples was performed. Image pairs from each camera were captured before and after deformation. Analysis was conducted using the open-source 3D DIC software DuoDIC within MATLAB, which involves three steps: 2D DIC analysis, 3D reconstruction and post-processing. Details on 3D DIC analysis were included in the publication, however this has been expanded below.

2D DIC Analysis

The region of interest (ROI) and parameters were selected within the 2D DIC (Ncorr) interface enabling the displacement of subsets between reference and deformed images. This produced 2D displacement fields for each camera.

3D Reconstruction

The 2D points defined within the ROI were used to complete 3D reconstruction. This involves Delaunay triangulation [168], [169], where the 2D points are used to construct triangular faces across the sample surface, ensuring that for a given set of discrete points, P, the triangulation, DT(P), contains no point inside the circumcircle of any triangle. The described triangular faces exist in the 2D plane, so the underlying code performs further triangulation using the identified matching points from each camera together with the calibration file. This enables the 2D points and triangular faces to be mapped into the corresponding 3D positions based on the relative camera position described by the camera extrinsic parameters output during system calibration (Figure 4.3.3). Any lens distortion calculated during calibration is removed from each of the speckled images automatically. This is unlike 2D DIC software such as GOM and Ncorr, in which lens distortion must be removed manually from each of the images using a MATLAB script prior to performing DIC analysis.

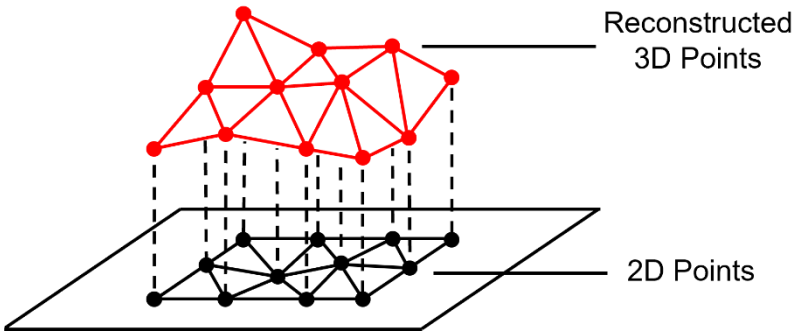


Figure 4.3.3: *Conceptual illustration showing the 2D points and triangulation from the master camera image, and how these are mapped to their reconstructed 3D positions following stereo matching between cameras.*

Post-processing

The final step involves the calculation of displacement and 3D sample deformations. This is performed for each of the triangular faces described, using Cosserat point element method. Note that the DuoDIC software enables removal of rigid body motion (RBM) from measures to account for misalignment of a given sample between imaging pre- and post-deformation. This is useful for the STAMPS3D insole application since the insole must be removed from the camera rig and worn for deformation before being placed back into the rig. Hence, any changes in placement after deformation, although minimal due to the gridded baseplate acting as a guide, will be accounted for by the RBM measure.

Additional tests were performed by shifting the insoles between pre- and post-deformation image capture by hand. The aim of this work was to assess whether the STAMPS3D system could detect misalignment between pre- and post-deformation images and apply appropriate RBM correction across different sample placements. In doing so, it confirmed whether the RBM correction procedure was robust to variations in sample positioning, ensuring that subsequent strain analyses throughout the thesis were not confounded by placement-related errors. Using the same calibration file and ROI, translations were detected in the RBM translation vector corresponding to the imposed shifts. The results are summarised in Table 4.3.3. The direction of translation reflects the geometry of the stereo rig. Shifts in the X-direction corresponds to the insole being shifted up (positive shift) or down (negative shift), while shifts in Y-direction correspond to the insole being shifted left (positive shift) or right (negative shift). Z-plane translations reflect differences in depth relative to the cameras and were observed more with larger shifts. In practice, insole repositioning is minimal, so Z-plane translations are expected to be negligible. No strain field was computed for these tests as the insoles were not deformed between image capture and only rigid-body translation was imposed.

Table 4.3.3: *RBM translation vectors produced when insole placement is shifted between images.*

Test	Shift		RBM Translation Vector
	X	Y	
1	0	0	(0.0018, 0.0034, -0.0012)
2	0	-10	(0.2215, -9.2770, -0.3887)
3	10	-10	(9.2742, -9.6733, -3.6329)
4	30	-10	(28.7327, -8.9789, -10.4017)

These results demonstrate that the RBM correction successfully captures misalignment between image capture, ensuring that displacement and strain calculations reflect true sample deformation rather than repositioning error. Minor discrepancies in values may be due to the manual repositioning guided by the 10 x 10 mm square grid on the baseplate. To minimise placement-related error in subsequent experiments, insoles were consistently aligned using this grid, and any residual misalignment was removed through RBM correction.

Strain Segmentation

A custom MATLAB post-processing script was developed to support the analysis presented in the published study (reported in the current and subsequent chapters) and to provide additional segmentation and interpretation of the raw strain fields generated by the 3D DIC workflow. Following computation of the Green–Lagrangian strain tensor, the three normal strain components (S_X, S_Y, S_Z) are extracted and used to calculate the strain magnitude (S_{MAG}). S_{MAG} represents the resultant deformation at each point and is therefore always positive. Although S_X, S_Y and S_Z are used during validation to understand directional behaviour, subsequent analysis focuses on S_{MAG} because it provides a single scalar measure that reflects the combined effects of shear- and pressure-related deformation, simplifying regional interpretation.

To enable anatomical analysis, the computed strain data is segmented using a masking protocol shown in Figure 4.2.7. The mask is scaled to the insole geometry and used to allocate datapoints into eleven anatomical regions (hallux, 2nd toe, toes 3-5, 1st MTH, 2nd MTH, 3rd MTH, 4th MTH, 5th MTH, medial midfoot, lateral midfoot and heel). Within each region, the peak S_{MAG} value is extracted to identify areas experiencing the highest localised deformation, which is clinically relevant for assessing elevated plantar loading.

Global peak values are also calculated for each repeat, however where multiple repeats are averaged, the global measure does not necessarily correspond to any single regional peak, as the location of the maximum strain can vary between repeats. For reporting, peak values (global and regional) are averaged across the three repeats, with standard deviations included to reflect variability. When data from multiple participants are analysed, a median measure is used to summarise patterns across individuals, minimising the influence of outliers that may skew using an average. This post-processing workflow ensures consistent interpretation of the strain fields and provides a link between the raw DIC output and the regional and global measures reported in the thesis.

4.3.4 Experimental Methods

To validate the accuracy of 3D DIC in capturing deformation geometry, a series of controlled tests were performed using 3D printed indenters, planar and non-planar samples and preliminary shear setups. These tests provided a framework that was progressed to assess DIC performance across increasingly complex geometries, with final methods reported in the publication.

Initial Validation Approaches

Early validation attempts involved fitting circles to cross-sections of the DIC and 3D scan data to estimate radius of curvature and its corresponding RMS error. This approach was limited by the small number of data points contained within cross-section (e.g., 6-10 points across the deformation), particularly at small deformation depths. Mesh comparison between DIC and 3D scan outputs was also attempted using CloudCompare. Initial alignment was performed manually by approximately matching the orientation of the two meshes, followed by fine registration using built-in alignment tool. Slice analysis was then used to extract cross-sections from each mesh for visual comparison. Although CloudCompare provides a function to quantify point-to-point distances between aligned slices, orientation and scale mismatches between datasets meant that the alignment error dominated the calculation differences, limiting the usefulness of this approach. In addition, the starting position for indentation tests was initially set based on expected sample thickness, which introduced error due to variability in thickness across samples.

Refinement of Test Procedure

To ensure consistent loading conditions, a revised procedure was implemented in which the indenter was lowered until a force of 0.01 N was detected, starting approximately 1 mm above the sample surface. This was repeated six times across a single sample, with DIC analysis confirming negligible deformation at this load. This procedure was adopted

to minimise error in subsequent deformation measurements and ensure consistency across tests.

Single vs Multiple Deformations

Tests comparing single and multiple indentations demonstrated that repeated deformations on the same planar sample introduced interference effects. Warping of the sample edges and delamination of the speckled pattern were observed, leading to inaccurate displacement measures. In contrast, single indentations produced more reliable results, with maximum displacement values of 2.19 mm compared to ~1.60 mm for multiple indentations. Despite these outputs, the estimated local radius of curvature was close to the expected 10 mm in both cases (10.06 and 10.01 mm). Single tests per sample were therefore adopted for subsequent experiments to eliminate any error due to interference.

Indentation Depth and Subset Spacing Sensitivity

Indentation tests using 10 and 15 mm radius 3D printed hemi-spherical indenters at depths of 0.5, 1, and 2 mm revealed high error at 0.5 and 1 mm depths. This was attributed to the small target ROI and limited number of datapoints, with only four points captured at 0.5 mm depth using the 10 mm radius indenter. To check if the subset spacing was a limiting factor, DIC analysis was repeated using subset spacing 1 and 4, increasing the number of ROI points from 4 to 103 and 15 respectively, but maximum depth values remained similar. This confirmed that errors at smaller depths were due to geometric limitations rather than DIC parameter choice, aligning with the findings from the work identifying DIC parameters in the previous chapter.

To increase the number of ROI points across the deformation, a 10 mm flat indenter with a 2 mm curved edge was trialled. While this produced larger deformation areas, significant warping and delamination were observed, particularly at greater depths (e.g. 4.51 mm measured at 2.5 mm indentation). Adjustments to edge curvature and the addition of talc had little effect. A bracket was therefore designed to hold planar samples during testing, with a 5 mm edge overlap and 4.5 mm sample space thickness, mimicking the total contact conditions of an insole.

Non-Planar Validation

Tests were extended to non-planar geometries using samples moulded to a 3D printed hemi-spherical cup with an inner radius of 45 mm. To ensure moulding of samples were uniform, an inner cup was also 3D printed with a 40 mm radius. Deformations on non-planar surfaces were smaller than expected, likely due to surface contact issues.

Sphere Fit with Edge Effect Removal

A refined post-processing method was developed to remove edge artefacts from sphere fitting for both planar and non-planar conditions. Thresholds of 0.5–2 mm were tested, with 1.25 mm edge removal selected as optimal for planar samples. This approach improved accuracy by excluding points from the transition region between undeformed and deformed surfaces. For non-planar samples, separate local and global fits were required to account for curvature changes, with edge removal thresholds of 1.9 mm (local) and 1.5 mm (global) applied.

Preliminary Shear Testing

Preliminary tests were conducted to assess the feasibility of capturing shear deformations using the Thorlabs multi-axial stage. As with the previous tests, an approach to identify the sample surface with the new setup was necessary. Based on previous data, the forces exceeded the load cells capacity for this setup, so visual identification was used. This relied on a subjective approach; however, this was performed by a single person to minimise error in identifying the perceived surface, resulting in negligible deformation. The initial tests following revealed visible flexion within the mounted parts of the setup resulting in errors in the measures captured. To address this, a rigid base plate was 3D printed so that the sample bracket was mounted directly to the stage. The maximum depth measured following deformation at 2 mm strictly in the Z-axis showed consistency with the previous planar tests. In addition to this, normal force increased consistently with indentation depth, supporting the validity of the mechanical setup despite displacement errors.

Finalised Approach for Subsequent Experiments

Based on these refinements, the following methods were implemented for subsequent experiments:

- Planar deformations: 10 and 15 mm radius hemi-spherical indenters at 2 mm depth, with 1.25 mm edge removal applied.
- Non-planar global geometry (undeformed): 40 mm radius fit.
- Non-planar local deformation and global fit: 15 mm radius hemi-spherical indenter at 2 mm depth, with 1.9 and 1.5 mm edge removal applied for local and global fits respectively.
- Shear tests: 10 mm radius hemi-spherical indenter at 2 mm depth, followed by shear distances applied as a controlled translation in the x-direction of 0, 1 and 2 mm.

These preliminary tests established a robust framework for validating 3D DIC geometry, ensuring that subsequent analyses were based on reliable and reproducible methods.

4.3.5 Case Study

Although the published case study presented the main findings, additional analysis is included here to provide a detailed comparison between 2D and 3D DIC methods. The aim of this work was to quantify baseline differences in strain measurement between 2D and 3D DIC under undeformed conditions, in order to determine whether 3D DIC provides a more accurate foundation for subsequent plantar strain analysis. This undeformed comparison complements the published case study, which examined differences in cumulative strain across ten steps during gait. Together, these components demonstrate both baseline and functional differences between 2D and 3D DIC, confirming that 3D DIC captures out-of-plane deformation that 2D DIC cannot resolve. This justified the use of 3D DIC over 2D for later plantar strain studies, demonstrating that the additional camera required for 3D acquisition provides a more representative measure of plantar deformation, with associated improvements in measurement accuracy, and therefore outweighs the increased system complexity. Peak S_{MAG} measures captured under undeformed (0% strain) samples is reported in Table 4.3.4, to demonstrate the difference in baseline error using 2D or 3D DIC analysis. Further details on the published results and analysis are included in Section 4.3.5 of the published study.

Table 4.3.4: *Average peak S_{MAG} captured using 2D and 3D DIC methods across anatomical regions of the foot for undeformed samples.*

	2D	**3D**	**3D**
Region	Peak S_{MAG} (x,y) $\times 10^{-14}$ (%)	Peak S_{MAG} (x,y) $\times 10^{-14}$ (%)	Peak S_{MAG} (x,y,z) $\times 10^{-14}$ (%)
Global	10.43	7.05	7.15
Hallux	9.77	5.36	5.95
2nd Toe	6.74	5.16	5.61
Toes 3-5	5.19	5.60	6.07
1st MTH	6.99	6.28	6.72
2nd MTH	6.77	6.79	6.40
3rd MTH	3.29	6.04	6.51
4th MTH	3.07	6.28	6.54
5th MTH	3.69	5.60	6.03
Midfoot (Medial)	4.55	6.53	7.15
Midfoot (Lateral)	6.44	6.62	6.86
Heel	9.35	6.53	6.76

Table 4.3.4 reports the average peak S_{MAG} computed using 2D and 3D DIC analysis across the three undeformed samples. In this case the expected strain across all regions of the foot was 0%. The results show that the strains calculated using each of the methods were of the same order ($\times 10^{-14}$). The results produced using 3D methods were more consistent across each region of the foot compared with that using 2D methods which fluctuated. Both measures of S_{MAG} using 3D methods show a similar pattern. This provides assurance in each of the methods, with both showing low error when compared against a known/expected strain profile.

4.4 Chapter Discussion

This chapter aimed to establish the rig setup and calibration procedures, alongside the development of a robust methodology for validating the STAMPS3D system prior to its application in the published study (Section 4.2). The preliminary tests presented were exploratory but also formed a critical part in understanding the capabilities and limitations of 3D DIC in the context of this project. The iterative refinements developed through this work underpin the methods reported in the publication and provide the foundation for the later chapters.

Before validating the system, it was essential to establish a stable DIC setup, as the accuracy of 3D DIC measures is dependent on several interconnected elements. Camera positioning, calibration quality, lighting conditions and speckle pattern characteristics together determine the reliability of resulting displacement and strain fields. The speckle pattern developed in a previous project provided sufficient variability and contrast and was retained to act as a starting point. Initial adjustments therefore focused on camera positioning and calibration, allowing the stereo angle, FOV and RPE to be optimised iteratively. Taking this approach meant that the camera pair captured the full FOV while achieving the desired stereo angle (35°) and low RPE. Independent validation of the extrinsic calibration parameters using an optical motion capture system (Qualisys) to provide an important external check on the DIC setup, but it also highlighted several limitations. The motion capture outputs for the baseline components and stereo angle were consistent across trials and broadly aligned with hand measurements, demonstrating that the overall camera geometry was stable and that the DIC calibration procedure did not produce inconsistent outputs. The differences observed in the baseline components (t_x, t_z) highlighted variability introduced by marker placement, slight differences in coordinate system origin and the lower accuracy of hand measurements, which likely contributed to these differences. Despite this, the strong agreement in stereo angle across all three methods provided confidence in the camera setup, given its influence on depth resolution, in addition to the established calibration workflow. This allowed later tests to focus solely on understanding the factors influencing measurement accuracy, rather than any error arising from the DIC setup itself.

The preliminary validation tests highlighted both the strengths and limitations of 3D DIC in capturing deformation geometry. Initial approaches, such as sphere fitting and mesh comparison, demonstrated feasibility but were constrained by small deformation sizes and alignment challenges. Refinements to the experimental setup, including the adoption of a 0.01 N load threshold for surface detection, reduced variability in initial positioning and improved reproducibility of tests, although further work could be performed to refine the threshold load for surface detection. The comparison of single versus multiple indentations showed that repeated loading introduced issues such as warping and

pattern delamination, which created interference between tests, reinforcing the decision to perform single tests per sample. Indenter design also showed variable effects. While the flat indenter increased the number of datapoints, substantial warping was generated, leading to the use of hemi-spherical indenters and a bracket to maintain planar form. For non-planar samples, uniform moulding using an inner cup ensured that the undeformed samples had a known starting geometry. Post-processing refinements, particularly the use of edge removal in sphere fits, were also necessary, as the extent of removal varied between planar and non-planar geometries, and between local and global fits. Applying a tailored, geometry-specific approach improved accuracy by excluding outliers at the transition site and was especially important for non-planar samples, where separate local and global fits were required to account for curvature changes. Similar considerations were found during the preliminary shear tests, where subjective identification of the surface and flexion in the initial rig design limited accuracy. The adoption of a rigid base plate improved consistency for the main tests, though displacement values remained slightly lower than expected due to surface detection limitations. The limitations highlighted during the initial tests helped to identify the conditions under which STAMPS3D performs reliably and informed the final methodology reported in the published study (Sairally et al., 2024).

An important outcome of this development process was the spatial resolution achievable using the final STAMPS3D workflow. In the case study presented in Section 4.2, the 3D DIC analysis generated 15,669 datapoints across the participant's insole, providing a dense strain field suitable for detailed spatial interpretation. For comparison, commonly used in-shoe measurement systems capture substantially fewer measurement locations. For example, the Pedar insole incorporates 99 sensors across the plantar surface, while the shear sensitive insole developed by Lord and Hosein includes only three sensors positioned at the metatarsal heads and heel [114]. This quantitative contrast demonstrates the markedly higher spatial resolution achieved by the STAMPS3D system and supports the statement made in the published work that this method enables high resolution plantar strain analysis.

Together, these refinements helped establish a rigorous and reproducible methodological framework for validating STAMPS3D, enabling potential transferability to other DIC-based projects. The workflow developed here also aligned with the software requirements defined in Chapter 3, ensuring that the tool-chain remained open-source, extensible to non-planar geometries and fully interoperable with MATLAB-based analysis. By addressing the sources of error and variability in the camera setup and mechanical testing, it ensured confidence in the STAMPS3D system and the use of 3D DIC as a tool for plantar strain analysis in the context of the overarching PhD narrative.

4.5 Chapter Conclusions

This chapter established the rig setup, calibration workflow, and validation methodology required for reliable application of the STAMPS3D system. By iteratively refining the camera placement, mechanical testing procedures and post-processing steps, the conditions under which 3D DIC can accurately capture insole deformation were identified, along with the limitations that must be considered when interpreting its outputs. These developments provided a robust and reproducible methodological foundation for the published validation study and for the subsequent technical work undertaken in this PhD.

While this chapter focused on the technical performance of STAMPS3D, the successful implementation of any measurement tool in clinical or real-world contexts also depends on its perceived value, usability, and acceptability by users. To address this, the next chapter presents a PPIE activity exploring stakeholder perspectives on diabetic foot ulceration, including current assessment and management practices and the challenges they face. This work then considers their perceptions of STAMPS3D and what they view as its potential applications. This transition from methodological development to stakeholder perspectives provides a bridge between technical capability and clinical relevance, ensuring that the system is influenced by both engineering and clinical considerations, supporting clinical pathways that focus on the early detection, prevention and management of diabetic foot ulcers.

Chapter 5

Engagement with Patients and Clinicians to Inform STAMPS3D Research and Development

5.1 Introduction

DFUs represent a significant clinical and economic burden, with high recurrence rates and serious consequences including infection, amputation and mortality. Despite routine foot assessments in clinical practice, gaps remain in patient awareness, communication and the integration of mechanical risk factors such as plantar pressure and shear stress. To address these challenges, the novel STAMPS3D tool has been developed to quantify plantar strain using 3D DIC, offering potential improvements in risk assessment and patient understanding.

To ensure that STAMPS3D is both clinically relevant and usable in real-world settings, patient and public involvement and engagement (PPIE) activities were conducted involving clinicians and patients. The insights gathered through this engagement will inform the development and potential clinical integration of STAMPS3D, ensuring that both clinician and patient perspectives are considered in its refinement. In addition, this work explores how STAMPS3D could fit into patient care pathways, how technology could be implemented in home and clinical settings, and potential barriers that may need to be addressed in future research. This chapter outlines the structure of the sessions, summarises the findings and reflects on the implications for future research in diabetic foot care.

5.2 Methodology

5.2.1 Overall Approach and Objectives

This chapter reports on a PPIE activity that sought stakeholder input to help shape the future development and evaluation of the STAMPS3D system. Rather than setting formal research objectives, the sessions were designed to gather practical insights from clinicians and patients to inform the kinds of questions future research should address, how studies using novel equipment might be conducted and how best to involve and

recruit people into such work. Specifically, we asked contributors to share their experience of diabetic foot care, reflect on the strengths and limitations of current assessment practices and comment on the potential role, feasibility and usability of STAMPS3D in both clinical and home environments.

This activity was conducted as an involvement exercise rather than a formal research study, meaning ethical approval was not required. Nonetheless, sessions were designed and delivered in line with best practice for working with potentially vulnerable groups, ensuring informed consent, confidentiality and sensitivity.

Development of this activity was in line with Responsible Research and Innovation (RRI) principles and the Anticipate, Reflect, Engage and Act (AREA) framework [170] set by the Engineering and Physical Sciences Research Council (EPSRC):

Anticipate - Anticipate possible implications for patient care, healthcare workflows and societal issues. This is in addition to challenges related to accessibility, usability and clinical applicability. Anticipate that there may be a lack of understanding around the need for risk identification techniques and, in particular, the social and financial costs associated, in regard to diabetes-related foot health conditions.

Reflect - Reflect on feedback given from various groups. For example, patients may focus on areas such as usability and comprehending the technique itself or need for it, whereas healthcare professionals may instead focus on clinical applicability and implementation of the tool into practice. In doing so, STAMPS3D can be evaluated in consideration of multiple stakeholders who may interact with it differently.

Engage - Engagement with the public, patients and healthcare professionals to gather diverse insights from groups outside of research, ensuring that it is relevant and practical. This enables research development which addresses real-world issues and is that which is conducted inclusively and responsibly.

Act - Act upon the insights from contributors to shape how future research with STAMPS3D is designed and delivered. This includes ensuring that studies are inclusive and accessible, that recruitment approaches reflect what clinicians and people with lived experience consider acceptable, and that future research questions address the priorities identified during the sessions. The feedback will also guide how information about the system is communicated, how contributors are supported to take part, and how the research environment can be made more comfortable and engaging for those involved.

5.2.2 PPIE Engagement

5.2.2.1 PPIE Groups

Recruitment of a diverse PPIE group was achieved through multiple channels, including diabetes care clinics, podiatry and orthotics practices, with a focus on achieving a balanced representation of individuals in terms of age, gender, ethnicity and clinical setting. Three stakeholder groups were engaged:

1. Clinician Group 1: Leeds Diabetes Limb Salvage Service team members (LDLSS), 30-minute session consisting of 8 individuals.
2. Clinician Group 2: Bradford Diabetic Foot MDT Team 60-minute session consisting of 15 individuals.
3. Patient Group: 2-hour session consisting of 7 individuals living with diabetes, both with and without experience of DFUs.

PPIE members included podiatrists, orthotists and individuals living with diabetes, both with and without experience of foot ulceration. This mix of professional and patient perspectives enabled an understanding of both clinical practice and lived experience.

5.2.2.2 Session Format and Facilitation

Each session explored three key areas to inform the design of future research involving the STAMPS3D system:

Key Area 1. Awareness and knowledge of DFUs.
Key Area 2. Perceptions of current assessment methods.
Key Area 3. Acceptance and attitudes towards the STAMPS3D tool.

Sessions began with an introduction to DFUs and the STAMPS3D tool, including a short video demonstration and handouts illustrating strain maps. Contributors were encouraged to discuss openly, with questions used to prompt conversation. Questions asked during these sessions are included in Appendix C.1.

Sessions were facilitated by the PhD candidate, with co-facilitation support from clinicians to ensure safeguarding and sensitivity. All sessions were recorded so that the PhD candidate could concentrate on listening to PPIE members and subsequently identify key areas for future research. No direct quotes or identifiable data were retained.

5.2.2.3 Ethical Considerations

Although formal ethics approval was not required, ethical integrity was prioritised for the PPIE activity. Contributors received an information sheet outlining the purpose, format

and confidentiality of the sessions. Consent was obtained prior to recording, and individuals were free to withdraw at any time. Discussion materials and questions were reviewed by the supervisory team and the National Institute for Health and Care Research (NIHR) Biomedical Research Centre (BRC) PPIE team to ensure appropriateness and sensitivity.

5.2.2.4 Funding and Resources

The activity was supported by a NIHR BRC £500 RRI award. This funding enabled reimbursement of travel expenses, refreshments and the commissioning of a graphic artist to produce illustrated summaries of the discussions. Sessions were hosted at St James Hospital, Thornbury centre and Healthwatch Leeds.

5.2.2.5 Reviewing and Summarising the Discussions

Recordings and notes from the sessions were revisited to help us reflect on what contributors had shared. Comments were organised broadly by discussion topic and by stakeholder group (clinicians and people with lived experience), and the main points were summarised in plain language rather than captured by verbatim. These summaries were then used to create visual infographics, produced by a commissioned graphic artist, to make the insights more accessible and engaging.

We looked across the different groups to identify where views aligned or differed, and to understand what contributors felt was important for future research involving STAMPS3D. This process helped highlight practical considerations for study design, recruitment and communication, as well as areas where further exploration may be needed. Clinicians provided insights into how data should be presented and interpreted, while patients highlighted usability in everyday settings. This feedback will guide future improvements in material selection and data capture methods, ensuring better integration into patient routines and clinical pathways. Accordingly, this activity was designed to provide information on the following topics:

- Identifying the main areas of clinical utility for STAMPS and how it may then integrate into existing diabetes foot care pathways as well as everyday patient life.
- Evaluating alternative materials to improve comfort and usability, while maintaining data accuracy.
- Exploring the potential to collect complementary data. For example, walking characteristics like speed will allow us to better understand plantar load and improve clinical applicability. However, we need to understand if people would find this obtrusive. This has the potential to inform treatment and prevention strategies for DFUs.

- Adapting data collection methods to enable longer durations of wear and capture strain during daily activities, increasing applicability outside of clinical settings.

5.2.3 Clinical Stakeholder Engagement

To complement the inputs gathered through the PPIE groups, engagement with two clinicians who had experience using the STAMPS system with patients in parallel clinical studies was conducted. The clinical stakeholder engagement explored the practical realities of implementing the STAMPS system within a clinical setting and provided user insights that could not be captured through the PPIE activity alone. Discussions were similarly guided by prompt questions and focused on areas including:

- General usability of the tool: fabrication, handling and workflow.
- Patient interaction with the tool: comfort, stability and ease of use.
- Analysis and post-processing: feasibility of current MATLAB-based pipeline
- Areas of improvement to support clinical usability and integration into clinical pathways.

5.3 Collective Review of Findings

The PPIE activity generated a wide range of insights into how clinicians and patients view DFU assessment and the potential role of the STAMPS3D tool. To make sense of what was shared, the discussions were reflected on across the three key areas introduced in Section 5.2.2.2. For each area, we outline what contributors told us, noting where views aligned or differed between stakeholder groups.

To provide an overview of the language used across groups, a word cloud was also generated from the group summaries (Figure 5.3.1). This highlights the most frequently mentioned terms, with words such as ‘patient’, ‘pressure’ and ‘tool’ appearing prominently. The word cloud offers a visual snapshot of recurring concerns, which are explored in greater depth through the summary of findings below.

Graphical summaries from the clinician and patient groups, as well as common themes across groups are also presented in Figure 5.3.2, Figure 5.3.3 and Figure 5.3.4. Research articles produced highlighting outcomes from this chapter’s work are included in Appendix C.2.

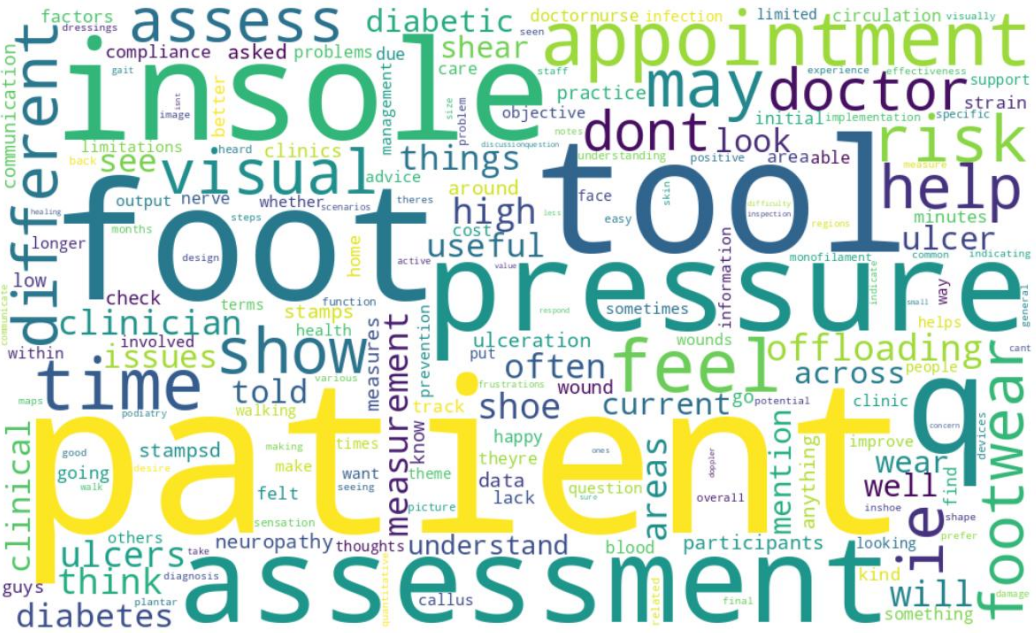


Figure 5.3.1: *Word cloud generated from group summaries, illustrating the most frequently used terms across clinician and patient discussions.*

5.3.1 Key Area 1: Awareness and Knowledge of DFUs

Clinicians across both groups described DFU assessment as a multifactorial process, drawing on circulation, diabetes control, neuropathy and footwear as key elements. In Leeds, clinicians emphasised wound-specific assessments, including probing for depth, measuring size and photographing ulcers to track progression, often using these to communicate findings with patients. Bradford clinicians highlighted structured risk stratification, categorising patients into low, medium or high risk and tailoring advice accordingly. Across both groups, assessments also incorporated broader indicators of foot health, such as callus formation, areas of high pressure, previous ulceration or amputation, and signs of Charcot foot when present. Clinicians noted that their involvement spans different stages of the patient pathway, from initial screening at diabetes diagnosis to annual reviews and ongoing prevention or management, resulting in variable frequency of assessments. Despite this variation, both groups relied heavily on visual inspection and physical measurements, supported by tools such as Doppler waveforms, monofilaments and tuning forks to assess vascular and neurological function. Importantly, neither group reported routine measurement of plantar shear stress, reflecting a gap in current practice.

In contrast, patients demonstrated limited awareness of DFUs prior to the session. Most had not heard of the condition and of those who had, often learned through personal experience of ulceration or infection rather than explanations from clinicians. Causes

identified included poor circulation, inappropriate footwear, friction from shoes or bed sheets and nerve damage. Several contributors described experiences of cellulitis and related complications, which had shaped their understanding of foot health risks. However, many expressed uncertainty about what a DFU actually was and how it might be prevented, highlighting a lack of consistent education during routine appointments.

Taken together, these findings reveal a clear gap between clinical knowledge and patient awareness. Clinicians possess detailed technical understanding of DFU risk factors and general practices, but patients often lack even basic information about the condition. This disconnect reinforces the need for future research to explore how information about foot health can be communicated more effectively, and how tools such as visual aids might support understanding and engagement. Contributors' reflections suggest that research involving STAMPS3D should consider not only the technical aspects of the system, but also how visual outputs could be used to support education, shared decision-making and risk prevention.

5.3.2 Key Area 2: Perceptions of Current Assessment Methods

Clinicians in both groups expressed mixed confidence in the tools currently available for DFU risk assessment. Vascular assessments were generally seen as reliable, with Doppler waveforms and pulse checks forming routine practice. However, neuropathy testing was consistently described as a weak area, with monofilament use regarded as subjective and insufficient for early detection. Leeds clinicians highlighted the absence of in-shoe pressure measurement devices and limited access to gait labs, while Bradford clinicians emphasised the broader issue of time and cost constraints that restrict the use of advanced technologies. Both groups noted that assessments often rely on visual inspection and patient history, which, while practical, lack the objectivity needed to guide treatment decisions. A recurring frustration was the difficulty of monitoring patient behaviour outside the clinic, particularly compliance with offloading approaches.

Patients described their experiences of foot checks as fragmented and rushed. Appointment slots were often limited to 15 minutes, leaving little time for detailed discussion. Continuity of care was a major concern, with contributors reporting seeing different doctors or nurses at appointments, which led to repeated explanations and a sense of being treated as 'just a number'. Communication was frequently basic, with advice restricted to moisturising or checking feet, and few patients recalled being categorised into risk levels. Several contributors expressed frustration at the difficulty of accessing timely appointments, noting long waits and challenges in booking. Others felt that information was not tailored to their needs, leaving them uncertain about whether they were managing their foot health appropriately.

These findings highlight systemic limitations in current practice. Clinicians emphasised the lack of objective tools and resource constraints, while patients raised issues regarding communication gaps and the absence of continuity. Time pressures emerged as a shared barrier across groups, affecting both the thoroughness of clinical assessments and the quality of patient education. These insights point to several areas where future research is needed. This includes how objective measurement technologies might be integrated into routine care, how information can be communicated more effectively, and how appointment structures could better support understanding and engagement. These issues raised by contributors therefore help shape the questions and priorities that future studies involving STAMPS3D should address.

5.3.3 Key Area 3: Acceptance and Attitudes Towards the STAMPS3D Tool

Clinicians across both groups responded positively to the demonstration of the STAMPS3D tool, recognising its potential as both an educational aid and a clinical assessment device. Leeds clinicians emphasised its value in helping patients understand the link between strain (indicative of pressure and shear) and the development of calluses or ulcers, particularly for those who struggle to accept that their footwear or walking patterns contribute to their condition. They saw the tool as a way to provide concrete, visual evidence that could improve compliance with offloading strategies. Bradford clinicians similarly highlighted the strength of visual strain maps, noting that clear graphical outputs could support patient communication and motivate behavioural change. In addition, they valued the potential for quantitative data to standardise risk categorisation and track changes over time, especially where multiple clinicians are involved in a patient's care. Practical considerations were also raised, including the need for efficiency in busy clinics, compatibility with different footwear and automation of post-processing to reduce workload and minimise error.

Patients expressed enthusiasm for STAMPS3D, describing the visual strain maps as clear, accessible and empowering. They appreciated the opportunity to see and track changes in their own feet over time and felt that such outputs would help them understand whether treatments or footwear were effective. Several contributors welcomed the idea of home use, provided the insoles were easy to insert and instructions were clear. Cost and simplicity were valued, with patients noting that current insoles are often purchased privately without guidance, leaving them overwhelmed by choice. Importantly, patients emphasised that clinician involvement remained essential and that while they were happy to use the tool, they wanted doctors and nurses to interpret the results and integrate them into their care.

These findings reveal positivity toward STAMPS3D across both clinicians and patients, but with differing priorities. Clinicians focused on workflow feasibility, integration into existing pathways and the need for objective data to support decision making. Patients emphasised usability, communication and empowerment, seeing the tool as a way to bridge gaps in understanding and continuity of care. Across groups, visual outputs were consistently highlighted as a way to improve understanding and engagement. These insights point to several areas where future research is needed. This includes how visual strain information can best support shared decision-making, how the tool might be used in real-world clinical and home settings, and what practical considerations should shape study design and recruitment. Contributors' views therefore help guide the next stages of research involving STAMPS3D and highlight the questions that future studies should address.

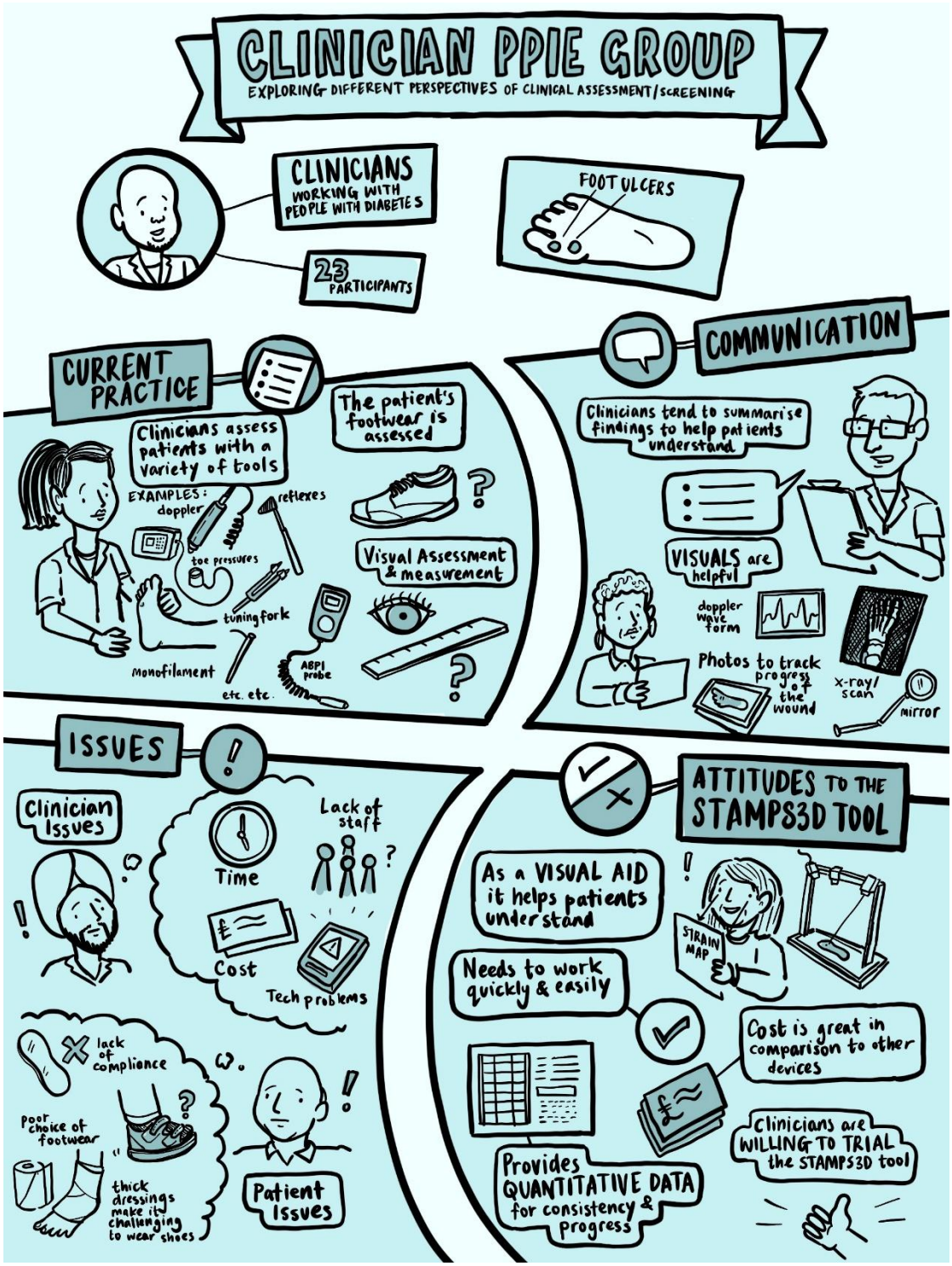


Figure 5.3.2: *Graphic summary of clinician perspectives on DFU assessment and STAMPS3D.*

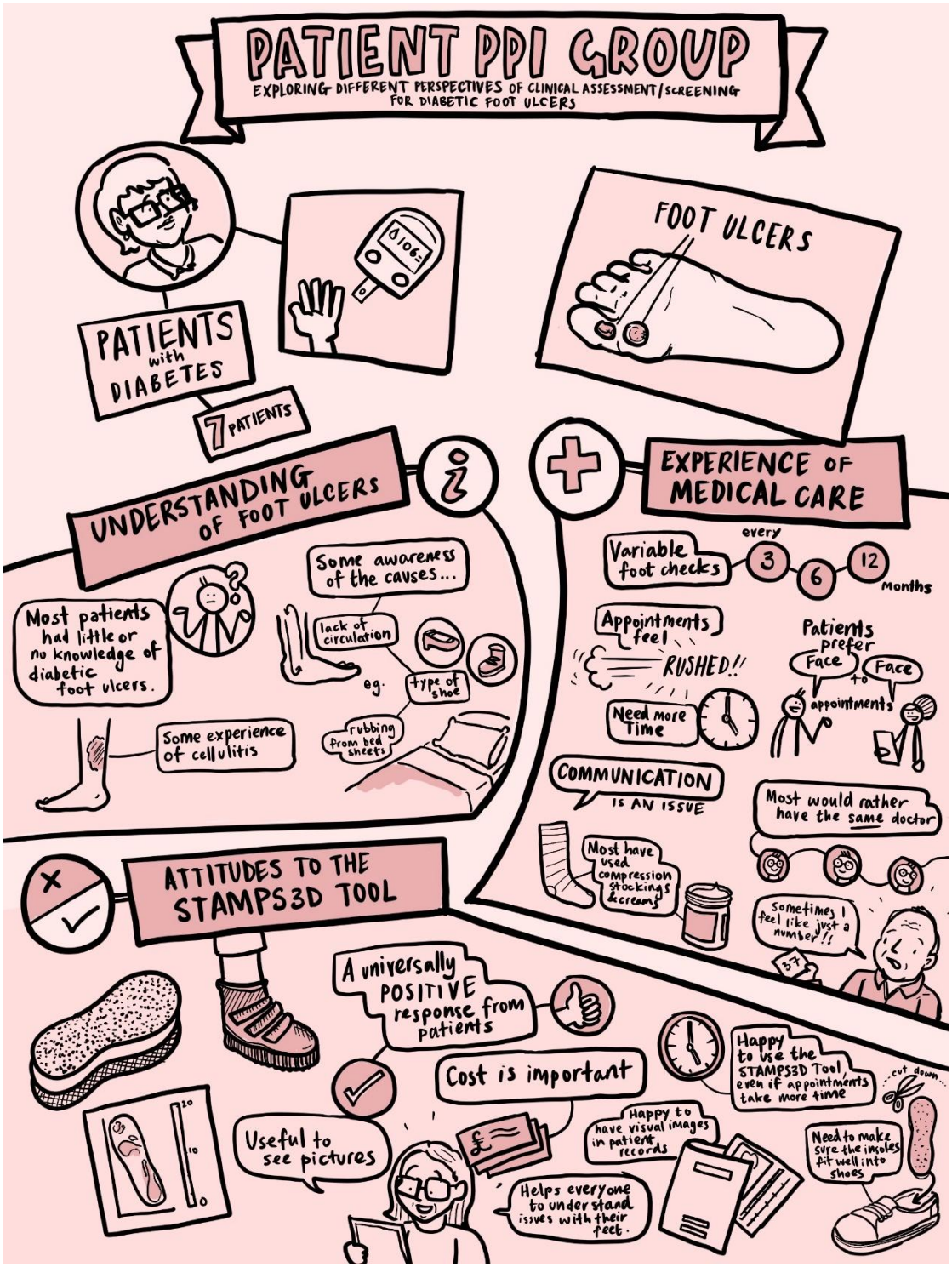


Figure 5.3.3: *Graphic summary of patient perspectives on DFU assessment and STAMPS3D.*



Figure 5.3.4: *Graphic summary of common themes across clinician and patient groups.*

5.3.4 Summary of Clinical Stakeholder Feedback

In addition to the insights gathered from the PPIE stakeholder discussions, reflections from two clinicians who used the STAMPS system with patients shared important insights into the system's practical implementation. These insights offer useful context for shaping future research questions and understanding the practical considerations that may influence clinical usability.

Clinicians highlighted several positive aspects of the system. The found the walking and image-capture process straightforward and noted that patients generally responded well to using the insole. Compared with systems such as Pedar, the absence of trailing wires was seen as a clear advantage. The ability to select specific regions of interest was valued and the visualisation of outputs was described as intuitive and helpful for communication. Both clinicians appreciated the innovation behind the system and felt that its low per use cost and clear visual outputs could support wider global health applications, particularly in settings where access to advanced gait technologies is limited.

Alongside these strengths, the clinicians also identified practical challenges. The current insole materials were described as sensitive to temperature, bulky to store and prone to distortion during insertion or removal, sometimes requiring repeat trials. Maintaining strict control over step counts, preventing early loading and managing waiting times between repeats were difficult within standard appointment slots. These waiting periods arise because, after each walking trial, the insole must be removed to capture a post-deformation image and then prepared for the next pre-deformation image before reinsertion. The software and post-processing pipeline were viewed as too complex for routine clinical use, requiring specialist training and involving coding environment that may be intimidating for non-technical users. Importantly, the clinicians could not determine whether the data were usable until after analysis, meaning that issues could not be addressed while the patient was still present. Together, these factors made the current workflow too time-consuming for typical clinical appointments.

The clinicians also shared views on how a future workflow might operate. They expressed interest in a fully streamlined and automated pipeline in which image capture, whether during an appointment or over a longer duration, is followed by a single action that completes both the analysis and post-processing, then generating a printable custom insole reflecting the strain outputs measured. As such, they emphasised the need for an orthotist-centred workflow requiring minimal specialist training, real-time quality checks to allow immediate repeats where needed, and clarity around where STAMPS might sit within screening pathways (e.g., diabetes reviews, high-risk monitoring or follow-up after ulceration). They also noted the system's potential as an educational too

and its relevance for global health contexts. A visual summary of the shared insights is presented in Figure 5.3.5.

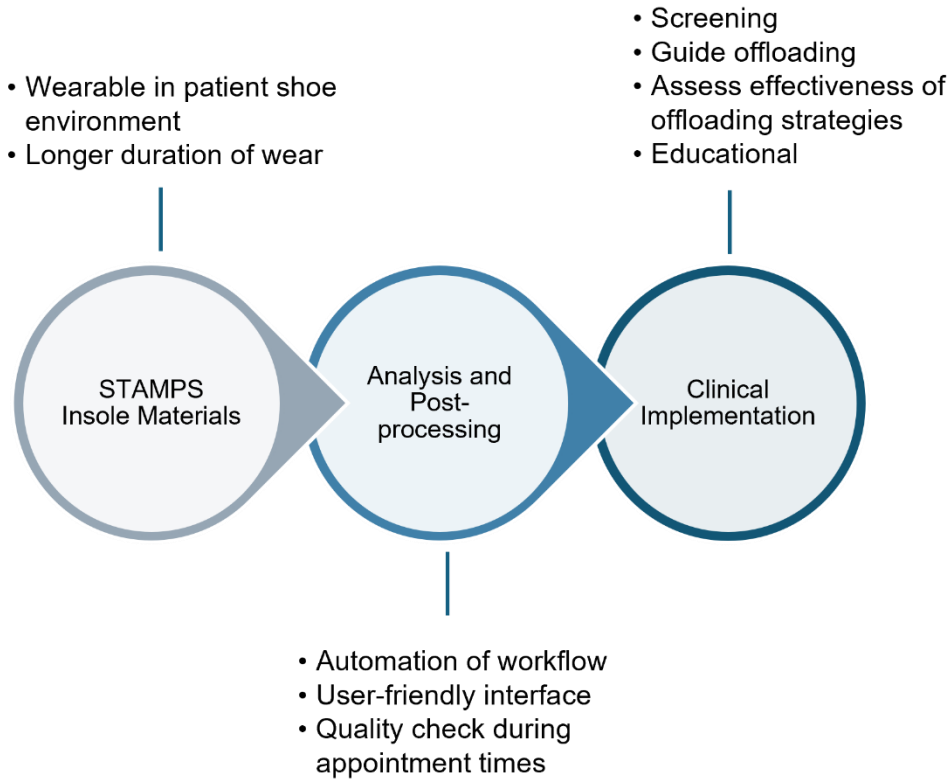


Figure 5.3.5: *Key areas identified by clinicians as priorities for enabling implementation of the STAMPS system.*

5.4 Chapter Discussion

This chapter interprets the insights generated through the PPIE activity, using the summarised findings to contextualise stakeholder views within diabetic foot care and the ongoing development of the STAMPS3D system. Instead of formal qualitative analysis, this discussion explores the three key areas in relation to existing clinical and patient pathways and highlights how these perspectives can inform the design of future research involving STAMPS3D, including questions around DFU prevention, patient engagement and the system's potential role in clinical pathways. In doing so, it demonstrates how stakeholder feedback can guide technical changes to the system and its integration into routine clinical care.

Across the three key areas, the PPIE activity highlighted a set of common themes and gaps within current diabetic foot care. Clinicians demonstrated strong technical knowledge, yet patients had limited understanding of DFU risk, which reflects short appointment times, communication challenges and additional barriers for those with

language needs or disabilities. Both groups recognised that the existing assessment methods used heavily rely on visual inspection and subjective judgement, with a lack of accessible technologies such as in-shoe pressure devices. These constraints, combined with staffing pressures and the inability to track patient compliance outside of a clinical setting, limit opportunities for early and objective risk identification.

Despite these limitations, there was clear enthusiasm around the potential applications of STAMPS3D. Clinicians valued the tool's ability to provide objective strain data, visualise what occurs inside the patient's shoe and support consistent decision making on patient foot care, including evaluation of orthotics and offloading strategies. Patients found the personalised visual outputs particularly informative and empowering, enabling greater involvement in their clinical care. A key aspect was that both groups viewed the STAMPS3D tool as a complement to, rather than a replacement for clinical expertise and highlighted practical needs such as compatibility with patient footwear, ease of home use and automated post-processing of data. Overall, the insights gathered indicate that STAMPS3D aligns with the current gap found in DFU care, particularly around communication, education and early risk identification, while offering a low-cost and customisable approach that could be integrated into existing pathways.

In interpreting these findings, several methodological considerations must be acknowledged, as the design and delivery of the PPIE activity shaped both the depth and nature of the perspectives captured. This PPIE activity was designed as an involvement exercise rather than formal qualitative research, which meant that discussions were summarised rather than line-by-line interpretation, resulting in a higher-level summary of findings. However, this less structured format may have supported a more relaxed conversational environment, enabling contributors to speak more freely. The duration of sessions varied, being dependent on stakeholder availability, which influenced the number of questions explored and the depth of discussion. To address this, questions were adapted to ensure that all groups contributed across the key areas. Group size also varied, with the larger clinician session making it challenging to capture contributions from all contributors, while smaller groups created a more intimate setting that facilitated clarification, engagement and ease of demonstrating the STAMPS3D tool. A key strength of the activity was the inclusion of a broad range of stakeholders, bringing together both clinical and patient perspectives. The combination of structured prompt questions, verbal explanation and visual aids helped maintain a shared pace of understanding, particularly for patients, supporting meaningful engagement with the sessions.

These insights were complemented by reflections from two clinicians who had previously used the STAMPS system with patients. Although based on limited experience, their observations cross-over several points raised in the PPIE discussions. Like the wider

stakeholder groups, they valued the clarity of the visual outputs and the potential for the tool to support communication and shared understanding. They also highlighted practical considerations around workflow, time pressures and the need for streamlined processes, aligning with broader concerns about the feasibility of integrating new technologies into routine care. These converging insights reinforce the importance of future research that examines not only the technical performance of STAMPS3D, but also its usability, acceptability and fit within real clinical pathways.

From this, several important implications for future development of STAMPS3D have been highlighted, both within and beyond this PhD. The system offers a unique opportunity to capture objective in-shoe strain data indicative of both pressure and shear, with clear potential to enhance early risk identification, guide management strategies and evaluate their effectiveness over time. Building on this, the next stages of work within this PhD will explore the application of STAMPS3D to contoured insoles to determine whether 3D strain patterns can be reliably captured across different orthotic materials and local stiffness variations, and to examine how strain distributions relate to callus formation and DFU risk. Although the current plasticine-based insole offers customisability, its use is restricted to controlled footwear and environments. Future development beyond this PhD will therefore focus on identifying alternative materials that reduce fabrication time, support use in patients' own shoes, and allow data collection across natural gait and daily activities. Alongside these technical refinements, further work beyond this PhD will also consider the automation of DIC post-processing to streamline clinical workflows. Together, these directions form the basis for the proof-of-concept studies presented in the following chapters, with additional opportunities for system enhancement extending beyond the scope of this PhD and representing longer-term development priorities for the system.

5.5 Chapter Conclusions

This chapter has examined the perspectives of clinicians and patients gathered through the PPIE activity, highlighting current gaps in diabetic foot care and how these inform the ongoing development of the STAMPS3D system. Across the key areas, contributors identified persistent challenges in communication, limited access to objective assessment tools and the constraints of time and staffing that shape routine practice. Despite these barriers, both groups expressed strong enthusiasm for the potential of STAMPS3D to provide objective in-shoe strain data, enhance patient understanding, and support more consistent clinical decision-making. Methodological reflections acknowledged the format of the work, variability in session structure and the value of combining verbal discussion with visual aids to support engagement.

The insights shared by contributors point toward clear priorities for future research, including exploring STAMPS3D's application to contoured insoles, assess its ability to detect differences in strain across orthotic materials and investigate how strain patterns relate to callus formation and DFU risk. These areas underpin the proof-of-concept studies presented in the following chapter, which begin by evaluating the capability of STAMPS3D to measure plantar load in contoured orthoses.

Chapter 6

Measuring Plantar Load with STAMPS3D: A Preliminary Study on the Impact of Contoured Orthoses

The work reported in Section 6.2 of this chapter has been published as:

Francesca Sairally, David A. Russell, Heidi J. Siddle, Kate Chauhan, Daniele Trinca, Claire Brockett and Pete Culmer. *Frontiers in Bioengineering and Biotechnology*, 13, p.1648649. (2025)

Journal Article: https://doi.org/10.3389/fbioe.2025.1648649

Dataset DOI: https://doi.org/10.5518/1706

6.1 Preface

This chapter reports a proof-of-concept study that explores the feasibility of capturing 3D strain data across the non-planar surfaces of contoured orthoses using the STAMPS3D system. In this context, orthoses refer to custom or prefabricated insoles shaped to match the contoured geometry of an individual's foot and designed to redistribute plantar load, support foot structures, or offload high-risk regions. The work reported in Section 6.2 was published as 'Measuring Plantar Load with STAMPS3D: A Preliminary Study on the Impact of contoured orthoses'. It addressed the questions raised from the PPIE activities (Chapter 5) on whether STAMPS3D could be applied to contoured orthoses and Objective 4 of this project. Demonstrating this feasibility is an important step toward using the system to potentially inform offloading strategies and evaluate the effectiveness of orthotic interventions.

As first author, my contribution to the paper comprised the design and performance of the case study, calibration of the STAMPS3D system (as described in Chapter 4) and all data processing, analysis, interpretation and writing of the manuscript. The dataset generated from the study is in the Research Data Leeds Repository (DOI: https://doi.org/10.5518/1706). Section 6.3 presents unpublished preliminary work with associated supporting data. This provides additional details on the mechanical testing, moulding development and preliminary tests that led to the final methodology. Sections 6.4 and 6.5 present the Discussion and Conclusions, summarising the key findings and limitations of the preliminary work and outlining how they inform the design of the final study.

6.2 Publication

The following publication presents a proof-of-concept study examining plantar strain behaviour under different orthotic conditions. To support interpretation of the findings discussed within the thesis, three research questions are provided to clarify the specific areas of focus within this work:

- Can STAMPS3D successfully capture cumulative plantar strain across a contoured orthotic surface, and do strain patterns differ between flat and contoured substrates in a way that reflects the load-redistribution effects reported in the orthotic literature?
- Can STAMPS3D detect differences in plantar strain arising from orthoses with different material stiffness, despite the combined mechanical behaviour of the orthosis and STAMPS insole system?
- How do plantar strain patterns measured using STAMPS3D relate to plantar pressure patterns measured using a commercial in-shoe system (Pedar)?

Abstract

Introduction: Diabetes-related foot disease including foot ulcers (DFU) are a growing concern with a huge associated socio-economic impact. Bespoke contoured orthoses are a common clinical intervention used to help prevent DFU formation in regions at risk through offloading, by implementing various design features such as arch support, cuts-outs, metatarsal pads and variable density materials. Research surrounding contoured orthoses has been limited to measuring plantar pressure to assess effectiveness and guide insole modifications necessary for individual patients. However, there is currently no in-shoe measurement tool capable of measuring all components of plantar load (plantar pressure and shear stresses).

Methods: The STAMPS3D system has been developed to address this gap and has been successfully shown to measure the cumulative effect of plantar strain indicative of pressure and shear stresses that arise at the plantar interface. In this work, the STAMPS3D system has been used in a proof-of-concept study to explore the efficacy of capturing 3D strain data across a non-planar surface of different contoured orthoses.

Results: Plantar strain patterns were shown to vary across anatomical regions of the foot, with statistically significant increases in plantar strain found for contoured conditions across the midfoot due to offloading associated with contoured orthoses. Differences in plantar strain were also observed across the toe and forefoot regions as a result of changing the material stiffness of the orthoses.

Discussion: This work demonstrates the utility of employing 3D measurement to improve our understanding of plantar load under the influence of design features implemented in contoured orthoses and their ability to offload regions at risk of DFU formation. In doing so, improvements in management and prevention of diabetes-related ulceration can be made, tackling the social and financial costs associated.

Introduction

The global population with diabetes is a growing concern with an expected increase in prevalence from 537 million to 783 million from 2021 to 2045 [164]. Consequently, a rise in associated diabetes-related foot health complications is also expected, with up to 25% of people with diabetes developing a diabetic foot ulcer (DFU) during their lifetime [41]. DFUs place a significant burden on both patients and the healthcare system. For those who develop a DFU, roughly 20% will remain unhealed at one year, with 65% experiencing subsequent recurrence within five years after successful healing [39], [41]. The mortality rate at 5 years is approximately 40%, increasing to more than 70% after amputation [41], [46]. The resulting financial cost is significant with estimates of up to £1 billion or 0.9% of the NHS England annual budget spent between 2014-2015 [44].

To address the social and financial costs associated, a set of guidelines on the prevention and management of diabetes-related foot disease was developed by the International World Group on the Diabetic Foot (IWGDF) [28]. Additionally, prevention was identified in 6/10 of the top diabetic foot research priorities set by the National Institute for Health and Care Research (NIHR) James Lind Alliance [91]. This has driven the development of assessment techniques used as a predictive tool for DFU formation, such as the emed® (Novel GmbH, Munich, Germany) pressure platform and Pedar® (Novel GmbH, Munich, Germany) in-shoe system. However, commercial measurement systems can be expensive making them less accessible for clinical use and are limited to capturing the pressure component of plantar load. Plantar load comprises of vertical (plantar pressure) and tangential (plantar shear stress) components. Increased plantar pressure has been reported in people with diabetes and even more so in those with existing DFUs, associating it with DFU formation [96], [101]. Although research on the influence of plantar pressure on DFU formation is extensive, peak plantar pressure alone is an unreliable marker for ulceration [96], [171]. Veves et al found that only 38% of ulcers were located at peak pressure sites, with others reporting that ulceration could still occur at pressures that are commonly considered normal [101], [102]. This suggests that there may be other factors contributing to the development of DFUs. Pollard et al found that ulcer formation occurred at both peak pressure and peak shear sites but the dominant mechanical force of the two was unclear [82]. A recent systematic review of 16 studies investigating plantar shear stress in people with diabetes showed that patients with an existing or pre-existing DFU displayed increased shear stress levels in contrast to those without ulceration [90]. Although plantar pressure and plantar shear have been described as influential in DFU formation, the technical demands of capturing both components of plantar load simultaneously have limited the availability of appropriate measurement instrumentation, particularly for plantar shear. Within research settings measurement systems have begun to address this gap. Yavuz et al developed a custom measurement platform with 80 embedded sensors, capable of capturing all components of plantar load [111], [112]. However, this technique is limited to capturing unshod conditions and therefore data is not representative of the plantar loads that occur while wearing shoes over a period of gait. More recently, in-shoe measurement devices have been reported capable of determining both plantar pressure and shear load components, employing electronic sensors either adhered to the plantar surface or imbedded in an insole, examples include [113], [114], [166]. Machine-learning techniques have also been used to enhance the measurements obtained from sensing elements within such in-shoe systems, demonstrating the potential to predict features such as tissue deformation, tissue injury risk and abnormalities occurring during gait [172], [173], [174]. While these advances demonstrate the potential for combining real-time in-shoe plantar load measures with AI-based analysis, their spatial resolution is constrained by the number of sensing elements on the plantar surface (typically N=4-8) and their positioning.

Accordingly, our work at the University of Leeds has pursued an alternative approach for full-field plantar load characterisation through development of the STrain Analysis and Mapping of the Plantar Surface (STAMPS) system [116]. This technique comprises a multi-layer plastically deformable insole together with Digital Image Correlation (DIC) to record the cumulative plantar strain after a period of gait. This differs from sensor-based systems which capture real-time data, but this approach enables high spatial resolution of the data captured across the plantar surface. Additionally, this system allows for high adaptability compared to other devices, in which the size and shape of the insole can be tailored to user requirements. The STAMPS system initially used a 2D DIC approach, which has been successfully validated in a number of studies, including a study of 18 participants identifying a range of 'normal' values within a healthy cohort [115], [116], [117]. Use of STAMPS with 2D DIC showed the potential to characterise plantar load, but its application is limited to planar surfaces and therefore measures may not accurately record contoured surfaces of the foot. To address this limitation, we have developed STAMPS3D, enhancing the original STAMPS system with 3D DIC techniques to enable the capture of 3D strain measures [175].

Currently, clinicians act to reduce risk of ulceration by offloading clinically indicated areas of high plantar load e.g. site of callus or previous DFU. Plantar pressure measurements are used within research to measure the effect of interventions such as contoured orthoses. However, due to the complexities and time needed for data capture and analysis, the available pressure measurement systems are not routinely used in clinical practice. The insole design features for offloading vary, including arch support, shape, thickness, material stiffness or hardness and variable stiffness/density across an insole [176]. Modifications can also be made through material cut-outs or addition of corrective pads [176], [177]. For insole designs that are implemented based on both pressure data and the individual's foot shape, offloading was found to be more effective [177]. In particular, improved forefoot offloading has been reported where multi-density, lower stiffness materials are used to make contoured orthoses, with increased arch support found to further reduce plantar pressures in the forefoot region [177]. Overall, the literature indicates that offloading is more effective using contoured orthoses with custom arch supports in comparison to those that are completely flat, in addition to material stiffness being influential in how well the foot is offloaded. In cases where in-shoe pressure measurements were used to modify footwear (in particular to the insoles), together with high patient adherence, risk of DFU recurrence was reduced by more than 50% [178]. Footwear modifications alone were found to relieve peak plantar pressures in local regions by 30%, however this varies among the literature with some showing conflicting results [179]. This may be due to difficulty in distinguishing design features that have the greatest impact on offloading or other contributing factors that lack investigation, such as shear [176], [179], [180]. Current literature focusses only on

plantar pressure, hence the STAMPS3D system offers an approach that has the potential to measure plantar strain indicative of all components of strain at the orthosis-foot interface, to identify whether differences can be identified for insole design features such as material stiffness and arch support.

This paper presents a proof-of-concept study to investigate whether STAMPS3D can be used to capture 3D strain data across the orthosis-foot interface and to identify the impact of contoured orthoses varying in stiffness compared to normal flat conditions. By evaluating how orthosis design influences strain distribution, this work builds on previous research demonstrating the potential of STAMPS3D for DFU risk prediction and supports applications in preventative clinical strategies.

Materials and Methods

A proof-of-concept study consisting of five healthy participants was conducted. Ethical approval was obtained from the University of Leeds Ethics Committee to conduct this study (EPS FREC-2024 1462-2517). Prior to assessment, participants read the participant information sheet and provided written consent. Participants were included if they were >18 years old and capable of walking unaided for 50 metres. Individuals were excluded if they were diagnosed with diabetes or associated foot health conditions.

Insole Fabrication

Foot impressions were taken by a qualified orthotist using a foam impression box. The impressions were scanned and used to create a 3D mesh, prior to 3D printing the bespoke contoured orthoses. Variation in the stiffness of the printed orthoses was achieved by adjusting the infill settings within a proprietary software, which uses a numeric scale to control infill density. This manufacturing process was conducted by an orthotics company (Steeper) that supply the NHS. For each participant, two pairs of contoured orthoses were printed defined as being either low (setting 1.3) or high (setting 5) stiffness. The stiffness of the insoles was controlled through the density of the print, temperature and speed of the 3D printer (Arkad P1, Qwadra, France), selected to ensure each insole type was significantly different. More detailed print-specific parameters such as temperature and head-speed are not directly accessible from this commercial software. An additional 1.5 mm Ethylene Vinyl Acetate (EVA) foam layer was added to the top of each insole as a standard feature for all contoured orthoses.

The development of the STAMPS system and the subsequent 3D DIC enhancement has previously been described [116], [175]; however a brief overview is provided here for convenience. The STAMPS insole has a multi-layer structure. The 5 mm mid-layer is made of industrial plasticine, enabling plastic deformation and can be easily adapted to fit a range of shoe sizes and shapes. The top layer consists of a high contrast stochastic

speckle pattern adhered to the surface using water-activated temporary tattoo paper. The speckle pattern was created using a commercial pattern generator (Correlated Solutions Inc.) and defined to have 65% density, 0.8 mm diameter and 75% variation. Pre- and post-walking image pairs with a resolution of 1920x1200 were captured using a custom 3D camera setup consisting of two high resolution USB cameras (Basler, Germany, A2A 1920-160UCBAS). Image pairs were analysed using open-source 3D DIC software (DuoDIC) and post-processed further using custom scripts (MATLAB, Mathworks, USA). The raw DIC strain data was anatomically segmented using a masking protocol employed by a commercial plantar analysis software (PEDAR INC., Novel GmbH, Munich, Germany): Global, hallux, 2nd toe, toes 3-5, 1st Metatarsal Head (MTH), 2nd MTH, 3rd MTH, 4th MTH, 5th MTH, medial and lateral Midfoot, heel. The mask was scaled and rotated based on the insoles shape and size, enabling the strain data to be allocated to the corresponding anatomical regions. The strain measures calculated include the magnitude of strain (S_{MAG}), anterior and posterior strain (S_{ANT}, S_{POST}), medial and lateral strain (S_{MED}, S_{LAT}) and the z-component of strain (S_Z). While each of the strain components were captured and analysed, only the overall strain magnitudes, S_{MAG}, are reported in the main text to provide a concise summary.[2] Detailed directional strain data for each anatomical region and condition are available in sections 1 and 2.1 of the Supplementary Material.

Experimental Protocol

Participant shoe size was measured to ensure the STAMPS insoles and supportive neoprene boots (Ninewells Boot, Chaneco) were correctly sized. The STAMPS insoles were made >24 hours prior to use. The STAMPS insoles were vacuum moulded to the orthoses surface, ensuring a consistent moulding approach and to avoid excessive deformation to the surface through manual moulding with hands. Any excess material was trimmed, and insoles were stored in a temperature-controlled cooler (15°C) until use. Prior to testing, insoles were manually checked for full contact with the orthosis surface. A pre-walk image was captured of the insole and inserted into the right shoe, with a similarly sized insole inserted into the left shoe to prevent any unwanted difference in insole depth. For consistency, the right foot was used for measurements for each participant. Participants were required to walk along a 10 m walkway at a self-selected walking speed, ensuring a consistent number of steps were taken. In total, participants were asked to complete three walking conditions: 1. Low stiffness orthosis with STAMPS overlayed (contoured), 2. high stiffness orthosis with STAMPS overlayed (contoured) and 3. STAMPS alone (flat). The insole was carefully removed, and a post-walk image was captured. Each of the walking conditions were repeated three times, with a new STAMPS

[2] The directional strain components here represent deformation in the local surface coordinate system of the contoured insole and therefore do not correspond uniformly to anatomical directions.

insole used for each assessment. Following the walking assessments using the STAMPS insole, a final walking assessment was performed using the Pedar® (Novel GmbH, Munich, Germany) in-shoe plantar pressure measurement system. Since the Pedar system cannot be used where there is pronounced and/or compound curvature (i.e. curvature in more than axis), direct comparisons between peak plantar pressure (PPP) and S_{MAG} will only be made with flat STAMPS condition. Measures of interest include the global and anatomical regions for median peak S_{MAG} and PPP. Median measures were used to provide a more robust representation of data and less susceptible to being skewed by extreme measures. Figure 6.2.1 outlines the method setup using STAMPS3D, DIC analysis and post-processing.

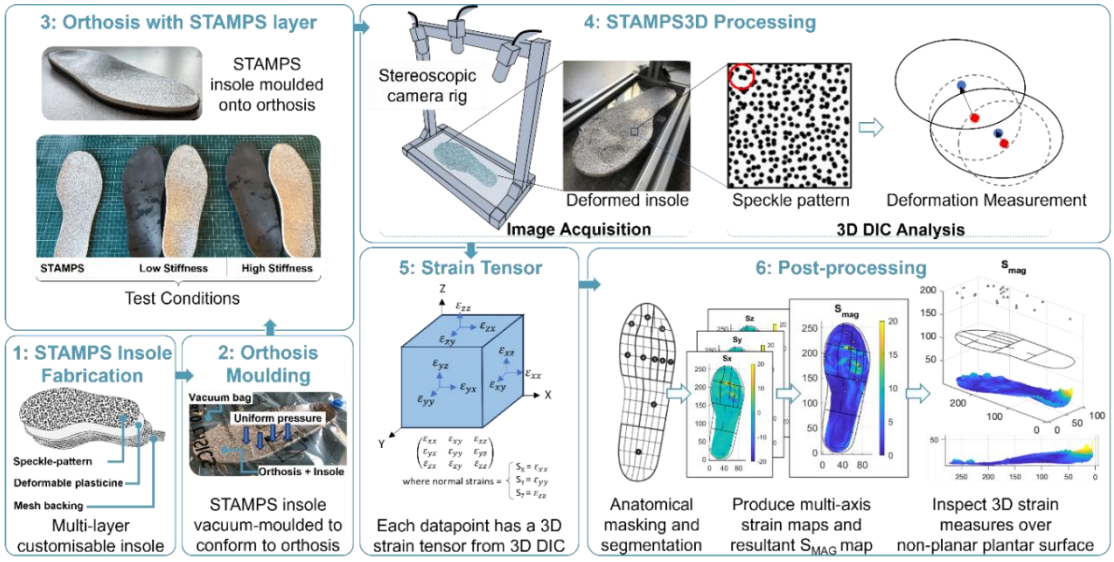


Figure 6.2.1: *Overview of methods, STAMPS3D and post-processing of 3D strain data.*

Statistical Analysis and Post-processing

The data was assessed for normality using the Shapiro-Wilk test. The results indicated non-normal distribution across multiple anatomical regions and test conditions. Due to the small sample size (n = 5) and the repeated measures design, the non-parametric Friedman's test was employed to compare plantar strain across the three test conditions. This test is appropriate for non-normally distributed data and does not assume homogeneity of variance. A post-hoc test with a Bonferroni correction was applied to adjust for multiple comparisons and identify which conditions showed statistically significant differences ($P < 0.05$). While the sample size of five participants limits the statistical power of the study, the repeated measures design and anatomical segmentation yielded a substantial amount of data per participant. The findings should be interpreted as preliminary, and future studies with larger cohorts are planned to

confirm and expand the results. PPP for each anatomical region and globally were extracted using the multimask application (Novel, GmbH, Munich, Germany) with the mask previously described. Spearman's correlation coefficient was used to assess the relationship between peak S_{MAG} and PPP, with a significant relationship being where a moderate and statistically significant correlation was found ($0.4 < rho < 0.69$ and $P < 0.05$). This was consistent with the approach used in the healthy cross-sectional study using STAMPS [117]. Median coefficients of variation (CV) of PPP and S_{MAG} was calculated for each region across all participants to determine repeatability of the study conditions.

Results

Five healthy participants were recruited and all successfully completed the walking assessments without reporting discomfort.

Across all the participants, the global median peak S_{MAG} was 28.34% ranging from 19.97-52.96%, 42.00% ranging from 21.19-102.11% and 22.70% ranging from 16.03-42.21% for the low stiffness, high stiffness and STAMPS conditions respectively. The global median PPP was 412.54 kPa, ranging from 293.00-542.00 kPa. The corresponding S_{MAG} strain maps and absolute plots displaying different coloured strain brackets across the plantar surface are shown in Figure 6.2.2. A single strain map representative of all three repeats for each condition and participant is displayed. The strain brackets were selected to better highlight local regions of high strain, e.g. 0-2.5% (blue), 2.5-5% (green), 5-7.5% (yellow), 7.5-10% (magenta) and > 10 (red). The figure shows patterns across the participants, with high strain regions varying across the cohort. For the low stiffness condition, peak S_{MAG} was located at toes 3-5 in one participant, at the 5th MTH in one and at the heel in three. For the high stiffness condition, peak S_{MAG} was located at the 4th MTH in one participant, at the 5th MTH in one and at the heel in three participants. For the flat condition, peak S_{MAG} was located at the hallux in one participant, at toes 3-5 in one, at the 4th MTH in one, at the 5th MTH in one and at the heel in one. PPP was located at the hallux in three participants, at the 2nd MTH in one and at the heel in one. Peak S_{MAG} for all conditions and PPP occurred at the same region in one participant.

The region of peak S_{MAG} showed consistency across all repeats for all conditions in 1/5 participants. All other participants showed consistency across in two of the repeats for all conditions except for P05 during the flat condition. The median CV of S_{MAG} and PPP was computed across participants to compare across the three repeats. For the low stiffness condition, the median CV was 45%, for high stiffness was 30%, for the flat condition was 23% and for PPP was 5%.

Median regional strain and PPP measures across the five participants are shown in Table 6.2.1.[3] Across each condition the region of highest S_{MAG} and PPP were at different locations, being at toes 3-5 (23.22%), heel (20.80%), 5th MTH (13%) and hallux (399.99 kPa) respectively. For the contoured conditions, the regions with highest S_{MAG} were the toes 3-5, 5th MTH and heel, whereas for the flat condition S_{MAG} was highest at the hallux, 4th MTH and 5th MTH. The distribution of median peak S_{MAG} across each anatomical region for all participants is shown in Figure 6.2.3. Significant differences between conditions were found at the hallux, 1st MTH, 2nd MTH, 3rd MTH, 4th MTH, medial and lateral midfoot and heel. To complement the overview provided in Figure 6.2.3, section 2.2 of the Supplementary Material presents individual boxplots for each of the 12 anatomical regions, allowing for more in-depth interpretation of regional strain patterns across conditions.

[3] Repeat-level averaging was performed first to obtain one dataset per participant per condition, after which the median was calculated across participants.

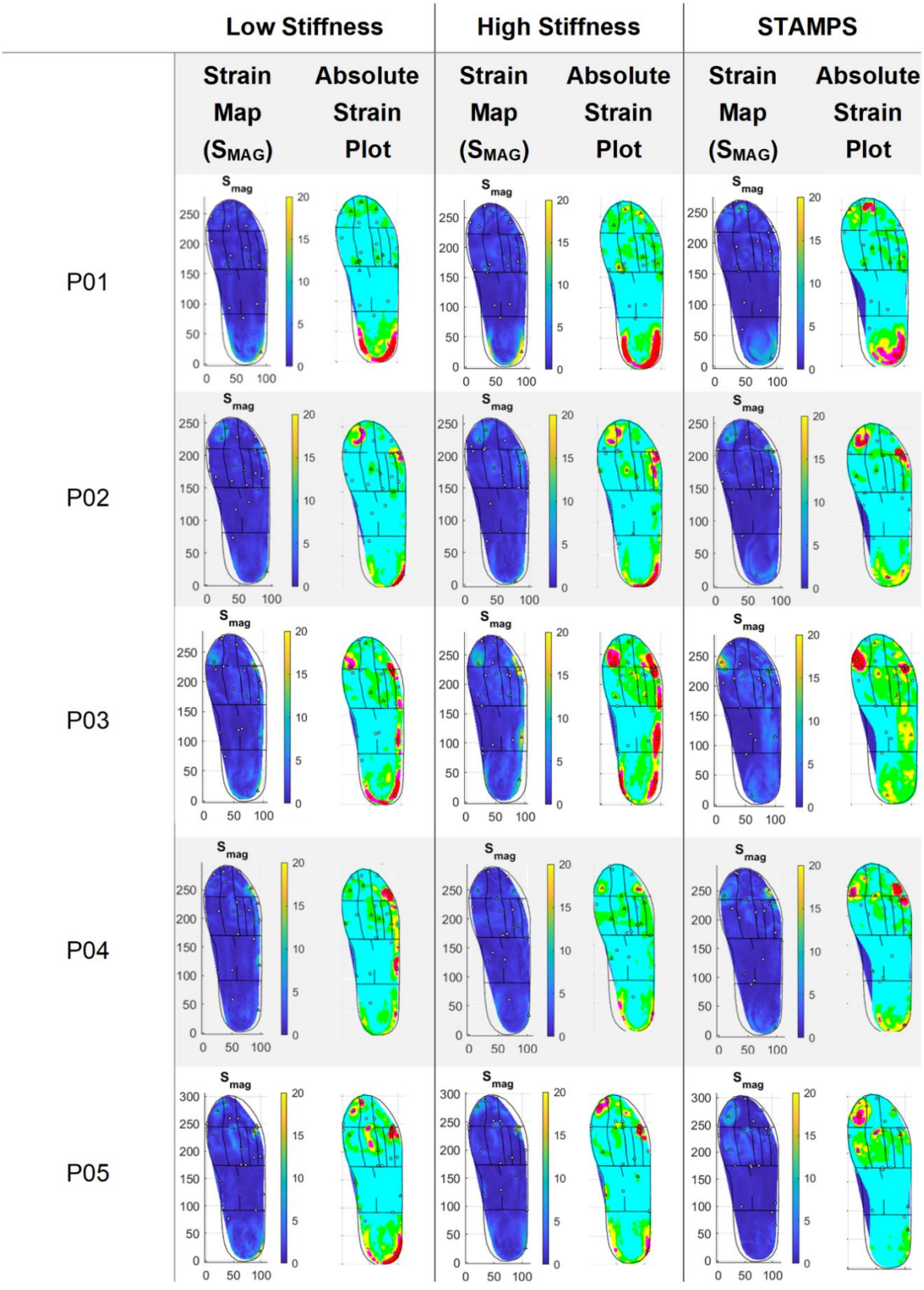


Figure 6.2.2: *Representative strain maps for S_{MAG} across each participant and condition, with absolute plots demonstrating strain brackets: 0-2.5% (blue), 2.5-5% (green), 5-7.5% (yellow), 7.5-10% (magenta) and > 10 (red).*

Table 6.2.1: *Regional median peak S_{MAG} for each condition and PPP across all participants, with interquartile range (IQR) reported in brackets.*

Anatomical Region	*Low Stiffness, Peak S_{MAG} (%)*	*High Stiffness, Peak S_{MAG} (%)*	*STAMPS, Peak S_{MAG} (%)*	*PPP (kPa)*
Global	28.34 (21.59-48.71)	42.00 (23.40-75.30)	22.70 (16.90-39.00)	412.54 (328.31-517.13)
Hallux	8.37 (5.58-11.27)	10.38 (6.62-12.20)	12.36 (8.34-16.00)	399.99 (281.65-503.94)
2nd Toe	7.35 (4.53-10.83)	7.36 (4.85-9.61)	8.56 (5.39-12.30)	140.75 (107.94-283.97)
Toes 3-5	23.22 (11.59-27.30)	12.10 (8.84-19.20)	11.50 (7.51-24.70)	86.33 (66.00-145.27)
1st MTH	4.06 (2.91-6.70)	4.20 (3.21-7.17)	7.45 (3.92-11.30)	210.08 (85.73-309.56)
2nd MTH	4.31 (4.24-7.11)	5.52 (4.66-6.15)	5.51 (4.68-9.92)	193.50 (149.26-248.10)
3rd MTH	4.67 (3.07-5.64)	3.77 (3.27-5.45)	5.60 (4.15-6.78)	173.33 (120.42-221.02)
4th MTH	8.56 (4.73-22.84)	8.21 (5.24-16.10)	11.85 (6.31-24.20)	173.33 (120.42-219.42)
5th MTH	15.21 (6.70-34.43)	14.20 (6.23-59.10)	13.00 (8.64-32.70)	97.63 (93.40-136.17)
Medial Midfoot	2.77 (2.21-4.92)	3.01 (2.24-5.78)	2.16 (1.50-5.05)	23.92 (1.56-40.33)
Lateral Midfoot	5.08 (3.30-13.84)	5.42 (4.21-11.60)	3.01 (2.76-6.94)	74.67 (58.57-148.79)
Heel	18.88 (11.78-32.04)	20.80 (17.10-43.80)	11.69 (9.37-14.00)	286.00 (208.13-364.07)

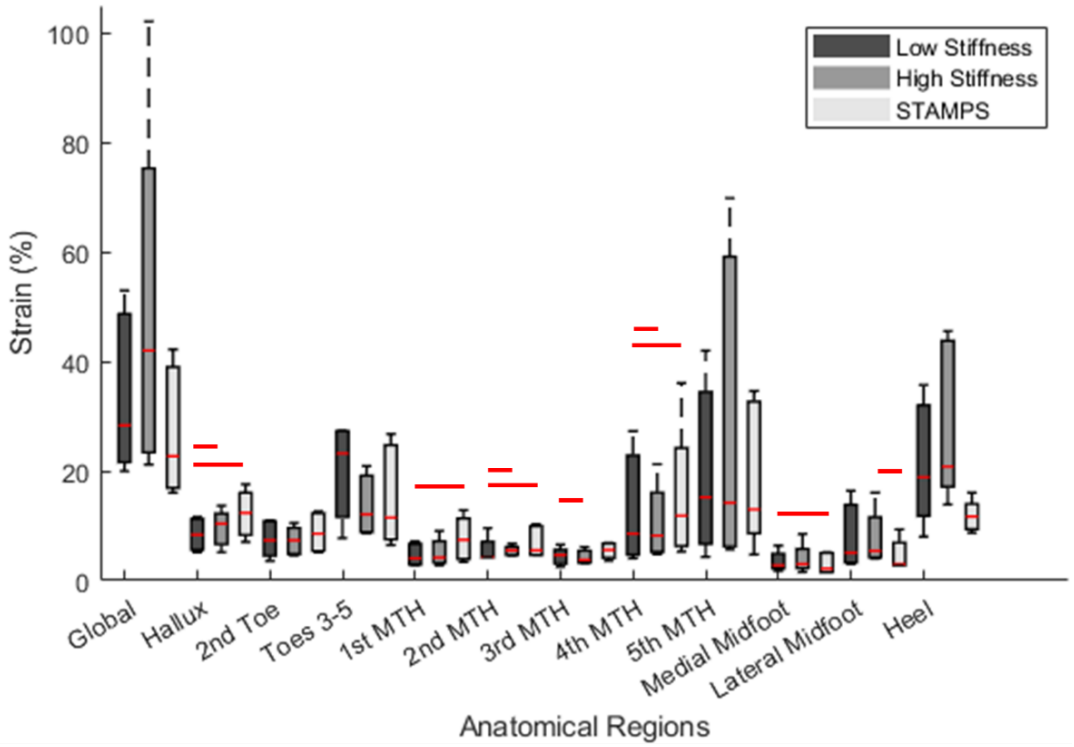


Figure 6.2.3: *Boxplot demonstrating regional distribution of peak S_{MAG} across all participants for the low stiffness, high stiffness and STAMPS conditions. Red lines above boxplots represent significance ($P < 0.05$) between the corresponding conditions based on median measures. For detail regional breakdowns, see section 2.2 of the Supplementary Material.*

Peak S_{MAG} and PPP were found to be moderately correlated, with PPP increasing with increased S_{MAG}. Spearman's correlation coefficient was found to be 0.52, $P < 0.001$. The relationship between the two plantar measures is demonstrated in Figure 6.2.4. For each participant there was moderate to strong correlation between peak S_{MAG} and PPP for 4/5 participants, ranging from 0.53-0.74. Only one participant showed a weak correlation between peak S_{MAG} and PPP (rho = 0.21). Regional correlation analysis between peak S_{MAG} and PPP revealed moderate to very strong positive correlations in 4 out of 12 regions. The remaining regions showed weak or inconsistent relationships. These findings may reflect limitations in pressure measurement systems sensor resolution, which varies across anatomical regions and may not fully capture localised strain patterns measured by STAMPS3D.

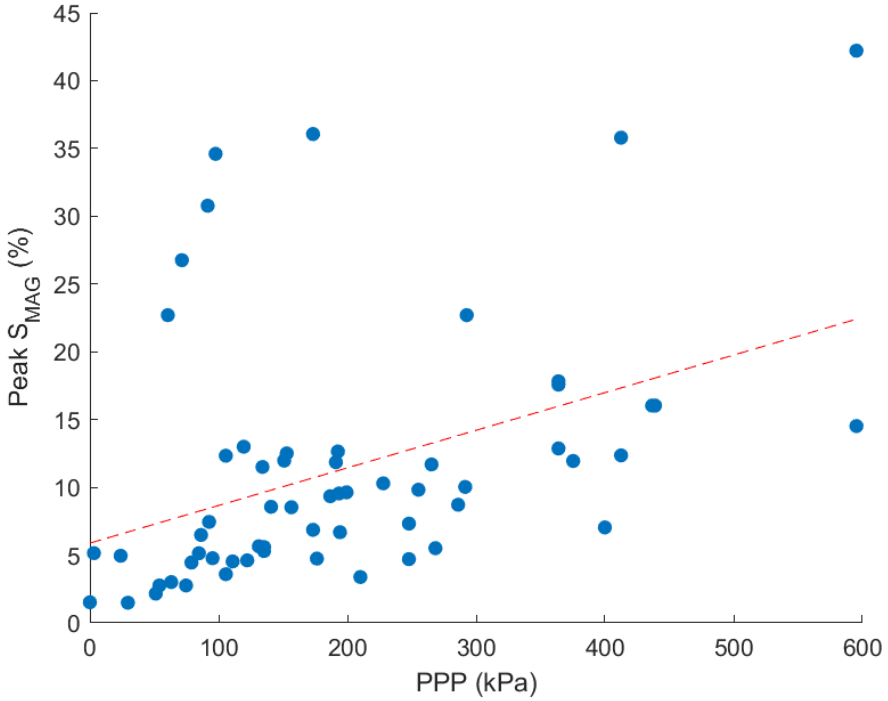


Figure 6.2.4: *Scatter plot demonstrating the correlation between peak S_{MAG} and PPP across all participants. Points included are an average across three repeats for each region and participant.*

Discussion

This study has demonstrated the successful application of the STAMPS3D system to identify whether differences in plantar strain measures can be observed when an individual's foot posture is altered using bespoke contoured orthosis compared to a standard flat insole. It also examined how plantar strain changes as a result of the material stiffness of the orthosis.

Plantar strain patterns were shown to vary across the foot between conditions in each participant (Figure 6.2.2), particularly between the contoured (low and high stiffness) and flat (STAMPS) conditions. The absolute plots highlight the edge of the heel and lateral side of the foot, indicating strain levels > 10%. This differs for the flat condition where little to no high-level strain measures are located in those regions. For the flat condition of P01, the heel region is highlighted more centrally compared to the contoured conditions, which suggest that the raised edges of the heel and lateral side of the orthosis result in greater interaction with the individual's foot, therefore increasing strain measures captured.

The relationship between PPP and peak S_{MAG}, shown in Figure 6.2.4, was found to have significant moderate correlation (rho = 0.52, P < 0.001), aligning with results from a

healthy cross-sectional study which also showed moderate correlation (rho = 0.65, P < 0.001) [117]. Differences in correlation may be due to a smaller sample size in the present study. Although direct measures of in-shoe shear stress are not measured, the STAMPS3D system captures the resultant strain from both shear stress and plantar pressure at the foot's surface interface. Therefore, the 3D strain data provides a proxy for assessment of plantar load under the tested conditions. Note that the reported correlation is between the peak S_{MAG} measures corresponding to the flat STAMPS3D condition and PPP, since plantar pressure comparison measurements could only be captured under flat conditions due to limitations of the Pedar system. The difference in resolution between STAMPS3D and pressure measurement insoles such as Pedar presents a challenge for regional correlation analysis. STAMPS3D captures strain at higher spatial resolution and across the full plantar surface, while Pedar relies on fewer sensors per region. This may lead to underrepresentation of pressure data in some areas, affecting the strength and reliability of regional correlations. Future studies may benefit from integrating higher-resolution pressure mapping or interpolative techniques to improve regional comparability.

For the low and high stiffness conditions, the highest S_{MAG} occurred at the same three regions including toes 3-5, 5th MTH and heel (Table 6.2.1). Whereas for the STAMPS condition, the highest S_{MAG} occurred at the hallux, 4th MTH and 5th MTH, with the latter being the only region appearing in all three conditions with the highest measures. Within the toe region, the hallux and 2nd toe regions showed lower S_{MAG} in the contoured conditions compared to the flat condition with statistical significance between low and STAMPS at the hallux (P = 0.003). Within the forefoot region, the 1st, 3rd and 4th MTH showed lower S_{MAG} measures in the contoured conditions compared to the flat condition. Strain measures were found to be significantly lower in the low stiffness condition compared to STAMPS across the 1st, 2nd and 4th MTH (P = 0.01, P = 0.006, P = 0.019). A number of studies found a decrease in plantar pressure in forefoot regions of those who wore contoured orthoses in comparison to a flat insole, with one finding a 34% pressure reduction at the 1st MTH [176], [181], [182]. Since this study showed that peak S_{MAG} correlates with PPP, the decreased magnitude of strain reported may be as a result of a decreased pressure component. This can be found when contoured orthoses with a raised arch profile is present, enabling the forces to be redistributed from the front of the foot to the midfoot [181]. This may explain why at the medial and lateral midfoot, the reported S_{MAG} is significantly increased in the contoured conditions (P = 0.003, P = 0.019). Similarly, S_{MAG} is increased at the heel for the contoured conditions. This again may be resulting from the raised edge prominent along the lateral side of the orthosis and around the heel cup, leading to increased resultant effect of shear and pressure in those regions as shown by the strain maps in Figure 6.2.2. In addition to this, these high strain regions may also be due to ill-fitted footwear since the footwear used in this study

had to be able to accommodate for a range of sizes, leading to greater movement within the shoes and against the orthosis during gait. The regions where the highest PPP occurred were the hallux, 1st MTH and heel. However, there were regions that reported relatively high peak S_{MAG} in comparison to PPP such as toes 3-5, 4th MTH and 5th MTH. Since the plantar pressure exhibited was low in the presence of high plantar strain, it suggests that these regions may have experienced elevated shear stress.

A comparison between the low and high stiffness conditions within the contoured group showed fewer differences. As mentioned previously, the highest median S_{MAG} occurred in the same three anatomical regions, however some significant differences were found at the hallux ($P = 0.019$), 2nd MTH ($P = 0.002$), 3rd MTH ($P = 0.019$), 4th MTH ($P = 0.019$) and lateral midfoot ($P = 0.019$). At the hallux, 2nd MTH and lateral midfoot the median peak S_{MAG} was found to be significantly higher in the high stiffness group, whereas at the 3rd and 4th MTH significantly increased S_{MAG} was found in the low stiffness group. From Table 6.2.1, measures reported in the medial forefoot and toe regions appear to be generally reduced when low stiffness insoles were worn compared to the lateral toe and forefoot region, even though the arch profile was consistent in both contoured conditions. This suggests that differences in the distribution of plantar load may occur in differing regions depending on the stiffness of insole used. From the literature, multiple papers have reported differences in plantar pressures depending on insole material stiffness, hardness or density [20], [177], [183], [184]. However, whether the pressure reductions are found in the lower or upper margin of these material properties (i.e. low or high stiffness) are conflicted among studies. Therefore, from the current data it is difficult to determine if these results are significant and whether pressure or shear stress has greater influence in these regions depending on material stiffness. It is also worth highlighting that since this study consists of a healthy cohort, the expected impact of using a low or high stiffness insole may not be as pronounced in comparison to a cohort with diabetes-related foot complications. This could be due to a ‘healthy’ individual having relatively normal distribution of plantar load compared to those with foot issues.

The key limitations of the STAMPS3D system are similar to those of the 2D STAMPS system which have previously been discussed and relates to measurement capability, variability in outcomes and clinical utility [116], [175]. Most notably, the STAMPS measurement approach involves a trade-off between temporal measurement frequency and spatial resolution; using DIC to record the cumulative strain incurred through gait inherently precludes the ability to capture real-time or dynamic data but does allow for high resolution measurement across the full plantar surface. This differentiates the STAMPS (2D and 3D) systems from electronic-sensor based in-shoe systems which are capable of real-time measurement but lack spatial resolution and full coverage. Both approaches have virtue and there is potential to use them together as complementary

technologies to obtain a more complete understanding of plantar loading. In this study, the outcome measures obtained from STAMPS3D exhibited a relatively high coefficient of variation across gait repeats. However, this level of variability is consistent with previous STAMPS2D in-shoe testing, where natural gait variation contributed to higher CVs compared to bench testing [116], [117]. Notably, regions with lower absolute strain tended to show higher CVs, which may exaggerate variability without reflecting clinically meaningful differences. In prior studies involving diabetic participants, regions with higher strain magnitudes were associated with lower CVs [185], suggesting improved measurement stability under clinically relevant load regimes and contexts, and an aspect that will be pursued in future work. The STAMPS systems have been co-developed with clinical stakeholders with the aim of being appropriate for clinical use in the future. In its current form, STAMPS3D system does have some limitations in this respect; although data capture can be completed within 10-15 minutes (deemed clinically appropriate), it requires additional preparation time (to mould insoles to the contours of the orthosis) and to perform the post-hoc analysis steps (including DIC, masking and determining summary metrics). Addressing these aspects is an important part of our future work, firstly to optimise the fitting process and secondly to automate the analysis process guided by expert clinical input, combining to produce a streamlined process suitable for use within clinical sessions.

This study was conducted with healthy participants to establish the baseline performance and repeatability of the STAMPS3D system.[4] While this does limit extrapolation to understand potential clinical efficacy, it is an important first step in evaluating system feasibility prior to future clinical studies. Using this approach, our previous work using STAMPS2D demonstrates greater strain differentiation in diabetic populations [185] suggesting that STAMPS3D may offer similar capabilities coupled with the ability to evaluate non-planar insoles. Future clinical studies involving participants with diabetes (including those with neuropathy and foot deformities), are planned to evaluate the clinical utility of STAMPS3D. In doing so, the effect of bespoke orthoses and the various design features used to offload regions at risk of DFU formation in patients with diabetes, can be better understood and used to improve management and prevention procedures.

In conclusion, this proof-of-concept study demonstrates the potential of the STAMPS3D system to capture 3D strain patterns indicative of plantar loads at the foot-orthosis interface. The system was successfully applied to compare strain patterns across flat and contoured orthoses of varying stiffness, revealing significant differences in local strain distribution. Notably, regions of high plantar strain did not always align with regions of high plantar pressure, suggesting the influence of shear stress components. While

[4] Baseline performance refers to characterising system behaviour under controlled conditions in healthy participants, whereas repeatability was assessed through consistency of strain and pressure measurements across repeated trials.

these findings are promising, the repeatability and clinical applicability of STAMPS3D requires further investigation. The current study was limited to healthy participants, and future work will involve individuals with diabetes, including those with neuropathy and foot deformity, to assess robustness and relevance in clinical settings. These efforts aim to improve our understanding of orthotic intervention and their role in preventing diabetic foot ulceration.

6.3 Preliminary Work and Supporting Data

This section presents the supplementary experimental work that supported the development of the methodology used in the published work in Section 6.2. While the paper reports the final methodological procedure and key findings, several stages of mechanical characterisation, moulding development and preliminary testing were involved in the development phases leading up to this work and were required to ensure that STAMPS3D could be reliably applied to contoured orthoses. This iterative approach in the development process is illustrated in Figure 6.3.1.

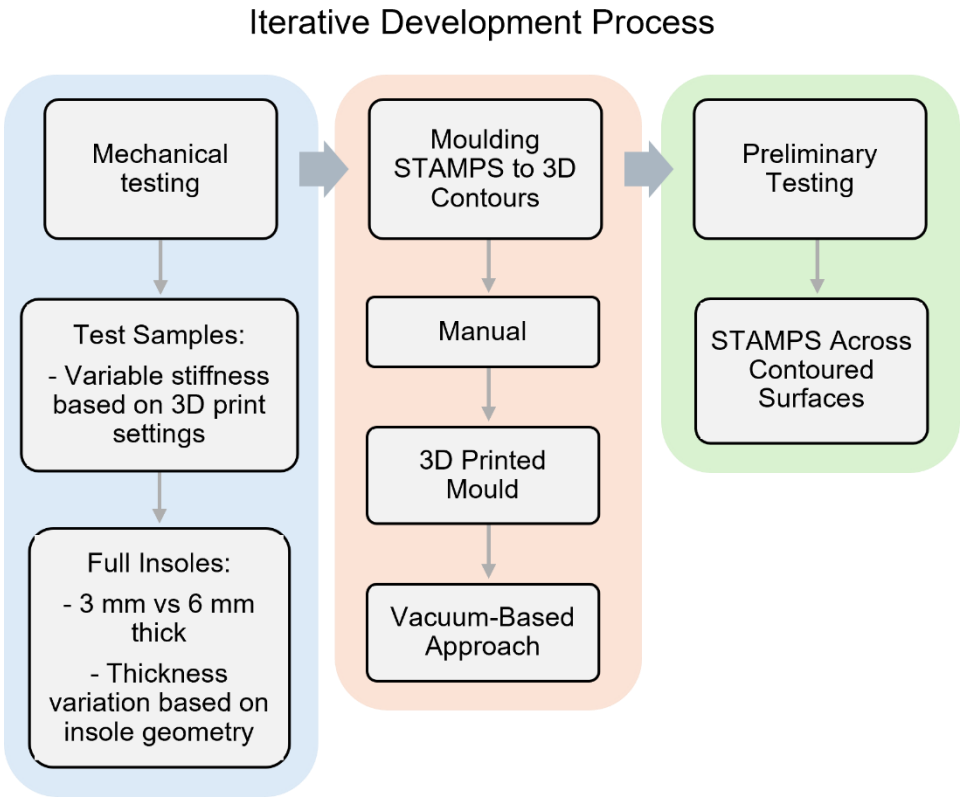


Figure 6.3.1: *Illustration of the iterative development process carried out prior to the final proof-of-concept study presented in Section 6.2.*

During this methodology development work, key research areas of interest were also highlighted by an industrial collaborator (Steeper) including the influence of orthotic material stiffness, insole thickness variation, localised regions of differing stiffness, edge

effects around these local regions and the impact of using loaded versus unloaded foot scans for custom orthotic design. Of these areas, this section focuses on material stiffness, insole thickness and localised stiffness variability, as these were both clinically relevant and feasible to evaluate experimentally within the scope of the preliminary stage of work. These factors also aligned with the overarching aim of determining whether the STAMPS3D system could capture plantar strain across contoured orthotic surfaces.

6.3.1 Mechanical Characterisation of Orthotic Insoles

Mechanical testing was undertaken to quantify the stiffness of orthotic materials and insoles used in the study, including those that are routinely produced for clinical use. The aim of this work was to characterise the mechanical stiffness of the 3D printed contoured orthoses materials, assess consistency across regions of varying thickness and to determine the combined mechanical behaviour when the STAMPS insole is overlaid. Characterising these materials ensured that the materials selected for subsequent strain testing within the proof-of-concept study were mechanically distinct. Although the orthoses used in the study were manufactured through 3D printing, this is not a universal method of production. The selected orthoses (Steeper Ltd) are manufactured using an additive manufacturing process in a proprietary commercial 3D printing system. A foamed polymer material is used, where print temperature and print speed influences the amount of foaming and therefore the final material density. For example, slower, hotter print settings produce greater foaming and a lower density, while faster, cooler print settings reduce foaming and result in a more dense and stiffer structure. These settings are controlled within a commercial software, however further details on print temperature and speed are not directly accessible, limiting the ability to directly control or understand the exact 3D printer settings implemented.

To characterise these behaviours, mechanical testing was performed using a consistent protocol across all samples and tests. A 10 mm diameter flat 3D printed indenter was attached to the Instron 5943 testing machine equipped with a 500 N load cell and a preload of 0.1 N was applied to ensure contact with the sample surface. A 10 mm indenter was used to target localised regions of the insole, accounting for areas of intervention and variability in the insole geometry. Compression testing was then conducted to 50% strain at a constant rate of 5 mm/min, which was selected to ensure slow and control testing, with this rate being used in a study on 3D printed custom insoles [186]. Each test was repeated three times with insoles left to recover for 24 hours between tests. Young's Modulus was calculated between 10-20% strain for each test, providing a standardised measure of stiffness within the linear region of the corresponding stress-strain curve. Three repeats were performed for each sample to account for variability.

Evaluation of Test Samples

A set of seventeen test samples were provided by Steeper to characterise the full stiffness range achievable through their 3D printing process. These samples were expected to show a controlled gradient of material stiffness, increasing linearly from Sample 1 (lowest stiffness) to Sample 5 (highest stiffness), with intermediate variants (e.g., 1.1, 1.2, 1.3) produced by adjusting print parameters. Quantifying the stiffness of these samples was important for establishing reference values that could later be compared with plantar strain measurements obtained using STAMPS3D.

For each of the seventeen samples, three compression tests were performed with a 24-hour recovery period between repeats to ensure full material recovery. Figure 6.3.2 presents the combined stress–strain curves for a single representative repeat of each sample and Figure 6.3.3 shows the corresponding averaged Young's modulus values calculated between 10–20% strain. A full table of stiffness values is provided in Appendix D.1.

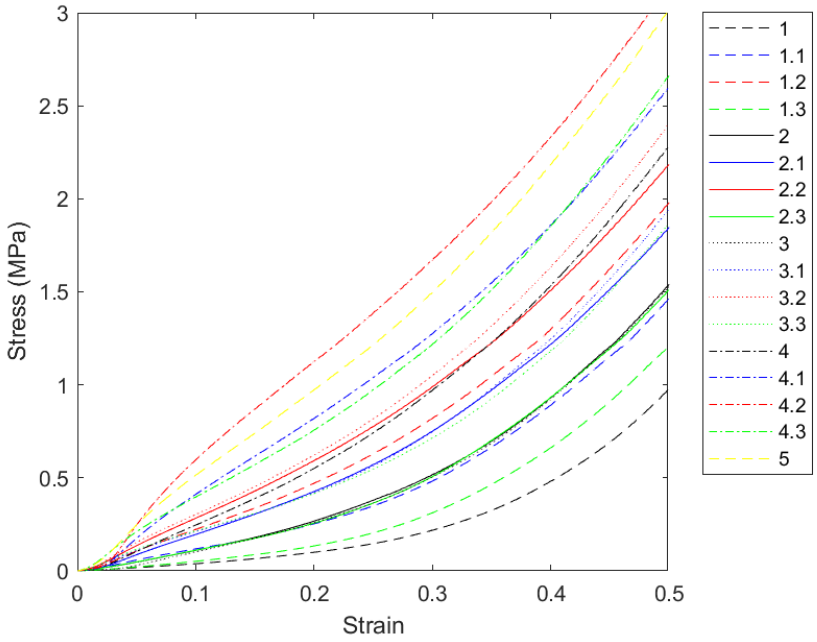


Figure 6.3.2: *Stress-strain curves for all 17 test samples (1-5 and intermediate variants), showing a single representative repeat for each.*

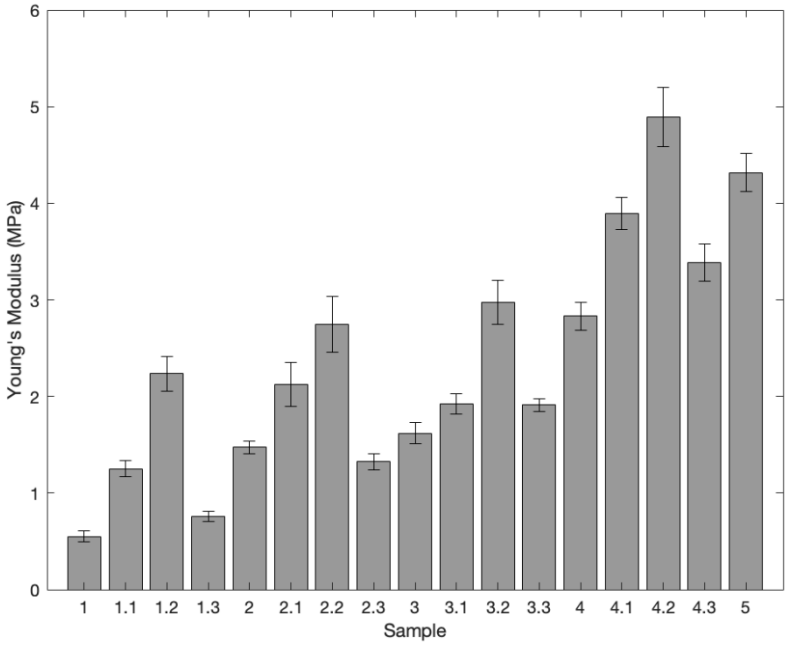


Figure 6.3.3: *Average Young's Modulus for each test sample, calculated between 10-20% strain. Error bars represent variability across the three repeats.*

Unexpectedly, the samples did not follow the linear increase in stiffness. Instead, the first three samples showed an initial rise in stiffness (1 to 1.2), followed by a decrease at Sample 1.3 to a value only slightly above Sample 1. A similar pattern was observed across the remaining groups, with stiffness increasing again up to Sample 2.2 before dropping at Sample 2.3, and this repeating through to Sample 5. Figure 6.3.3 shows some samples expected to be low stiffness (e.g., 1.2) were comparable to, or even stiffer than, samples intended to represent medium or high stiffness (e.g., 3.3). Repeat tests were consistent, confirming that this pattern reflected true material behaviour rather than measurement error.

Evaluation of Full Insoles

Mechanical testing was next performed on complete orthotic insoles to examine both inter- and intra-insole variability in stiffness. The insoles were manufactured with minimum thicknesses of either 3 mm or 6 mm (range used for clinical applications), but their geometry varied across the surface due to features such as the medial arch support and heel cup. As a result, stiffness was expected to differ across regions within a single insole as well as between insoles of different nominal thicknesses.

To capture this variability, tests were conducted at four anatomically relevant locations (Figure 6.3.4):

- Hallux region (intervention site)
- Lateral forefoot (comparison site)
- Lateral midfoot (thickest region)
- Central heel (thinnest region)

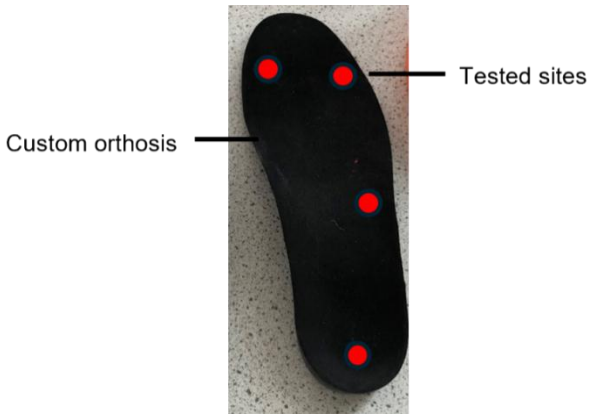


Figure 6.3.4: *Illustration of regions on the custom orthoses that underwent compression testing.*

In addition to the orthotic materials themselves, the influence of the 5 mm plasticine STAMPS layer was assessed by placing a 50 x 50 mm STAMPS samples over selected regions of each insole and repeating the compression tests. This allowed the combined stiffness of the orthosis-STAMPS layers to be quantified, reflecting the configuration used during plantar strain measurement.

Steeper provided insoles categorised clinically as low, medium or high stiffness. However, specific details linking these categories to the test samples were not available and instead the classifications reflected the material options routinely supplied in clinical practice and informed by podiatrist expertise. An additional medium stiffness insole was supplied with a localised modification at roughly the hallux region, described as a ‘spot’. These represented targeted stiffness alterations intended to redistribute plantar load.

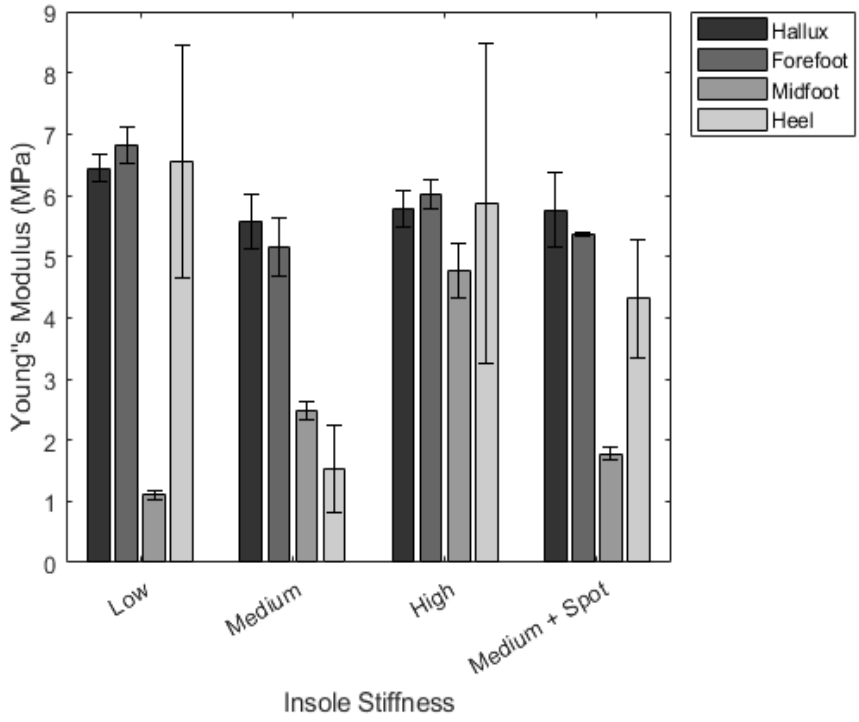
The combinations tested varied intentionally, reflecting the staged nature of the methodological development. Initial four-region testing characterised intra-insole stiffness variation associated with differences in insole features such as arch height, heel cup depth. Subsequent testing was restricted to the forefoot regions, where insole thickness was more uniform and therefore more appropriate for controlled comparison across the material types and set print thicknesses. The insole-STAMPS combined tests were similarly focused on these regions, using a 5 mm STAMPS layer consistent with the thickness used in the fabricated STAMPS3D insoles. The combinations tested are outlined in Table 6.3.1.

Table 6.3.1: *Summary of the insole thickness, stiffness conditions and anatomical regions tested during the preliminary work.*

Condition	Stiffness Conditions	STAMPS Layer (50 x 50 x 5 mm)	Test Regions
3 mm insoles	Low / Medium / High / Medium + Spot	No	Hallux, Lateral Forefoot, Lateral Midfoot, Heel
6 mm insoles	Low / Medium / High / Medium + Spot	No	Hallux, Lateral Forefoot, Lateral Midfoot, Heel
3 mm insoles	Low / Medium / High / Medium + Spot	Yes	Hallux, Lateral Forefoot
6 mm insoles	Low / Medium / High / Medium + Spot	Yes	Hallux, Lateral Forefoot
STAMPS only	-	STAMPS only	50 x 50 mm sample

All tests followed the same protocol described at the start of Section 6.3.1, ensuring consistency across materials and conditions. Figure 6.3.5 and Figure 6.3.6 summarise the Young's modulus values for all the full insole mechanical tests. Figure 6.3.5 presents stiffness measurements for the 3 mm and 6 mm insoles alone across the four anatomical regions, while Figure 6.3.6 shows the combined stiffness of each insole when tested with a 5 mm STAMPS layer. The 5 mm STAMPS sample alone had an average Young's Modulus of 3.69 MPa (Confidence Interval = +/- 0.06). Full numerical data is provided in Appendix D.2.

a)



b)

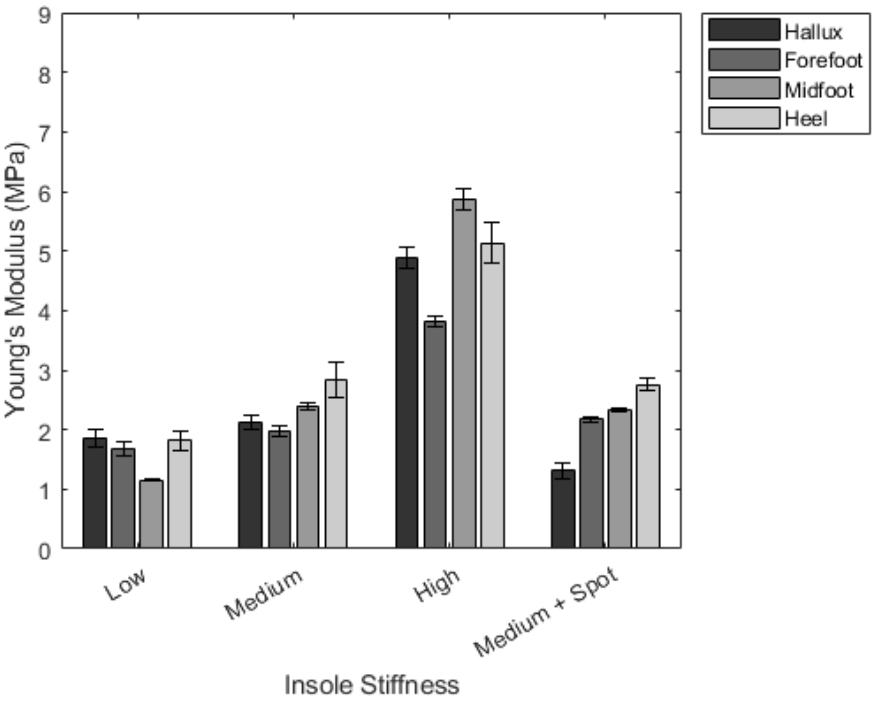
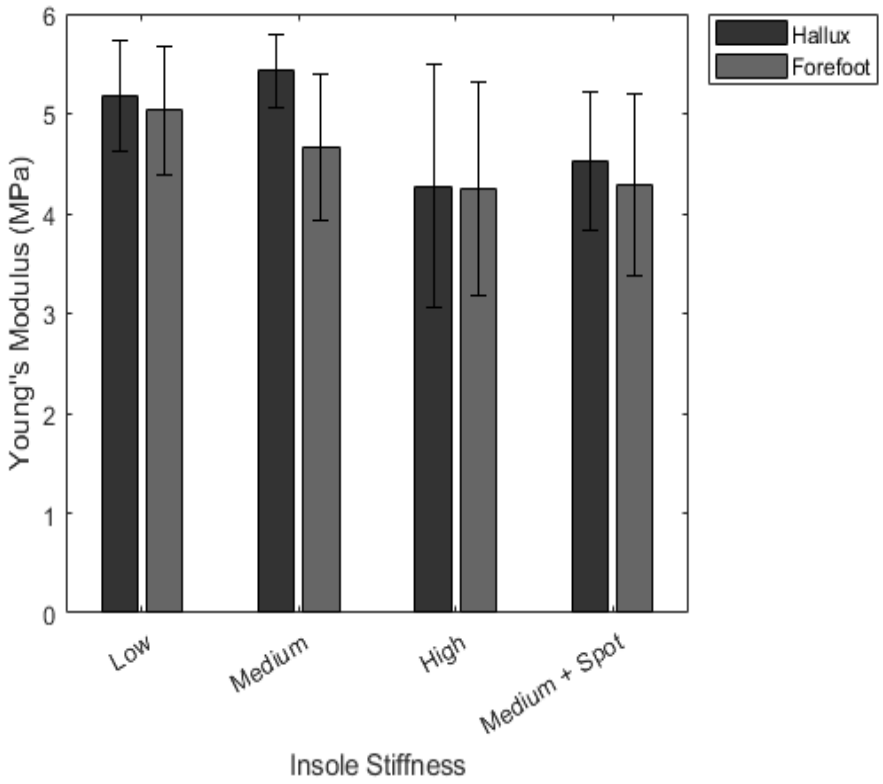


Figure 6.3.5: *Young's Modulus values for a) 3 mm and b) 6 mm orthotic insoles tested at the hallux, forefoot, midfoot and heel. Results are shown for low, medium, high and (where applicable) medium + spot materials. Error bars represent the 95% confidence interval across three repeats.*

Across the 3 mm and 6 mm insoles (Figure 6.3.5), stiffness varied both between materials and across anatomical regions. This was particularly evident for the 3 mm insoles, where fluctuations in stiffness were seen across regions of the foot. The lateral midfoot consistently showed lower stiffness, consistent with the greater thickness present in this area. At the other sites, where insole thickness was smaller, stiffness was more variable, with no clear linear increase in overall stiffness from low to high stiffness insoles. Stiffness at these thinner regions was typically higher than in the 6 mm insoles, which may reflect a denser structure when printed at a thinner baseline. No clear differences were observed between the medium stiffness insoles with and without intervention at the hallux site, further demonstrating the unexpected stiffness behaviour at thinner regions of the insoles. In contrast, for the 6 mm insoles an overall pattern of increasing stiffness was seen from low to high stiffness categories. Stiffness across regions of the insoles was relatively consistent, except at the lateral midfoot and forefoot for the low and high stiffness insoles respectively, which showed slightly lower values across insole types. At the intervention sites, a lower stiffness was observed for the modified insole, aligning with the intended localised change in mechanical properties.

a)



b)

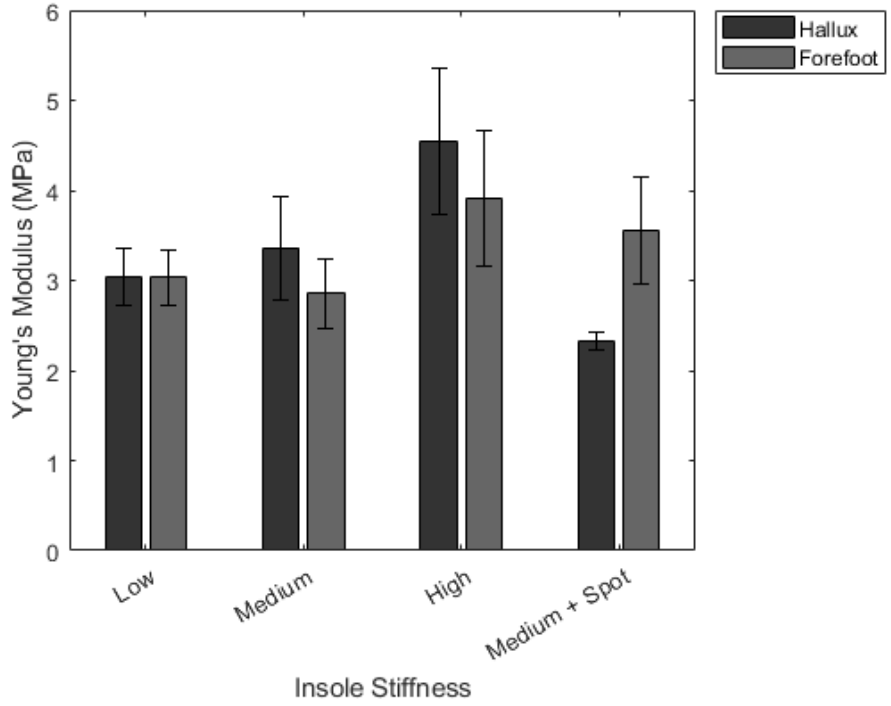


Figure 6.3.6: *Combined stiffness of 3 mm and 6 mm orthotic insoles with a 5 mm STAMPS layer, tested at the hallux and forefoot. Results are shown for low, medium, high and (where applicable) medium + spot materials. Error bars represent the 95% confidence interval across three repeats.*

When the 5 mm STAMPS layer was added (Figure 6.3.6), the combined stiffness changed in accordance with the relative stiffness of the plasticine layer and the underlying insole. For example, where the plasticine was stiffer than the insole (as in the 6 mm insoles), the combined stiffness increased, whereas where the plasticine was softer (as in the 3 mm insoles at the hallux and forefoot), the combined stiffness decreased. For the 3 mm insoles, measured stiffness at the hallux and forefoot was consistently high across all material categories, with little distinction between low, medium, and high stiffness types. For the 6 mm insoles, although the effect was more subtle than in the insole-only tests, an overall increase in stiffness from low to high material categories was still apparent. The intervention insoles again showed reduced stiffness at the hallux, as expected. Across all other tests, stiffness at the hallux and forefoot was consistent, indicating that these regions were comparable between conditions. These findings suggest that the 6 mm insoles retained stiffness differences seen in Figure 6.3.5 once the STAMPS layer was added, supporting their use in the subsequent strain testing.

6.3.2 Moulding STAMPS to 3D Contours

The aim of this stage of the preliminary work was to identify a reliable method for moulding the STAMPS insole onto a contoured orthosis surface. The moulding procedure for adapting the STAMPS3D insoles to the 3D printed orthoses underwent

several iterations as part of the methodological development. Initial work involved creating a stencil to extend the STAMPS insole outline to include the medial midfoot region, ensuring full coverage of the orthotic surface. This stencil was later adjusted once moulding was attempted.

The first approach involved manually moulding the entire STAMPS insole directly onto the 3D printed orthosis. While this allowed the insole to conform reasonably well to the overall shape, this process was time consuming and introduced uncertainty regarding the uniformity of the final insole thickness. This highlighted the need for a more controlled and repeatable method.

To improve consistency, a 3D printed mould was produced by inverting the scanned foot file into a negative mould surface (Figure 6.3.7). This approach aimed to provide a more controlled shaping process by matching the geometry of the orthosis. Although the mould improved alignment across much of the insole, the heel cup region still required manual shaping. This was due to the inverted mould not being offset to account for the additional plasticine material, meaning the STAMPS layer could not match up to the heel contour.



Figure 6.3.7: *Illustration of 3D printed mould and STAMPS insoles moulded to the orthoses.*

A vacuum-based approach was next trialled, intended to draw the STAMPS insole and orthosis surfaces together by removing air between them. While this method improved conformity across the midfoot and forefoot, some discrepancies, although reduced, remained at the heel. These were attributed to air becoming trapped in the heel cup, potentially due to excess material around the edge of the insole. Minor cracking of the plasticine was also observed, likely related to moulding being performed immediately after removing the material from the cooler, when it was less pliable (Figure 6.3.8).

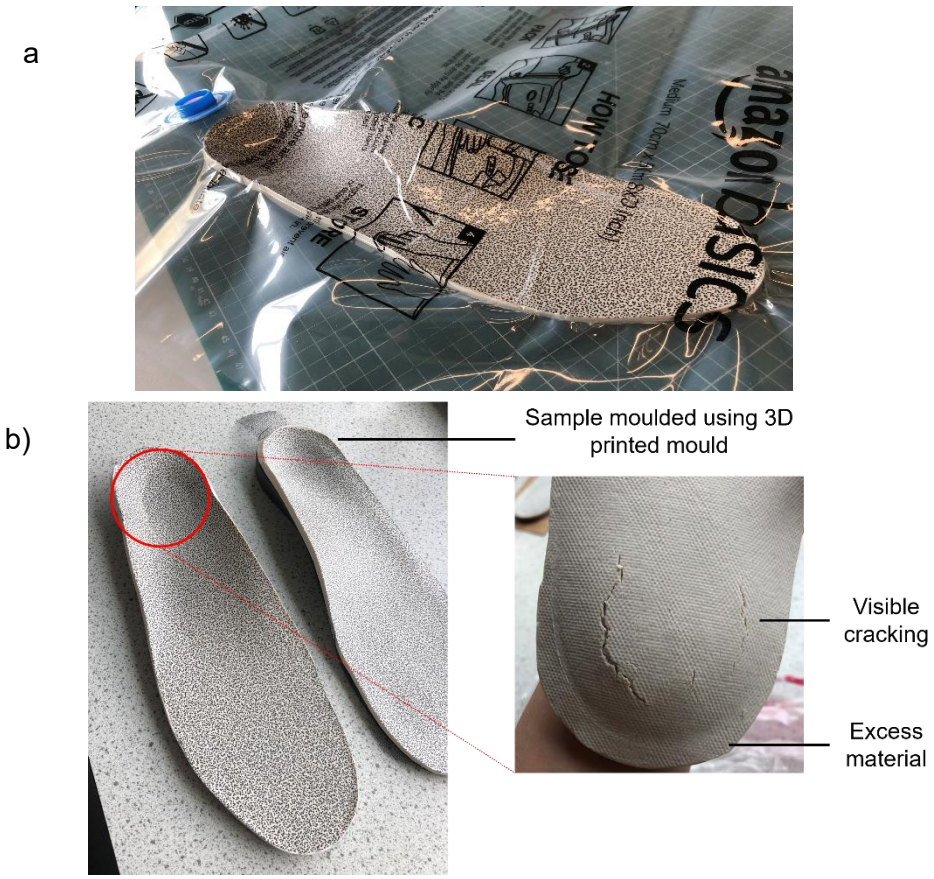


Figure 6.3.8: *Demonstration of the vacuum bag moulding approach (a), with initial attempts showing surface cracking and remaining excess material (b).*

Selected Moulding Methodology

These iterative trials informed the final moulding procedure used in the study, highlighting the practical challenges of achieving consistent conformity between the STAMPS layer and contoured orthotic geometries. The final approach that was used was:

- Initial moulding of the STAMPS insoles prior to storage in the cooler.
- Removal of excess material around the edge of the insole, leaving a small margin to accommodate areas requiring further shaping.
- Final vacuum bag moulding to achieve accurate conformity before storage.
- A final check immediately before use, overlaying the insole onto the orthosis and gently correcting any remaining areas requiring manual adjustment.

6.3.3 Preliminary Testing of STAMPS Across Contoured Surfaces

A series of preliminary tests were conducted to explore the strain response of the STAMPS3D system when used with contoured orthotic insoles, aiming to determine whether strain could be captured across a curved surface and how these patterns compared with those obtained from flat STAMPS insoles. These tests also helped refine the stiffness conditions included in the final protocol by evaluating whether global

stiffness differences or localised stiffness modifications (such as spot features) produced interpretable strain patterns suitable for inclusion in the proof-of-concept study. Although initial testing was performed on both 3 mm and 6 mm insole types, only the 6 mm results are presented here, as the thicker insoles demonstrated a more stable and representative mechanical response (as shown in Section 6.3.1). Strain maps were generated for low, medium, high and medium + spot insole types, as well as for flat STAMPS samples.

Across all contoured insoles, pronounced edge effects were observed, particularly along the lateral side (Figure 6.3.9). This was later corroborated by Steeper clinicians, who reported that some patients had described similar sensations at the lateral foot during orthotic use. While the strain maps themselves did not always show distinct regional differences, the corresponding numerical strain values revealed clear variation across anatomical regions under different material conditions, consistent with the patterns reported in the published study.

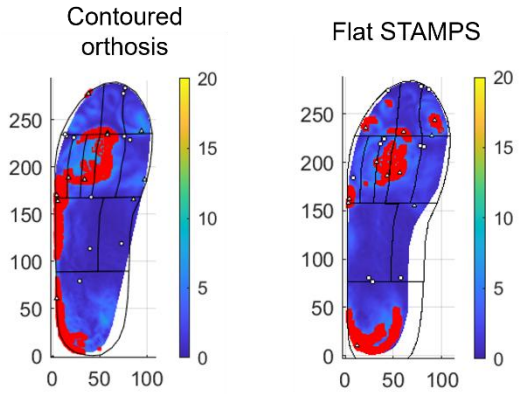


Figure 6.3.9: *Example strain maps from preliminary testing, with contoured insoles showing pronounced lateral edge effects, illustrated by the upper 10% of strain values highlighted in red, compared to flat STAMPS insole demonstrating.*

These tests were instrumental in refining the scope of the final experimental protocol. Specifically, they demonstrated that localised modifications produced less distinct strain differences at the intervention site than anticipated, whereas global differences in insole stiffness produced clearer and more interpretable patterns. Discussions with clinical and industry stakeholders highlighted a broad range of potential research directions relating to orthosis design, including material stiffness and geometry, thickness variation and localised stiffness features. Of these, the topic most relevant to this PhD focused on comparing contoured versus flat insoles and low versus high global stiffness conditions, rather than investigating more complex localised stiffness changes. By doing this, it ensured that the main aim of demonstrating that STAMPS3D can capture plantar strain

across contoured surfaces remained the focus, while incorporating material-related difference of relevance to clinical practice.

6.4 Chapter Discussion

This chapter presented the supplementary methodological work undertaken to support and extend the findings of the published study. The aim was to evaluate the feasibility of using the STAMPS3D system with contoured orthoses, understand the mechanical behaviour of the insole materials and refine the moulding and testing procedures required for reliable strain capture. Together, these investigations provide important context for interpreting the main study and demonstrate the broader potential of the STAMPS3D approach.

The mechanical testing showed clear differences in stiffness between materials and across anatomical regions of the insoles, with the 6 mm versions exhibiting a more consistent and representative mechanical response. In contrast, the 3 mm insoles showed greater variability, particularly in the forefoot where the reduced thickness appeared to influence the printed density and resulted in higher than expected stiffness values. This was shown in Figure 6.3.5, where the medium stiffness 3 mm insole reached approximately 5–6 MPa in the forefoot, compared with around 2 MPa for the equivalent 6 mm insole, despite both showing comparable stiffness in the midfoot region (~2.5 MPa). These findings indicated that the behaviour of the 3 mm insoles was influenced by thickness-related printing effects rather than material properties alone. For this reason, the preliminary strain testing focused on the 6 mm insoles, ensuring that the strain behaviour observed reflected true material differences. It should be noted that the contoured geometry of the insoles made it difficult to ensure perfectly parallel loading surfaces during mechanical testing, particularly in the midfoot region. For this reason, the lateral midfoot was selected as the most suitable location for testing, as it provided a flatter and more repeatable surface than the medial midfoot arch. The earlier mechanical test samples also confirmed which material categories were mechanically distinct, preventing the selection of materials whose stiffnesses were too similar and reducing the risk of generating strain responses that were insufficiently different to interpret meaningfully. These preliminary investigations ensured that the conditions chosen for the main study were both mechanically robust and capable of producing interpretable strain outcomes.

The preliminary strain tests revealed consistent lateral edge effects across all contoured insoles, a finding later corroborated by clinicians at Steeper who reported similar sensations described by patients. Although the strain maps themselves did not consistently show distinct regional differences, the numerical strain values demonstrated measurable variation across anatomical regions under different material conditions,

aligning with the patterns reported in the published study. These findings helped refine the final experimental design, narrowing the focus to comparisons between contoured and flat insoles and between low and high stiffness conditions, rather than localised modifications where strain differences were less pronounced. It is also important to note that both the preliminary tests and the main study were conducted using healthy participants. As reported in the published study, plantar strain differences arising from variations in orthotic stiffness may be more subtle in individuals with intact sensation and typical foot biomechanics. This likely contributed to the modest magnitude of strain differences observed here and reinforces the need for future testing in clinical populations where orthotic effects may be more pronounced.

The moulding development work highlighted the practical challenges of achieving consistent conformity between the STAMPS layer and complex orthotic geometries. Manual moulding proved feasible but inconsistent, while the 3D printed mould improved alignment but could not fully accommodate the heel cup due to the lack of offset for the plasticine layer. In addition, this approach would require a custom mould for each individual orthosis, limiting its practicality for wider clinical use. The vacuum bag moulding offered the most consistent conformity, though some heel discrepancies and material cracking remained. However, these were accounted for by making adjustments to insole size and moulding temperature. Despite these challenges, the final moulding protocol provided a reliable and repeatable method for preparing the STAMPS3D insoles for testing.

Several limitations should be acknowledged. The insole materials supplied by the 3D printing company lacked detailed mechanical specifications, and the proprietary nature of the printing software meant that print temperature, speed and foaming parameters could not be directly accessed or controlled. This limited the ability to fully characterise the manufacturing conditions and introduced uncertainty into the interpretation of stiffness differences. The moulding process could not be fully automated, requiring some degree of manual adjustment, and the combined thickness of the orthosis and STAMPS layer (6 mm + 5 mm) resulted in a device thicker than typical clinical orthoses. These constraints inevitably influenced the behaviour of the system. However, they do not detract from the central finding of this chapter that the STAMPS3D system is capable of capturing strain across contoured surfaces and therefore shows potential to be applied to clinically relevant orthotic geometries. Confidence in the curved-insole results was supported by two observations from the published study presented in Section 6.2. First, the strain patterns obtained on contoured orthoses (Figure 6.2.2) show consistent and interpretable behaviour relative to the flat condition, including expected redistribution of strain. Second, the contoured conditions demonstrate offloading patterns that align with the established pressure literature, with forefoot strain reducing and load shifting towards

the midfoot, particularly the lateral midfoot, when using full-contact contoured orthoses. These findings indicate that STAMPS3D performs appropriately on curved geometries and that the strain responses observed on contoured insoles are both biomechanically plausible and consistent with known offloading behaviour.

Overall, the supplementary work presented in this chapter strengthens the methodological foundation of the published study and demonstrates the feasibility of extending the STAMPS3D approach to more complex, patient specific devices. While further refinement is needed to optimise material selection, moulding consistency and device thickness, the results highlight the potential for STAMPS3D to support future clinical applications in orthotic assessment and design.

6.5 Chapter Conclusions

This chapter identified the key steps required to adapt the STAMPS3D system for use with contoured orthotic devices. Through characterising the mechanical behaviour of the insole materials, refining the moulding protocol and conducting preliminary strain testing, the work clarified the conditions under which reliable strain capture can be achieved on complex geometries. These developments ensured that the experimental choices made in the main study, including the selection of stiffness categories, insole thickness and testing configurations, were supported by evidence rather than assumption.

Although several practical constraints were encountered, including limited material information and the need for some manual moulding adjustments, the final protocol provided a consistent and repeatable approach for preparing STAMPS3D insoles. Importantly, the chapter demonstrated that strain data can be obtained from contoured orthoses, supporting the feasibility of extending the system beyond flat or simplified geometries.

Overall, this work strengthens the methodological foundation of the thesis and positions the STAMPS3D system for further refinement and application. The insights gained here directly inform the interpretation of the main study and provide a clear platform for the broader considerations explored in the following chapter.

Chapter 7

Measuring In-Shoe Plantar Strain Outcomes in the Presence of Callus: A Preliminary Study using the STAMPS3D Measurement System

The work reported in Section 7.2 of this chapter has been published as:

Francesca Sairally, David A. Russell, Heidi J. Siddle, Daniele Trinca, Claire Brockett and Pete Culmer. *Journal of Foot and Ankle Research*, 19(2), p.e70169, 2026.

Article DOI: https://doi.org/10.1002/jfa2.70169

The graphical abstract for this paper is shown in Figure 7.1.1, with corresponding dataset available at: https://doi.org/10.5518/1820

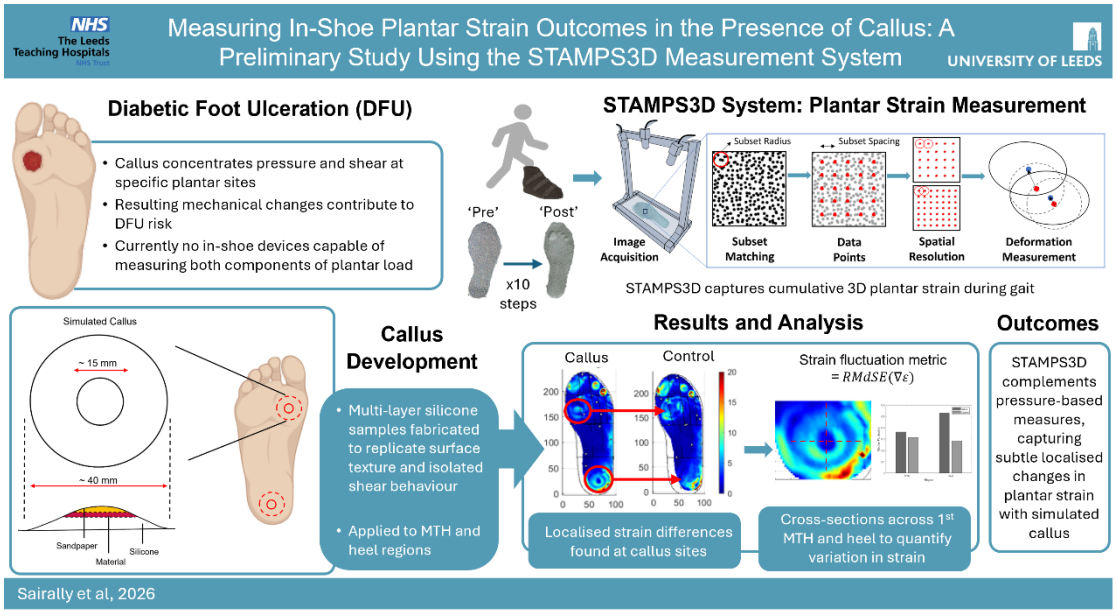


Figure 7.1.1: *Graphical abstract for the paper: Measuring In-Shoe Plantar Strain Outcomes in the Presence of Callus: A Preliminary Study using the STAMPS3D Measurement System.*

7.1 Preface

This chapter reports the development and evaluation of a simulated plantar callus designed to investigate how a healthy foot responds to a localised region of increased stiffness, designed to represent a callus, using the STAMPS3D system. This work was also motivated by insights from the PPIE activities described in Chapter 5, where stakeholders highlighted the clinical importance of callus in diabetic foot ulcer risk and raised questions about whether STAMPS3D could be used to study callus-related loading. The proof-of-concept study presented in Section 7.2 was submitted as 'Measuring In-Shoe Plantar Strain Outcomes in the Presence of Callus: A Preliminary Study using the STAMPS3D Measurement System' and represents a key step toward understanding how localised mechanical changes influence plantar strain patterns.

As first author, my contribution to the paper comprised the design and fabrication of the callus samples, development of the testing protocol, all STAMPS3D data collection and the full processing, analysis and interpretation of strain data. The dataset is available in the Research Data Leeds Repository (DOI: https://doi.org/10.5518/1820). Section 7.3 presents the Preliminary Work and Supporting Data, which expands on the iterative material tests, sample refinement and exploratory strain assessments that informed the final methodology. These components of work were not included in the published manuscript but are essential for demonstrating the methodological reasoning and rigour underpinning the study. Sections 7.4 and 7.5 present the Discussion and Conclusions, summarising the key findings and limitations of the preliminary work and outlining how they inform the design of the final study.

7.2 Publication

The following publication presents a proof-of-concept study examining plantar strain behaviour in the presence of simulated callus and comparing strain-based measurements with pressure-based measurements of plantar loading. To support interpretation of the findings discussed within the thesis, two research questions are provided to clarify the specific areas of focus within this work:

- Can STAMPS3D detect localised or global changes in plantar strain in the presence of a simulated callus that replicates key tactile and mechanical features of biological callus?
- How do plantar strain patterns measured using STAMPS3D relate to plantar pressure patterns measured using Pedar, and do callus and no-callus conditions reveal differences between pressure-based and strain-based indicators of plantar loading?

More broadly, these components of the study evaluate the sensitivity of the STAMPS3D system to local stiffness contrasts that may occur in real callus tissue and differences in

plantar loading, providing insight into how the system performs relative to established sensor-based technologies.

Abstract

Introduction: Diabetes-related foot ulcers (DFU) are growing in prevalence, driven by the global rise in diabetes [28]. Plantar callus has been identified as a risk factor for DFU formation, with its presence considered highly predictive for ulceration [29], [31]. Preventative strategies, such as debridement and offloading aim to reduce the thickness of localised hard skin formed through repetitive high pressure and shear stress [30], [187]. Although several studies have looked at the quantitative effects of callus and its removal in the neuropathic foot, assessments have relied solely on pressure measurements, neglecting the contribution of shear stress [87], [88]. A lack of in-shoe measurement devices capable of measuring shear, either independently or alongside pressure, limits our understanding of how the foot behaves in the presence of callus or responds as a result of debridement.

Methods: This proof-of-concept study investigates the use of the STAMPS3D system to capture cumulative 3D plantar strain data across the foot in the presence of simulated callus in healthy participants. By introducing multi-layer silicone inserts that replicate key mechanical features of callus at the 1st metatarsal head and heel regions, this study explores plantar strain responses in healthy participants.

Results: The simulated callus produced subtle redistribution of strain across the foot with distinct local changes at the callus sites.

Conclusion: Findings may inform future approaches to objective callus assessment, guide debridement practices and contribute to DFU prevention strategies.

Introduction

Plantar callus is a dermatological response to repetitive high pressure and shear, resulting in localised thickening of the skin [28]. While often asymptomatic and protective in healthy individuals, callus can become pathological when pain develops or mechanical stress acts between callus, underlying soft tissue and prominent bone [29], [30]. In people with diabetes, and particularly peripheral neuropathy, this may go unnoticed, elevating the risk of tissue breakdown and ulcer formation. Accordingly, plantar callus is recognised as a risk factor and predictive marker for diabetic foot ulcers (DFUs) [29], [30], [31], [84], [86]. Callus debridement is a common intervention to reduce risk; in those with diabetic neuropathy studies report plantar pressure reductions by up to 30% after debridement [86], [87], [88] yet outcomes in other groups are mixed, with no significant change in rheumatoid arthritis [31], [89] or healthy cohorts [30]. These differences may

suggest context-dependent biomechanics influenced by pathology and sensory feedback.

Despite extensive literature linking callus to elevated plantar pressure, few studies have examined how callus and debridement impact plantar shear stress, an important contributor to plantar loading and skin breakdown. Increased peak-to-peak shear stress has been reported at callus sites in people with diabetes, even when plantar pressures do not differ between callused and non-callused regions [188]. This suggests that shear may play a distinct role in callus formation and DFU risk.

Currently, no commercially available in-shoe measurement devices can capture both pressure and shear, or shear alone, so plantar pressure remains a gold-standard. Furthermore, existing technologies are typically time-consuming, costly and complex to use, therefore not routinely used in clinical practice. Debridement is therefore guided largely by visual assessment and physical measurements rather than objective biomechanical data and neglect the influence of plantar shear.

While increased plantar pressure has been long associated with DFU formation [96], [101], peak pressure alone is an unreliable predictor [96], [171]. Veves et al found that only 38% of ulcers were located at peak pressure sites, with some occurring at pressures considered ‘normal’ [101], [102]. Others report ulceration occurring at both peak pressure and peak shear sites, though the dominant mechanical force remained unclear [82], and a recent systematic review reported elevated shear stress levels in patients with existing or prior DFUs compared to un-ulcerated individuals [90].

Despite DFU formation being associated with plantar pressure and shear, the availability of measurement devices capable of capturing both components of plantar load simultaneously are limited due to the technical difficulty involved. However, research teams have begun to address this gap. Custom platforms with embedded sensors have been developed, and can capture both plantar pressure and shear, with this being at the expense of capturing data strictly under barefoot conditions [111], [112]. While in-shoe devices have been reported that measure both components of plantar load using sensors adhered to the plantar surface or imbedded in an insole [97], [113], [114], [166], [189]. Machine-learning techniques further enhance such measurements, enabling prediction of tissue deformation, tissue injury risk and abnormalities occurring during gait [172], [173], [174]. Although the described sensor-based insoles offer data capture that is real-time and reflect in-shoe walking dynamics, the spatial resolution is constrained by the number and positioning of the sensors integrated.

To address these limitations, the University of Leeds developed the STrain Analysis and Mapping of the Plantar Surface (STAMPS) in-shoe measurement tool, which uses a

plastically deformable insole and Digital Image Correlation (DIC) to capture cumulative plantar strain during gait [116]. Measures of plantar strain reflects the combined mechanical effect of both vertical pressure and shear components of plantar load, providing insight into how the plantar surface of the foot deforms under load, with a spatial resolution of ca. 100 points per cm^2. The STAMPS and STAMPS3D systems use this principle by quantifying cumulative strain across ten steps through DIC, enabling assessment of combined loading even in the absence of direct shear measurement. This offers a novel approach to in-shoe strain mapping in addition to enabling increased adaptability to a range of foot sizes and shapes, compared to other devices set to specific sizes. Technical development and validation of the system are reported in previous work [116], [175]. STAMPS provides a measure that reflects the plantar pressure and shear stresses acting across the foot by capturing their combined effect. Previous work validated the 2D system and identified 'normal' strain measures within a healthy cohort (n=18) [115], [117], however the 2D approach is limited to planar surfaces. STAMPS3D extends this to contoured surfaces using 3D DIC, which has been demonstrated in a proof-of-concept study involving custom orthoses varying in stiffness [175], [190].

This paper presents a proof-of-concept study to evaluate whether STAMPS3D can detect localised and global strain changes in the presence of a simulated plantar callus. By introducing anatomically placed silicone inserts replicating key tactile and mechanical features of callus, this study aims to characterise how these localised changes in stiffness and surface roughness are captured by the STAMPS3D measurement system. These findings will inform future applications in diabetic populations, where subjective offloading strategies and elevated, but undetected, shear pose significant risks for DFU formation.

Methods

A proof-of-concept study consisting of five healthy participants was conducted. Ethical approval was obtained from the University of Leeds Ethics Committee to conduct this study (EPS FREC-2024 1462-2517). Prior to the walking assessments, participants were given participant information sheets and asked for written consent. Participants were included if they were > 18 years old and able to walk unaided for 50 metres. Participants were excluded if they had a diabetes diagnosis, any diabetes-related foot issues (e.g., peripheral neuropathy, peripheral vascular disease, inflammatory arthritis), plantar callus associated with pain and/or underwent regular debridement of plantar callus.

Simulated Callus Development

To replicate the biomechanical effects of plantar callus, multi-layer silicone samples were fabricated and applied to the heel and the 1st metatarsal head (MTH). A 3D printed mould

with a 40 mm diameter indent and maximum central depth of 2 mm was used to cast the silicone samples. This geometry was selected to produce a gradual taper at the sample edge, ensuring a smooth integration to the surrounding plantar skin and to minimise gait disruption. Silicone (Ecoflex 00-30, Smooth-On Inc.) was chosen for final testing based on its values on the Shore OO hardness scale, which aligns with reported values for plantar callus at both the MTH and heel [191]. Some literature reports characteristics of plantar callus such as thickness, hardness, elasticity, hydration and surface texture compared to non-callus sites [191], [192]. However, due to limited quantitative data on the mechanical properties of plantar callus, a representative yet simplified model was developed in consultation with experienced clinicians to encompass the most relevant tactile and structural features. The samples were cured in stages to embed two features; an embedded sandpaper layer (Grit 120) at the surface provided increased roughness (emulating coarse skin layer of callus) and beneath this a layer of woven fabric to provide localised reduction in shear strain within the callus in contrast to surrounding tissue (Figure 7.2.1). A 15 mm diameter piece of 120 grit sandpaper was first adhered to the base of the mould indent to ensure it remained at the surface of the sample. A small volume of silicone was poured into the mould, and a second material insert was placed directly under the sandpaper layer to maintain its proximity to the surface. Once cured, the mould was filled to the top and levelled to create a smooth contact interface. These features introduced a surface texture and an isolated region with altered shear behaviour, consistent with the mechanical characteristics of plantar callus.

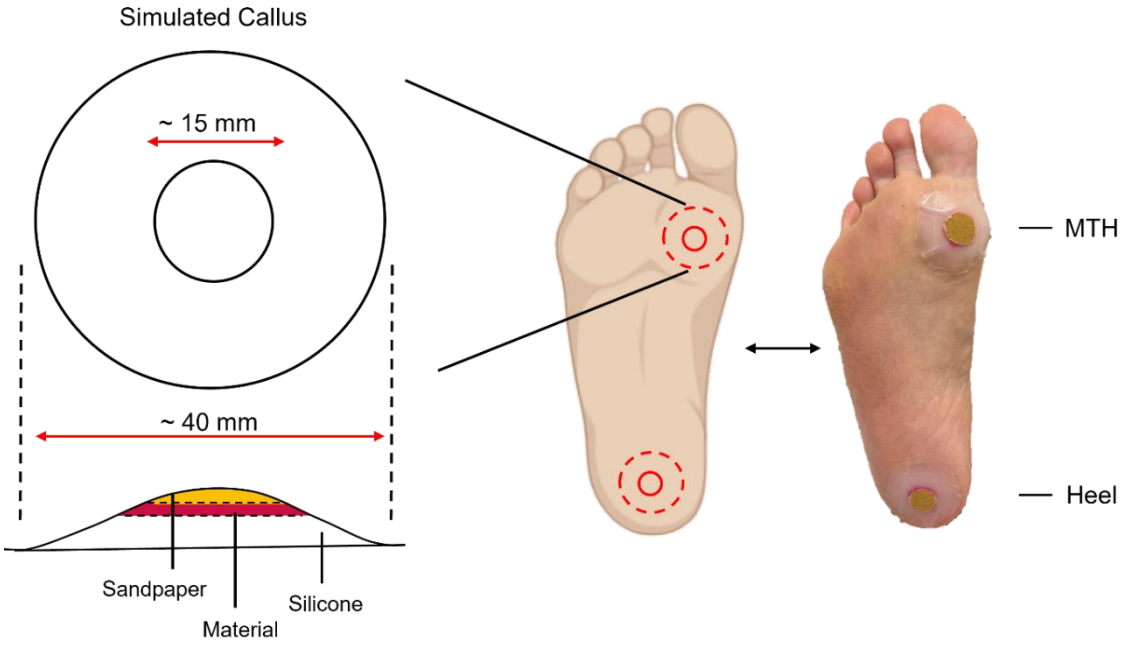


Figure 7.2.1: *Schematic illustrating components of the multi-layer silicone callus samples, adhered to the MTH and heel regions of participants feet.*

Experimental Protocol

Participant shoe size was measured to size STAMPS insoles and corresponding neoprene boots (Ninewells Boot, Chaneco). Details of the STAMPS3D insole fabrication, DIC methods and analysis are reported in previous work [116], [175]. Silicone samples were adhered to the 1st MTH and heel regions of the foot using double-sided tape, as shown in Figure 1. These regions were selected due to their clinical relevance in callus formation, with the 1st MTH also being a common site for DFUs [38], [187]. Thin knee-high nylon socks were used to provide a consistent plantar interface.

A pre-walk image was captured of the STAMPS insole prior to use. The STAMPS insole was then inserted into the right neoprene boot, with a similarly sized insole inserted into the left boot to prevent any differences in insole depth. Participants were asked to walk at a self-selected walking pace for 10 steps on the right foot. This approach was adopted to promote natural gait behaviour, with consistency maintained between participants by standardising the number of steps rather than controlling walking speed. Following the walk, the insole was removed carefully, and a post-walk image was captured of the worn STAMPS insole. This procedure was repeated with and without (control) the simulated callus adhered to each region of the participant's foot, with conditions repeated three times to account for any variability. Subsequent walking assessments were conducted using the Pedar (PEDAR INC., Novel GmbH, Munich, Germany) in-shoe plantar pressure measurement system under both conditions. It is important to note that the STAMPS3D system captures cumulative strain, which reflects the combined effects of vertical pressure and shear stresses, whereas the Pedar system measures only vertical plantar pressure. This enabled comparison between strain and pressure distributions.

The images captured were processed using DuoDIC, a 3D DIC software, following procedures outlined in previous work [175]. Peak magnitude of strain (S_{MAG}) was defined as the maximum strain value observed within each region of interest. This measure was used to identify differences between callus and control conditions across anatomical regions and whether the presence of callus has a global effect on the foot. To quantify localised variation in strain patterns, horizontal and vertical cross-sections were extracted through the centre of the callus samples and corresponding regions in control samples. A strain-fluctuation metric was calculated as the Root Median Squared Error (RMdSE) of the differentiated strain values along each cross-section, using median to minimise the influence of outliers. The process of determining the strain-fluctuation metric is demonstrated in Figure 7.2.2. Peak plantar pressure (PPP) measurements were also analysed to evaluate potential correlations between

pressure and strain, and to determine whether peak pressure regions aligned with the simulated callus sites.

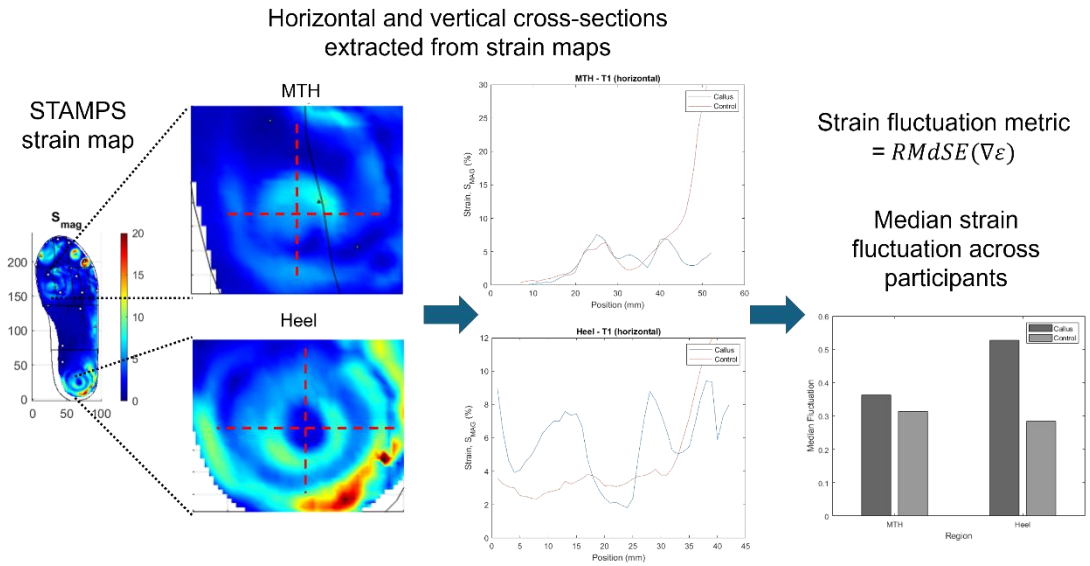


Figure 7.2.2: *Process used to calculate the median strain fluctuation metric across participants for each region and test condition. The x-axis on the cross-section plots represents the distance along the extracted cross-section and is shown at the same scale as the strain maps.*

Post-processing and Statistical Analysis

Descriptive statistics were used to summarise strain and pressure data, with median values and interquartile ranges reported to capture central tendency and variability across participants. Paired t tests were performed for each participant and repeated to compare strain fluctuation between callus and control conditions separately for MTH and heel regions. These analyses were intended to illustrate consistency and variability across individuals, rather than to provide population level inference. Statistical significance was defined as $p < 0.05$.

PPP for each anatomical region and globally were extracted using a software mask (Novel, GmbH, Munich, Germany). Spearman's correlation coefficient was used to assess the relationship between peak S_{MAG} and PPP for both test conditions, with a significant relationship being where a moderate and statistically significant correlation was found ($0.4 < rho < 0.69$ and $p < 0.05$). This approach was consistent with the healthy cross-sectional study using STAMPS [117].

Results

Five healthy participants were recruited and successfully completed the walking conditions.

Representative examples of the strain and pressure maps for each condition are shown in Figure 7.2.3. While numerical differences between callus and control conditions were less clear, visual inspection revealed localised regions of changing strain in the callus condition corresponding to sample placement. These localised strain differences seen between the two conditions were particularly noticeable at the heel, where changes in strain pattern correspond to components of the callus sample. This could also be seen at the 1st MTH, however appears to be less distinct. While similar localised effects were seen in the pressure maps, visual differences between conditions were more difficult to distinguish, with increased pressure found at the forefoot and heel in both conditions. These maps illustrate the enhanced spatial resolution of STAMPS3D compared to PPP, with strain maps highlighting deformation patterns that do not always align with peak pressure regions.

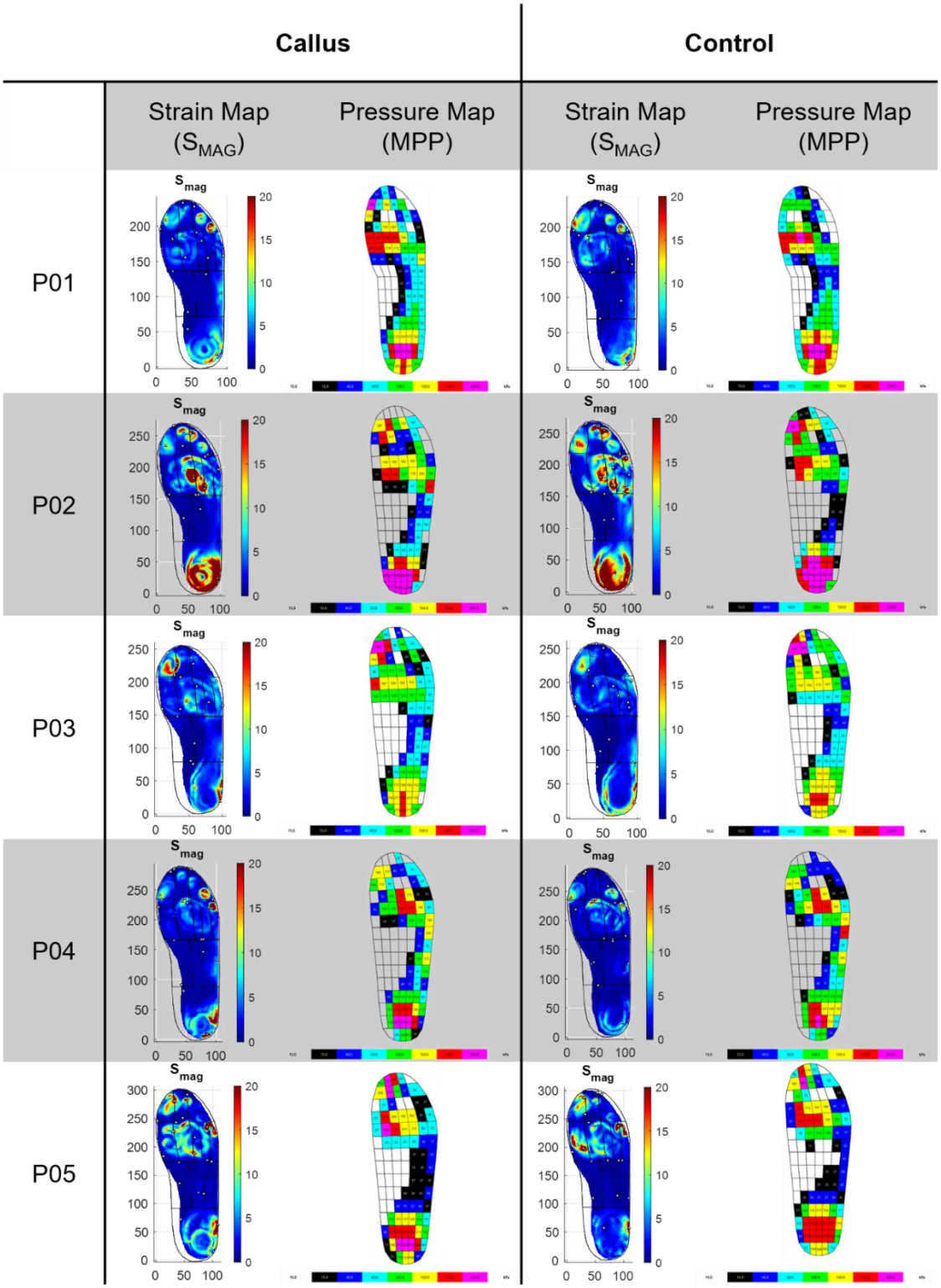


Figure 7.2.3: *Representative examples of plantar strain and pressure distribution maps for both callus and control conditions across five healthy participants.*

Across participants, peak S_{MAG} and PPP were often found at the same anatomical regions for both callus and control conditions, with this occurring at the Hallux, 5th MTH and heel. For example, peak S_{MAG} was found at the heel in 3/5 participants and at the 5th MTH in 2/5 participants in both conditions. PPP was also found at the heel in 3/5 participants and the hallux in 1/5 participants for both conditions. PPP was found at different locations for each condition in one participant with this being at the heel and hallux/2nd toe in the callus and control conditions respectively. PPP and peak S_{MAG} were found at the same location in 2/5 participants, with this being at the heel. Measures reported did not consistently align with the simulated callus sites, reflecting either anatomical variation or edge effects. These differences are summarised in Table 7.2.1, which combines peak S_{MAG} and PPP measures across anatomical regions, reported as a median across all participants and corresponding interquartile range (IQR).

Table 7.2.1: *Peak S_{MAG} and PPP reported for each condition and anatomical region of the foot, with median and IQR used to summarised data across all five participants.*

	Peak S_{MAG} (%)		**PPP (kPa)**	
Anatomical Region	**Callus**	**Control**	**Callus**	**Control**
Global	141.54 (40.22-304.18)	67.71 (59.98-361.23)	416.00 (376.50-420.50)	429.50 (328.00-462.00)
Hallux	21.29 (15.28-22.16)	15.26 (14.61-21.55)	280.00 (194.00-349.50)	333.00 (213.75-429.50)
2nd Toe	18.44 (11.80-18.47)	19.59 (11.07-22.96)	265.75 (157.75-272.50)	258.75 (108.25-306.00)
Toes 3-5	23.73 (12.71-24.02)	28.97 (11.80-34.26)	144.75 (83.50-161.00)	120.25 (72.50-121.25)
1st MTH	11.07 (10.63-12.25)	15.91 (10.34-18.55)	230.50 (114.50-253.25)	154.50 (121.00-250.25)
2nd MTH	15.04 (13.60-44.91)	24.46 (13.82-35.85)	219.00 (185.00-230.50)	236.25 (183.25-250.75)
3rd MTH	7.98 (7.00-21.12)	13.70 (8.21-14.89)	172.50 (169.25-174.25)	167.00 (166.25-191.00)
4th MTH	13.02 (11.23-90.70)	18.57 (13.09-26.72)	202.25 (174.25-224.75)	190.00 (167.00-240.50)
5th MTH	11.47 (9.94-127.98)	52.08 (13.78-54.98)	203.50 (94.00-238.00)	136.25 (126.25-239.25)
Medial Midfoot	1.78 (1.46-1.95)	1.78 (1.72-2.42)	13.00 (11.50-43.25)	25.00 (12.25-50.75)
Lateral Midfoot	6.80 (6.20-7.91)	10.05 (9.51-12.45)	94.75 (85.25-156.75)	93.75 (60.00-148.00)
Heel	42.11 (34.25-92.23)	38.69 (32.18-59.98)	376.5 (319.25-416)	302.00 (286.50-317.25)

For the summary metrics across participants shown in Table 7.2.1, peak S_{MAG} values were higher in the callus condition across the hallux (21.2 vs 15.3) and heel (42.1 vs 38.7) regions, with the remaining toes and forefoot region showing elevated peak S_{MAG} in the control condition. PPP values generally showed greater pressure across anatomical regions in the callus condition, with the most prominent differences found at the toes 3–5 (144.8 vs 120.3), 1st MTH (230.5 vs 154.5), 5th MTH (203.5 vs 136.3) and heel (376.5 vs 302). From the summarised data peak S_{MAG} and PPP were found at different locations for each condition, with peak S_{MAG} and PPP both found at the heel in the callus condition and at the 5th MTH and hallux respectively in the control condition.

Figure 7.2.4 summarises the median strain fluctuation across participants. Fluctuation analysis revealed consistent increases in localised strain variability within the callus condition, particularly at the heel. Vertical cross-sections through the heel region showed significantly greater fluctuation ($p < 0.005$) in all five participants, while horizontal cross-sections showed significant increases ($p < 0.05$) in three participants. In contrast, the MTH region demonstrated less consistent differences, with only two participants showing significant increases in vertical cross-sections and none in horizontal. These results concur with visual inspection of the strain maps, where samples at the heel produced more distinct and localised deformation patterns than those at the MTH.

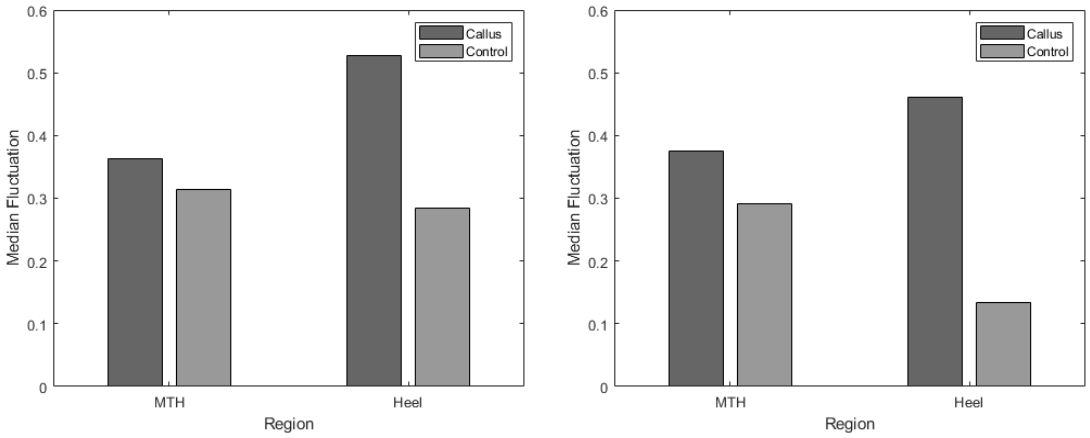


Figure 7.2.4: *A summary of median strain fluctuation measured across horizontal (left) and vertical (right) cross-sections across the MTH and heel regions for both callus and control conditions.*

Peak S_{MAG} and PPP were found to be moderately correlated for both conditions, with PPP increasing with increased S_{MAG}. Spearman's correlation coefficient was found to be 0.57, $p < 0.001$ for the callus condition and 0.55, $p < 0.001$ for the control. The relationship between the two plantar measures is demonstrated in Figure 7.2.5. For each participant there was moderate to strong correlation between peak S_{MAG} and PPP for all five participants across both conditions, ranging from 0.42-0.76.

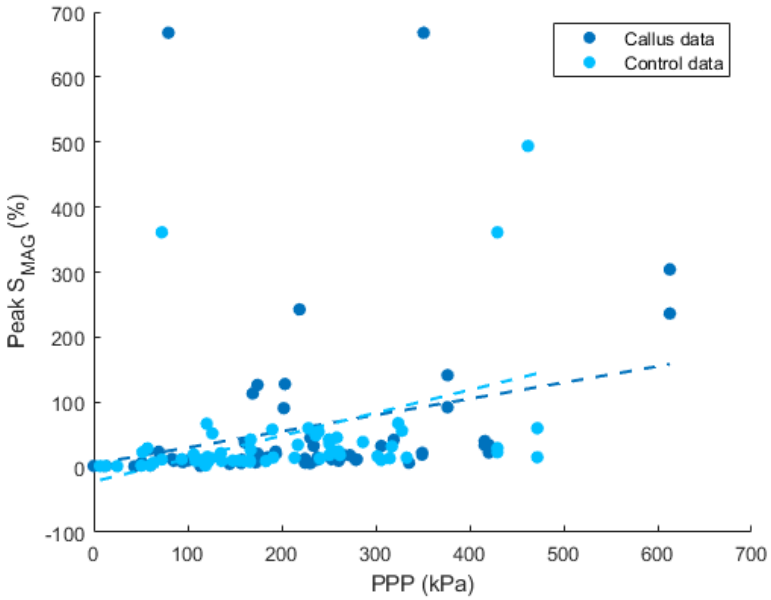


Figure 7.2.5: *Scatter plot demonstrating the correlation between peak S_{MAG} and PPP across all participants for callus and control conditions.*

Discussion

This proof-of-concept study demonstrates that STAMPS3D can quantify local and global plantar strain patterns in the presence of simulated callus, complementing traditional pressure measurement systems. Localised strain differences were consistently found at callus sites, particularly at the heel, whereas effects at the 1st MTH were less distinct. The control conditions are similar, suggesting the effects of MTH anatomy may dominate over those of callus. The effect in pressure distribution was less pronounced but showed similar trends, consistent with typical loading patterns of walking [193], [194]. The reduced sensitivity in pressure measures may reflect the reduced spatial resolution compared to STAMPS3D, (ca. 8 vs 560 datapoints at 1st MTH respectively). These findings highlight the enhanced spatial resolution of strain-based metrics compared to pressure alone, enabling STAMPS3D to capture subtle, anatomically specific changes in plantar loading.

Across participants, peak S_{MAG} tended to increase at the heel and hallux with callus; regions typically experiencing high loads during gait and linked to ulceration [35], [38], [193], [194]. Since heel loading is largely unavoidable, this increased strain is consistent with heel-strike mechanics. Forefoot regions were varied, with some responses showing higher S_{MAG} without callus. Lower forefoot strain under the callus condition may reflect an individual's anatomical structures influencing load distribution and (in this cohort of healthy individuals with intact sensation) subconscious gait adaptation to offload areas where a foreign object is perceived. In this proof-of-concept study, anatomical foot shape was not recorded, but these results indicate that this

should be included in future studies. PPP measures were elevated in 8/11 regions under the callus condition, commensurate with reports of elevated pressure at callus sites in diabetic cohorts (particularly forefoot and heel) with reduction (25–30%) following debridement, increased to 54% when combined with orthoses [87], [88]. Healthy cohorts also show higher pressure with callus, but debridement does not reduce this, highlighting differences in tissue resilience and adaptation [30]. The larger global peak S_{MAG} observed in the callus condition may partly reflect inter-participant variability, as one participant exhibited substantially higher strain values at the heel in both conditions, influencing the overall median. In addition, STAMPS3D identified regions of elevated strain outside the simulated callus sites, features not detected by the Pedar system, which measures only vertical pressure. This likely contributes to the greater global difference in strain compared with PPP. It is also possible that the short walking protocol (10 steps) captured only the early response to altered local stiffness, where more pronounced differences around the callus regions may emerge over longer cumulative loading. Alternative measures such as median strain across each anatomical region were also considered to capture cumulative deformation effects. These showed similar trends but were less directly comparable to the PPP data, which reflect maximum vertical loading. For consistency in benchmarking between systems, peak S_{MAG} was used as the primary measure, though future work may explore median or cumulative strain metrics to assess broader intra-regional strain behaviour.

Peak S_{MAG} and PPP occurred at the heel under the callus condition, but their locations differed in the control condition. This suggests that shear strain measures may capture aspects of local tissue deformation not reflected in pressure alone. This hypothesis is consistent with studies showing elevated peak-to-peak shear at callus sites despite non-significant PPP differences [188]. Callus is a common precursor to ulceration in people with diabetes and peripheral neuropathy, where altered plantar loading and reduced protective sensation increases risk [29]. In contrast, healthy individuals may also develop callus, but typically without the same pathological consequences, reflecting differences in tissue resilience and mechanical adaptation. Our results show that strain variability can be detected even in non-neuropathic feet, supporting the notion that STAMPS3D may help distinguish adaptive and maladaptive callus in diabetic cohorts. Correlations were moderate and significant between PPP and peak S_{MAG} in both conditions (rho = 0.57 and rho = 0.55, $p < 0.001$), aligning with prior findings from a healthy cohort (rho = 0.62, $p < 0.001$) [117]. A moderate correlation was expected, as peak S_{MAG} reflects cumulative deformation arising from both vertical pressure and shear loading, whereas PPP represents only the vertical component. The two measures are therefore related but not interchangeable. The strength of the correlation observed here and consistency with previous findings in healthy cohorts, suggests that while pressure contributes substantially to overall strain, STAMPS3D

also captures additional shear-related deformation that is not represented in PPP alone. Beyond peak values, a strain variability metric was developed to provide a novel means to assess complex strain responses. Strain variability increased consistently under callus, particularly at the heel, concurring with visual differences in strain maps. This metric may help capture subtle load changes not evident from peak shear and may provide insight into why regions such as the MTH and heel are more prone to tissue breakdown in neuropathic feet. These local strain-fluctuation patterns further demonstrate the sensitivity of STAMPS3D to detect subtle variations in plantar loading that are not captured by vertical pressure systems. The high spatial resolution of the strain maps enables identification of localised deformation responses at the callus sites that remain invisible to pressure-only devices such as Pedar. This level of measurement resolution is beyond the capability of current in-shoe systems and highlights the potential of strain-based metrics to reveal clinically relevant loading behaviour that may otherwise go undetected.

Beyond the immediate findings, this work builds on a previous STAMPS3D study demonstrating the system's ability to quantify plantar load on contoured, variable stiffness orthoses, reinforcing its potential relevance to clinical offloading practice [190]. In contrast, the present study was focused on using the flat STAMPS insole, with no orthotic device, to isolate the effect of the simulated callus without interactions from contoured geometry. Offloading and debridement are the two primary management strategies recommended by the IWGDF for preventing and treating DFUs [28], yet current clinical decision making relies heavily on visual inspection and pressure-only metrics, which do not capture shear-related tissue deformation. By providing a cumulative, spatially detailed measure of plantar strain, STAMPS3D offers a practical, low-cost and potentially feasible for bedside implementation as an alternative to laboratory-based plantar load measurement systems. This positions STAMPS3D as a promising tool for objective assessment of callus-related loading, evaluation of debridement effectiveness and optimisation of offloading interventions in people with diabetes.

Limitations of the study relate primarily to the small proof-of-concept sample size, limiting the ability to generalise, therefore results should be interpreted with caution. The STAMPS3D technique is inherently a compound measure, thus precluding capture of dynamic data, but bringing increased spatial resolution compared to real-time sensor systems [175], [190]. The simulated callus may not fully replicate the complex mechanical properties of plantar callus in vivo but does recreate local variation in tissue stiffness reported in literature. Future work will evaluate STAMPS3D for clinical use, focusing on people with diabetes and neuropathy, to assess whether strain metrics can identify callus-associated deformation and DFU risk. Longitudinal

studies could reveal high-risk regions and evaluate whether STAMPS3D can guide debridement, individual susceptibility to ulceration and personalised off-loading approaches.

Conclusions

This proof-of-concept study in healthy participants demonstrates that STAMPS3D can detect localised differences in plantar strain associated with simulated callus, complementing pressure-based measures. While pressure metrics showed modest differences between callus and control conditions, strain measures revealed consistent, anatomically specific changes, particularly at the heel. These findings highlight the virtue of strain-based metrics in capturing tissue-level deformation that may be indistinct in pressure alone. The study establishes methodological feasibility and provides a foundation for future clinical evaluation. STAMPS3D can help bridge the gap between pressure-based monitoring and tissue-level biomechanics to support risk assessment and intervention planning; guiding debridement strategies and offering new insights into ulceration risk and prevention. Given its low-cost, adaptable design and minimal technical requirements, STAMPS3D has the potential to evolve into a clinically practical, bedside tool aligned with IWGDF offloading recommendations.

7.3 Preliminary Work and Supporting Data

Callus formation is a well-established marker of elevated plantar loading and a recognised precursor to diabetic foot ulceration [29], [30], [31], [84], [86]. Its presence reflects localised changes in mechanical behaviour characterised by features such as increased stiffness and hardness of tissue, reduced hydration and altered shear [192]. Consequently, this contributes to a concentration of stress within the underlying tissues. In Chapter 5, stakeholder discussions also highlighted callus and its link to ulceration risk, as a key clinical concern, emphasising the need for better understanding of how callus alters plantar loading and how this might inform prevention. These priorities aligned with the literature, which similarly identifies a lack of tools capable of capturing the combined pressure-shear environment associated with callus. Together, this motivated the development of a simulated callus model to explore how localised stiffness influences plantar strain and to support future preventative strategies.

During the early planning phase of the study, the intention was to use STAMPS3D to quantify changes in plantar strain before and after clinical debridement of callus tissue. However, the time and ethical requirements associated with recruiting individuals with active callus meant that this study could not be undertaken within the scope of the PhD. An alternative approach was adopted in which a physical model of a callus was used to

investigate how a healthy foot responds to a localised region of increased stiffness intended to mimic key biomechanical features of callus.

The following sections describe the iterative development of this simulation, beginning with exploratory tests to determine whether STAMPS3D could detect a distinct region of altered mechanical behaviour. These early trials informed the design of a 3D printed mould used to cast silicone samples with controlled geometry, followed by the refinement of material composition, embedded layers and surface texture. Preliminary strain assessments were conducted throughout this process to evaluate whether each iteration produced meaningful localised changes in plantar strain. This development process is illustrated in Figure 7.3.1. Together, this work established the rationale and final design of the callus samples used in the experimental study presented in Section 7.2.

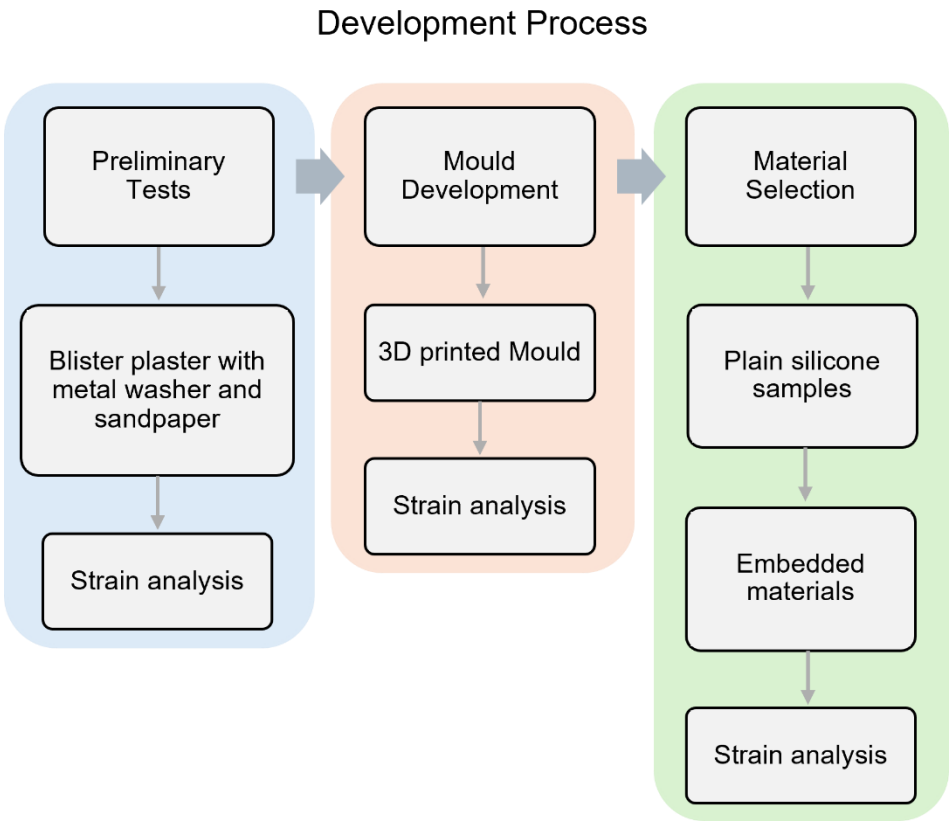


Figure 7.3.1: *Illustration of the development process carried out prior to the final proof-of-concept study presented in Section 7.2.*

7.3.1 Design Requirements for a Simulated Callus

The design of a simulated plantar callus required an understanding of the structural and mechanical characteristics that distinguish callused from non-callused skin. Holowka et al. reported barefoot measurements of callus thickness, hardness (Shore OO), and stiffness (N/mm) at the 1st MTH and heel, providing quantitative ranges for these properties in healthy individuals [191]. For shod conditions, callus thickness was

approximately 1.1 ± 0.2 mm at the 1st metatarsal head and 1.4 ± 0.3 mm at the heel, with corresponding hardness values of 31.1 ± 8.9 and 42.5 ± 10.2 Shore OO, and stiffness values of 7.01 ± 2.35 and 5.9 ± 1.4 N/mm respectively. These data indicate that callus is both thicker and mechanically stiffer than healthy skin.

Complementary work by Hashmi et al. described additional qualitative differences between callused and non-callused sites, including reduced hydration at the callus centre, greater elasticity at the periphery and subtle differences in surface texture [192]. Their observations suggest that callus does not present as a uniform block of stiff tissue but instead exhibits a gradual transition from a firmer, drier centre to a softer edge. This gradient is clinically relevant, as it influences how stresses are transferred to underlying and surrounding healthy tissue. Although the literature describes some of the mechanical properties of callus, it provides little information on typical callus diameter, which varies widely across sites and individuals. Therefore, clinical input was essential in guiding the size used in the simulated model.

Comparative measurements of non-callused plantar skin further contextualise these differences. Reported values include heel skin thickness of 0.78 ± 0.17 mm and hardness of 28.66 ± 7.9 Shore OO, and 1st metatarsal head skin thickness of 0.72 ± 0.10 mm with hardness of 29.1 ± 14 Shore OO [195]. These ranges overlap with the lower end of callus hardness values, reinforcing the need for a surrogate that is stiffer than healthy skin but still within physiologically limits reported.

Despite these insights, quantitative data on the full mechanical behaviour of plantar callus remain limited. As a result, a simplified but representative surrogate was developed in consultation with experienced clinicians. The design aimed to capture the most clinically relevant features: a slightly thickened central region, increased stiffness relative to surrounding skin, a gradual transition toward the edge and a roughened surface texture. The final design requirements for the simulated callus model are outlined in Table 7.3.1. These characteristics formed the basis for the material selection, mould geometry, and embedded-insert approach described in the following sections, which led to the final silicone callus model used in the proof-of-concept study presented in Section 7.2.

Table 7.3.1: *Final design requirements for the simulated callus model.*

Final Design Requirements
• Variable thickness ensuring distinct central region • Increased material stiffness to contrast healthy skin, guided by literature • Smooth transition to participants surrounding skin • Surface texture to reflect callus tissue roughness

7.3.2 Preliminary Tests of Early Callus Simulation

Before developing a bespoke silicone callus, an initial set of tests was conducted to determine the efficacy of using STAMPS3D to measure localised regions with altered mechanical properties on the plantar surface. Ethics approval was obtained from the University of Leeds Ethics Committee to conduct this exploratory work prior to the final study (EPS FREC-2024 1462-2517). A blister plaster was applied to the foot with a small metal washer adhered to its surface and sandpaper was added to introduce surface roughness. Although this configuration did not resemble true callus, it provided an extreme case of localised stiffness intended to test the sensitivity of the system. Figure 7.3.2 shows the construction of the sample and its placement at the 1st MTH and heel.

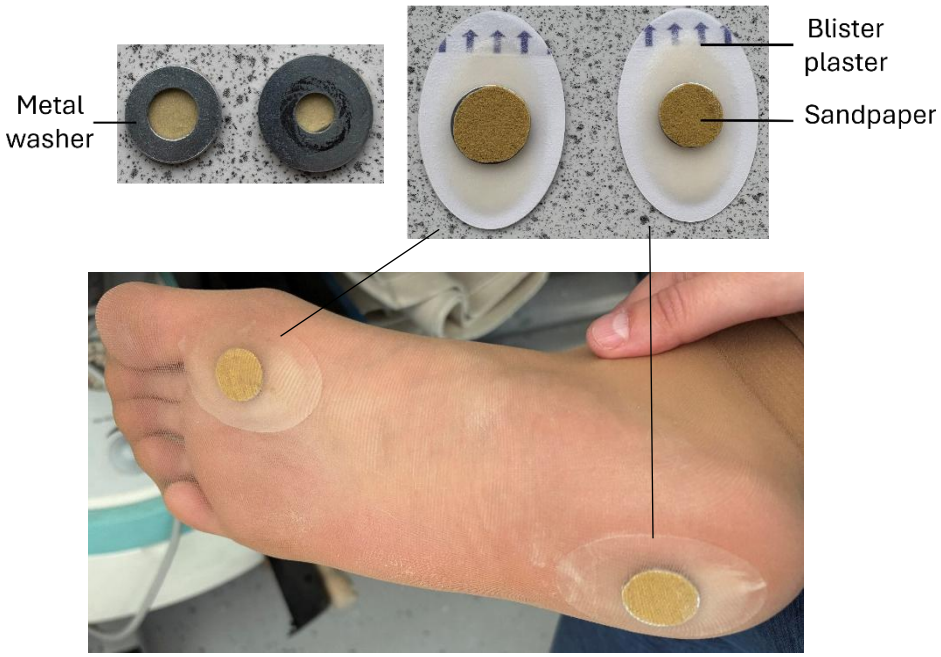


Figure 7.3.2: *Demonstration of initial simulated callus samples, using a blister plaster, metal washer and sandpaper, adhered to the 1st MTH and heel.*

When placed at the 1st MTH and heel, the simulated region produced measurable changes in plantar strain. At the MTH, peak strain values were similar to the control condition without the plaster, but increased strain was observed at the lateral midfoot,

suggesting offloading. At the heel, strain was substantially higher than in the control condition, consistent with the inability to naturally offload this region during gait. Local strain measurements were also taken at the centre and edge of the simulated callus, showing a small increase at the centre and a more pronounced increase at the edge compared to control. Cross-sectional strain profiles revealed localised peaks at both the 1st MTH and heel. These findings demonstrated that STAMPS3D could detect localised mechanical changes, but the extreme stiffness of the washer-based sample and its lack of anatomical resemblance indicated the need for a more representative material. These effects are illustrated in Figure 7.3.3, which shows the corresponding strain map, cross-sections and summary of central strain values for the callus and control conditions.

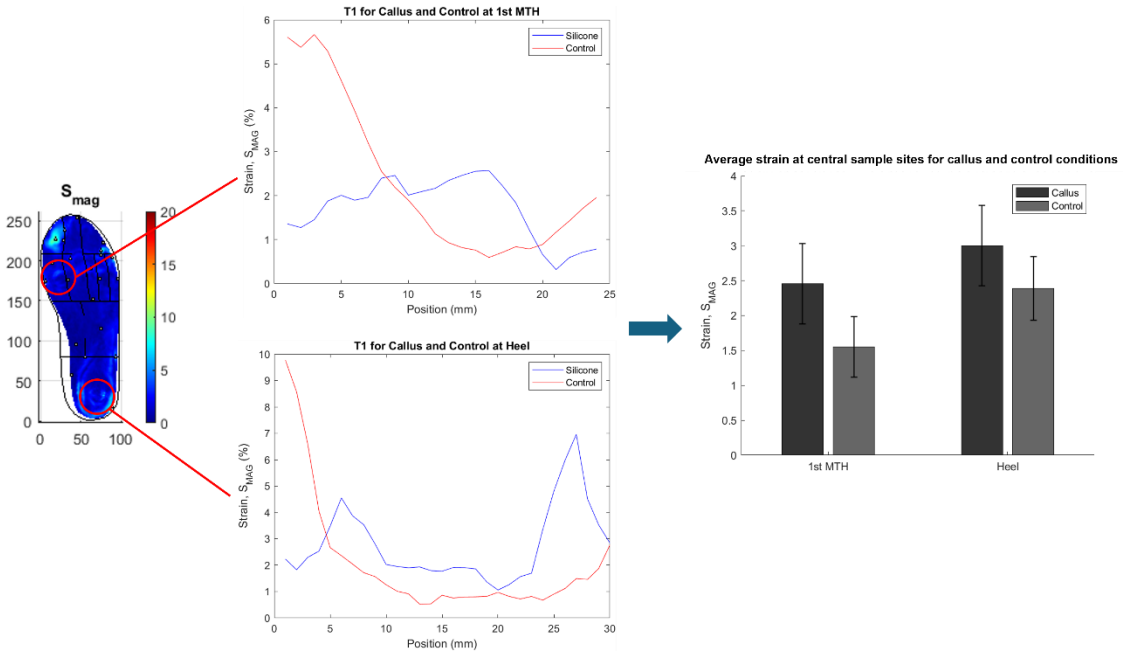


Figure 7.3.3: *Strain response to the initial exploratory callus simulation: The strain map illustrates localised changes in strain at the 1st metatarsal head and heel when the sample was applied, with corresponding cross-sections revealing distinct differences in strain distribution between callus and control conditions. The bar chart provides a summary of average strain at the central sample sites, confirming a measurable increase in strain in the surrogate condition (Error bars = +/- STD).*

7.3.3 Mould Development

To replicate the key mechanical and structural features of plantar callus, a model cast using silicone was developed incorporating a central thickened region, embedded material layers and surface texture. Silicone was selected as the base material as it allowed the sample geometry and mechanical characteristics to be adapted to meet the design requirements presented in Table 7.3.1.

To produce samples with a known geometry and a smooth transition to the surrounding skin, a 3D printed mould was designed. The mould consisted of a 50 × 50 × 10 mm plate

with a 40 mm diameter indent and a maximum depth of 2 mm. Although this thickness exceeded values reported in the literature, it was selected to ensure a clear biomechanical contrast while accommodating variability introduced during silicone curing.

A central raised region was incorporated to mimic the increased thickness typically observed at the centre of callus. Early mould iterations used a pointed central feature, which was later refined to a rounded 10 mm diameter dome to create a smoother, more anatomically comparable profile. As mentioned, there is limited quantitative evidence describing the typical size of plantar callus, with the studies highlighted reporting local mechanical characteristics rather than overall dimensions. Clinical input therefore guided the selection of the sample size. The central thickened region of the mould (10 mm diameter) was chosen to represent the area of greatest stiffness, with the tapered profile extending to an overall diameter of 40 mm. This geometry allowed the sample to taper gradually toward the edge, reducing any abrupt transitions that could influence gait or cause discomfort.

7.3.4 Material Selection

The development of the final silicone samples was carried out through an iterative approach to identify the most appropriate materials, ensuring a robust representation of the characteristics of plantar callus. As silicone Shore hardness increases, the material becomes stiffer and less deformable, providing a way to approximate the increased rigidity of callused tissue. This informed the initial exploration of silicones with different hardness values to determine whether stiffness alone could produce detectable changes in plantar strain.

Plain Silicone Samples

Initial samples were cast using commercially available silicones with a range of hardness values, including Dragon Skin 10, 20 and 30, and Ecoflex 00-30 and 00-50, based on the literature highlighted in Section 7.3.1. Equal parts of components A and B were mixed according to manufacturer instructions. Ecoflex 00-50 cured rapidly, beginning to set during degassing and resulted in trapped air bubbles, whereas the other silicones produced smoother samples.

These plain silicone samples were used to assess whether differences in material stiffness alone produced detectable changes in plantar strain. Although some localised effects were observed, the behaviour of the samples did not fully reflect the mechanical contrast expected of callus and the lack of surface texture limited their reflection of callus in vivo. This is because increasing silicone hardness primarily alters stiffness, whereas callus also exhibits altered resistance to shear. As a result, plain silicone could not

reproduce the dual mechanical response of callused tissue, and additional reinforcement was required to create a more distinct local contrast and better represent the shear-related behaviour observed clinically.

Samples with Embedded Materials

To introduce a more distinct region of altered shear behaviour, additional materials were embedded within the silicone. Ecoflex 00-30 samples were cast with mesh and three alternative insert materials. Clinicians were asked to compare the samples and identify which combination most closely replicated the characteristics of callus encountered in clinical practice. Feedback indicated that one of the materials (a pink, moderately stiff insert) produced a tactile response most comparable to callus when paired with silicone. Figure 7.3.4 shows examples of the plain silicone samples and those with embedded material.

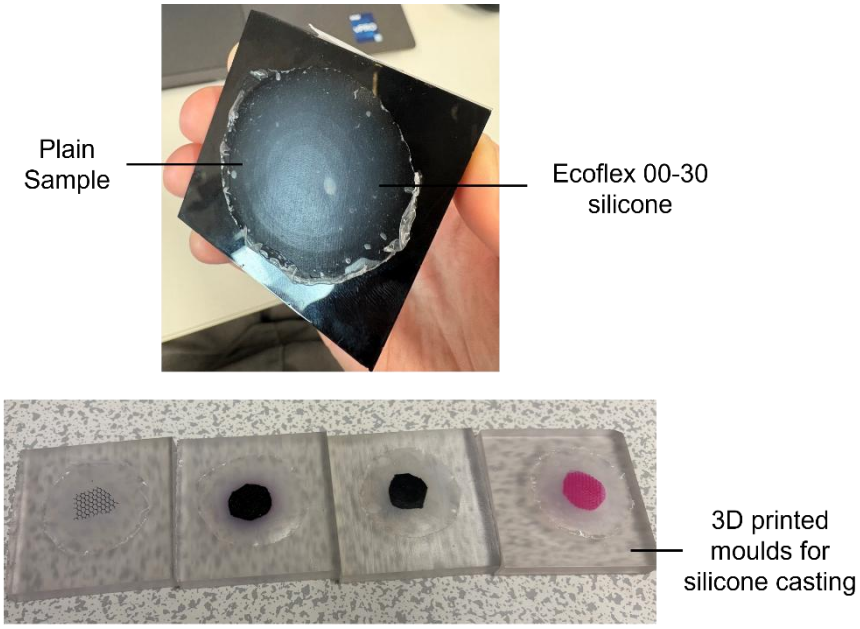


Figure 7.3.4: *Examples of silicone samples produced during the early development, including plain silicone sample cast using Ecoflex 00-30 and those with embedded materials.*

To replicate the roughened surface typical of callus, 120-grit sandpaper was incorporated into the samples using a two-stage curing process. A 15 mm diameter piece of sandpaper was adhered to the base of the mould using double-sided tape, a thin layer of silicone was poured, and the insert material was positioned beneath the sandpaper. Once cured, the mould was filled to the top and levelled to create a smooth contact interface. These features introduced a surface texture and an isolated region with altered shear behaviour, consistent with the mechanical characteristics of plantar callus described in the literature and observed clinically.

7.3.5 Preliminary Strain Assessments in the Presence of Callus

Preliminary strain assessments were conducted throughout the development process to evaluate whether each sample type produced meaningful localised changes in plantar strain and to guide the selection of the final design. These assessments were not intended as a comprehensive comparison of all materials, but instead as tests to determine whether specific design features, such as material stiffness, embedded inserts and surface texture, produced detectable and interpretable strain responses. Strain maps and cross-sectional strain profiles (generated using the approach described in Experimental Protocol of Section 7.2) were used to visualise both global and local strain behaviour for each sample type. A fluctuation metric was also calculated from these cross-sections by differentiating the strain values along the profile and summarising the magnitude of local variation using a robust RMS-like measure (square-root of the median squared gradient).

Plain Silicone Samples

Initial tests were performed using plain silicone samples placed at the 1st MTH and heel. Ecoflex 00-30 was tested at the 1st MTH and Ecoflex 00-50 at the heel to reflect the relative stiffness differences reported in the literature. Global strain measures were compared across anatomical regions and local strain values were extracted at the centre and edge of the sample region from the data to determine whether these differed from the peak or median strain within the broader region. Cross-sectional strain profiles were generated by extracting strain values from a single line of data corresponding to the centre of each sample, and were examined to visualise how strain varied across the region.

Differences in strain patterns with and without callus present were not clear from the strain maps, with global strain values not showing distinct differences except at the lateral midfoot which reported larger measures in the callus condition. As sample placement from the strain maps were not clear, extraction of accurate centre and edge sample measures was not possible. This reinforced the need for a sample that provides greater mechanical contrast.

Silicone Samples with Embedded Materials

Subsequent tests focused on samples incorporating embedded materials and surface texture, as shown in Figure 7.3.4. Ecoflex 00-30 samples containing a material insert and sandpaper produced the first clear appearance of localised ‘strain rings’ indicating a sharper transition in mechanical behaviour between the central region and surrounding silicone (Figure 7.3.5). Ecoflex 00-50 samples with the same configuration produced

similar patterns, though with differences in magnitude potentially reflecting the higher stiffness of the silicone itself.

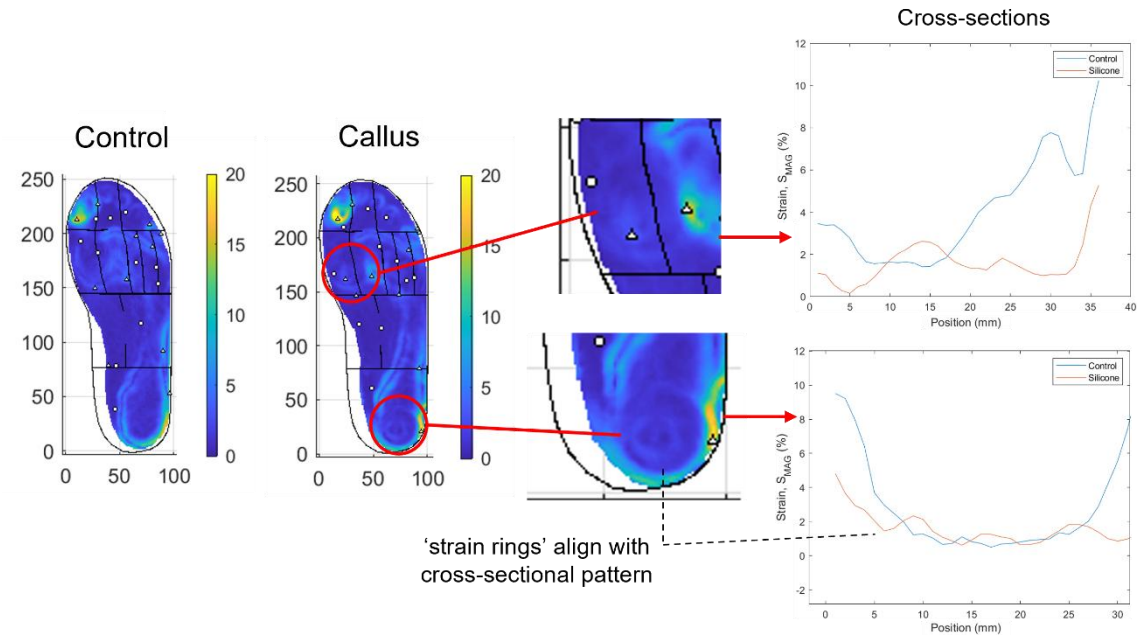


Figure 7.3.5: *Illustration of strain pattern produced in the presence of Ecoflex 00-30 samples at the 1st MTH and heel regions in comparison tests without. Altered strain behaviour seen at local sites, displaying 'strain rings' and corresponding strain variation in cross-sections.*

Testing Multiple Placements and Interaction Effects

To also assess whether the presence of two samples influenced each other's strain response, Dragon Skin 10 samples with embedded material and sandpaper were tested under three conditions: placement at the 1st MTH alone, at the heel alone, and at both sites simultaneously. These tests showed that while the absolute strain values varied between conditions, the presence of a second sample did not significantly alter the local strain response at each site. This indicated that introducing a callus at one site did not substantially influence the strain patterns at other anatomical locations.

Together, this preliminary work informed the selection of the final simulated callus samples used in the experimental study. The combination of Ecoflex 00-30, an embedded insert and a textured surface offered the best representation according to the literature and clinical input provided during the development process. The full testing protocol and analysis methods, including the strain-fluctuation metric used to quantify cross-section variability, are presented in Section 7.2. The strain fluctuation metric was calculated from the cross-sections by differentiating the strain values along the profile and summarising the magnitude of local variation using a robust RMS-like measure (square root of the median squared gradient).

7.4 Chapter Discussion

This chapter described the exploratory and developmental work required to create a practical and biomechanically meaningful simulated callus. The following discussion summarises the key findings from this iterative process, reflects on the constraints and uncertainties encountered, and considers how these shaped the final surrogate design and the direction of the experimental study.

The preliminary work demonstrated that STAMPS3D is capable of detecting subtle localised changes in plantar mechanical behaviour, from extreme cases through to more clinically representative examples. These early tests confirmed the system's sensitivity and justified further development of a more anatomically comparable model. The literature highlighted the complex nature of callus, characterised not only by increased stiffness and thickness but also by reduced hydration, altered elasticity and distinct surface texture [191], [192]. These insights informed the design requirements for the simulated callus, emphasising the need for a central thickened region, a gradual transition to the edge and a textured surface. The iterative development of silicone samples showed that stiffness differences alone were insufficient to produce clear strain responses. Embedding materials within the silicone introduced a more distinct mechanical contrast, and clinician feedback helped identify the insert that most closely resembled callus on palpation. Incorporating surface texture through sandpaper further improved the anatomical fidelity of the samples. Preliminary strain assessments confirmed that these combined features produced interpretable localised strain patterns, including the appearance of 'strain rings' and that samples placed at different anatomical sites had little effect on each other. Together, these findings supported the selection of Ecoflex 00-30 with an embedded insert and textured surface as the final callus samples for the experimental study.

Several limitations should be considered when interpreting this preliminary work. First, the assessments were exploratory rather than systematic, meaning not all material combinations were tested in a controlled manner, and trials were limited to a single participant. Consequently, the strain patterns observed should be viewed qualitatively. Second, the tactile evaluations used to select the embedded insert were inherently subjective and influenced by the absence of natural callus features such as hydration, microtopography and natural skin tension in silicone. Although clinician feedback was valuable, the samples cannot fully reproduce the complex viscoelastic behaviour of real callus tissue. Third, strain maps from plain silicone samples were sometimes ambiguous, making accurate centre and edge measurements difficult to extract. Rather than solely reflecting the limitations of the simulated callus model, this also highlights that callus mechanics are influenced by multiple interacting factors, including surrounding soft tissue, local anatomy and the combined effects of shear and pressure, which can mask

the mechanical contribution of callus itself. Finally, the developed samples capture only selected characteristics of callus, with aspects such as biological variability, progressive formation and interactions with footwear being beyond the scope of this work.

Despite these limitations, the preliminary work has several important implications for both the experimental study and the wider field of plantar biomechanics. Methodologically, it demonstrates a rigorous and transparent approach to the development of a simulated callus, integrating literature evidence, clinical insight and experimental testing. This strengthens the validity of the final experimental study by showing that the sample was not chosen arbitrarily but from a structured design process. However, this development process highlighted the limited quantitative understanding of callus characteristics, particularly in relation to shear behaviour. The need to approximate the natural features through silicone and embedded materials demonstrates the importance of further research aimed at characterising callus more comprehensively, using both mechanical testing and in-vivo imaging approaches. Additionally, the ability of STAMPS3D to detect subtle, localised changes in strain in the presence of an artificial callus demonstrates the potential of this method for future studies involving both healthy and clinical cohorts. This includes investigations comparing feet with and without callus, as well as studies examining the biomechanical consequences of debridement. The sensitivity of the system to local stiffness contrasts suggests that STAMPS3D could contribute to a deeper understanding of how callus formation influences plantar loading and how clinical interventions modify these patterns. In addition, the developed samples provide a controlled platform for investigating how localised stiffness influences plantar strain, an important step toward understanding the mechanical pathways that contribute to callus formation and ulcer risk. These aspects played a key role in producing interpretable strain responses and should be considered in future efforts to simulate or model callus-related loading, whether for experimental studies, computational modelling or the design of targeted interventions.

7.5 Chapter Conclusions

This chapter established the rationale, development and evaluation of the simulated callus. Through iterative testing, design choices informed by literature and preliminary assessments, a simple yet biomechanically meaningful sample was produced that enabled controlled investigation of localised stiffness effects on plantar strain. The work also demonstrated the sensitivity of STAMPS3D to subtle mechanical contrasts and highlighted key areas where further characterisation of callus is needed. Together, these findings highlight the potential of STAMPS3D to contribute to future investigations of callus-related loading and ulcer risk, supporting the development of more targeted preventative strategies for people with diabetes.

Chapter 8

Discussion and Conclusions

8.1 Review of Thesis Chapters and Research Objectives

The research aim and objectives were presented in Chapter 1 and provided an overview of the anticipated work of the project. This section provides a critical review of the chapters and publications included in this thesis, highlights where the research objectives were achieved across the chapters and discusses the potential impact of the work to the wider research field.

For clarity, the research questions and objectives from Chapter 1 are outlined below and are referred to throughout the chapter.

Research Questions

RQ1. Measurement feasibility – Can a 3D DIC based in-shoe measurement system reliably capture both pressure and shear components of plantar loading during gait?
RQ2. Stakeholder perspectives – How do stakeholders perceive the potential applications of STAMPS3D, and in what contexts do they see the greatest value?
RQ3. Clinical relevance – Do 3D plantar strain maps provide additional insights into DFU risk compared to conventional pressure-only measures?
RQ4. System validation – How does the performance of the 3D system compare to established tools in terms of accuracy, repeatability and usability?
RQ5. Translation potential – What are the practical considerations for integrating 3D plantar strain measurement into clinical risk assessment and management pathways?

Research Objectives

1. Develop appropriate open-source DIC workflow using DIC software to provide a foundation for subsequent 3D analysis.
2. Develop and implement a novel 3D DIC based in-shoe measurement system for plantar load, validating the system against established measurement devices under controlled experimental conditions.

3. Engage clinicians and patients through discussion groups to explore perceptions of STAMPS3D, identifying potential applications for DFU prevention and management strategies.
4. Conduct proof-of-concept experiments to assess feasibility of capturing plantar load data across contoured surfaces and local regions of varying surface stiffness.
5. Develop summary metrics for clinical use derived from measures of plantar shear loading.
6. Identify methodological and practical limitations of STAMPS3D and propose potential solutions to support future clinical translation.

Chapter 3: Parameter Selection for Digital Image Correlation

This chapter addressed a methodological challenge of DIC, focusing on the subjective and inconsistent nature of parameter selection. The work demonstrated the complex interdependence between camera setup, calibration quality, subset size, step size, smoothing and spatial resolution, reinforcing concerns around the lack of standardised workflows highlighted by the literature. The chapter then proposed a quantitative, transparent and open-source framework for evaluating DIC parameter selection, enabling a more objective approach to DIC setup. Although some subjectivity remained, the framework provided a reproducible method for identifying suitable parameters across different camera configurations and samples. In doing so, this work achieved Objective 1 by establishing the methodological foundation required for the subsequent 3D developments used within the STAMPS3D system.

Chapter 4: Development and Evaluation of a Novel 3D In-Shoe Plantar Strain Measurement System: STAMPS3D

(Publication - https://doi.org/10.1177/09544119251330738)

The development of STAMPS3D, a novel 3D in-shoe plantar strain measurement system capable of capturing deformation across the non-planar plantar surface of the foot. The system addresses a gap in current in-shoe technologies, which typically only measure pressure and rely on planar conditions. By integrating an open-source processing pipeline and validating the system against known deformation patterns, the study demonstrated the feasibility of capturing pressure and shear related strain components in three dimensions. In doing so, this work achieved Objective 2 and represents a significant methodological advance, providing the technical platform for the orthoses and callus studies that followed. The chapter also contributed to Objective 5 through the development of initial strain-based metrics that offer a starting point for future clinical interpretation of plantar loading. In addition, it addressed Objective 6 by identifying

methodological limitations, such as the constraints of the DIC workflow, that require refinement to support future clinical translation.

Chapter 5: Engagement with Patients and Clinicians to Inform STAMPS3D Research and Development

The PPIE discussion groups explored patient and clinician perspectives on DFU prevention, highlighting current barriers to effective communication, challenges with existing measurement tools and the need for accessible, clinically meaningful outputs. Stakeholders emphasised the importance of risk identification, the ability to test in patients' own footwear and automated post-processing, alongside practical considerations relating to workflow constraints and patient acceptability. Through these discussions, the work achieved Objective 3 by identifying the requirements and expectations of end-users and clarifying where STAMPS3D could add value within clinical care. The activity also contributed to Objective 6 by revealing practical limitations around usability and workflow integration, providing essential guidance for future system refinement and supporting the direction of clinical translation in the subsequent studies.

Chapter 6: Measuring Plantar Load with STAMPS3D: A Preliminary Study on the Impact of Contoured Orthoses

(Publication - https://doi.org/10.3389/fbioe.2025.1648649)

This study investigated whether STAMPS3D could capture strain across contoured orthosis surfaces, addressing a gap in the literature where most work focuses on pressure alone. The findings demonstrated that STAMPS3D can measure deformation across complex geometries and detect subtle differences between orthotic conditions. The study also identified practical limitations, including material interactions, insole moulding effects and the influence of orthosis thickness on the distribution of material stiffness. While conducted in healthy participants, the work highlights the potential for STAMPS3D to support orthosis evaluation and optimisation of offloading strategies in people with diabetes-related foot issues. In doing so, this work achieved Objective 4 by demonstrating the feasibility of capturing strain across contoured surfaces and contributed to Objective 6 by revealing key areas requiring refinement (e.g., alternative materials) before clinical implementation.

Chapter 7: Measuring In-Shoe Plantar Strain Outcomes in the Presence of Callus: A Preliminary Study using the STAMPS3D Measurement System

(Publication – https://doi.org/10.1002/jfa2.70169)

The final study explored the mechanical effects of callus using a simple multi-layered model to simulate its presence on the plantar surface of the foot. The study provided an initial investigation into how callus alters local strain patterns and assessed the feasibility of using STAMPS3D to measure these localised mechanical effects. STAMPS3D demonstrated sensitivity to subtle strain changes in the presence of simulated callus, suggesting potential applications in risk identification, monitoring callus progression, and guiding debridement. Although the model does not capture the full biological complexity of callus tissue, the work achieved Objective 4 by identifying feasibility of detecting localised strain changes associated with callus-related stiffness variations. It also contributed to Objective 6 by identifying methodological and practical limitations, such as the need for clinical validation and improved material properties of the simulated callus.

8.2 Discussion

The global population with diabetes is expected to increase [1], with related foot ulceration approximated to occur in up to 34% of these individuals [41]. Consequently, the social and financial burden of DFUs continues to be a growing issue. Healthcare services are faced with high costs associated with diabetes-related foot intervention [44]. Individuals directly affected by the disease effects also experience poor healing capacity, which contributes to elevated risk of recurrence, amputation and increased mortality rates [34], [41], [43]. Among the literature, it has been suggested that plantar pressure and shear stress may be influential in DFU formation [90], [101], [103], emphasising the need to capture the loads that occur at the plantar interface of the foot. However, no in-shoe devices are currently available that capture both components of plantar load, reflecting the pressure-focused assessment and offloading recommendations within current clinical guidelines, such as those from the IWGDF [28]. This gap in measurement capability has limited both research progress and clinical decision-making, particularly in relation to understanding how combined pressure and shear contribute to ulcer formation. Addressing this challenge required the development of a measurement approach capable of capturing plantar loading in a more comprehensive and clinically meaningful way. Early work prior to this PhD explored the use of 2D DIC to quantify plantar strain as a proxy for combined loading, providing an initial step toward addressing this gap [116]. Building on this, this PhD developed a 3D approach that required careful consideration of the methodological reliability of DIC, which forms the first theme of this discussion.

8.2.1 Technical Development of STAMPS3D

A key technical contribution of this work was the transition from a commercial DIC software (GOM Correlate) to an open-source workflow using Ncorr, enabling greater transparency, extensibility and control over the analytical process. This change addressed limitations acknowledged in commercial DIC systems, where restricted algorithm access, high costs and limited customisability remain significant barriers [134], [135]. These contribute to the broader challenge that DIC performance is highly sensitive to interdependent factors such as camera configuration, calibration quality, parameter selection, smoothing and spatial resolution. The literature consistently highlights that parameter selection remains largely subjective, often guided by user experience rather than objective criteria [126], [161], constraining reproducibility and limiting confidence in clinical or translational use. By developing a quantitative framework to evaluate parameter combinations, this work demonstrated the extent to which these elements interact and provided a more systematic basis for selecting appropriate DIC settings, reducing reliance on trial-and-error while acknowledging that some degree of subjective judgement remains unavoidable, as demonstrated in Chapter 3.

Establishing this methodological reliability was essential for addressing research question 1 highlighted in Chapter 1, as the feasibility of a 3D DIC-based in-shoe measurement system depends fundamentally on the robustness and transparency of the underlying workflow. The integrated nature of Ncorr within the DuoDIC analysis pipeline subsequently enabled extension to non-planar (3D) foot geometry in STAMPS3D, offering a technically robust means of capturing deformation patterns that reflect both pressure- and shear-related components of plantar loading [137], as detailed in Chapter 4. Although the transferability of parameters from 2D to 3D provided confidence in the stability of the workflow, this cannot be assumed across other software, and future users would need to undertake similar iterative evaluation to ensure methodological robustness. These insights also underpin the context for research question 4, as system validation must be interpreted in relation to the methodological assumptions and constraints inherent in the 3D workflow.

As part of the technical aspects of the system development, it is important to highlight that several sources of error and uncertainty influence the strain measurements obtained using STAMPS3D. DIC-related measurement error was reported in Chapter 3, where absolute error increased with strain magnitude (~0.005 at 5% strain and ~0.02 at 40% strain), but the relative error decreased (~0.1 vs ~0.05), indicating proportionally greater stability at higher strains. Sample placement variability between pre-and post-walk images was minimised through RBM correction, and a grid integrated into the base of the camera rig acts as a placement guide. The RBM correction implemented within the 3D DIC analysis workflow was demonstrated in Section 4.3.3 of Chapter 4, showing that

it successfully captures misalignment between images and ensures that strain measurements do not reflect repositioning error. This highlights a strength of 3D DIC over 2D DIC (with respect DuoDIC and Ncorr), where RBM correction is not performed. When using the STAMPS3D system with participants, repeat-level variability was reduced through averaging across three repeats per condition. Deformation arising during insertion and removal of the STAMPS insole was minimised by using a neoprene boot that can be opened fully, with any residual deformation being small relative to the cumulative strain captured over ten steps. Minor non-gait deformation outside the walking condition may also arise when participants place or remove their foot from the footwear and is similarly absorbed within the cumulative measure. Together, these factors consolidate the sources of error inherent to 3D DIC and within the STAMP3D workflow and demonstrate the overall reliability of the system.

Collectively, this progression from commercial software to a quantitatively optimised, open-source, 3D workflow represents a significant step toward improving the objectivity, reproducibility and clinical applicability of the STAMPS system for plantar load assessment. When considered in relation to established Technology Readiness Levels (TRLs) [196], this progression corresponds to advancement from early validation and proof-of-concept in both laboratory and relevant environments (TRL 5), as illustrated in Figure 8.2.1.

Beyond the context of plantar loading, 3D DIC has been widely applied across biomedical applications, including the characterisation of soft tissues such as tendon, ligament and skin, as well as hard tissues such as bone [197]. These studies demonstrate the suitability of DIC for capturing complex, heterogeneous deformation patterns in biological structures, reinforcing the relevance of this approach for non-planar, anisotropic behaviour of the plantar soft tissues. Related volumetric techniques such as Digital Volume Correlation have further extended this capability by enabling full-field strain measurement within trabecular bone and intervertebral discs [198], highlighting the broader utility of correlation-based methods for understanding tissue mechanics. These wider applications highlight the versatility of 3D DIC, with this PhD contributing to the growing field by providing an objective approach to determining suitable DIC parameters and demonstrating its feasibility within clinically relevant, in-shoe settings.

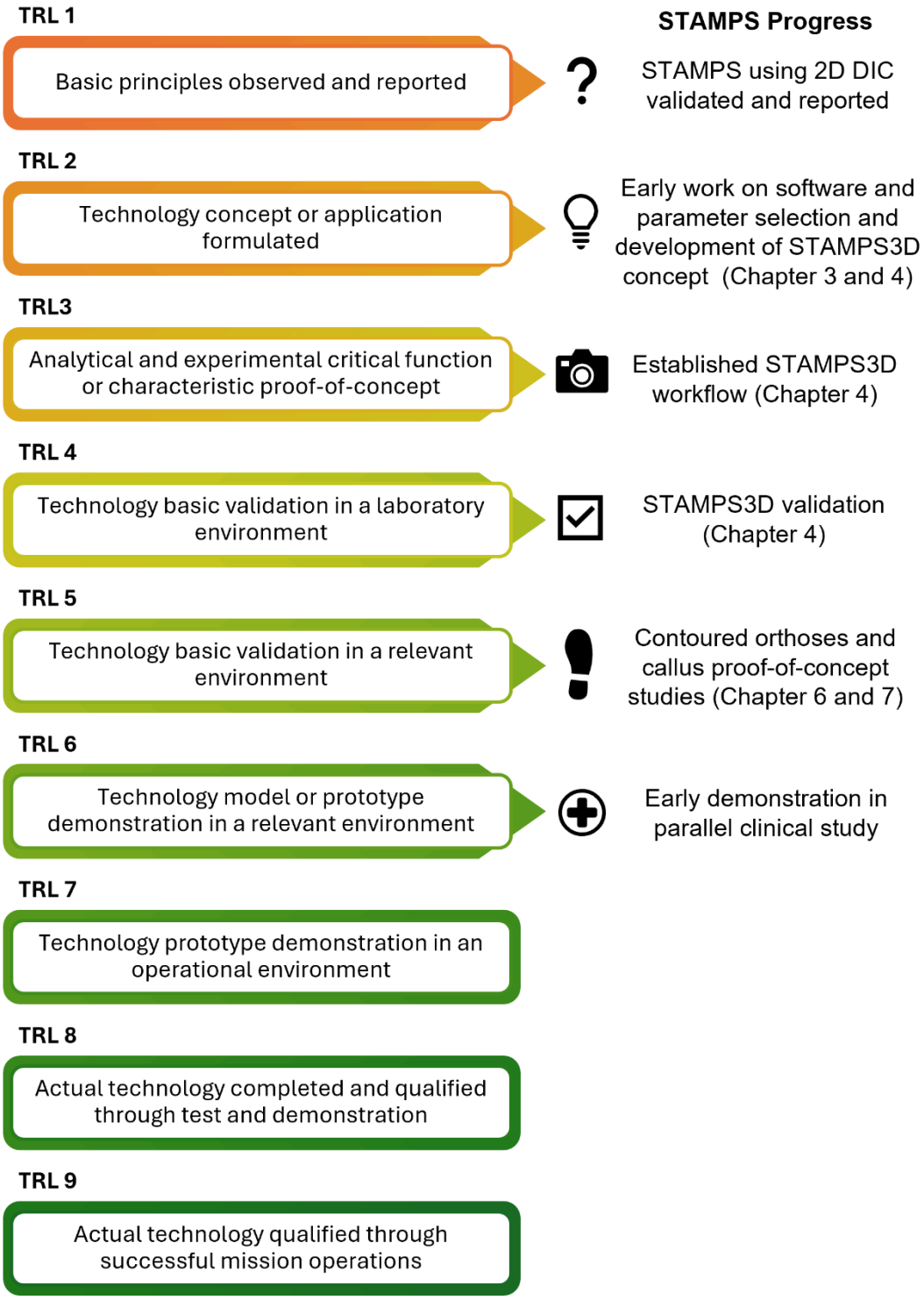


Figure 8.2.1: *TRLs (adapted from UKRI definitions) with corresponding stages of STAMPS3D development, illustrating how the work presented in this thesis progressed the system from proof-of-concept toward validation in relevant environments [196].*

8.2.2 Shear-Related Measurement Capability of STAMPS3D

A key motivation for developing STAMPS3D was the lack of in-shoe measurement systems capable of capturing plantar shear, either independently or alongside pressure. While STAMPS3D does not directly measure shear force or plantar pressure, the system captures cumulative strain arising from the combined effects of vertical and tangential loading at the plantar interface. The degree to which shear-related deformation can be detected is therefore an important consideration.

Evidence from the developmental studies supports the sensitivity of the STAMPS approach to shear loading. The original 2D STAMPS work demonstrated that measured strain increased when tangential shear stress was applied, confirming that strain reflects both normal pressure and shear components [116]. Similarly, in the 3D developmental study (Chapter 4), indentation tests followed by controlled shear displacements of 1–2 mm produced clear increases in strain magnitude [175]. These findings indicate that STAMPS3D can detect deformation arising from shear loading, even though shear force itself is not directly measured.

Within the participant-based studies (Chapters 6 and 7), regions of elevated strain were frequently observed in areas where PPP was not elevated. These patterns suggest that shear-related deformation contributes to the measured strain, particularly in locations such as the toes and central forefoot (Figure 7.2.3) [199]. Correlation between peak S_{MAG} and PPP in the participant-based studies (Chapters 6 and 7) consistently demonstrated moderate relationships. As discussed in the Chapter 7 publication, a moderate correlation was expected since peak S_{MAG} reflects cumulative deformation arising from both vertical pressure and shear loading, whereas PPP represents only the vertical component. Therefore, pressure and strain are considered related but not interchangeable. The consistency of these correlations across proof-of-concept studies presented in this thesis, together with previous findings using the 2D system, suggests that while pressure contributes substantially to overall strain, STAMPS3D also captures additional shear-related deformation that is not represented in PPP alone. This is notable given that plantar pressure magnitudes are reported to be substantially higher than shear magnitudes (e.g., ~189 kPa vs ~33 kPa respectively in Perry et al. [102]).

However, the individual contributions of pressure and shear cannot be separated within the strain measure. STAMPS3D is therefore able to detect deformation arising from shear loading but cannot quantify the magnitude of shear or isolate shear from pressure. Interpretation of strain maps must also consider the influence of local plantar geometry. Curved or prominent anatomical structures, such as the metatarsal heads, produce sharper deformation gradients than flatter regions such as the heel, potentially amplifying strain independent of shear magnitude. The 3D validation work demonstrated that STAMPS3D can accurately capture deformation across both planar and non-planar

surfaces, reducing the confounding influence of out-of-plane motion compared with 2D DIC [175]. Nonetheless, anatomical shape remains an important factor when interpreting strain patterns.

Based on these points, it is acknowledged that the system does not directly measure shear force, cannot separate pressure from shear, and cannot quantify the relative contribution of each. These limitations should be considered when interpreting strain maps and when evaluating the role of shear in plantar loading. However, it is equally important to recognise that STAMPS3D has been demonstrated to be sensitive to shear-related deformation and can detect changes in strain arising from combined pressure and shear loading. Despite the constraints inherent to strain-based measurement, the system offers a low-cost, high resolution, in-shoe method for capturing cumulative plantar loading that is not available in current commercial devices. This capability provides a meaningful basis for considering how STAMPS3D may be translated into clinical practice.

8.2.3 Clinical Translation of the STAMPS3D System

Another major theme emerging from this work is the clinical translation of engineering methods, particularly in the context of measuring both pressure and shear at the plantar interface. Within the wider field, there is growing recognition that shear plays a critical role in the development of callus and ulceration [103], yet most clinically available systems continue to measure pressure alone. This mismatch between what is biomechanically important and what can currently be measured in practice has limited the ability to personalise offloading, evaluate intervention effectiveness and understand why some patients continue to ulcerate despite apparently adequate pressure reduction. This highlights the ongoing need for clinically feasible tools capable of capturing combined loading at the plantar interface, given that existing systems remain expensive, time-consuming, research-focused or requiring specialist training, and therefore poorly align with routine clinical workflows [109], [110], [112], [113], [114].

Stakeholder discussions held within this project directly addressed research question 2, revealing perceptions of STAMPS3D's potential value, desired implementation and practical limitations, as well as highlighting issues such as patient compliance, communication and the practical constraints of time-limited appointments (Chapter 5). Their insights pointed toward clear priorities for future development, including exploring how STAMPS3D could support clinical offloading decisions, assess effectiveness of orthotic interventions, automation of data post-processing and be adapted for use within patients' own footwear through alternative materials. However, these discussions also indicated that the level of control achievable in laboratory settings is unlikely to be replicated in clinical environments, where workflow pressures, variable patient presentations and limited setup time may influence system performance. This highlights

that tools developed in research conditions may not readily translate directly into routine clinical practice, demonstrating the need for continued co-design or collaborative approach with stakeholders to ensure systems such as STAMPS3D can progress toward higher TRL levels (Figure 8.2.1) and be integrated effectively within clinical pathways. Together, these findings address research question 5, highlighting that while STAMPS3D addresses a clear measurement gap, its successful translation will depend on continued refinement of usability, workflow integration and material choice to ensure that the system can operate effectively within the constraints of clinical care pathways.

This is consistent with broader developments in healthcare technology, where research-based systems often require multiple iterations before they can be adopted into routine practice. Recent reviews emphasise that technologies only achieve clinical impact when they are aligned with real-world workflows, interoperable with existing systems and designed around usability and training needs, with examples ranging from digital monitoring tools to advanced sensing and imaging technologies [200], [201]. This reinforces the importance of iterative refinement and stakeholder collaboration as STAMPS3D progresses to higher TRL levels.

8.2.4 Clinical Applications and Impact of STAMPS3D

The final discussion theme drawn from this work relates to the clinical applications and implications of STAMPS3D, particularly how strain-based information can support prevention and management of diabetes-related foot complications, in addition to where STAMPS3D could meaningfully fit within existing care pathways. As shown in the updated patient pathway figure from Chapter 2 (Figure 8.2.2), STAMPS3D has potential to contribute at several points within clinician-led assessment, directly addressing research question 3 by providing strain-based indicators of elevated mechanical loading that may precede callus formation or ulceration [29], [104]. This includes early risk identification (screening), guiding offloading selection and evaluating the effectiveness of orthotic or footwear interventions (clinical management and offloading). Early proof-of-concept work using contoured orthoses and callus-related models (Chapters 6 and 7) demonstrated that STAMPS3D can detect clinically relevant differences in strain distribution, reinforcing its potential utility in informing both preventative and therapeutic decision-making.

Early clinical implementation of STAMPS3D within a parallel study provided further insight into the translational aspects of research question 5, providing an initial indication of how the system functions without researcher oversight, identifying both its practical benefits and the challenges associated with integrating a technically complex measurement tool into real-world practice. Feedback from both clinicians who implemented the tool and those involved in the stakeholder discussions highlighted not only the aspects of the system that translated effectively into practice, such as the

intuitive visualisation of strain patterns, but also the elements that require refinement, including time, integration and the need for streamlining the workflow from image capture to post-processing. In addition, practical considerations that would influence adoption of the tool in a clinical setting include cost of equipment, the training required for healthcare professionals and the need for systems that can be incorporated into existing budgets. This is particularly important given the substantial financial burden associated with managing diabetes-related foot complications [44].

The combined insights from these groups were particularly valuable in shaping an understanding of how STAMPS3D could be improved for real-world use and how its usability and implementation could be optimised within clinical settings (Figure 8.2.2). Their insights also helped identify where STAMPS3D could realistically sit within the clinical pathway, with particular emphasis on its use during general foot assessments, orthotic review appointments and situations where clinicians need rapid feedback on the mechanical effects of footwear or offloading interventions. Engagement with industry partners, including Steeper, further highlights opportunities for integration within existing orthotic provision pathways.

In addition to its clinical applications, STAMPS3D also has potential value within the self-management pathway, as illustrated in Figure 8.2.2. The visual nature of strain heat maps offers a powerful tool for patient education, helping individuals understand how pressure and shear contribute to callus formation and ulcer risk, and supporting more informed engagement with offloading strategies. Similar benefits have been reported in diabetes care, where qualitative studies of continuous glucose monitoring show that real-time visual feedback enhances patients' understanding of their condition, supports behaviour change and improves engagement with recommended management approaches, demonstrating how accessible engineering outputs can drive meaningful changes in healthcare provision [202]. Therefore, by enabling patients to see the effects of different footwear or orthotic choices, STAMPS3D could enhance compliance and facilitate ongoing self-monitoring between clinical appointments.

These possibilities align with models of shared care and contribute to research question 5 by identifying specific points at which STAMPS3D could add value across both clinical and self-management pathways. When considered alongside the TRLs presented in Figure 8.2.1, these insights also highlight the specific developments required for progression toward higher TRLs, particularly in relation to clinical workflow integration, material optimisation and automation of post-processing. Other available systems provide useful indication of how STAMPS3D might translate to clinical and home use. Commercial in-shoe pressure measurement systems (E.g., Pedar, Novel Ltd.) have been widely used in research to quantify plantar loading and evaluate orthotic interventions, with its real-time data capture enabling quick assessment of data. However, the

associated cost and time needed for use, limits its integration within both clinical environments and patient-facing self-management. By contrast, systems such as the Orpyx Sensory Insole extends plantar monitoring into daily life by continuously measuring pressure, temperature and general activity, while delivering real-time alerts to users and healthcare teams. A recent longitudinal study in people with a history of DFU has suggested that such systems may promote engagement and compliance through multi-layer care models that combine patient feedback with remote clinical oversight [203]. However, these systems typically offer lower spatial resolution compared to STAMPS3D, constrained by the limited number and distribution of embedded sensors, and therefore may be less sensitive to localised mechanical changes associated with callus formation or early tissue breakdown. While this higher spatial sensitivity is a key advantage of STAMPS3D, systems such as the Orpyx Sensory Insole nevertheless highlight the opportunity to develop similarly intuitive, clinically relevant interfaces that support timely feedback and patient engagement. Overall, this theme illustrates how STAMPS3D moves beyond technical feasibility to offer a clinically meaningful tool with the potential to enhance preventative care and support more targeted management of diabetes-related foot risk.

Together these themes demonstrate how this work has developed STAMPS3D from a technical concept toward a tool with clear clinical potential. Although the work discussed across this thesis has identified the potential applications of STAMPS3D and highlighted where the system may fit within clinical and self-management pathways, further research is needed to address the limitations of the current studies and to refine the system to enable clinical utility. Insights shared by contributors in Chapter 5 helped identify priorities for future development, while the proof-of-concept studies in Chapters 6 and 7 provide a basis for which the next phase of work can build on.

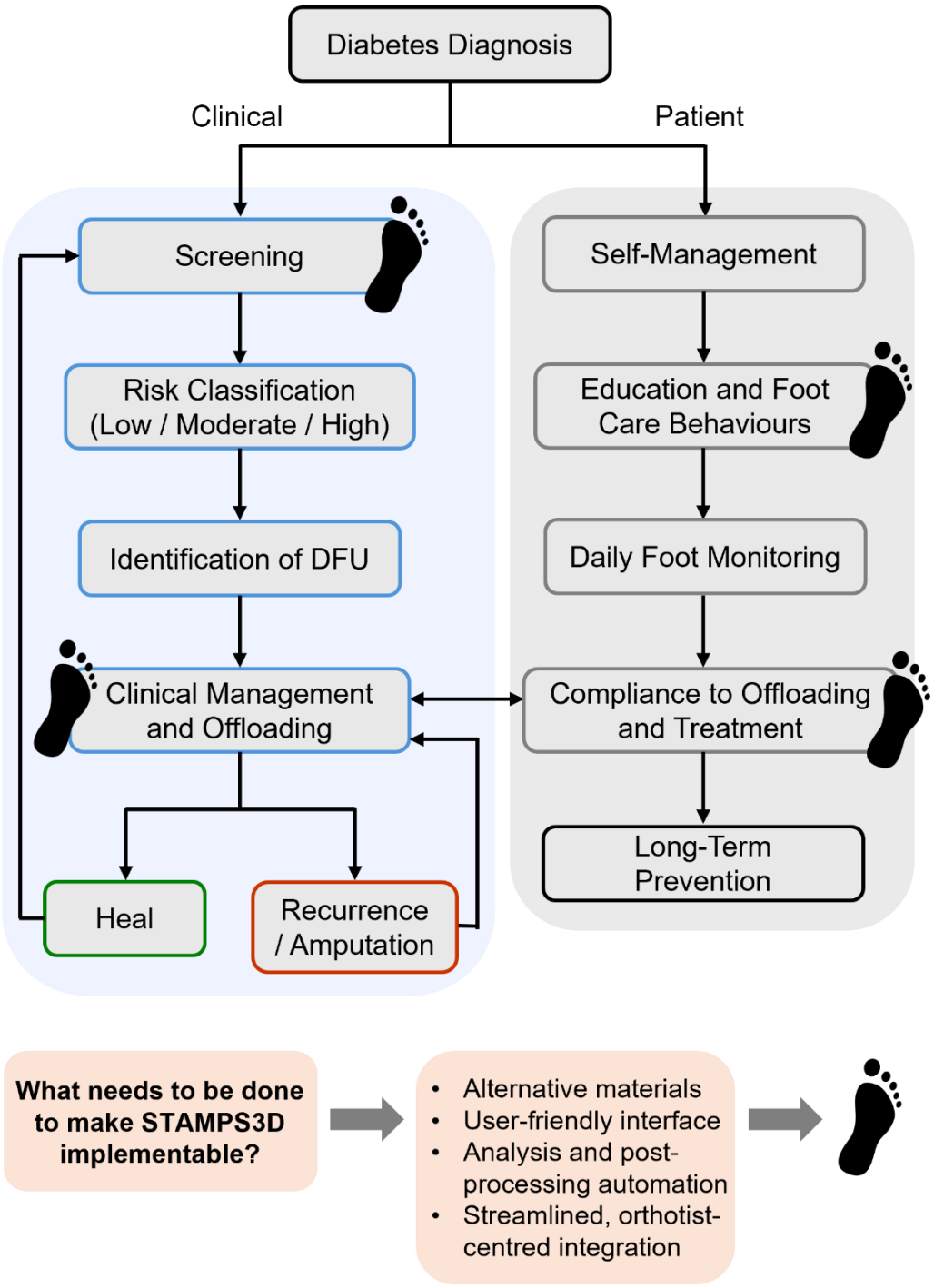


Figure 8.2.2: *Updated overview of the patient pathway for diabetes-related foot care (adapted from Chapter 2), with foot icons indicating points at which the STAMPS3D system could potentially be implemented and the work needed to enable this.*

8.3 Future Work

This section outlines the key areas where further research and development are needed to strengthen the system, address limitations identified in this thesis and support its progression toward clinical implementation.

8.3.1 Alternative Materials for the STAMPS Insole

A key priority for future development is the identification and evaluation of alternative materials for the STAMPS insole that would enable use within patients' own footwear and support longer wear durations. The plasticine-based insoles used in this thesis were appropriate for proof-of-concept testing, but its limited durability, temperature sensitivity and challenges around fabrication, limits its suitability for clinical use. The next iteration of STAMPS3D therefore requires materials that balance mechanical sensitivity, structural stability, manufacturability, and clinical practicality.

From a design perspective, several mechanical requirements emerge from the findings of this thesis. First, the material must exhibit slow rebound or partial permanent deformation, enabling strain to be captured reliably post loading using DIC. This implies a material with low stiffness, low density, and a controlled compression set, ensuring that deformation patterns reflect loading rather than elastic recovery. Second, the material must support reliable speckle pattern application, either through surface application or by integrating a pattern directly into the material during manufacturing, which would streamline production and improve consistency, by removing the need for manual pattern application to individual insoles. Thickness is also a critical design parameter. A material thickness of <5 mm would allow the insole to be used within patients' own footwear and applied to contoured orthoses without substantially increasing overall stack height. However, this must be balanced against the need to avoid 'bottoming out' under higher loads, particularly in people with diabetes who may generate greater plantar forces. This may require exploring multi-layer insoles, where a softer top layer is paired with a more supportive base layer. While a single material design simplifies manufacturing and may be sufficient for short duration assessments, layered structures could offer a more optimal combination of sensitivity, durability and load-bearing capacity. Practical considerations also influence material selection. The insole must be easy to insert and remove, customisable in shape and size, and low cost to produce at a clinical scale. In addition, any candidate material must be biocompatible and safe for contact with skin, particularly given the heightened vulnerability of skin associated with diabetes. The current STAMPS insole costs approximately £2.50 per unit and so maintaining a similar low cost will be important for clinical use. Environmental sustainability is another important consideration, suggesting value in exploring recyclable or reusable material options.

These requirements point toward evaluating materials already used in orthotic manufacturing, such as polyethylene, polyurethane and memory foams, as well as silicone-based elastomers and thermoplastic elastomers with variable mechanical properties. Building on the combined material effects observed in Chapter 6, future studies should assess how these materials behave on complex, contoured surfaces and

under real-world gait conditions to ensure accurate strain capture in clinically relevant scenarios. Establishing a clinically viable, manufacturable material is therefore a foundational step in progressing STAMPS3D toward higher TRL levels, enabling longer wear durations, integration into patients' own footwear, and eventual translation into routine clinical care.

8.3.2 Automation of STAMPS3D Post-Processing

Another key priority for future development is the automation of STAMPS3D post-processing to support clinical feasibility. The current workflow requires multiple manual steps, from image import to correlation, strain calculation and map generation, which would increase the time needed to assess each patient in a clinical setting and may introduce user-dependent variability. Developing an automated or semi-automated analysis pipeline would streamline workflow, reduce the burden on clinicians and researchers, and ensure greater consistency in output. Examples of similar automation among other clinical technologies demonstrate how such developments support translation. Ultrasound systems incorporate automated segmentation, quality checks and workflow enhancing tools to reduce operator variability and enable assessments within time-limited settings [204]. Markerless motion capture technologies similarly enable automated clinical reporting and reduced setup time, supporting their emerging use in rehabilitation and clinical gait assessment [205], [206]. With respect to STAMPS3D, a robust pipeline would need to incorporate automated quality checks (e.g., pattern integrity and correlation confidence), standardised strain map generation and automated reporting of key quantitative outputs, enabling the system to operate reliably within time-limited clinical environments.

8.3.3 Larger Cohort Studies Involving Healthy and Diabetes Individuals

While this thesis provides initial proof-of-concept evidence for the feasibility of STAMPS3D, further work is required to evaluate the system in larger and more diverse populations. However, the next steps must be guided by the current limitations of the system, particularly its suitability for use in high-risk groups. At this stage, the material properties, workflow demands, and short wear duration mean that STAMPS3D can not yet be safely or practically use in people with active ulceration or severe deformity of the feet. Early clinical studies should therefore focus on healthy individuals and people with diabetes at low ulcer risk, enabling further refinement of the system under controlled and lower-risk conditions.

Once the system has been refined and automated, larger healthy participant cohorts will be needed to establish normative strain distributions across a wider range of foot types. This data would provide essential reference data for interpreting individual results and identifying any deviations due to pathology present. Building on this, the next clinically

meaningful study would be to assess whether STAMPS3D can identify differences between groups at varying levels of ulcer risk (e.g., low-risk individuals compared against those with history of ulceration). In doing so, we can determine the sensitivity of STAMPS3D to pathological loading patterns and assess its ability to detect early mechanical indicators of tissue breakdown. As the system progresses through higher TRL stages (summarised in Figure 8.2.1), study designs would similarly need to move from single-centre feasibility studies and cohort studies, toward multi-centre evaluations and randomised controlled trials, to establish generalisability and clinical effectiveness of STAMPS3D. This process is essential to demonstrate not only technical performance but also real-world clinical value, ensuring that STAMPS3D can support earlier intervention and improved DFU prevention.

Subsequent work would then explore the use of STAMPS3D to evaluate offloading interventions, such as contoured orthoses or callus debridement, within clinical populations. As noted in the proof-of-concept studies reported in Chapter 6 and 7, the effects observed in healthy individuals may underestimate the magnitude or clinical relevance of changes seen in higher-risk groups, so targeted studies would help inform whether STAMPS3D can support personalised offloading strategies.

8.3.4 Automated Risk Classification

In the longer term, larger datasets involving healthy, low-risk and high-risk groups would provide the foundation for developing machine-learning approaches to support automated risk classification. However, this requires large quantities of data and evidence distinguishing different risk groups and their corresponding strain profiles. Therefore, this reinforces the need for the proposed stages of future work, beginning with proof-of-concept studies in low-risk groups, before progressing toward larger clinical cohorts as the STAMPS3D system becomes more refined and clinically viable.

Examples from related areas demonstrate the potential value of automated classification tools in diabetes-related foot care. The FootSnap system uses computer vision to automatically quantify foot shape and detect changes associated with ulcer risk [207], ultimately aiming to eventually aid monitoring and prevention of foot ulceration over time. Similar approaches could eventually enable STAMPS3D to convert the current large quantities of strain data into simplified indicators of mechanical risk, such as highlighting regions of elevated deformation or generating risk scores that could support clinical decision making. While such developments remain a longer-term goal, they highlight the potential for machine-learning methods to enhance the usability and clinical impact of STAMPS3D once sufficient datasets become available.

8.4 Concluding Remarks

This research project set out to develop a 3D DIC-based in-shoe system capable of measuring pressure and shear on non-planar surfaces, with the intention of generating clinically relevant information to support DFU prevention and management. Across the work presented in this thesis, each of the research objectives have been addressed and demonstrated how the system can be implemented, interpreted and positioned within clinical and self-management pathways.

The technical developments presented in Chapters 3 and 4 established a transparent and reproducible workflow using 3D DIC, providing the foundation for reliable strain measurement. Subsequent studies explored the clinical relevance of strain patterns and examined how STAMPS3D could be applied to orthotic interventions and callus-related loading, offering early evidence of its potential to support risk identification, guide offloading decisions and evaluate intervention effectiveness. Stakeholder discussions also supported these findings, highlighting priorities for future development and clarifying where the STAMPS3D system may add value in practice.

Collectively, this work advances understanding of STAMPS3D's capabilities and limitations, identifies the contexts in which the system may be clinically meaningful and outlines the steps required to enable clinical implementation. While further research is required to provide further clinical validation and refine the system for real-world use, the findings presented in this thesis provide a robust platform on which future development can be built. In doing so, systems like STAMPS3D have the potential to provide clinicians with clearer, earlier indicators of ulcer risk, supporting faster and more targeted intervention and ultimately helping to prevent DFU formation and its associated burden on patients and healthcare services. Importantly, these developments align closely with national and international research priority initiatives, notably the James Lind Alliance Priority Setting Partnership, which highlights the need for improved early detection of ulcer risk, better tools to guide personalised offloading, and technologies that support prevention and self-management. By directly addressing several of these priority areas, this work contributes to the direction of future research and innovation in diabetes-related foot care.

List of References

[1] K. L. Ong *et al.*, 'Global, regional, and national burden of diabetes from 1990 to 2021, with projections of prevalence to 2050: a systematic analysis for the Global Burden of Disease Study 2021', *The Lancet*, vol. 402, no. 10397, pp. 203–234, Jul. 2023, doi: 10.1016/S0140-6736(23)01301-6.

[2] 'IDF Diabetes Atlas 2025', Diabetes Atlas. Accessed: Feb. 17, 2026. [Online]. Available: https://diabetesatlas.org/resources/idf-diabetes-atlas-2025/

[3] 'How many people in the UK have diabetes?', Diabetes UK. Accessed: Feb. 17, 2026. [Online]. Available: https://www.diabetes.org.uk/about-us/about-the-charity/our-strategy/statistics

[4] A. Sapra and P. Bhandari, 'Diabetes', in *StatPearls*, Treasure Island (FL): StatPearls Publishing, 2025. Accessed: Feb. 18, 2026. [Online]. Available: http://www.ncbi.nlm.nih.gov/books/NBK551501/

[5] C. Solis-Herrera, C. Triplitt, C. Reasner, R. A. DeFronzo, and E. Cersosimo, 'Classification of Diabetes Mellitus', in *Endotext*, K. R. Feingold, R. A. Adler, S. F. Ahmed, B. Anawalt, M. R. Blackman, G. Chrousos, E. Corpas, W. W. de Herder, K. Dhatariya, K. Dungan, E. Hamilton, J. Hofland, S. Jan de Beur, S. Kalra, G. Kaltsas, N. Kapoor, M. Kim, C. Koch, P. Kopp, M. Korbonits, C. S. Kovacs, W. Kuohung, B. Laferrère, M. Levy, E. A. McGee, R. McLachlan, R. Muzumdar, J. Purnell, R. Rey, R. Sahay, A. S. Shah, M. A. Sperling, C. A. Stratakis, D. L. Trence, and D. P. Wilson, Eds., South Dartmouth (MA): MDText.com, Inc., 2000. Accessed: Feb. 18, 2026. [Online]. Available: http://www.ncbi.nlm.nih.gov/books/NBK279119/

[6] S. A. Antar *et al.*, 'Diabetes mellitus: Classification, mediators, and complications; A gate to identify potential targets for the development of new effective treatments', *Biomedicine & Pharmacotherapy*, vol. 168, p. 115734, Dec. 2023, doi: 10.1016/j.biopha.2023.115734.

[7] T. Quattrin, L. D. Mastrandrea, and L. S. K. Walker, 'Type 1 diabetes', *The Lancet*, vol. 401, no. 10394, pp. 2149–2162, Jun. 2023, doi: 10.1016/S0140-6736(23)00223-4.

[8] U. Galicia-Garcia *et al.*, 'Pathophysiology of Type 2 Diabetes Mellitus', *Int J Mol Sci*, vol. 21, no. 17, p. 6275, Aug. 2020, doi: 10.3390/ijms21176275.

[9] S. Nam, C. Chesla, N. A. Stotts, L. Kroon, and S. L. Janson, 'Barriers to diabetes management: Patient and provider factors', *Diabetes Research and Clinical Practice*, vol. 93, no. 1, pp. 1–9, Jul. 2011, doi: 10.1016/j.diabres.2011.02.002.

[10] F. Hill-Briggs *et al.*, 'Social Determinants of Health and Diabetes: A Scientific Review', *Diabetes Care*, vol. 44, no. 1, pp. 258–279, Jan. 2021, doi: 10.2337/dci20-0053.

[11] N. G. Clark, K. M. Fox, S. Grandy, and for the SHIELD Study Group, 'Symptoms of Diabetes and Their Association With the Risk and Presence of Diabetes: Findings from the Study to Help Improve Early evaluation and management of risk factors Leading to Diabetes (SHIELD)', *Diabetes Care*, vol. 30, no. 11, pp. 2868–2873, Nov. 2007, doi: 10.2337/dc07-0816.

[12] M. G. Yu, D. Gordin, J. Fu, K. Park, Q. Li, and G. L. King, 'Protective Factors and the Pathogenesis of Complications in Diabetes', *Endocr Rev*, vol. 45, no. 2, pp. 227–252, Apr. 2024, doi: 10.1210/endrev/bnad030.

[13] 'Complications | Background information | Diabetes - type 2 | CKS | NICE'. Accessed: Feb. 18, 2026. [Online]. Available: https://cks.nice.org.uk/topics/diabetes-type-2/background-information/complications/

[14] J. Zhu *et al.*, 'Diabetic peripheral neuropathy: pathogenetic mechanisms and treatment', *Front. Endocrinol.*, vol. 14, Jan. 2024, doi: 10.3389/fendo.2023.1265372.
[15] U. V. Shukla and K. Tripathy, 'Diabetic Retinopathy', in *StatPearls*, Treasure Island (FL): StatPearls Publishing, 2025. Accessed: Feb. 18, 2026. [Online]. Available: http://www.ncbi.nlm.nih.gov/books/NBK560805/
[16] R. Agarwal, 'Pathogenesis of Diabetic Nephropathy', in *Chronic Kidney Disease and Type 2 Diabetes*, in ADA Clinical Compendia Series. , Arlington (VA): American Diabetes Association, 2021. Accessed: Feb. 18, 2026. [Online]. Available: http://www.ncbi.nlm.nih.gov/books/NBK571720/
[17] N. D. Wong and N. Sattar, 'Cardiovascular risk in diabetes mellitus: epidemiology, assessment and prevention', *Nat Rev Cardiol*, vol. 20, no. 10, pp. 685–695, Oct. 2023, doi: 10.1038/s41569-023-00877-z.
[18] K. Papatheodorou, M. Banach, E. Bekiari, M. Rizzo, and M. Edmonds, 'Complications of Diabetes 2017', *J Diabetes Res*, vol. 2018, p. 3086167, Mar. 2018, doi: 10.1155/2018/3086167.
[19] M. E. Fernando, R. G. Crowther, M. Cunningham, P. A. Lazzarini, K. S. Sangla, and J. Golledge, 'Lower limb biomechanical characteristics of patients with neuropathic diabetic foot ulcers: the diabetes foot ulcer study protocol', *BMC Endocrine Disorders*, vol. 15, no. 1, p. 59, Oct. 2015, doi: 10.1186/s12902-015-0057-7.
[20] U. H. Tang, R. Zügner, V. Lisovskaja, J. Karlsson, K. Hagberg, and R. Tranberg, 'Foot deformities, function in the lower extremities, and plantar pressure in patients with diabetes at high risk to develop foot ulcers', *Diabetic Foot & Ankle*, vol. 6, no. 1, p. 27593, Jan. 2015, doi: 10.3402/dfa.v6.27593.
[21] D. Allan *et al.*, 'Increased exposure to loading is associated with decreased plantar soft tissue hardness in people with diabetes and neuropathy', *Diabetes Research and Clinical Practice*, vol. 187, p. 109865, May 2022, doi: 10.1016/j.diabres.2022.109865.
[22] D. O. Soyoye, O. O. Abiodun, R. T. Ikem, B. A. Kolawole, and A. O. Akintomide, 'Diabetes and peripheral artery disease: A review', *World J Diabetes*, vol. 12, no. 6, pp. 827–838, Jun. 2021, doi: 10.4239/wjd.v12.i6.827.
[23] 'Peripheral Arterial Disease in People With Diabetes | Diabetes Care | American Diabetes Association'. Accessed: Nov. 17, 2022. [Online]. Available: https://diabetesjournals.org/care/article/26/12/3333/21851/Peripheral-Arterial-Disease-in-People-With
[24] J. Ahmad, 'The diabetic foot', *Diabetes & Metabolic Syndrome: Clinical Research & Reviews*, vol. 10, no. 1, pp. 48–60, Jan. 2016, doi: 10.1016/j.dsx.2015.04.002.
[25] S. Pai and W. R. Ledoux, 'The shear mechanical properties of diabetic and non-diabetic plantar soft tissue', *J Biomech*, vol. 45, no. 2, pp. 364–370, Jan. 2012, doi: 10.1016/j.jbiomech.2011.10.021.
[26] U. Srinivas-Shankar, A. Kimyaghalam, and R. Bergman, 'Diabetic Foot Ulceration and Complications', in *StatPearls*, Treasure Island (FL): StatPearls Publishing, 2025. Accessed: Feb. 19, 2026. [Online]. Available: http://www.ncbi.nlm.nih.gov/books/NBK499887/
[27] K. McDermott, M. Fang, A. J. M. Boulton, E. Selvin, and C. W. Hicks, 'Etiology, Epidemiology, and Disparities in the Burden of Diabetic Foot Ulcers', *Diabetes Care*, vol. 46, no. 1, pp. 209–221, Jan. 2023, doi: 10.2337/dci22-0043.
[28] International Working Group on the Diabetic Foot, 'IWGDF Guidelines', IWGDF Guidelines. Accessed: May 18, 2023. [Online]. Available: https://iwgdfguidelines.org
[29] J. H. Collier and C. A. Brodbeck, 'Assessing the Diabetic Foot: Plantar Callus and Pressure Sensation'. Accessed: Jul. 21, 2025. [Online]. Available: https://journals.sagepub.com/doi/10.1177/014572179301900605
[30] J. Potter and M. J. Potter, 'Effect of callus removal on peak plantar pressures', *The Foot*, vol. 10, no. 1, pp. 23–26, Mar. 2000, doi: 10.1054/foot.2000.0576.

[31] J. Woodburn, Z. Stableford, and P. S. Helliwell, ‘Preliminary investigation of debridement of plantar callosities in rheumatoid arthritis’, *Rheumatology*, vol. 39, no. 6, pp. 652–654, Jun. 2000, doi: 10.1093/rheumatology/39.6.652.
[32] M. Á. Tresierra-Ayala and A. García Rojas, ‘Association between peripheral arterial disease and diabetic foot ulcers in patients with diabetes mellitus type 2’, *Medicina Universitaria*, vol. 19, no. 76, pp. 123–126, Jul. 2017, doi: 10.1016/j.rmu.2017.07.002.
[33] A. Berbudi, N. Rahmadika, A. I. Tjahjadi, and R. Ruslami, ‘Type 2 Diabetes and its Impact on the Immune System’, *Curr Diabetes Rev*, vol. 16, no. 5, pp. 442–449, May 2020, doi: 10.2174/1573399815666191024085838.
[34] D. G. Armstrong, T.-W. Tan, A. J. M. Boulton, and S. A. Bus, ‘Diabetic Foot Ulcers: A Review’, *JAMA*, vol. 330, no. 1, pp. 62–75, Jul. 2023, doi: 10.1001/jama.2023.10578.
[35] D. M. Eastman and M. A. Dreyer, ‘Neuropathic Ulcer’, in *StatPearls*, Treasure Island (FL): StatPearls Publishing, 2025. Accessed: Dec. 15, 2025. [Online]. Available: http://www.ncbi.nlm.nih.gov/books/NBK559214/
[36] J. S. Bevans and P. Bowker, ‘Foot structure and function: aetiological risk factors for callus formation in diabetic and non-diabetic subjects’, *The Foot*, vol. 9, no. 3, pp. 120–127, Sep. 1999, doi: 10.1054/foot.1999.0535.
[37] P. Pit’hová, H. Pátková, I. Galandáková, L. Dolezalová, and M. Kvapil, ‘[Differences in ulcer location in diabetic foot syndrome]’, *Vnitr Lek*, vol. 53, no. 12, pp. 1278–1285, Dec. 2007.
[38] S. O. Oyibo *et al.*, ‘The effects of ulcer size and site, patient’s age, sex and type and duration of diabetes on the outcome of diabetic foot ulcers’, *Diabetic Medicine*, vol. 18, no. 2, pp. 133–138, 2001, doi: 10.1046/j.1464-5491.2001.00422.x.
[39] L. Prompers *et al.*, ‘Prediction of outcome in individuals with diabetic foot ulcers: focus on the differences between individuals with and without peripheral arterial disease. The EURODIALE Study’, *Diabetologia*, vol. 51, no. 5, pp. 747–755, May 2008, doi: 10.1007/s00125-008-0940-0.
[40] A. M. Galea, K. Springett, H. Bungay, S. Clift, S. Fava, and M. Cachia, ‘Incidence and location of diabetic foot ulcer recurrence’, vol. 12, no. 4, 2009.
[41] D. G. Armstrong, A. J. M. Boulton, and S. A. Bus, ‘Diabetic Foot Ulcers and Their Recurrence’, *New England Journal of Medicine*, vol. 376, no. 24, pp. 2367–2375, Jun. 2017, doi: 10.1056/NEJMra1615439.
[42] ‘NDFA Interval Review: July 2014-March 2021’. Accessed: May 18, 2023. [Online]. Available: https://digital.nhs.uk
[43] M. Yavuz, A. Tajaddini, G. Botek, and B. L. Davis, ‘Temporal characteristics of plantar shear distribution: Relevance to diabetic patients’, *Journal of Biomechanics*, vol. 41, no. 3, pp. 556–559, Jan. 2008, doi: 10.1016/j.jbiomech.2007.10.008.
[44] M. Kerr *et al.*, ‘The cost of diabetic foot ulcers and amputations to the National Health Service in England’, *Diabetic Medicine*, vol. 36, no. 8, pp. 995–1002, 2019, doi: 10.1111/dme.13973.
[45] A. Jodheea-Jutton, S. Hindocha, and A. Bhaw-Luximon, ‘Health economics of diabetic foot ulcer and recent trends to accelerate treatment’, *The Foot*, vol. 52, p. 101909, Sep. 2022, doi: 10.1016/j.foot.2022.101909.
[46] D. C. Jupiter, J. C. Thorud, C. J. Buckley, and N. Shibuya, ‘The impact of foot ulceration and amputation on mortality in diabetic patients. I: From ulceration to death, a systematic review’, *International Wound Journal*, vol. 13, no. 5, pp. 892–903, 2016, doi: 10.1111/iwj.12404.
[47] J. A. Rubio, S. Jiménez, and J. L. Lázaro-Martínez, ‘Mortality in Patients with Diabetic Foot Ulcers: Causes, Risk Factors, and Their Association with Evolution and Severity of Ulcer’, *J Clin Med*, vol. 9, no. 9, p. 3009, Sep. 2020, doi: 10.3390/jcm9093009.
[48] C. Miranda, G. Zanette, and R. Da Ros, ‘Diabetic foot disease during the COVID-19 pandemic: lessons learned for our future’, *Arch Med Sci Atheroscler Dis*, vol. 7, pp. e94–e103, Aug. 2022, doi: 10.5114/amsad/151047.

[49] National Institute for Health and Care Excellence (NICE), 'Diabetic foot problems: prevention and management', 2019, [Online]. Available: www.nice.org.uk
[50] I. G. Costa, D. Tregunno, and P. Camargo-Plazas, 'Patients' Journey Toward Engagement in Self-Management of Diabetic Foot Ulcer in Adults With Types 1 and 2 Diabetes: A Constructivist Grounded Theory Study', *Canadian Journal of Diabetes*, vol. 45, no. 2, pp. 108-113.e2, Mar. 2021, doi: 10.1016/j.jcjd.2020.05.017.
[51] K. Stevens, D. Moralejo, S. Ersser, and C. MacLean, 'Patient, Support-Person and Health-Care Provider Perspectives on Foot Self-Management for Adults With Type 1 and Type 2 Diabetes: Personal Challenges', *Canadian Journal of Diabetes*, vol. 46, no. 1, pp. 40–46, Feb. 2022, doi: 10.1016/j.jcjd.2021.04.011.
[52] P. Manickum, T. Mashamba-Thompson, R. Naidoo, S. Ramklass, and T. Madiba, 'Knowledge and practice of diabetic foot care – A scoping review', *Diabetes & Metabolic Syndrome: Clinical Research & Reviews*, vol. 15, no. 3, pp. 783–793, May 2021, doi: 10.1016/j.dsx.2021.03.030.
[53] CDC, 'Diabetes and Your Feet', Centers for Disease Control and Prevention. Accessed: Jan. 22, 2023. [Online]. Available: https://www.cdc.gov/diabetes/library/features/healthy-feet.html
[54] C. Seery, 'Foot care amongst diabetics is incredibly important as foot related complications are common for those of us with diabetes.', Diabetes. Accessed: Jan. 22, 2023. [Online]. Available: https://www.diabetes.co.uk/diabetes-footcare.html
[55] E. K. Untari, T. M. Andayani, N. M. Yasin, and R. H. Asdie, 'A Review of Patient's Knowledge and Practice of Diabetic Foot Self-Care', *Malays J Med Sci*, vol. 31, no. 1, pp. 33–50, Feb. 2024, doi: 10.21315/mjms2024.31.1.3.
[56] N. G. Méndez *et al.*, '"New technologies applied in self-care to patients with diabetic foot ulcers: a scoping review"', *Diabetol Metab Syndr*, vol. 17, no. 1, p. 262, Jul. 2025, doi: 10.1186/s13098-025-01822-5.
[57] F. Pouwer, B. Perrin, A. Lavender, B. Najafi, K. Ismail, and L. Vileikyte, 'The quest for wellness: How to optimise self-care strategies for diabetic foot management?', *Diabetes/Metabolism Research and Reviews*, vol. 40, no. 3, p. e3751, 2024, doi: 10.1002/dmrr.3751.
[58] W. J. Jeffcoate and K. G. Harding, 'Diabetic foot ulcers', *The Lancet*, vol. 361, no. 9368, pp. 1545–1551, May 2003, doi: 10.1016/S0140-6736(03)13169-8.
[59] N. Amin and J. Doupis, 'Diabetic foot disease: From the evaluation of the "foot at risk" to the novel diabetic ulcer treatment modalities', *World J Diabetes*, vol. 7, no. 7, pp. 153–164, Apr. 2016, doi: 10.4239/wjd.v7.i7.153.
[60] E. Everett and N. Mathioudakis, 'Update on management of diabetic foot ulcers', *Ann N Y Acad Sci*, vol. 1411, no. 1, pp. 153–165, Jan. 2018, doi: 10.1111/nyas.13569.
[61] A. Buggy and Z. Moore, 'The impact of the multidisciplinary team in the management of individuals with diabetic foot ulcers: a systematic review', *Journal of Wound Care*, vol. 26, no. 6, pp. 324–339, Jun. 2017, doi: 10.12968/jowc.2017.26.6.324.
[62] S. Krishnan, F. Nash, N. Baker, D. Fowler, and G. Rayman, 'Reduction in Diabetic Amputations Over 11 Years in a Defined U.K. Population: Benefits of multidisciplinary team work and continuous prospective audit', *Diabetes Care*, vol. 31, no. 1, pp. 99–101, Jan. 2008, doi: 10.2337/dc07-1178.
[63] J. A. Rubio *et al.*, 'Reducing Major Lower Extremity Amputations After the Introduction of a Multidisciplinary Team for the Diabetic Foot', *The International Journal of Lower Extremity Wounds*, vol. 13, no. 1, pp. 22–26, Mar. 2014, doi: 10.1177/1534734614521234.
[64] F. L. Bowling, S. T. Rashid, and A. J. M. Boulton, 'Preventing and treating foot complications associated with diabetes mellitus', *Nat Rev Endocrinol*, vol. 11, no. 10, Art. no. 10, Oct. 2015, doi: 10.1038/nrendo.2015.130.
[65] D. Chen *et al.*, 'Development and validation of an incidence risk prediction model for early foot ulcer in diabetes based on a high evidence systematic review and

meta-analysis', *Diabetes Research and Clinical Practice*, vol. 180, p. 109040, Oct. 2021, doi: 10.1016/j.diabres.2021.109040.
[66] F. Crawford *et al.*, 'A systematic review and individual patient data meta-analysis of prognostic factors for foot ulceration in people with diabetes: the international research collaboration for the prediction of diabetic foot ulcerations (PODUS)', *Health Technology Assessment*, vol. 19, no. 57, pp. 1–210, Jul. 2015, doi: 10.3310/hta19570.
[67] V. Blanchette, J. Kuhnke, M. Botros, and S. Rosenthal, 'Inlow's 60-second Diabetic Foot Screen: Update 2022', *Limb Preservation Journal*, vol. 4, Apr. 2023, doi: 10.56885/HRJU7789.
[68] M. G. Woodbury, R. G. Sibbald, B. Ostrow, R. Persaud, and J. M. Lowe, 'Tool for Rapid & Easy Identification of High Risk Diabetic Foot: Validation & Clinical Pilot of the Simplified 60 Second Diabetic Foot Screening Tool', *PLOS ONE*, vol. 10, no. 6, p. e0125578, Jun. 2015, doi: 10.1371/journal.pone.0125578.
[69] 'NHS England — North West » Diabetes footcare blueprint, report and key documents'. Accessed: Dec. 20, 2022. [Online]. Available: https://www.england.nhs.uk/north-west/north-west-coast-strategic-clinical-networks/our-networks/diabetes/protocols-and-standards/diabetes-footcare-blueprint-report-and-key-documents/
[70] L. Dhoonmoon, 'The relevance of skin tones in the diabetic foot'. Accessed: Feb. 23, 2026. [Online]. Available: https://diabetesonthenet.com/diabetic-foot-journal/the-relevance-of-skin-tones-in-the-diabetic-foot/
[71] J. Black and A. Simende, 'Ten top tips: assessing darkly pigmented skin', *Clinical practice*, vol. 11, no. 3, 2020.
[72] J. Fletcher, 'The challenges of dark skin tone assessment: the importance of language', vol. 18, no. 2, 2022.
[73] Jack, 'Handbook: Diabetes footcare in dark skin tones', Diabetes Africa. Accessed: Feb. 23, 2026. [Online]. Available: https://diabetesafrica.org/footcare-handbook/
[74] 'Wound care and skin tone: Signs, symptoms and terminology for all skin tones – Wounds International'. Accessed: Feb. 23, 2026. [Online]. Available: https://woundsinternational.com/consensus-documents/wound-care-and-skin-tone-signs-symptoms-and-terminology-for-all-skin-tones/
[75] B. A. Lipsky *et al.*, '2012 Infectious Diseases Society of America Clinical Practice Guideline for the Diagnosis and Treatment of Diabetic Foot Infectionsa', *Clin Infect Dis*, vol. 54, no. 12, pp. e132–e173, Jun. 2012, doi: 10.1093/cid/cis346.
[76] P. Ince *et al.*, 'Use of the SINBAD Classification System and Score in Comparing Outcome of Foot Ulcer Management on Three Continents', *Diabetes Care*, vol. 31, no. 5, pp. 964–967, May 2008, doi: 10.2337/dc07-2367.
[77] J. L. Mills *et al.*, 'The Society for Vascular Surgery Lower Extremity Threatened Limb Classification System: Risk stratification based on Wound, Ischemia, and foot Infection (WIfI)', *Journal of Vascular Surgery*, vol. 59, no. 1, pp. 220-234.e2, Jan. 2014, doi: 10.1016/j.jvs.2013.08.003.
[78] B. M. Schmidt *et al.*, 'On diabetic foot ulcer knowledge gaps, innovation, evaluation, prediction markers, and clinical needs', *Journal of Diabetes and its Complications*, vol. 36, no. 11, p. 108317, Nov. 2022, doi: 10.1016/j.jdiacomp.2022.108317.
[79] B. Manna, P. Nahirniak, and C. A. Morrison, 'Wound Debridement', *StatPearls*, Sep. 2021, Accessed: Nov. 28, 2021. [Online]. Available: https://www.ncbi.nlm.nih.gov/books/NBK507882/
[80] S. A. Bus, 'The Role of Pressure Offloading on Diabetic Foot Ulcer Healing and Prevention of Recurrence', *Plastic and Reconstructive Surgery*, vol. 138, no. 3S, p. 179S, Sep. 2016, doi: 10.1097/PRS.0000000000002686.
[81] S. Racaru, L. Bolton Saghdaoui, J. Roy Choudhury, M. Wells, and A. H. Davies, 'Offloading treatment in people with diabetic foot disease: A systematic scoping review on adherence to foot offloading', *Diabetes & Metabolic Syndrome: Clinical Research & Reviews*, vol. 16, no. 5, p. 102493, May 2022, doi: 10.1016/j.dsx.2022.102493.

[82] J. P. Pollard and L. P. Le Quesne, 'Method of healing diabetic forefoot ulcers.', *Br Med J (Clin Res Ed)*, vol. 286, no. 6363, pp. 436–437, Feb. 1983.
[83] M. Westra, J. J. van Netten, H. A. Manning, J. G. van Baal, and S. A. Bus, 'Effect of different casting design characteristics on offloading the diabetic foot', *Gait & Posture*, vol. 64, pp. 90–94, Jul. 2018, doi: 10.1016/j.gaitpost.2018.05.022.
[84] H. J. Murray, M. J. Young, S. Hollis, and A. J. Boulton, 'The association between callus formation, high pressures and neuropathy in diabetic foot ulceration', *Diabet Med*, vol. 13, no. 11, pp. 979–982, Nov. 1996, doi: 10.1002/(SICI)1096-9136(199611)13:11<979::AID-DIA267>3.0.CO;2-A.
[85] A. Amemiya *et al.*, 'Factors Associated with Callus Formation in the Plantar Region through Gait Measurement in Patients with Diabetic Neuropathy: An Observational Case-Control Study', *Sensors (Basel)*, vol. 20, no. 17, p. 4863, Aug. 2020, doi: 10.3390/s20174863.
[86] M. j. Young, P. r. Cavanagh, G. Thomas, M. m. Johnson, H. Murray, and A. j. m. Boulton, 'The Effect of Callus Removal on Dynamic Plantar Foot Pressures in Diabetic Patients', *Diabetic Medicine*, vol. 9, no. 1, pp. 55–57, 1992, doi: 10.1111/j.1464-5491.1992.tb01714.x.
[87] D. L. Pitei, A. Foster, and M. Edmonds, 'The effect of regular callus removal on foot pressures', *The Journal of Foot and Ankle Surgery*, vol. 38, no. 4, pp. 251–255, Jul. 1999, doi: 10.1016/S1067-2516(99)80066-0.
[88] R. A. Slater, I. Hershkowitz, Y. Ramot, A. Buchs, and M. J. Rapoport, 'Reduction of digital plantar pressure by debridement and silicone orthosis', *Diabetes Research and Clinical Practice*, vol. 74, no. 3, pp. 263–266, Dec. 2006, doi: 10.1016/j.diabres.2006.04.006.
[89] H. J. Davys, D. E. Turner, P. S. Helliwell, P. G. Conaghan, P. Emery, and J. Woodburn, 'Debridement of plantar callosities in rheumatoid arthritis: a randomized controlled trial', *Rheumatology (Oxford)*, vol. 44, no. 2, pp. 207–210, Feb. 2005, doi: 10.1093/rheumatology/keh435.
[90] A. D. Jones, J. De Siqueira, J. E. Nixon, H. J. Siddle, P. R. Culmer, and D. A. Russell, 'Plantar shear stress in the diabetic foot: A systematic review and meta-analysis', *Diabet Med*, vol. 39, no. 1, p. e14661, Jan. 2022, doi: 10.1111/dme.14661.
[91] 'Diabetic Foot Top 10 Priorities (priority setting in association with the JLA) | James Lind Alliance'. Accessed: Jan. 06, 2023. [Online]. Available: https://www.jla.nihr.ac.uk/priority-setting-partnerships/Vascular/diabetic-foot-top-10-priorities.htm
[92] Ming Zhang and V. C. Roberts, 'The effect of shear forces externally applied to skin surface on underlying tissues', *Journal of Biomedical Engineering*, vol. 15, no. 6, pp. 451–456, Nov. 1993, doi: 10.1016/0141-5425(93)90057-6.
[93] V. V. Broderick and L. J. Cowan, 'Pressure Injury Related to Friction and Shearing Forces in Older Adults'.
[94] E. Roux, P. Bougaran, P. Dufourcq, and T. Couffinhal, 'Fluid Shear Stress Sensing by the Endothelial Layer', *Frontiers in Physiology*, vol. 11, 2020, Accessed: Feb. 02, 2023. [Online]. Available: https://www.frontiersin.org/articles/10.3389/fphys.2020.00861
[95] S. (née K. Rajala and J. Lekkala, 'Plantar shear stress measurements — A review', *Clinical Biomechanics*, vol. 29, no. 5, pp. 475–483, May 2014, doi: 10.1016/j.clinbiomech.2014.04.009.
[96] K. E. Chatwin, C. A. Abbott, A. J. M. Boulton, F. L. Bowling, and N. D. Reeves, 'The role of foot pressure measurement in the prediction and prevention of diabetic foot ulceration—A comprehensive review', *Diabetes Metab Res Rev*, vol. 36, no. 4, p. e3258, May 2020, doi: 10.1002/dmrr.3258.
[97] L. Wang *et al.*, 'An Inductive Force Sensor for In-Shoe Plantar Normal and Shear Load Measurement', *IEEE Sensors Journal*, vol. 20, no. 22, pp. 13318–13331, Nov. 2020, doi: 10.1109/JSEN.2020.3006316.
[98] V. H. Chuter, M. J. Spink, M. David, S. Lanting, and A. Searle, 'Clinical foot measurements as a proxy for plantar pressure testing in people with diabetes',

Journal of Foot and Ankle Research, vol. 14, no. 1, p. 56, Oct. 2021, doi: 10.1186/s13047-021-00494-4.

[99] L. A. Lavery, D. G. Armstrong, S. A. Vela, T. L. Quebedeaux, and J. G. Fleischli, 'Practical Criteria for Screening Patients at High Risk for Diabetic Foot Ulceration', *Arch Intern Med*, vol. 158, no. 2, pp. 157–162, Jan. 1998, doi: 10.1001/archinte.158.2.157.

[100] M. Yavuz, A. Erdemir, G. Botek, G. B. Hirschman, L. Bardsley, and B. L. Davis, 'Peak Plantar Pressure and Shear Locations: Relevance to diabetic patients', *Diabetes Care*, vol. 30, no. 10, pp. 2643–2645, Oct. 2007, doi: 10.2337/dc07-0862.

[101] A. Veves, H. J. Murray, M. J. Young, and A. J. M. Boulton, 'The risk of foot ulceration in diabetic patients with high foot pressure: a prospective study', *Diabetologia*, vol. 35, no. 7, pp. 660–663, Jul. 1992, doi: 10.1007/BF00400259.

[102] J. E. Perry, J. O. Hall, and B. L. Davis, 'Simultaneous measurement of plantar pressure and shear forces in diabetic individuals', *Gait & Posture*, vol. 15, no. 1, pp. 101–107, Feb. 2002, doi: 10.1016/S0966-6362(01)00176-X.

[103] M. Yavuz *et al.*, 'Plantar Shear Stress in Individuals With a History of Diabetic Foot Ulcer: An Emerging Predictive Marker for Foot Ulceration', *Diabetes Care*, vol. 40, no. 2, pp. e14–e15, Nov. 2016, doi: 10.2337/dc16-2204.

[104] C. Y. L. Chao, Y.-P. Zheng, and G. L. Y. Cheing, 'Epidermal Thickness and Biomechanical Properties of Plantar Tissues in Diabetic Foot', *Ultrasound in Medicine & Biology*, vol. 37, no. 7, pp. 1029–1038, Jul. 2011, doi: 10.1016/j.ultrasmedbio.2011.04.004.

[105] Y. P. Zheng, Y. K. C. Choi, K. Wong, S. Chan, and A. F. T. Mak, 'Biomechanical assessment of plantar foot tissue in diabetic patients using an ultrasound indentation system', *Ultrasound in Medicine & Biology*, vol. 26, no. 3, pp. 451–456, Mar. 2000, doi: 10.1016/S0301-5629(99)00163-5.

[106] A. Gefen, M. Megido-Ravid, M. Azariah, Y. Itzchak, and M. Arcan, 'Integration of plantar soft tissue stiffness measurements in routine MRI of the diabetic foot', *Clinical Biomechanics*, vol. 16, no. 10, pp. 921–925, Dec. 2001, doi: 10.1016/S0268-0033(01)00074-2.

[107] Y.-K. Jan, C.-W. Lung, E. Cuaderes, D. Rong, and K. Boyce, 'Effect of viscoelastic properties of plantar soft tissues on plantar pressures at the first metatarsal head in diabetics with peripheral neuropathy', *Physiol. Meas.*, vol. 34, no. 1, p. 53, Dec. 2012, doi: 10.1088/0967-3334/34/1/53.

[108] P. A. Lazzarini *et al.*, 'Measuring Plantar Tissue Stress in People With Diabetic Peripheral Neuropathy: A Critical Concept in Diabetic Foot Management', *Journal of Diabetes Science and Technology*, vol. 13, no. 5, pp. 869–880, Sep. 2019, doi: 10.1177/1932296819849092/FORMAT/EPUB.

[109] M. N. Orlin and T. G. McPoil, 'Plantar Pressure Assessment', *Physical Therapy*, vol. 80, no. 4, pp. 399–409, Apr. 2000, doi: 10.1093/ptj/80.4.399.

[110] A. H. Abdul Razak, A. Zayegh, R. K. Begg, and Y. Wahab, 'Foot Plantar Pressure Measurement System: A Review', *Sensors*, vol. 12, no. 7, Art. no. 7, Jul. 2012, doi: 10.3390/s120709884.

[111] M. Yavuz, 'Plantar shear stress distributions in diabetic patients with and without neuropathy', *Clin Biomech (Bristol, Avon)*, vol. 29, no. 2, pp. 223–229, Feb. 2014, doi: 10.1016/j.clinbiomech.2013.11.003.

[112] M. Yavuz, G. Botek, and B. L. Davis, 'Plantar shear stress distributions: Comparing actual and predicted frictional forces at the foot–ground interface', *Journal of Biomechanics*, vol. 40, no. 13, pp. 3045–3049, Jan. 2007, doi: 10.1016/j.jbiomech.2007.02.006.

[113] A. Amemiya, H. Noguchi, M. Oe, H. Sanada, and T. Mori, 'Establishment of a measurement method for in-shoe pressure and shear stress in specific regions for diabetic ulcer prevention', in *2016 38th Annual International Conference of the IEEE Engineering in Medicine and Biology Society (EMBC)*, Aug. 2016, pp. 2291–2294. doi: 10.1109/EMBC.2016.7591187.

[114] M. Lord and R. Hosein, 'A study of in-shoe plantar shear in patients with diabetic neuropathy', *Clinical Biomechanics*, vol. 15, no. 4, pp. 278–283, May 2000, doi: 10.1016/S0268-0033(99)00076-5.
[115] S. R. Crossland, H. J. Siddle, P. Culmer, and C. L. Brockett, 'A plantar surface shear strain methodology utilising Digital Image Correlation', *Journal of the Mechanical Behavior of Biomedical Materials*, vol. 136, p. 105482, Dec. 2022, doi: 10.1016/j.jmbbm.2022.105482.
[116] A. D. Jones, S. R. Crossland, J. E. Nixon, H. J. Siddle, D. A. Russell, and P. R. Culmer, 'STrain Analysis and Mapping of the Plantar Surface (STAMPS) – A novel technique of plantar load analysis during gait', Mar. 15, 2023, *medRxiv*. doi: 10.1101/2023.03.10.23287086.
[117] A. D. Jones, S. Crossland, J. E. Nixon, H. J. Siddle, P. R. Culmer, and D. A. Russell, 'A cross sectional pilot study utilising STrain Analysis and Mapping of the Plantar Surface (STAMPS) to measure plantar load characteristics within a healthy population', *Gait & Posture*, vol. 113, pp. 246–251, Sep. 2024, doi: 10.1016/j.gaitpost.2024.06.018.
[118] A. D. Jones, S. Crossland, J. E. Nixon, H. J. Siddle, P. R. Culmer, and D. A. Russell, 'Comparing plantar shear strain in patients with a previous diabetes-related foot ulcer and those at low risk for ulceration using the STrain Analysis and Mapping of the Plantar Surface (STAMPS) system', *Diabetic Medicine*, vol. 43, no. 2, p. e70164, 2026, doi: 10.1111/dme.70164.
[119] N. McCormick and J. Lord, 'Digital Image Correlation', *Materials Today*, vol. 13, no. 12, pp. 52–54, Dec. 2010, doi: 10.1016/S1369-7021(10)70235-2.
[120] B. Pan, 'Digital image correlation for surface deformation measurement: historical developments, recent advances and future goals', *Meas. Sci. Technol.*, vol. 29, no. 8, p. 082001, Jun. 2018, doi: 10.1088/1361-6501/aac55b.
[121] J. Zhao, Y. Sang, and F. Duan, 'The state of the art of two-dimensional digital image correlation computational method', *Engineering Reports*, vol. 1, no. 2, p. e12038, 2019, doi: 10.1002/eng2.12038.
[122] Y. L. Dong and B. Pan, 'A Review of Speckle Pattern Fabrication and Assessment for Digital Image Correlation', *Exp Mech*, vol. 57, no. 8, pp. 1161–1181, Oct. 2017, doi: 10.1007/s11340-017-0283-1.
[123] J. Park, S. Yoon, T.-H. Kwon, and K. Park, 'Assessment of speckle-pattern quality in digital image correlation based on gray intensity and speckle morphology', *Optics and Lasers in Engineering*, vol. 91, pp. 62–72, Apr. 2017, doi: 10.1016/j.optlaseng.2016.11.001.
[124] Y. Su and Q. Zhang, 'Glare: A free and open-source software for generation and assessment of digital speckle pattern', *Optics and Lasers in Engineering*, vol. 148, p. 106766, Jan. 2022, doi: 10.1016/j.optlaseng.2021.106766.
[125] H. Tu, Z. Gao, C. Bai, S. Lan, Y. Wang, and Q. Zhang, 'Single-camera 3D-DIC system based on a fiber bundle', *Optics and Lasers in Engineering*, vol. 147, p. 106743, Dec. 2021, doi: 10.1016/j.optlaseng.2021.106743.
[126] E. M. C. Jones and M. A. Iadicola, 'A Good Practices Guide for Digital Image Correlation', International Digital Image Correlation Society. Accessed: Oct. 05, 2022. [Online]. Available: https://doi.org/10.32720/idics/gpg.ed1.
[127] G. Crammond, S. W. Boyd, and J. M. Dulieu-Barton, 'Speckle pattern quality assessment for digital image correlation', *Optics and Lasers in Engineering*, vol. 51, no. 12, pp. 1368–1378, Dec. 2013, doi: 10.1016/j.optlaseng.2013.03.014.
[128] B. Pan, K. Qian, H. Xie, and A. Asundi, 'Two-dimensional digital image correlation for in-plane displacement and strain measurement: a review', *Meas. Sci. Technol.*, vol. 20, no. 6, p. 062001, Apr. 2009, doi: 10.1088/0957-0233/20/6/062001.
[129] B. Pan, A. Asundi, H. Xie, and J. Gao, 'Digital image correlation using iterative least squares and pointwise least squares for displacement field and strain field measurements', *Optics and Lasers in Engineering*, vol. 47, no. 7, pp. 865–874, Jul. 2009, doi: 10.1016/j.optlaseng.2008.10.014.
[130] J. Blaber, & B. Adair, and & A. Antoniou, 'Ncorr: Open-Source 2D Digital Image Correlation Matlab Software', doi: 10.1007/s11340-015-0009-1.

[131] B. Wattrisse, A. Chrysochoos, J.-M. Muracciole, and M. Némoz-Gaillard, ‘Analysis of strain localization during tensile tests by digital image correlation’, *Experimental Mechanics*, vol. 41, no. 1, pp. 29–39, Mar. 2001, doi: 10.1007/BF02323101.
[132] M. A. Sutton, J. L. Turner, H. A. Bruck, and T. A. Chae, ‘Full-field representation of discretely sampled surface deformation for displacement and strain analysis’, *Experimental Mechanics*, vol. 31, no. 2, pp. 168–177, Jun. 1991, doi: 10.1007/BF02327571.
[133] L. B. Meng, G. C. Jin, and X. F. Yao, ‘Application of iteration and finite element smoothing technique for displacement and strain measurement of digital speckle correlation’, *Optics and Lasers in Engineering*, vol. 45, no. 1, pp. 57–63, Jan. 2007, doi: 10.1016/j.optlaseng.2006.04.012.
[134] J. C. A. de Deus Filho, L. C. da Silva Nunes, and J. M. C. Xavier, ‘iCorrVision-2D: An integrated python-based open-source Digital Image Correlation software for in-plane measurements (Part 1)’, *SoftwareX*, vol. 19, p. 101131, Jul. 2022, doi: 10.1016/j.softx.2022.101131.
[135] D. Lunt *et al.*, ‘Comparison of sub-grain scale digital image correlation calculated using commercial and open-source software packages’, *Materials Characterization*, vol. 163, p. 110271, May 2020, doi: 10.1016/j.matchar.2020.110271.
[136] M. Arza-García *et al.*, ‘Evaluation of a low-cost approach to 2-D digital image correlation vs. a commercial stereo-DIC system in Brazilian testing of soil specimens’, *Archiv.Civ.Mech.Eng*, vol. 22, no. 1, p. 4, Nov. 2021, doi: 10.1007/s43452-021-00325-0.
[137] D. Solav and A. Silverstein, ‘DuoDIC: 3D Digital Image Correlation in MATLAB’, *Journal of Open Source Software*, vol. 7, no. 74, p. 4279, Sep. 2022, doi: 10.21105/JOSS.04279.
[138] D. Solav, K. M. Moerman, A. M. Jaeger, K. Genovese, and H. M. Herr, ‘MultiDIC: An Open-Source Toolbox for Multi-View 3D Digital Image Correlation’, *IEEE Access*, vol. 6, pp. 30520–30535, 2018.
[139] ‘Correlated Solutions Digital Image Correlation’, Correlated Solutions Digital Image Correlation. Accessed: Feb. 01, 2023. [Online]. Available: https://www.correlatedsolutions.com
[140] ‘ARAMIS - GOM correlate’. Accessed: Feb. 01, 2023. [Online]. Available: https://www.gom.com/en/topics/aramis-high-speed-dic-systems
[141] ‘MatchID’. Accessed: Feb. 01, 2023. [Online]. Available: https://www.matchid.eu/
[142] ‘LaVision - StrainMaster’. Accessed: Feb. 01, 2023. [Online]. Available: https://www.lavision.de/en/products/strainmaster/
[143] S. Jaminion, N. W. Nelson, J. P. Chambard, N. Swiergel, and F. Hild, ‘CorreliSTC: A Global Approach in Digital Image Correlation’, in *International Digital Imaging Correlation Society*, M. Sutton and P. L. Reu, Eds., in Conference Proceedings of the Society for Experimental Mechanics Series. Cham: Springer International Publishing, 2017, pp. 277–279. doi: 10.1007/978-3-319-51439-0_66.
[144] ‘Digital Image Correlation (DIC) - Dantec Dynamics’, Dantec Dynamics | Precision Measurement Systems & Sensors. Accessed: Feb. 01, 2023. [Online]. Available: https://www.dantecdynamics.com/notes/digital-image-correlation-dic-a-complementary-method-for-strain-gauge-measurements/
[145] ‘Image Systems’. Accessed: Feb. 01, 2023. [Online]. Available: https://imagesystems.se/dic-embedded/
[146] D. Turner, P. Crozier, and P. Reu, ‘Digital Image Correlation Engine’, Sandia National Laboratories (SNL), Albuquerque, NM, and Livermore, CA (United States), DICE; 003748MLTPL00, Oct. 2015. Accessed: Feb. 01, 2023. [Online]. Available: https://www.osti.gov/biblio/1245432
[147] V. Belloni, R. Ravanelli, A. Nascetti, M. Di Rita, D. Mattei, and M. Crespi, ‘py2DIC: A New Free and Open Source Software for Displacement and Strain Measurements in the Field of Experimental Mechanics’, *Sensors*, vol. 19, no. 18, Art. no. 18, Jan. 2019, doi: 10.3390/s19183832.

[148] S. N. Olufsen, M. E. Andersen, and E. Fagerholt, ‘µDIC: An open-source toolkit for digital image correlation’, *SoftwareX*, vol. 11, p. 100391, Jan. 2020, doi: 10.1016/j.softx.2019.100391.
[149] P. P. Das, M. R. P. Elenchezhian, V. Vadlamudi, K. Reifsnider, and R. Raihan, ‘RealPi2dDIC: A Low-cost and open-source approach to in situ 2D Digital Image Correlation (DIC) applications’, *SoftwareX*, vol. 13, p. 100645, Jan. 2021, doi: 10.1016/j.softx.2020.100645.
[150] D. Atkinson and T. Becker, ‘A 117 Line 2D Digital Image Correlation Code Written in MATLAB’, *Remote Sensing*, vol. 12, no. 18, Art. no. 18, Jan. 2020, doi: 10.3390/rs12182906.
[151] R. Seghir, J. F. Witz, and S. Coudert, ‘YaDICs - Digital Image Correlation 2/3D software’. Accessed: Feb. 01, 2023. [Online]. Available: https://yadics.univ-lille1.fr/wordpress/index.html
[152] J. Yang and K. Bhattacharya, ‘Combining Image Compression with Digital Image Correlation’, *Exp Mech*, vol. 59, no. 5, pp. 629–642, Jun. 2019, doi: 10.1007/s11340-018-00459-y.
[153] J. Filho, L. Nunes, and J. Xavier, ‘iCorrVision-3D: An integrated python-based open-source Digital Image Correlation Software for in-plane and out-of-plane measurements (Part 2)’, *SoftwareX*, vol. 19, p. 101132, Jul. 2022, doi: 10.1016/j.softx.2022.101132.
[154] Z. Jorge, P. Ronny, and O. Sotomayor, ‘On the Digital Image Correlation Technique’, *Materials Today: Proceedings*, vol. 49, pp. 79–84, Jan. 2022, doi: 10.1016/j.matpr.2021.07.476.
[155] H. R and M. Ramji, ‘Adaptation of Open Source 2D DIC Software Ncorr for Solid Mechanics Applications’, Nov. 2014. doi: 10.13140/2.1.4994.1442.
[156] A. F. Ab Ghani, M. B. Ali, S. Dhar Malingam, and J. Mahmud, ‘Digital Image Correlation (DIC) Technique in Measuring Strain Using Opensource Platform Ncorr’, *Journal of Advanced Research in Applied Mechanics*, vol. 26, pp. 2289–7895, Oct. 2016.
[157] S. L. Kumar, H. B. Aravind, and N. Hossiney, ‘Digital image correlation (DIC) for measuring strain in brick masonry specimen using Ncorr open source 2D MATLAB program’, *Results in Engineering*, vol. 4, p. 100061, Dec. 2019, doi: 10.1016/j.rineng.2019.100061.
[158] K. Genovese, L. Casaletto, J. A. Rayas, V. Flores, and A. Martinez, ‘Stereo-Digital Image Correlation (DIC) measurements with a single camera using a biprism’, *Optics and Lasers in Engineering*, vol. 51, no. 3, pp. 278–285, Mar. 2013, doi: 10.1016/j.optlaseng.2012.10.001.
[159] H. Luo, L. Yu, and B. Pan, ‘Design and validation of a demand-oriented single-camera stereo-DIC system with a four-mirror adapter’, *Measurement*, vol. 186, p. 110083, Dec. 2021, doi: 10.1016/j.measurement.2021.110083.
[160] J. Pisonero *et al.*, ‘A Comparative Study of 2D and 3D Digital Image Correlation Approaches for the Characterization and Numerical Analysis of Composite Materials’, *IEEE Access*, vol. 9, pp. 160675–160687, 2021, doi: 10.1109/ACCESS.2021.3132393.
[161] I. Eshraghi, M. R. Yadegari Dehnavi, and N. Soltani, ‘Effect of subset parameters selection on the estimation of mode-I stress intensity factor in a cracked PMMA specimen using digital image correlation’, *Polymer Testing*, vol. 37, pp. 193–200, Aug. 2014, doi: 10.1016/j.polymertesting.2014.05.017.
[162] B. Pan, H. Xie, Z. Wang, K. Qian, and Z. Wang, ‘Study on subset size selection in digital image correlation for speckle patterns’, *Opt. Express, OE*, vol. 16, no. 10, pp. 7037–7048, May 2008, doi: 10.1364/OE.16.007037.
[163] C. Lim, Y. Jeong, S. Limkatanyu, and M. Kwon, ‘Strain Measuring of Composite Grid Using Digital Image Correlation’, *Advances in Materials Science and Engineering*, vol. 2022, pp. 1–12, Apr. 2022, doi: 10.1155/2022/6041887.
[164] International Diabetes Federation, ‘IDF Diabetes Atlas 10th edition’. Accessed: May 16, 2023. [Online]. Available: https://diabetesatlas.org

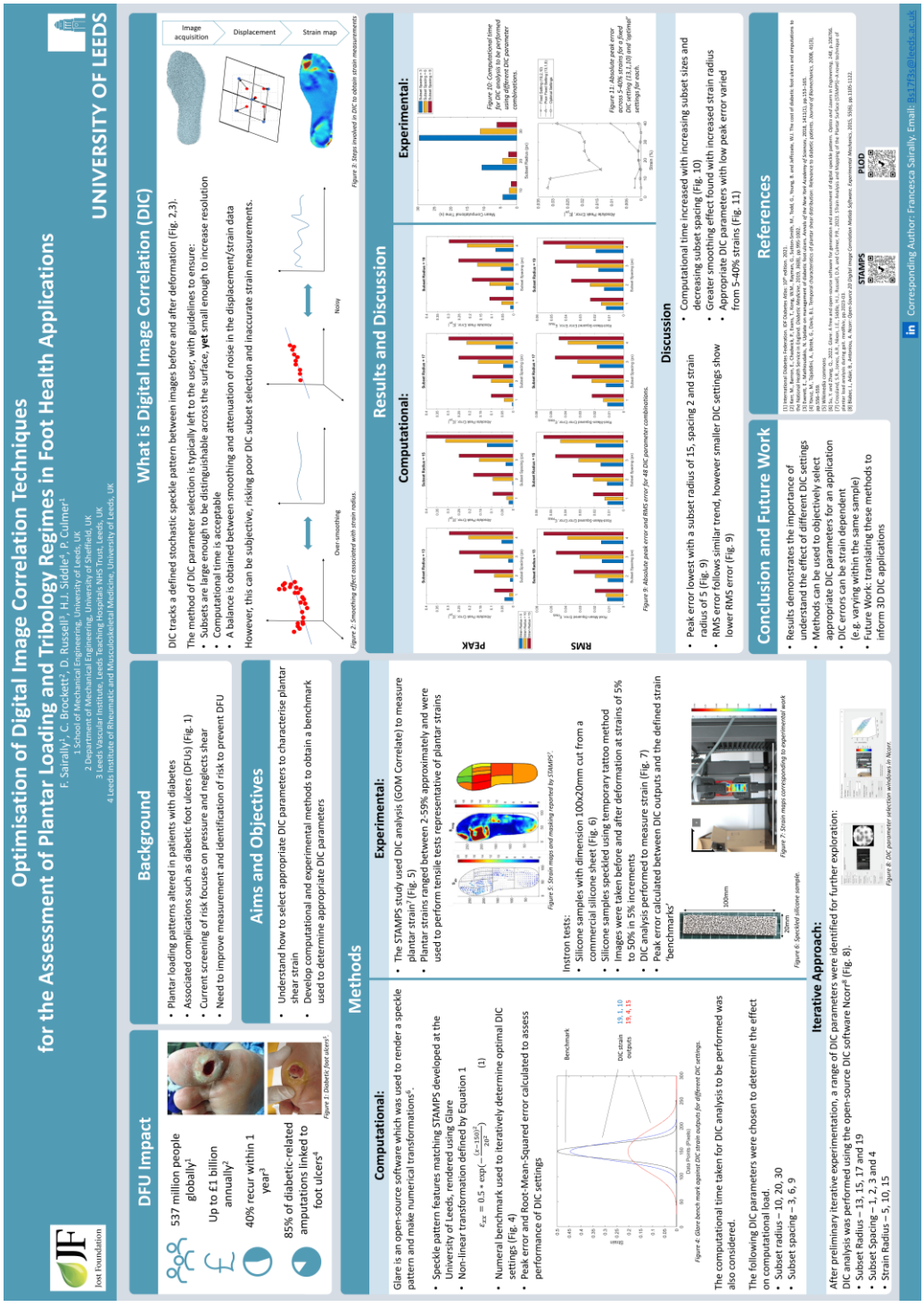
[165] S. White, M. B. A. McCullough, and P. M. Akangah, 'The Structural Effects of Diabetes on Soft Tissues: A Systematic Review', *Crit Rev Biomed Eng*, vol. 49, no. 6, pp. 11–27, 2021, doi: 10.1615/CritRevBiomedEng.2022043200.
[166] A. H. Haron *et al.*, 'In-shoe plantar shear stress sensor design, calibration and evaluation for the diabetic foot', *PLOS ONE*, vol. 19, no. 9, p. e0309514, Sep. 2024, doi: 10.1371/journal.pone.0309514.
[167] P. Reu, 'Hidden Components of 3D-DIC: Triangulation and Post-processing – Part 3', *Experimental Techniques*, vol. 36, no. 4, pp. 3–5, Jul. 2012, doi: 10.1111/j.1747-1567.2012.00853.x.
[168] H. Edelsbrunner, 'Triangulations and meshes in computational geometry', *Acta Numerica*, vol. 9, pp. 133–213, Jan. 2000, doi: 10.1017/S0962492900001331.
[169] 'Delaunay Triangulation | Computational Geometry | Faculty of Natural Science at Masaryk University'. Accessed: Mar. 12, 2026. [Online]. Available: https://is.muni.cz/do/sci/UMS/el/geometricke-alg/pages/10-delaun-triangulation.html?kod=MUKS11;predmet=625896;lang=cs
[170] 'Framework for responsible research and innovation'. Accessed: Mar. 18, 2026. [Online]. Available: https://www.ukri.org/who-we-are/epsrc/our-policies-and-standards/framework-for-responsible-innovation/
[171] L. A. Lavery, D. G. Armstrong, R. P. Wunderlich, J. Tredwell, and A. J. M. Boulton, 'Predictive Value of Foot Pressure Assessment as Part of a Population-Based Diabetes Disease Management Program', *Diabetes Care*, vol. 26, no. 4, pp. 1069–1073, Apr. 2003, doi: 10.2337/diacare.26.4.1069.
[172] S. Hu *et al.*, 'Triboelectric Insoles with Normal-Shear Plantar Stress Perception', *Advanced Functional Materials*, vol. 34, no. 16, p. 2313458, 2024, doi: 10.1002/adfm.202313458.
[173] X. Xiang *et al.*, 'Smart Cushions with Machine Learning-Enhanced Force Sensors for Pressure Injury Risk Assessment', *ACS Appl. Mater. Interfaces*, vol. 16, no. 29, pp. 38466–38477, Jul. 2024, doi: 10.1021/acsami.4c05964.
[174] K. Zhang *et al.*, 'Machine learning based finite element analysis for personalized prediction of pressure injury risk in patients with spinal cord injury', *Computer Methods and Programs in Biomedicine*, vol. 261, p. 108648, Apr. 2025, doi: 10.1016/j.cmpb.2025.108648.
[175] F. Sairally, R. P. Turnbull, H. J. Siddle, D. A. Russell, C. Brockett, and P. R. Culmer, 'Development and evaluation of a novel 3D in-shoe plantar strain measurement system: STAMPS3D', *Proc Inst Mech Eng H*, p. 09544119251330738, Apr. 2025, doi: 10.1177/09544119251330738.
[176] R. Collings, J. Freeman, J. M. Latour, and J. Paton, 'Footwear and insole design features for offloading the diabetic at risk foot—A systematic review and meta-analyses', *Endocrinol Diabetes Metab*, vol. 4, no. 1, p. e00132, Apr. 2020, doi: 10.1002/edm2.132.
[177] S. Ahmed, A. Barwick, P. Butterworth, and S. Nancarrow, 'Footwear and insole design features that reduce neuropathic plantar forefoot ulcer risk in people with diabetes: a systematic literature review', *Journal of Foot and Ankle Research*, vol. 13, no. 1, p. 30, Jun. 2020, doi: 10.1186/s13047-020-00400-4.
[178] M. L. J. Arts *et al.*, 'Data-driven directions for effective footwear provision for the high-risk diabetic foot', *Diabetic Medicine*, vol. 32, no. 6, pp. 790–797, 2015, doi: 10.1111/dme.12741.
[179] S. A. Bus, R. Haspels, and T. E. Busch-Westbroek, 'Evaluation and Optimization of Therapeutic Footwear for Neuropathic Diabetic Foot Patients Using In-Shoe Plantar Pressure Analysis', *Diabetes Care*, vol. 34, no. 7, pp. 1595–1600, Jun. 2011, doi: 10.2337/dc10-2206.
[180] S. A. Bus *et al.*, 'The effectiveness of footwear and offloading interventions to prevent and heal foot ulcers and reduce plantar pressure in diabetes: a systematic review', *Diabetes/Metabolism Research and Reviews*, vol. 24, no. S1, pp. S162–S180, 2008, doi: 10.1002/dmrr.850.
[181] S. A. Bus, J. S. Ulbrecht, and P. R. Cavanagh, 'Pressure relief and load redistribution by custom-made insoles in diabetic patients with neuropathy and

foot deformity', *Clinical Biomechanics*, vol. 19, no. 6, pp. 629–638, Jul. 2004, doi: 10.1016/j.clinbiomech.2004.02.010.
[182] M. Lord and R. Hosein, 'Pressure redistribution by molded inserts in diabetic footwear: a pilot study.', 1994.
[183] M. Nouman, T. Dissaneewate, W. Leelasamran, and S. Chatpun, 'The insole materials influence the plantar pressure distributions in diabetic foot with neuropathy during different walking activities', *Gait & Posture*, vol. 74, pp. 154–161, Oct. 2019, doi: 10.1016/j.gaitpost.2019.08.023.
[184] Q. Q. Shi, P. L. Li, K.-L. Yick, N.-W. Li, and J. Jiao, 'Effects of contoured insoles with different materials on plantar pressure offloading in diabetic elderly during gait', *Sci Rep*, vol. 12, no. 1, p. 15395, Sep. 2022, doi: 10.1038/s41598-022-19814-0.
[185] The Leeds Teaching Hospitals NHS Trust, 'Shear Load In-shoe Plantar Sensing/ Strain Analyses and Mapping in Diabetic Foot Ulcers (SLIPSTREAM)', clinicaltrials.gov, Clinical trial registration NCT05687643, Jul. 2023. Accessed: Aug. 27, 2025. [Online]. Available: https://clinicaltrials.gov/study/NCT05687643
[186] Y. Sterman, D. Solav, N. Rosen, E. Saffuri, and L. Shmilov Zaritsky, 'Custom orthotic insoles with gradual variable stiffness using 3D printed spacer technique', *Virtual and Physical Prototyping*, vol. 19, no. 1, p. e2336151, Dec. 2024, doi: 10.1080/17452759.2024.2336151.
[187] N. Baker, 'Debridement of the Diabetic Foot: A Podiatric Perspective', *The International Journal of Lower Extremity Wounds*, vol. 1, no. 2, pp. 87–92, Jun. 2002, doi: 10.1177/153473460200100203.
[188] M. Hamatani *et al.*, 'Factors Associated With Callus in Patients with Diabetes, Focused on Plantar Shear Stress During Gait'. Accessed: Jul. 22, 2025. [Online]. Available: https://journals.sagepub.com/doi/epub/10.1177/1932296816648164
[189] L. Wang *et al.*, 'A Portable Insole System to Simultaneously Measure Plantar Pressure and Shear Stress', *IEEE Sensors Journal*, vol. 22, no. 9, pp. 9104–9113, May 2022, doi: 10.1109/JSEN.2022.3162713.
[190] F. Sairally *et al.*, 'Measuring plantar load with STAMPS3D: a preliminary study on the impact of contoured orthoses', *Front. Bioeng. Biotechnol.*, vol. 13, Nov. 2025, doi: 10.3389/fbioe.2025.1648649.
[191] N. B. Holowka *et al.*, 'Foot callus thickness does not trade off protection for tactile sensitivity during walking', *Nature*, vol. 571, no. 7764, pp. 261–264, Jul. 2019, doi: 10.1038/s41586-019-1345-6.
[192] F. Hashmi, C. Nester, C. Wright, V. Newton, and S. Lam, 'Characterising the biophysical properties of normal and hyperkeratotic foot skin', *J Foot Ankle Res*, vol. 8, no. 1, p. 35, Aug. 2015, doi: 10.1186/s13047-015-0092-7.
[193] A. B. Putti, G. P. Arnold, L. A. Cochrane, and R. J. Abboud, 'Normal pressure values and repeatability of the Emed® ST4 system', *Gait & Posture*, vol. 27, no. 3, pp. 501–505, Apr. 2008, doi: 10.1016/j.gaitpost.2007.06.009.
[194] M. Mirando, C. Pavese, V. Pingue, S. Sozzi, and A. Nardone, 'Can Plantar Pressure Distribution During Gait Be Estimated from Quiet Stance in Healthy Individuals?', *J Funct Morphol Kinesiol*, vol. 10, no. 3, p. 301, Aug. 2025, doi: 10.3390/jfmk10030301.
[195] C. Zippenfennig, T. J. Drechsel, R. L. Monteiro, I. C. N. Sacco, and T. L. Milani, 'The Mechanoreceptor's Role in Plantar Skin Changes in Individuals with Diabetes Mellitus', *Journal of Clinical Medicine*, vol. 10, no. 12, p. 2537, Jan. 2021, doi: 10.3390/jcm10122537.
[196] 'Eligibility of technology readiness levels (TRL)'. Accessed: Mar. 31, 2026. [Online]. Available: https://www.ukri.org/councils/stfc/guidance-for-applicants/check-if-youre-eligible-for-funding/eligibility-of-technology-readiness-levels-trl/
[197] M. Palanca, G. Tozzi, and L. Cristofolini, 'The use of digital image correlation in the biomechanical area: a review', *International Biomechanics*, vol. 3, no. 1, pp. 1–21, Jan. 2016, doi: 10.1080/23335432.2015.1117395.

[198] E. Dall'Ara and G. Tozzi, 'Digital volume correlation for the characterization of musculoskeletal tissues: Current challenges and future developments', *Front. Bioeng. Biotechnol.*, vol. 10, Oct. 2022, doi: 10.3389/fbioe.2022.1010056.
[199] F. Sairally, D. A. Russell, H. J. Siddle, D. Trinca, C. Brockett, and P. R. Culmer, 'Measuring In-Shoe Plantar Strain Outcomes in the Presence of Callus: A Preliminary Study Using the STAMPS3D Measurement System', *Journal of Foot and Ankle Research*, vol. 19, no. 2, p. e70169, 2026, doi: 10.1002/jfa2.70169.
[200] V. Singhal, S. R., S. Singhal, A. Tiwari, and D. Mangal, 'Healthcare and cutting-edge technology: Advancements, challenges, and future prospects', *Computers in Biology and Medicine*, vol. 196, p. 110861, Sep. 2025, doi: 10.1016/j.compbiomed.2025.110861.
[201] R. Sinha, 'The role and impact of new technologies on healthcare systems', *Discov Health Systems*, vol. 3, no. 1, p. 96, Nov. 2024, doi: 10.1007/s44250-024-00163-w.
[202] P. Natale *et al.*, 'Patient experiences of continuous glucose monitoring and sensor-augmented insulin pump therapy for diabetes: A systematic review of qualitative studies', *J Diabetes*, vol. 15, no. 12, pp. 1048–1069, Aug. 2023, doi: 10.1111/1753-0407.13454.
[203] E. Matijevich, E. Minty, E. Bray, C. Bachus, M. Hajizadeh, and B. Liden, 'A Multi-Faceted Digital Health Solution for Monitoring and Managing Diabetic Foot Ulcer Risk: A Case Series', *Sensors (Basel)*, vol. 24, no. 9, p. 2675, Apr. 2024, doi: 10.3390/s24092675.
[204] J. Yi *et al.*, 'Technology trends and applications of deep learning in ultrasonography: image quality enhancement, diagnostic support, and improving workflow efficiency', *Ultrasonography*, vol. 40, no. 1, pp. 7–22, Jan. 2021, doi: 10.14366/usg.20102.
[205] L. Wade, L. Needham, P. McGuigan, and J. Bilzon, 'Applications and limitations of current markerless motion capture methods for clinical gait biomechanics', *PeerJ*, vol. 10, p. e12995, Feb. 2022, doi: 10.7717/peerj.12995.
[206] W. W. T. Lam, Y. M. Tang, and K. N. K. Fong, 'A systematic review of the applications of markerless motion capture (MMC) technology for clinical measurement in rehabilitation', *J Neuroeng Rehabil*, vol. 20, p. 57, May 2023, doi: 10.1186/s12984-023-01186-9.
[207] M. H. Yap *et al.*, 'A New Mobile Application for Standardizing Diabetic Foot Images', *J Diabetes Sci Technol*, vol. 12, no. 1, pp. 169–173, Jun. 2017, doi: 10.1177/1932296817713761.

Appendix A

A.1 STLE Conference Poster



A.2 Supplementary Computational Results

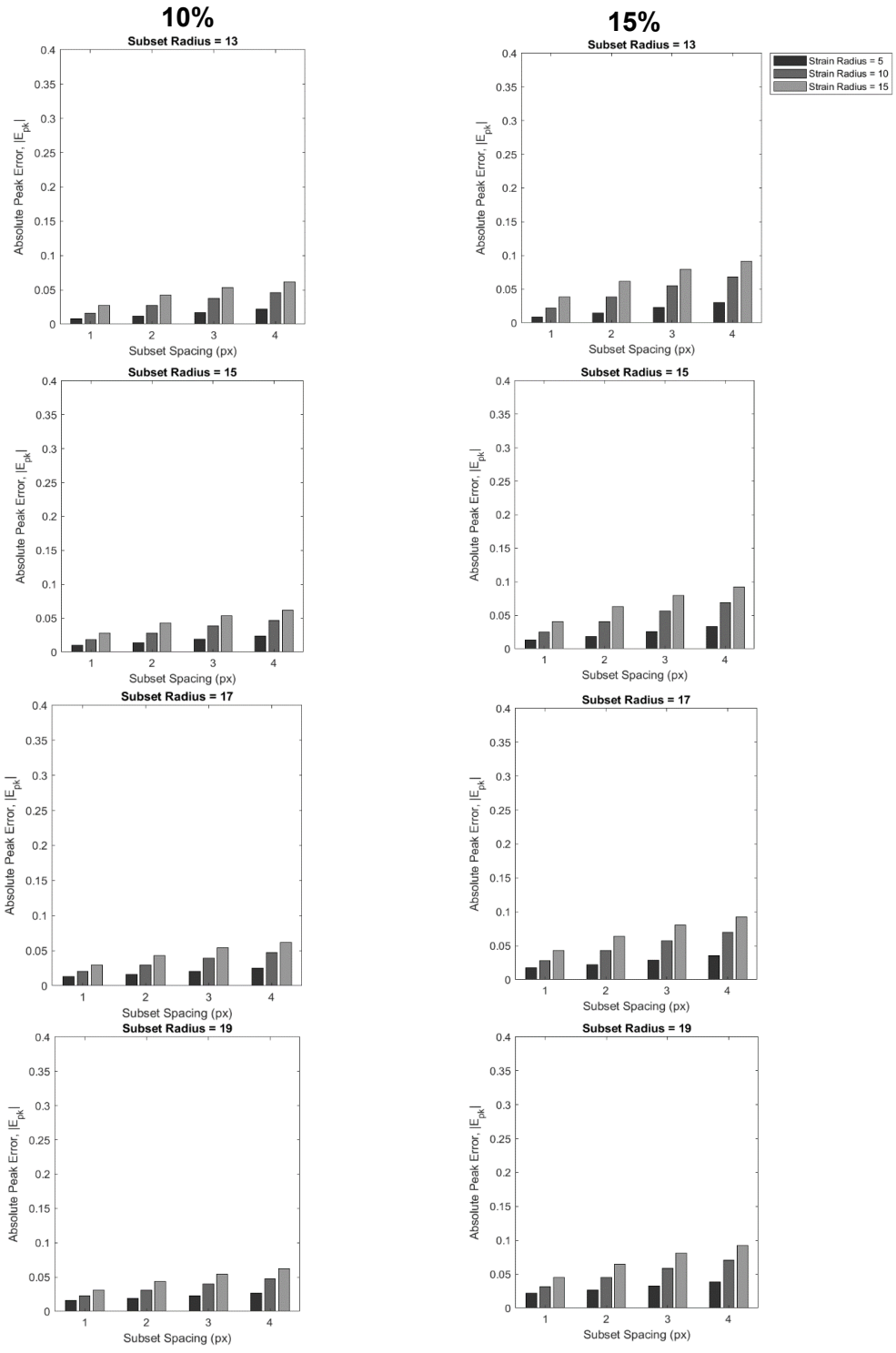


Figure A.1: *Magnitude of peak error corresponding to computational strain of 10% (left column) and 15% (right column) for different DIC parameter combinations, involving subset radius, subset spacing and strain radius.*

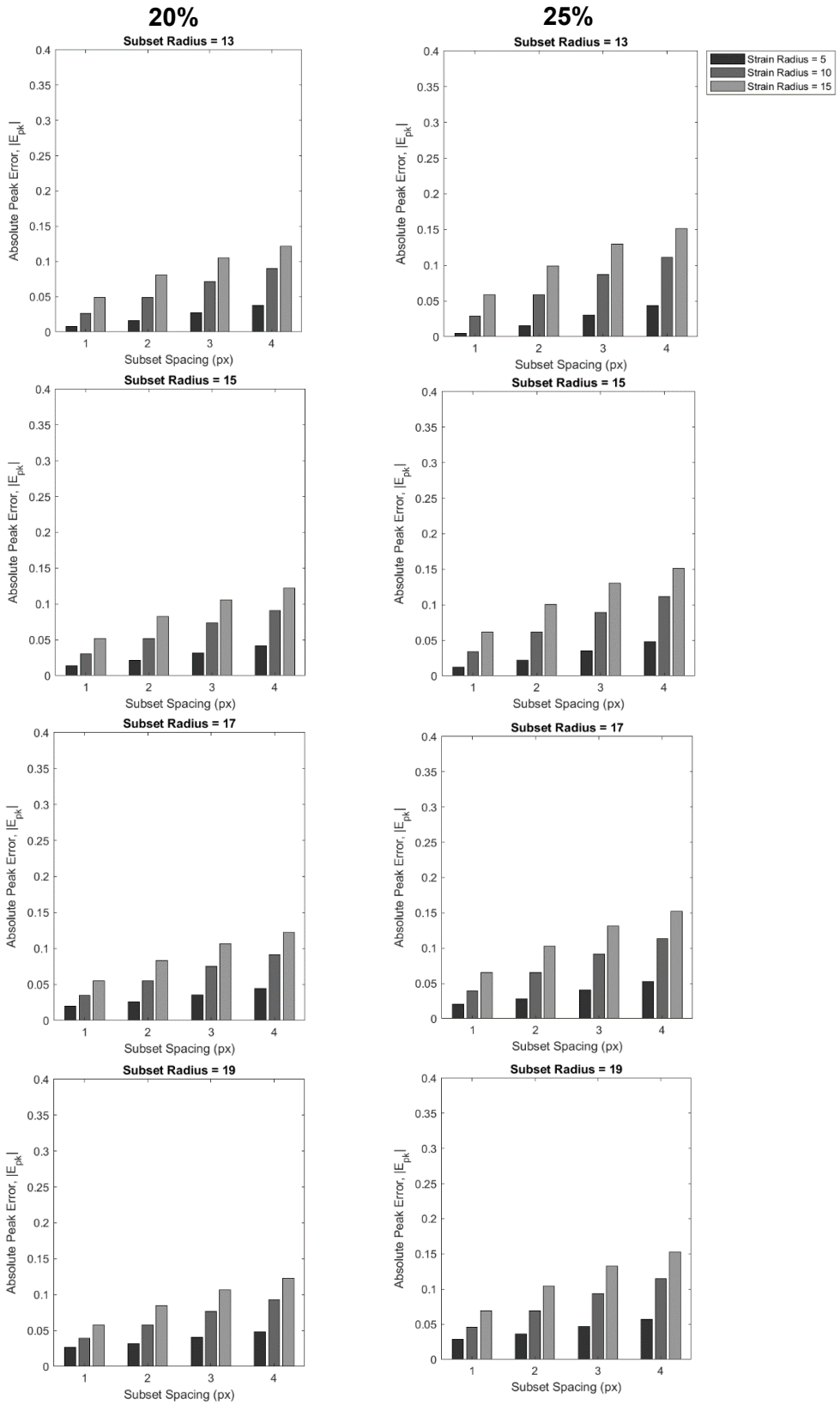


Figure A.2: *Magnitude of peak error corresponding to computational strain of 20% (left column) and 25% (right column) for different DIC parameter combinations, involving subset radius, subset spacing and strain radius.*

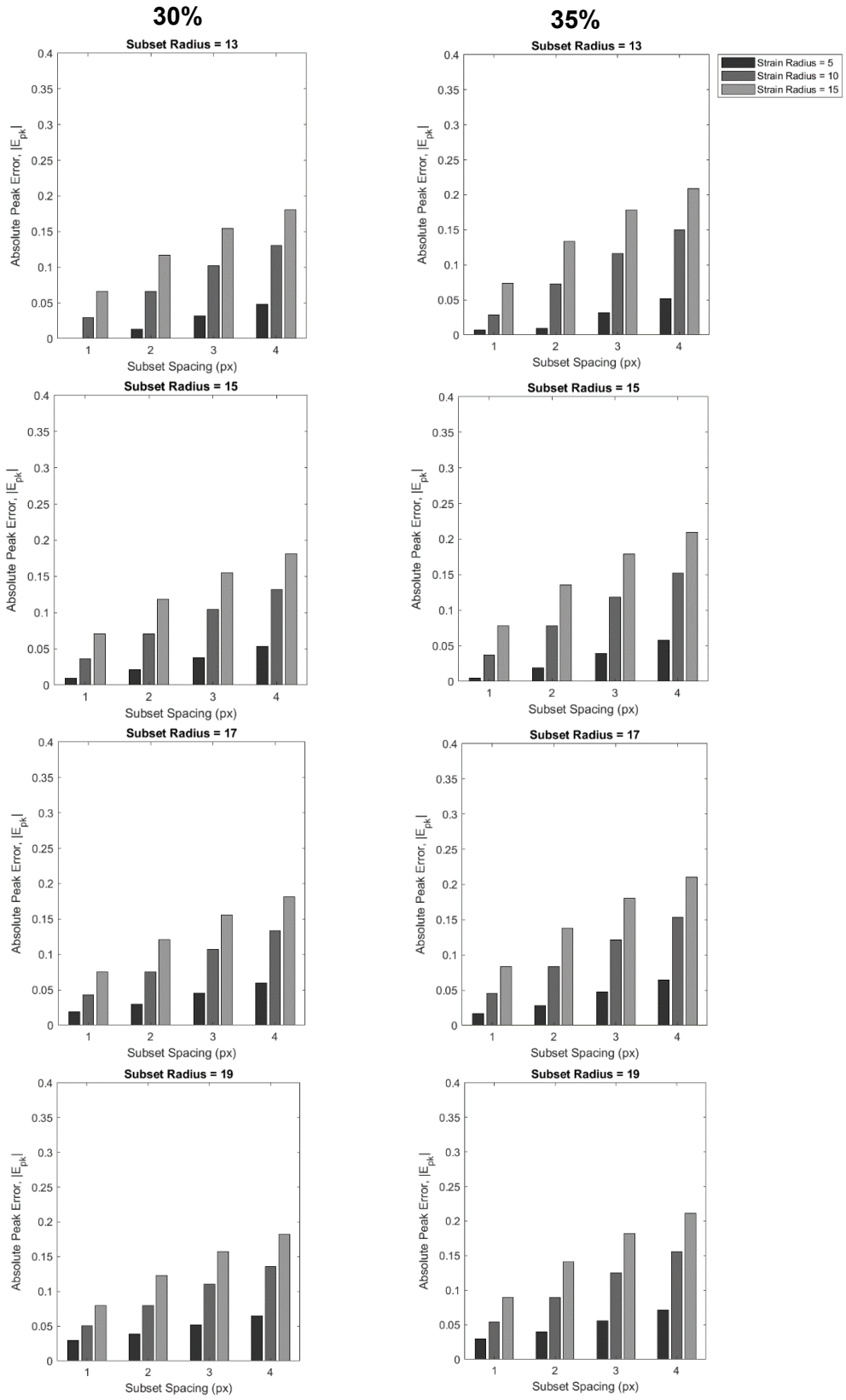


Figure A.3: *Magnitude of peak error corresponding to computational strain of 30% (left column) and 35% (right column) for different DIC parameter combinations, involving subset radius, subset spacing and strain radius.*

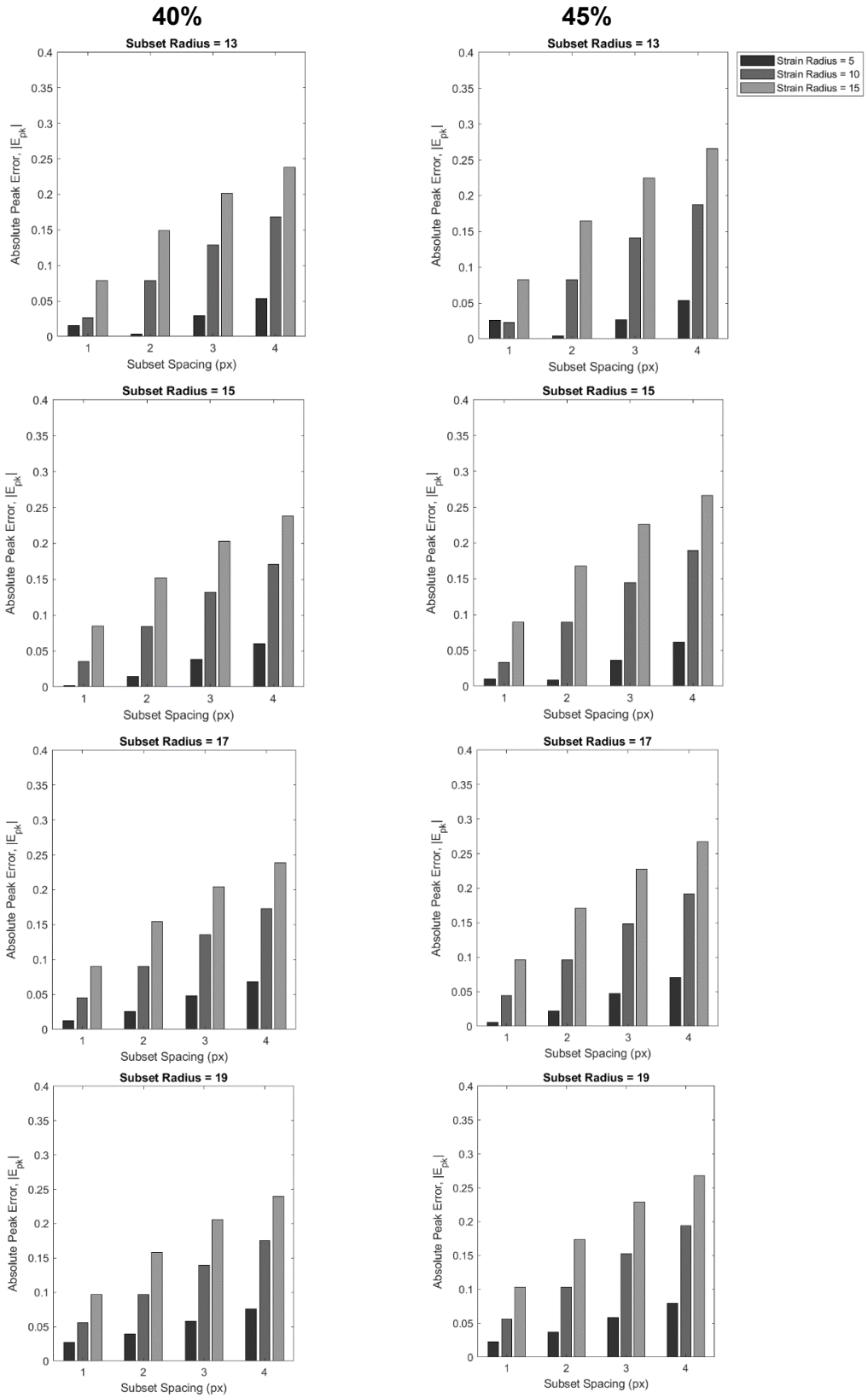


Figure A.4: *Magnitude of peak error corresponding to computational strain of 40% (left column) and 45% (right column) for different DIC parameter combinations, involving subset radius, subset spacing and strain radius.*

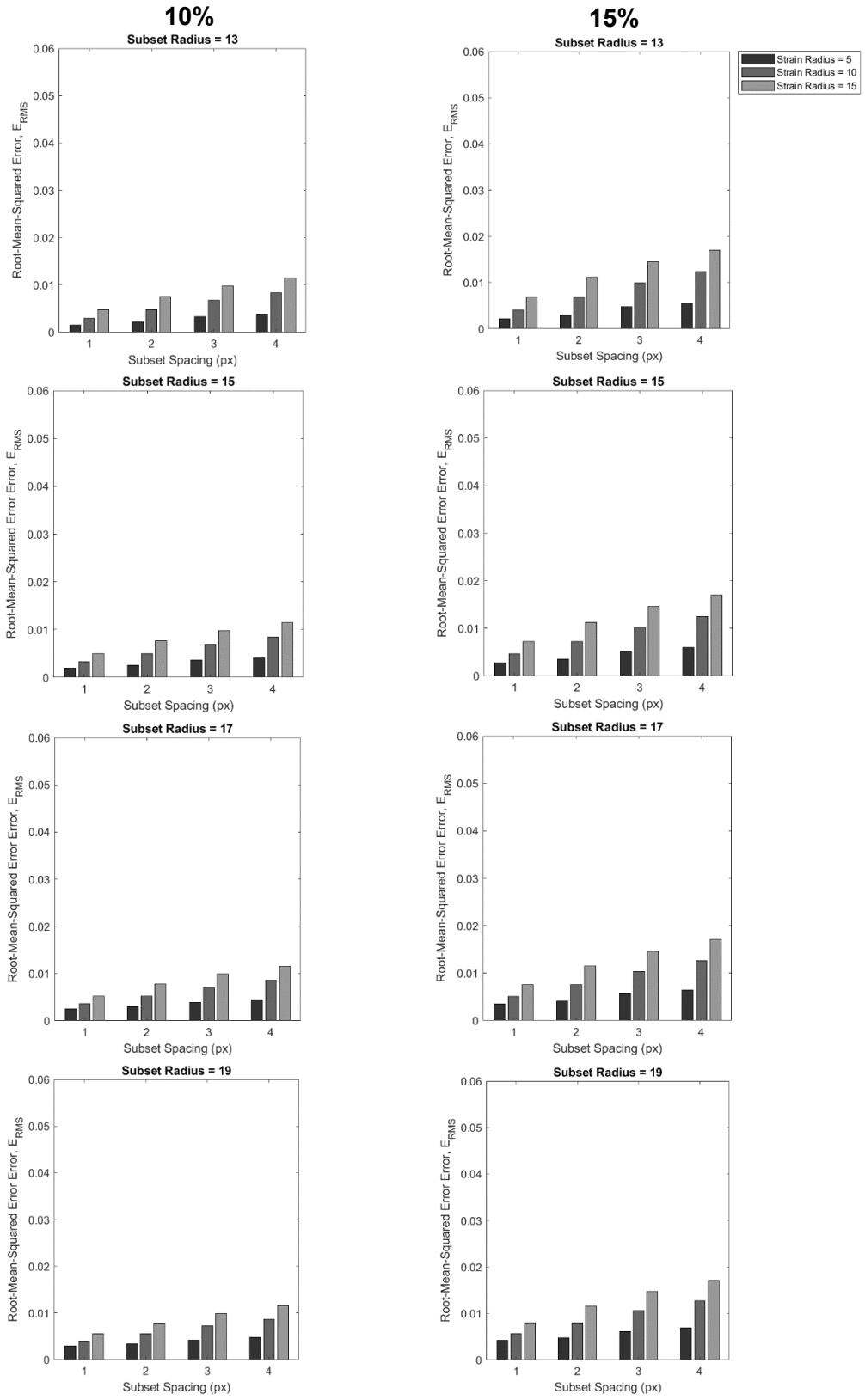


Figure A.5: *Root-mean-squared error corresponding to computational strain of 10% (left column) and 15% (right column) for different DIC parameter combinations, involving subset radius, subset spacing and strain radius.*

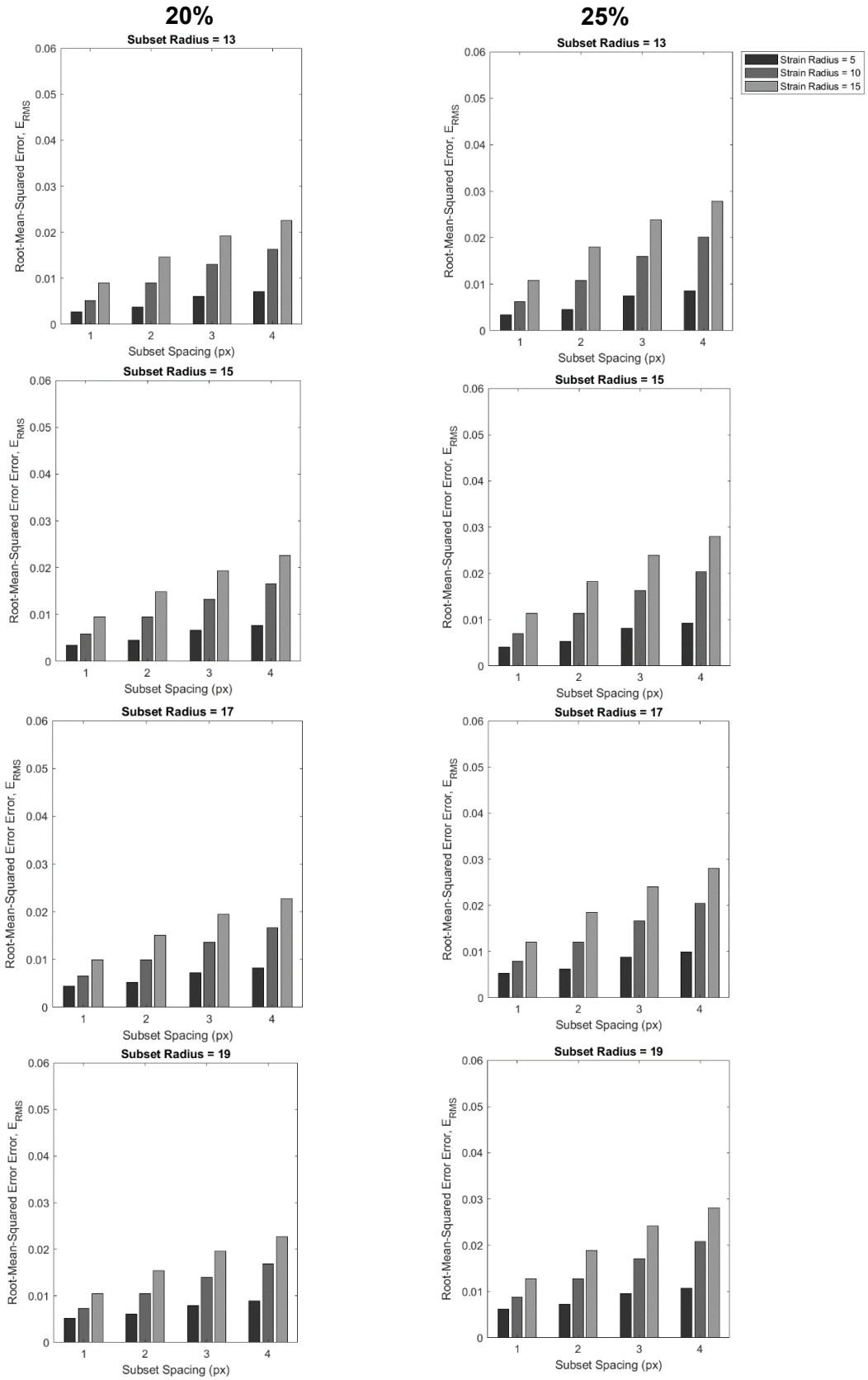


Figure A.6: *Root-mean-squared error corresponding to computational strain of 20% (left column) and 25% (right column) for different DIC parameter combinations, involving subset radius, subset spacing and strain radius.*

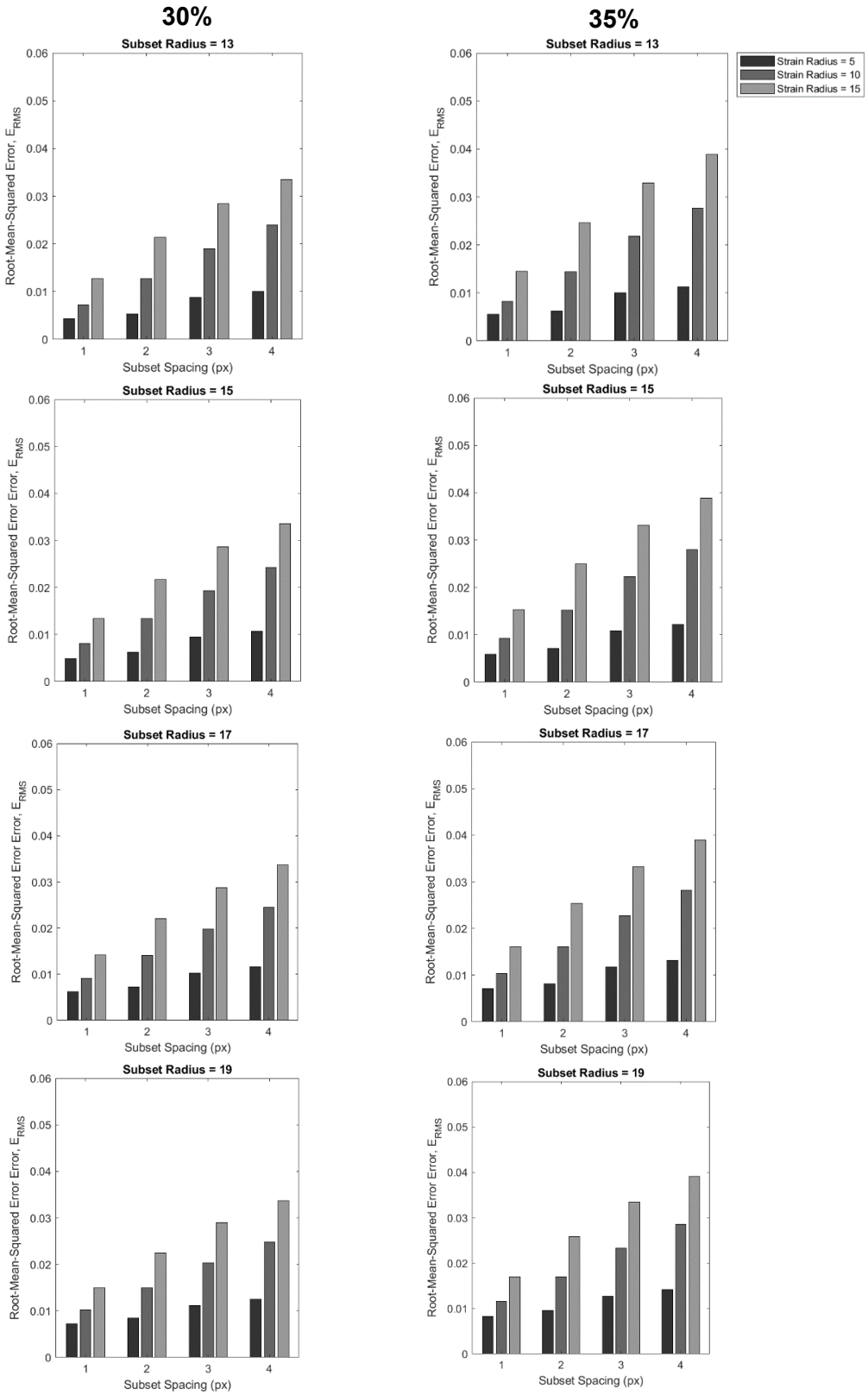


Figure A.7: *Root-mean-squared error corresponding to computational strain of 30% (left column) and 35% (right column) for different DIC parameter combinations, involving subset radius, subset spacing and strain radius.*

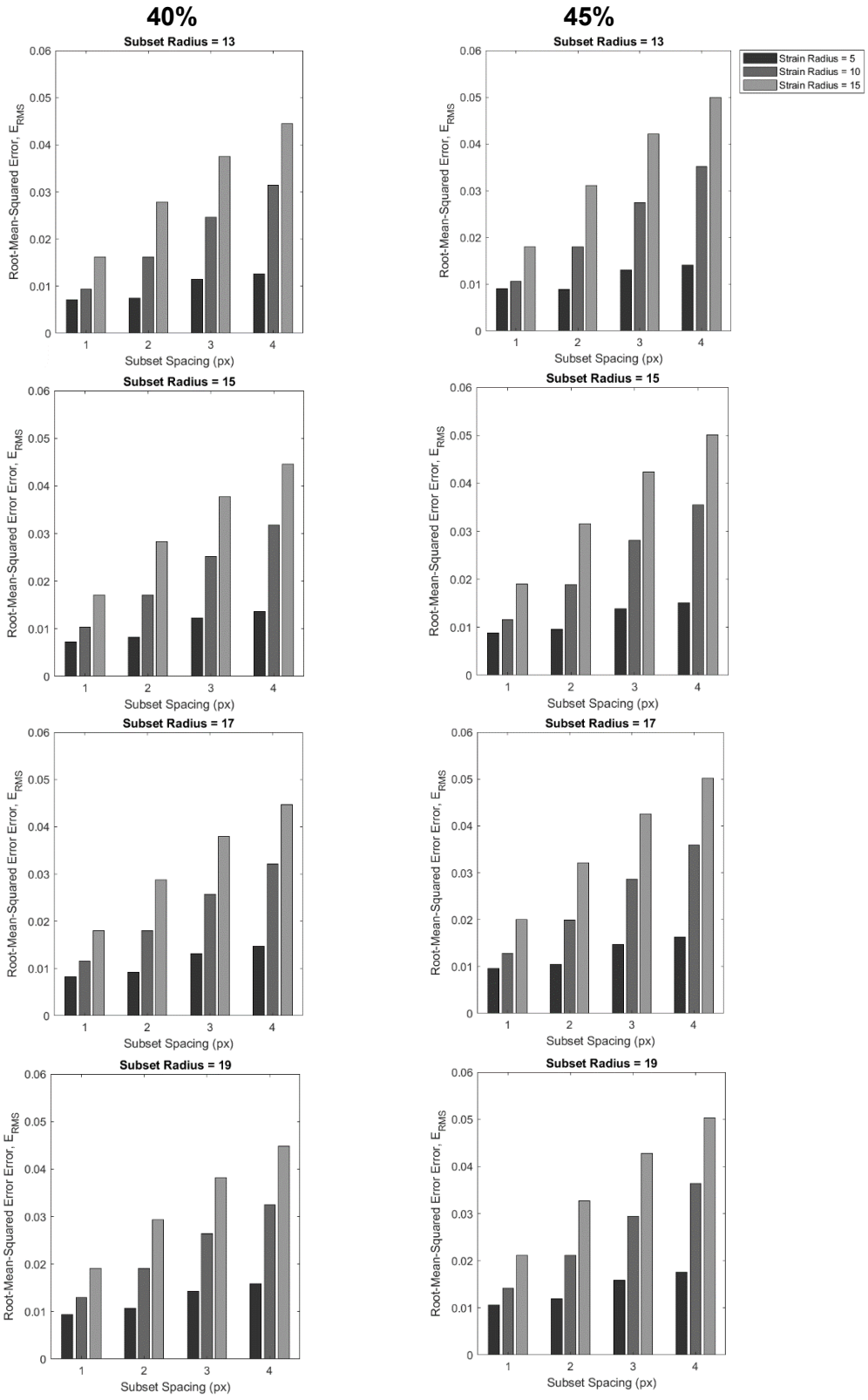


Figure A.8: *Root-mean-squared error corresponding to computational strain of 40% (left column) and 45% (right column) for different DIC parameter combinations, involving subset radius, subset spacing and strain radius.*

A.3 Supplementary Experimental Results

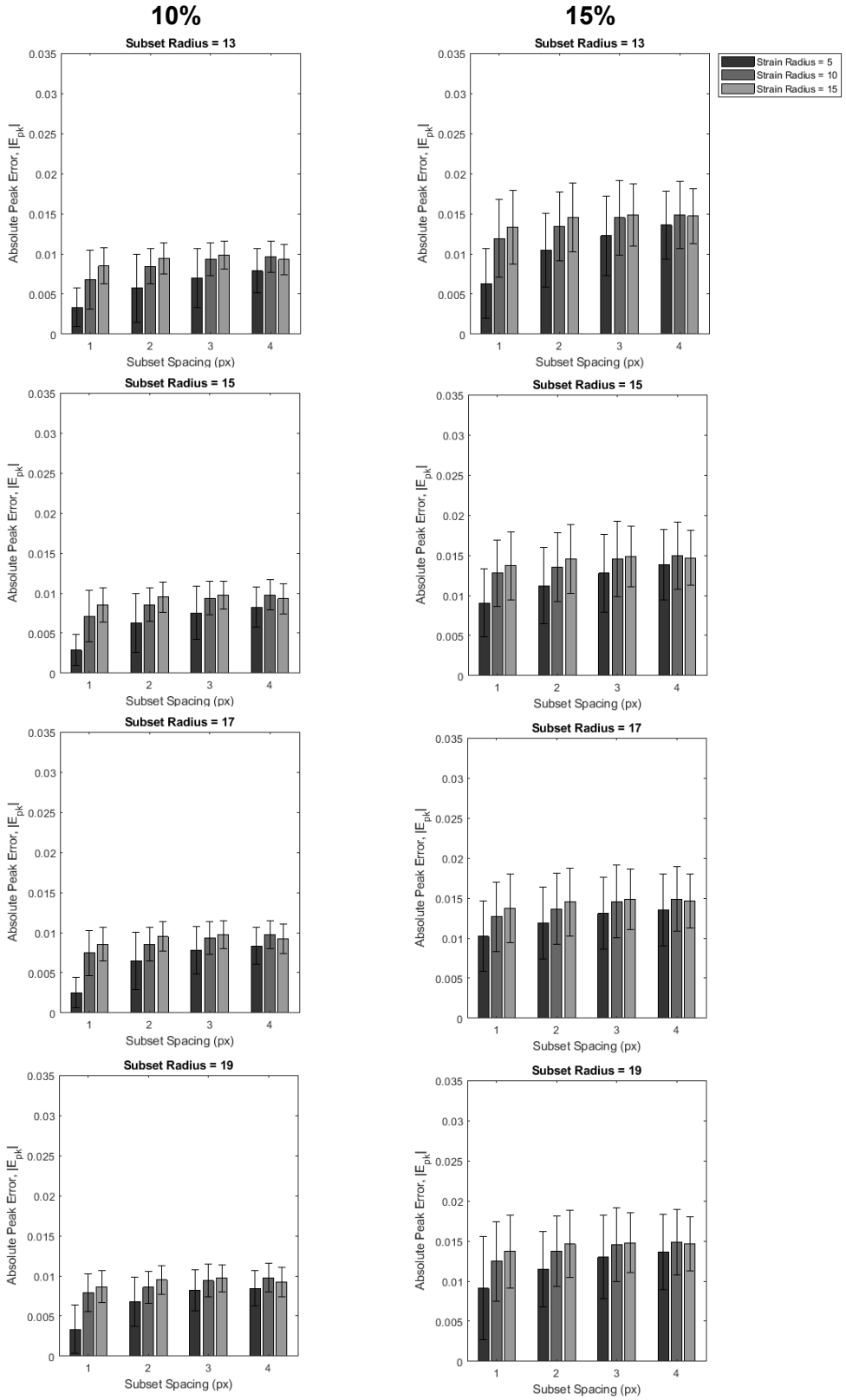


Figure A.9: Absolute peak error averaged across three samples *at 10 and 15% with error bars demonstrating standard deviation of error across the region of interest for each parameter combination.*

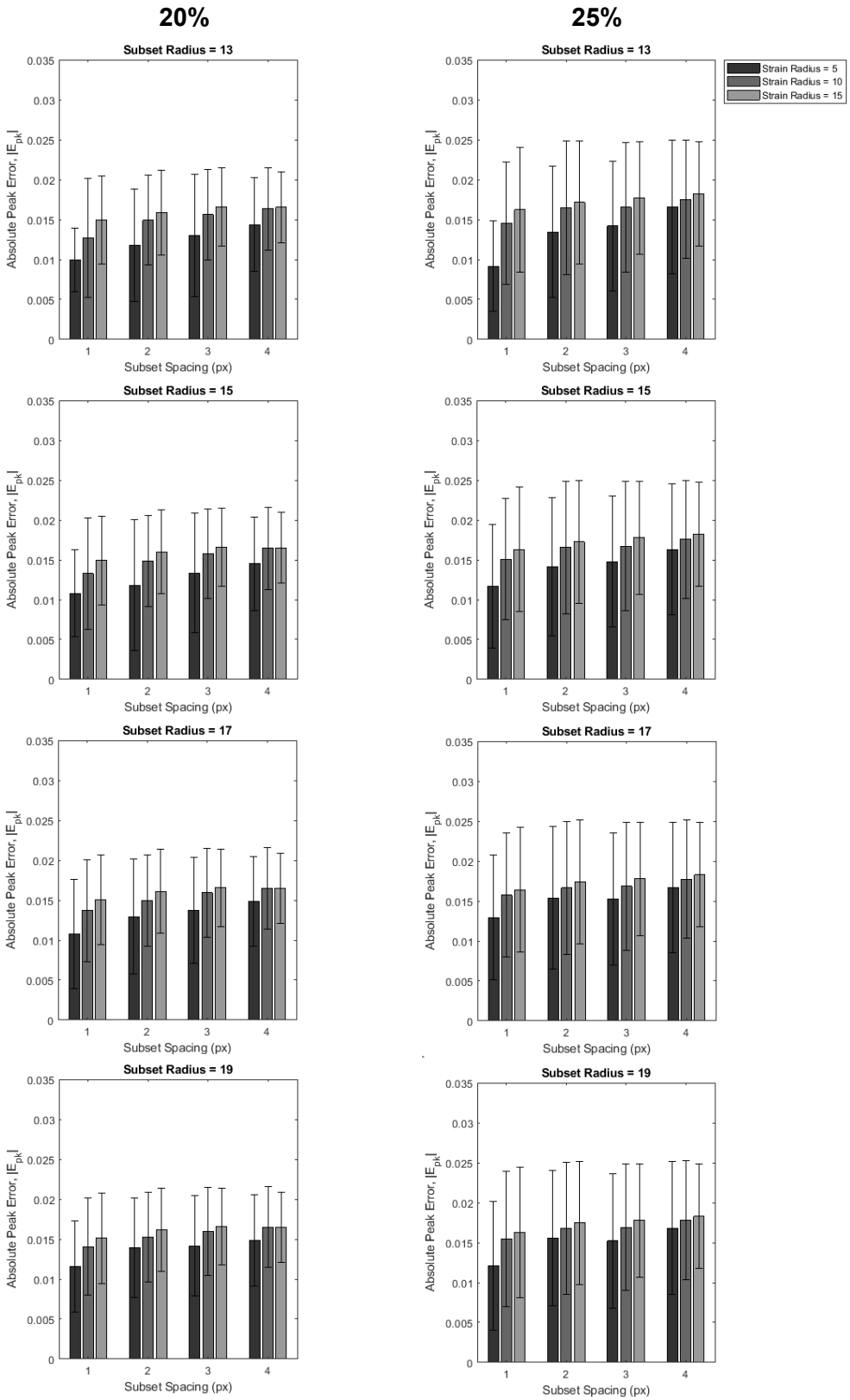


Figure A.10: Absolute peak error averaged across three samples *at 20 and 25% with error bars demonstrating standard deviation of error across the region of interest for each parameter combination.*

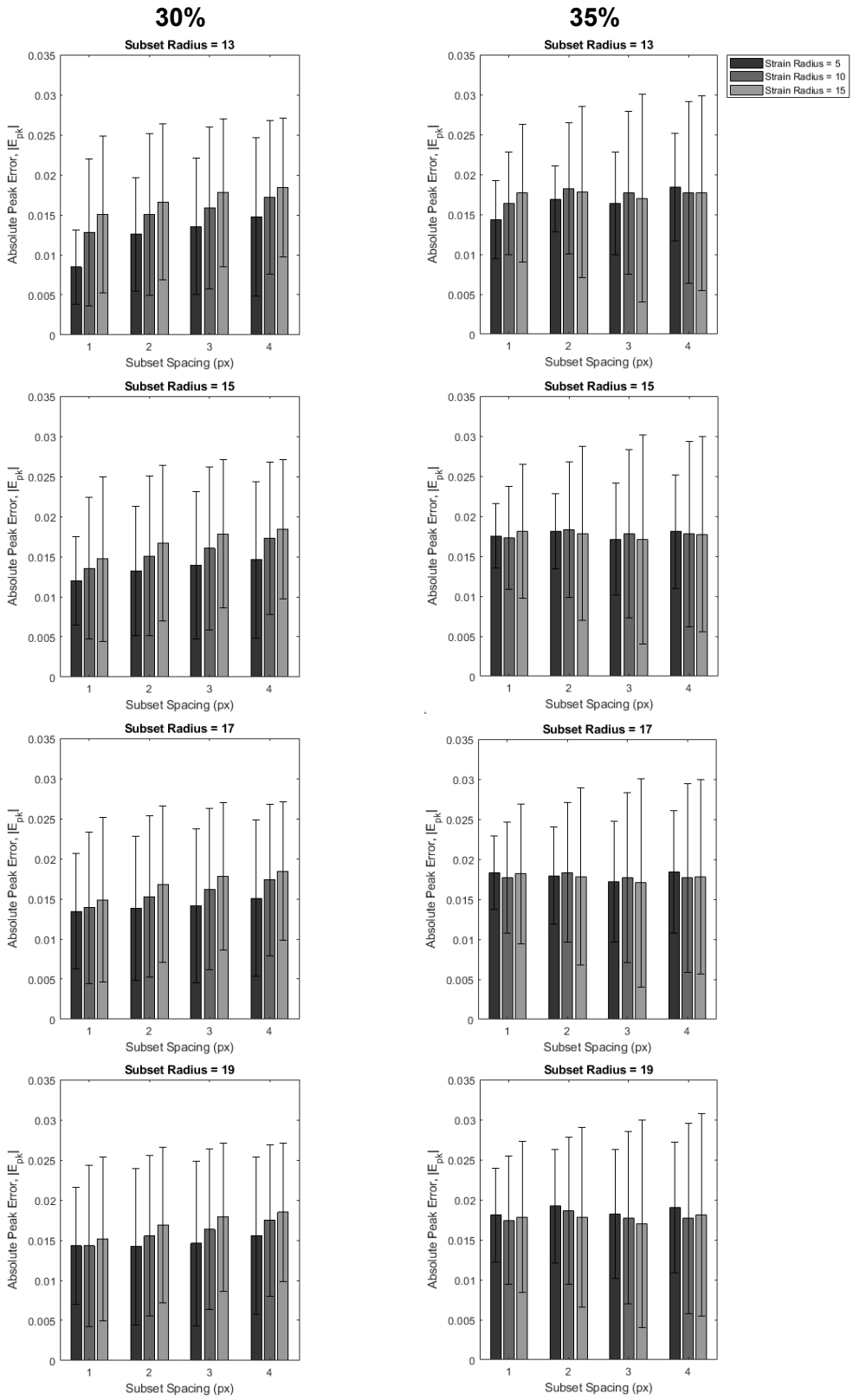


Figure A.11: Absolute peak error averaged across three samples *at 30 and 35% with error bars demonstrating standard deviation of error across the region of interest for each parameter combination*.

A.4 Ncorr vs GOM Strain Data

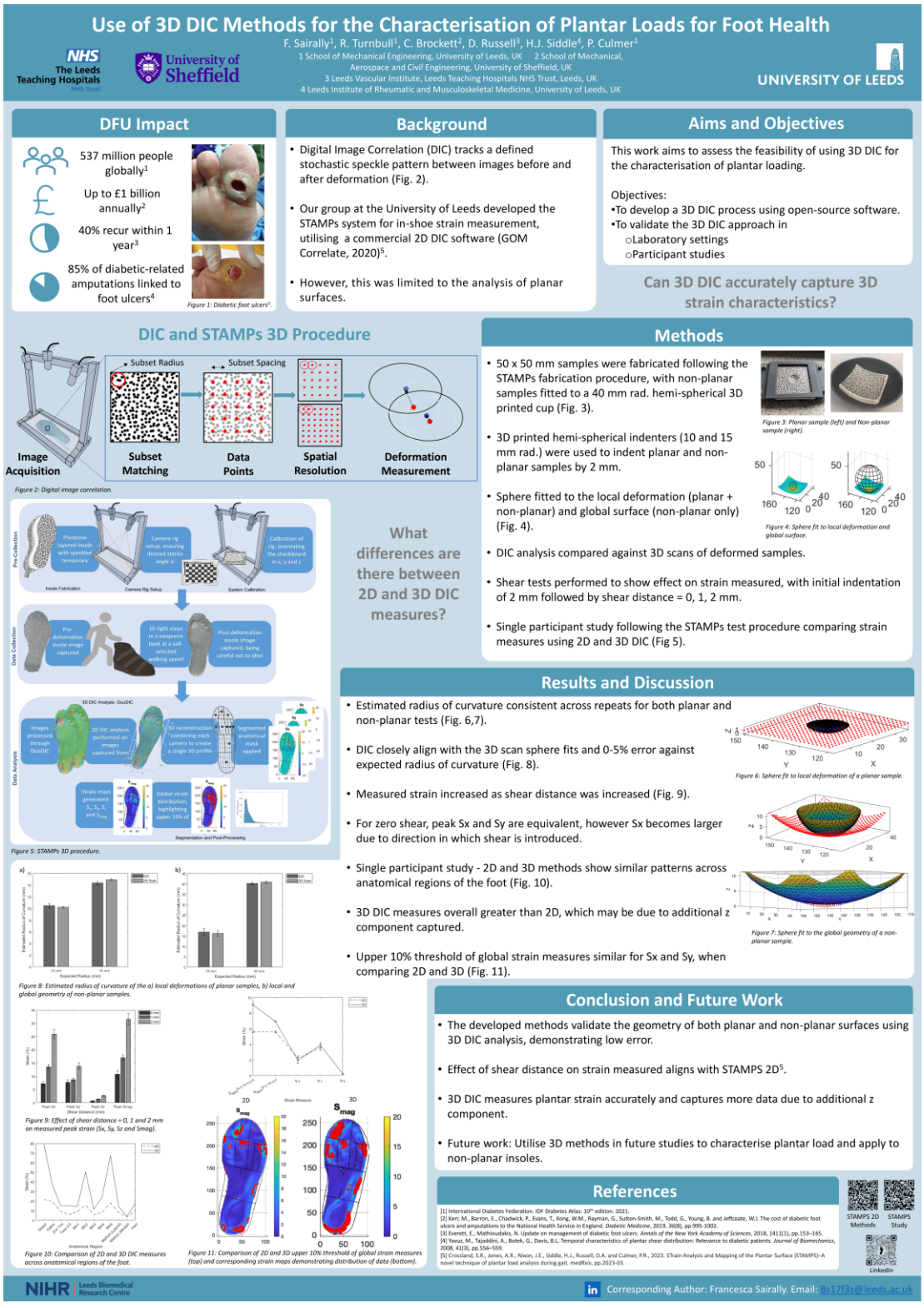
Table A.1: *Peak S_{MAG} values measured using Ncorr and GOM for participants 1-3 averaged across three repeats.*

Participant	Anatomical Region	Average Peak S_{MAG}	
		Ncorr	GOM
P01	Global	15.12328	16.83
	Hallux	10.63085	10.35
	2nd Toe	6.447343	4.66
	Toes 3-5	13.38179	15.31
	1st MTH	3.842575	4.15
	2nd MTH	4.098711	4.58
	3rd MTH	4.679564	5.1
	4th MTH	4.842832	5.26
	5th MTH	7.629929	7.08
	Midfoot (Medial)	1.585673	2.08
	Midfoot (lateral)	5.564032	5.51
	Heel	9.277924	9.33
P02	Global	34.29956	29.31
	Hallux	31.3885	29.31
	2nd Toe	17.68835	13.05
	Toes 3-5	20.35548	19.28
	1st MTH	14.42131	8.12
	2nd MTH	4.793052	4.39

	3rd MTH	6.021387	3.08
	4th MTH	6.921742	6.45
	5th MTH	4.923154	5.07
	Midfoot (Medial)	4.037896	3.29
	Midfoot (lateral)	2.632352	2.4
	Heel	27.61759	16.4
P03	Global	67.62924	58.85
	Hallux	24.35015	23.1
	2nd Toe	16.22876	14.79
	Toes 3-5	4.040427	5.33
	1st MTH	67.62924	58.85
	2nd MTH	47.64008	41.62
	3rd MTH	17.2563	14.84
	4th MTH	17.23725	18.54
	5th MTH	8.49966	7.13
	Midfoot (Medial)	5.824569	5.79
	Midfoot (lateral)	21.24648	24.17
	Heel	16.50336	16.64

Appendix B

B.1 BioMedEng24 Conference Poster



B.2 STAMPS3D Protocol Document

STAMPS Insole Fabrication

Plasticine preparation:

- Roll out the plasticine in stages until a uniform thickness of 5 mmm is achieved. Place three blocks of white plasticine side-by-side between the fabric sheets and roll them simultaneously.
- Blend the adjoining edges of the three white blocks before rolling to ensure they merge fully and do not separate during the process.
- After each rolling pass, separate the plasticine from the fabric to prevent adherence. Failure to do this can cause the plasticine to fold or roll onto itself.

Shaping the insoles:

- Use the insole as a template, tracing the outline with a pencil.
- Cut the traced shape using a Stanley knife or scalpel, ensuring clean, continuous edges.

Speckle pattern application:

- Print the speckle pattern onto temporary tattoo paper using an inkjet printer. Allow the printed sheet to dry for 24 hours, then apply the protective clear film.
- Cut the pattern to size and apply it to the plasticine surface using a wet tissue. Ensure the paper is fully saturated and the edges are adequately moistened to prevent lifting during removal.
- Take care to avoid air bubbles and incomplete edge adhesion. Excessive saturation may cause ink blurring, so moisture should be controlled.

Nylon mesh application:

- Cut the nylon mesh to size and adhere it to the plasticine after rolling.
- When inserting or removing the insole from the neoprene boot, slide it from the front to avoid it deforming the sample.

Surface finishing:

- Once the tattoo layer has dried, apply talcum powder to remove any residual moisture.
- Apply clear nail polish around the perimeter to minimise edge lifting if any moisture remains.

Storage and timing:

- Prepare insoles at least 24 hours before use.
- Store each insole at 15 °C in a cooler, with a moisture-absorbing sachet and a cardboard backing sheet to manage excess humidity.

STAMPS Data Collection Protocol

Pre-collection setup:

- Calibrate the camera system as described in the *3D DIC – DuoDIC* section.
- Select a STAMPS insole and supportive neoprene boot (Ninewells Boot, Chaneco Inc.) according to the participant's shoe size.
- Apply a light layer of talcum powder to the insole or participant's sock to minimise moisture transfer.

Baseline imaging:

- Capture a pre-deformation image of the prepared STAMPS insole before it is placed in the boot.

Insole placement and walking trial:

- Insert the STAMPS insole into the corresponding neoprene boot.
- Place a size-matched standard insole in the opposite shoe to avoid gait alterations caused by shoe depth differences.
- Instruct the participant to walk ten steps or traverse a 10 m walkway at their normal, self-selected walking speed on the measured foot.

Post-walking imaging:

- Remove the STAMPS insole by sliding it from the front of the neoprene boot to avoid deformation.
- Position the insole in the imaging rig and capture the post-deformation image.
- Repeat the full walking and imaging sequence three times.

3D DIC – DuoDIC

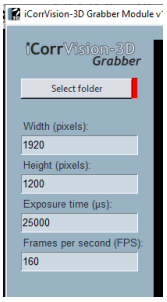
Software installation and setup:

- Install MATLAB via the University of Leeds licence - https://it.leeds.ac.uk/it?id=kb_article&sysparm_article=KB0011947
- Install the required MATLAB toolboxes for Ncorr and DuoDIC. These can be added directly through the MATLAB Add-On Explorer

- Download Ncorr (software, manual and associated publication) -
    - https://www.ncorr.com/index.php/downloads
    - https://link.springer.com/article/10.1007/s11340-015-0009-1
- Download DuoDIC (software, manual and associated publication) –
    - https://github.com/SolavLab/DuoDIC
- Install the Basler Pylon software package to enable communication with the Basler cameras - https://www.baslerweb.com/en/shop/a2a1920-160ucbas/#software=3032421996

Image Capture:

- Image capture for both calibration and deformation analysis is performed using the iCorrVison-3D open-source software, which includes an integrated Image Grabber toolbox. This tool automatically generates paired folders for the left and right cameras and stores both pre-deformation and post-deformation image sets.
- The software package and user manual can be downloaded from the project repository - https://github.com/ElsevierSoftwareX/SOFTX-D-22-00076?tab=readme-ov-file (Download the file iCorrVision-3D Grabber old.zip and refer to the included manual for setup guidance.)
- Connect the camera system to the laptop using the USB-C interface
- Launch the Image Grabber toolbox and create or select the folder in which images will be saved.
- Enter the required fields within the interface and shown below, before beginning acquisition.

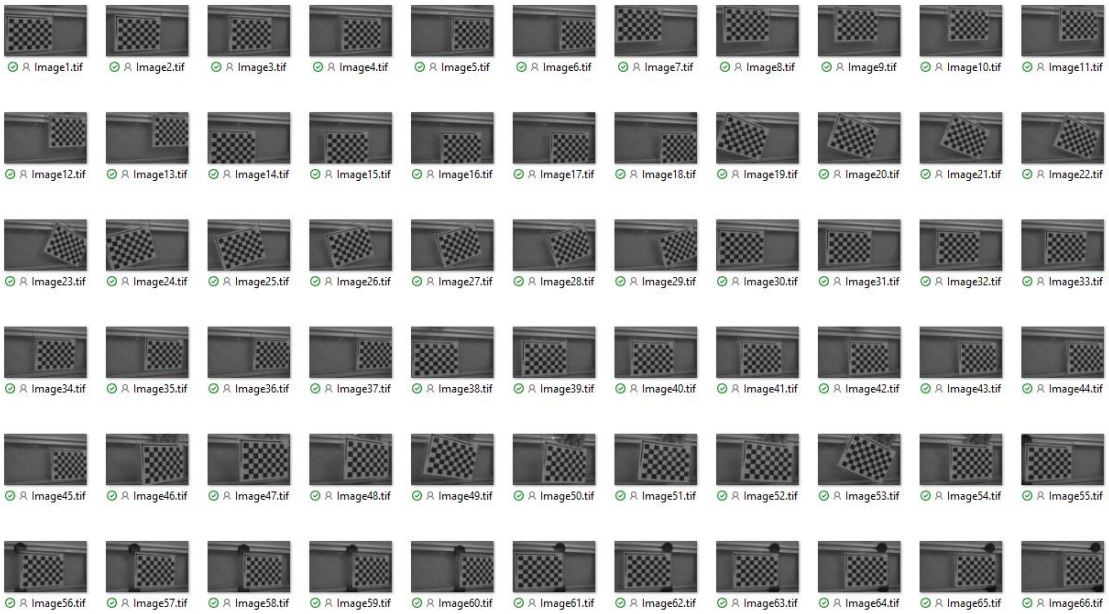


- Use the Preview window (bottom left of the interface) to confirm that both cameras have an unobstructed and correctly aligned view of the sample.
- Once the field of view is verified, select Snapshot to capture the image pair. Images are automatically saved to the designated left and right camera folders within the selected directory.

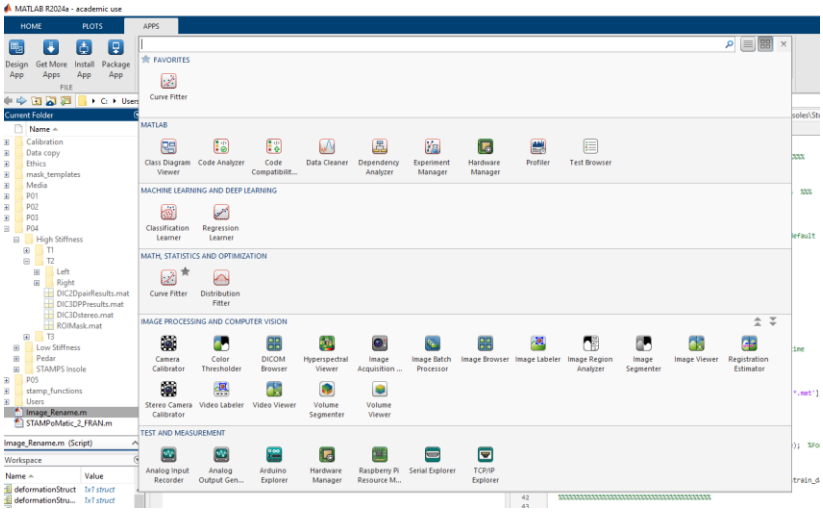
Calibration:

- Capture at least 50 image pairs of the calibration target. The dataset must include:
    - Rotations of the target in both x- and y-planes.
    - Translations across the entire field of view.

    - Images of the target held flat, then raised closer to the lenses.
    - Repeated captures at various angles and different depths relative to the cameras.
- Ensure the entire calibration target is visible in every image pair.
- An example calibration set is shown below.

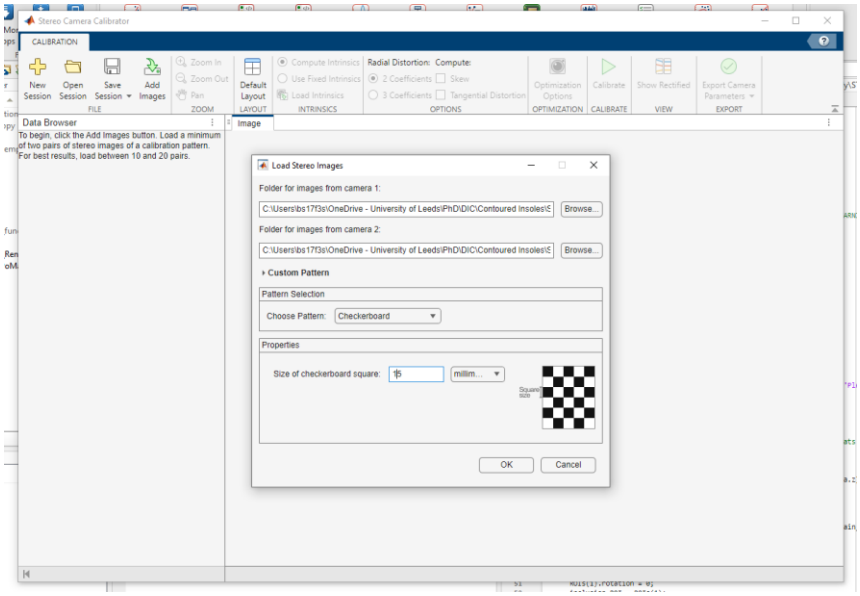


- Open MATLAB and navigate to the Apps tab.
- Select Stereo Camera Calibrator.



- Import all calibration image pairs and set the checkerboard square size to 15 mm.
- In the calibration settings, enable 3 Coefficients and Tangential Distortion.

- Run the calibration.



- Remove any image pairs with a reprojection error > 1.
- Confirm that the average reprojection error < 0.5.
- Verify that the stereo angle is approximately 35°.
    - Extract the rotation matrix R from the calibration output and convert the Euler angles using the equation shown below

$$\theta_y = -\sin^{-1}(r(3,1)), \qquad where\ R = \begin{bmatrix} r(1,1) & r(1,2) & r(1,3) \\ r(2,1) & r(2,2) & r(2,3) \\ r(3,1) & r(3,2) & r(3,3) \end{bmatrix}$$

- Select Show Rectified to confirm that the rectified stereo images are aligned along the y-axis.
- Save the calibration session. MATLAB will generate a file named calbrationSession.mat.

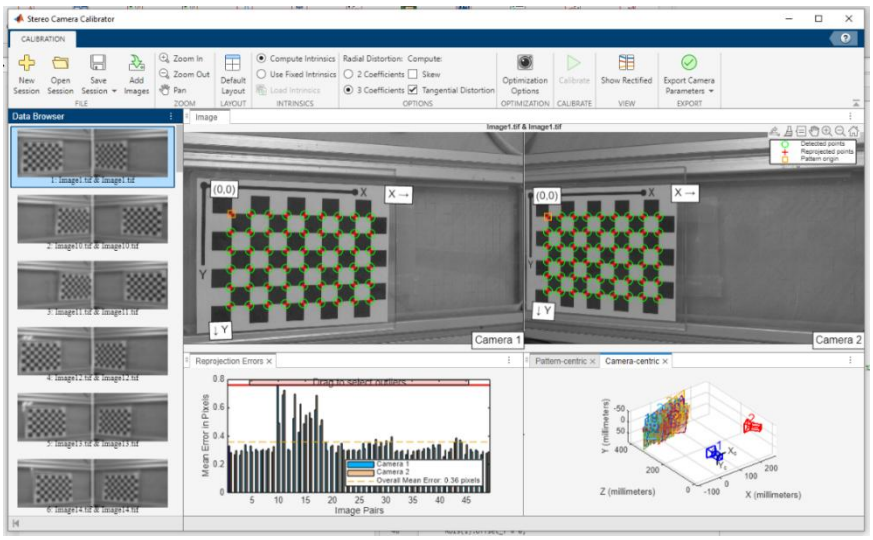


Image Renaming:

- Renaming the pre- and post-deformation images is required before running the DIC analysis. This is performed using the script Image_Rename.mat', which applies a consistent naming convention that DuoDIC can interpret correctly.

```
% Specify the current filenames with full paths
Left_oldFile1 = fullfile(imagedir_left, 'Image1.tif');
Left_oldFile2 = fullfile(imagedir_left, 'Image2.tif');

% Specify the new filenames with full paths
Left_newFile1 = fullfile(imagedir_left, 'Image_0001_0.tif');
Left_newFile2 = fullfile(imagedir_left, 'Image_0002_0.tif');

% Rename the files
movefile(Left_oldFile1, Left_newFile1);
movefile(Left_oldFile2, Left_newFile2);


imagedir_right = [repeat_no, 'Right\\'];

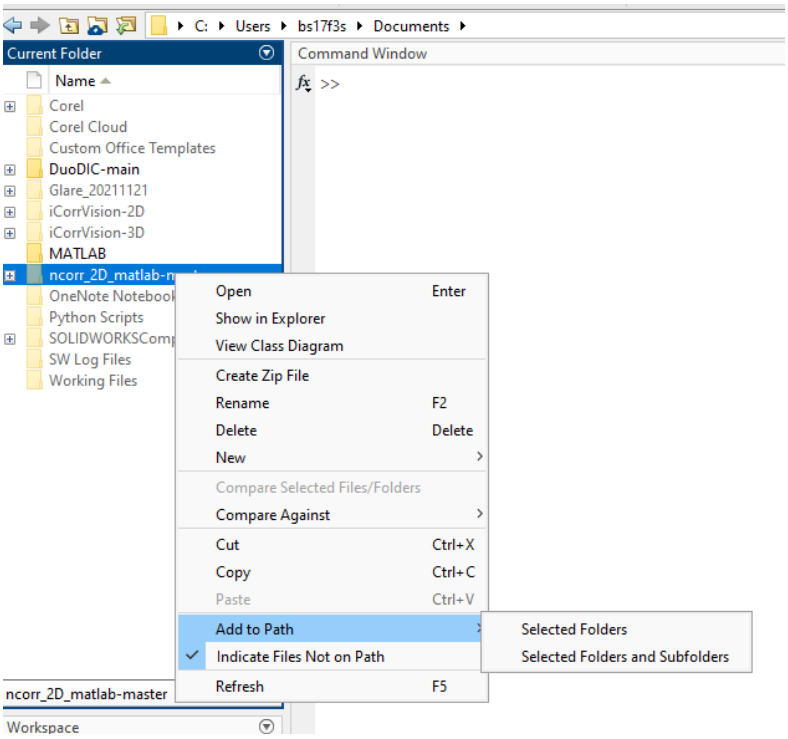
% Specify the current filenames with full paths
Right_oldFile1 = fullfile(imagedir_right, 'Image1.tif');
Right_oldFile2 = fullfile(imagedir_right, 'Image2.tif');

% Specify the new filenames with full paths
Right_newFile1 = fullfile(imagedir_right, 'Image_0001_1.tif');
Right_newFile2 = fullfile(imagedir_right, 'Image_0002_1.tif');
```

- The script assigns filenames that encode both the deformation state and the camera identify. For example:
    - 'Image_0001_0.tif' – 0001 indicates a pre-deformation image and _0 denotes the left/main camera.
    - 'Image_0002_1.tif' – 0002 indicates the corresponding post-deformation image and _1 denotes the right/additional camera.
- This renaming step must be completed before any DIC processing.
- Calibration images do not require renaming.

DIC Analysis:

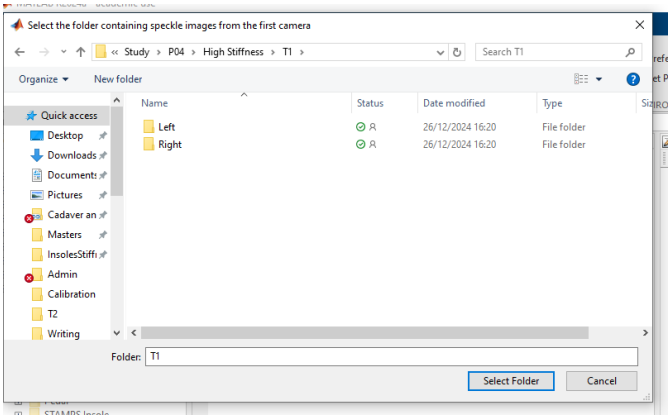
- Before beginning the analysis, add both 'DuoDIC – main' and 'ncorr_2D_matlab-master' to the MATLAB path. These must be loaded prior to running any DIC functions.

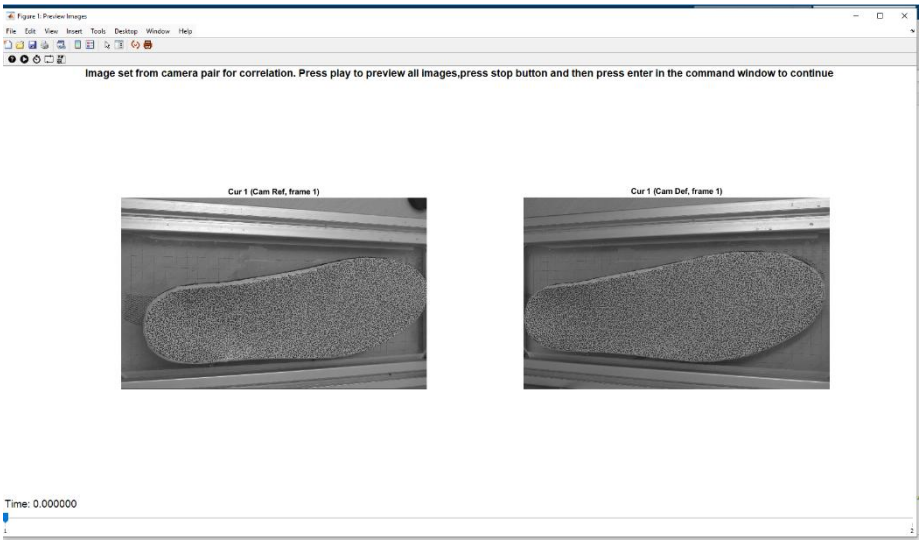


- Below are the functions you will write in the Matlab command window to complete each of the DIC steps

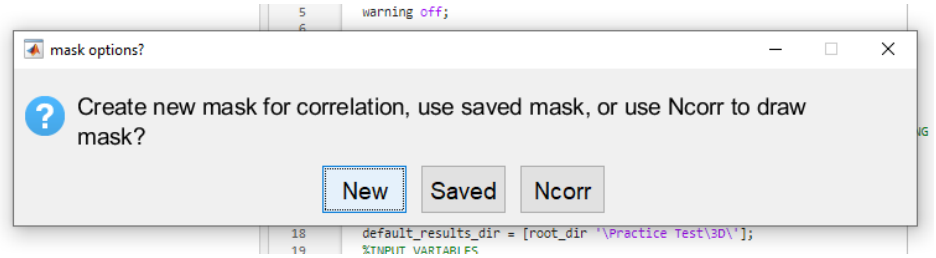
```
DuoDIC_STEP2_2DDIC_using_Ncorr
DuoDIC_STEP3_3D_reconstruction
DuoDIC_STEP4_Post_processing
```

- Step 2 – 2D DIC (Ncorr)
    - Run the first function in the MATLAB command window to initiate the 2D DIC workflow.
    - A window will open prompting you to select the folders containing the left and right camera images.
    - Save the output as ‘2D-DIC results’ within the participant’s directory (this directory should already be set).
    - A preview window will display the pre- and post-deformation images for each camera.
    - Return to the MATLAB command window and press any key to continue.

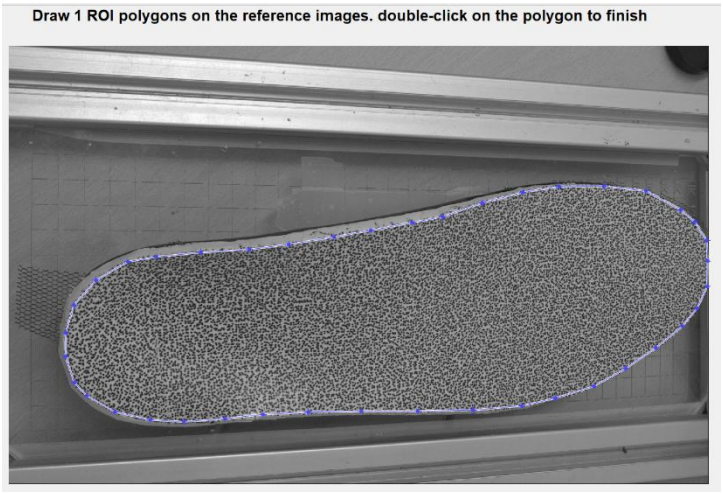




- Select New to create an ROI.



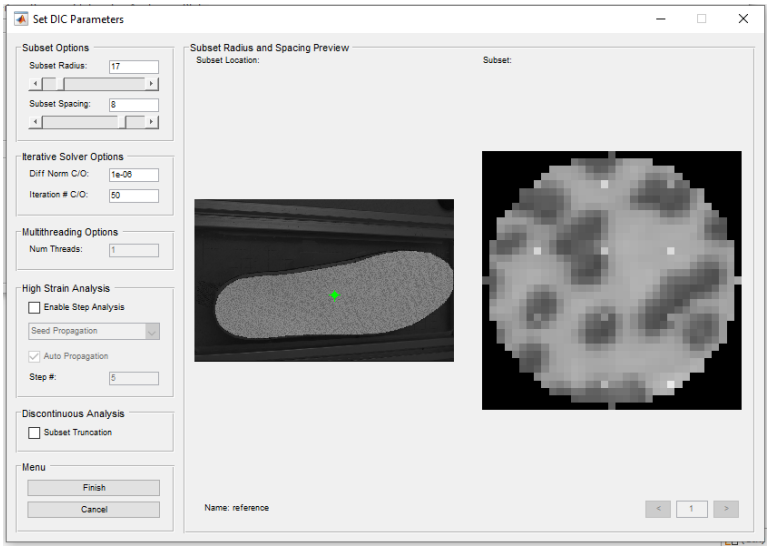
- When prompted for the number of ROIs, select OK for a single ROI.
- A new window will open for drawing the ROI. Place points around the perimeter of the sample, then zoom in to refine the boundary so that all points lie slightly inside the sample edge.
- Double-click the ROI and confirm with YES.
- Press FINISH to open the Ncorr user interface.



- Four sections must be completed on the Analysis tab.

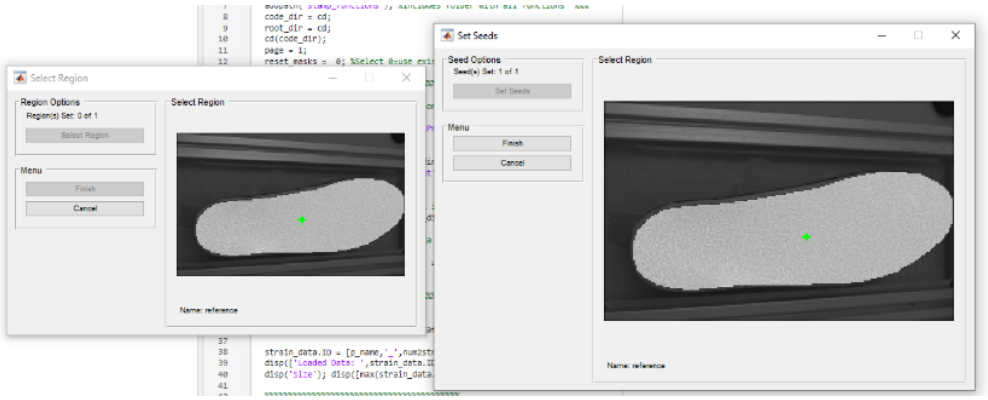


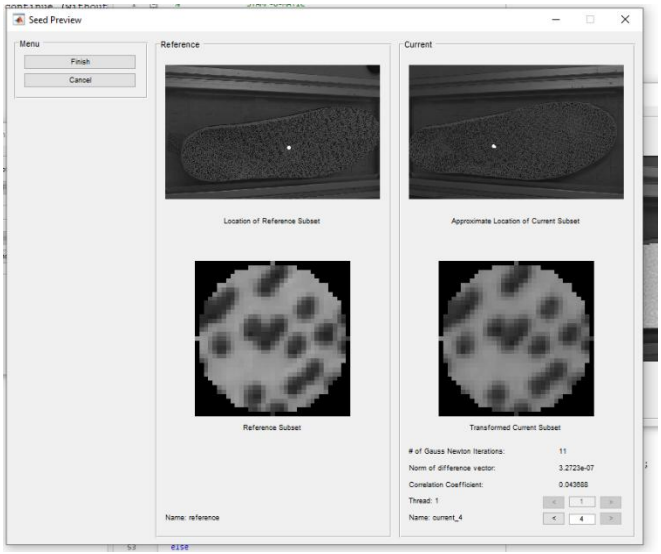
- Set DIC Parameters – subset radius = 17, subset spacing = 8. Select Finish.



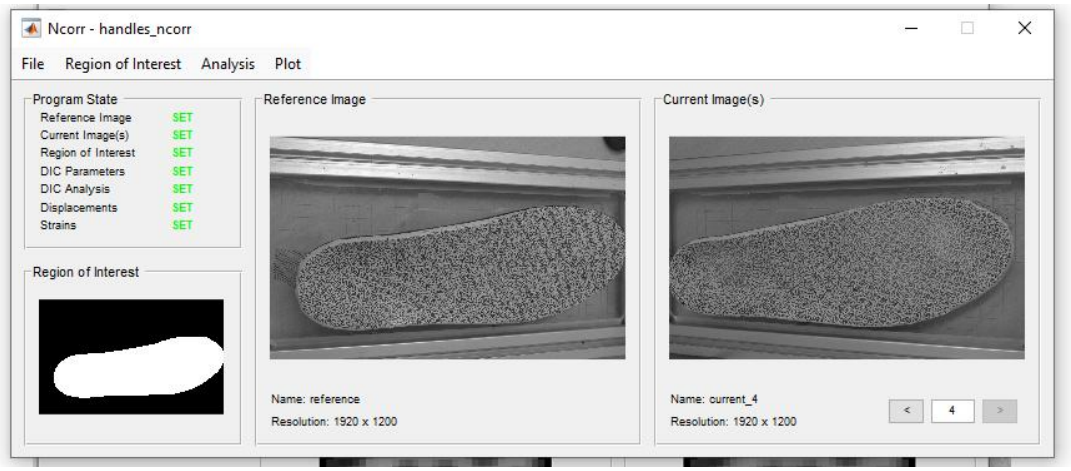
- Perform DIC Analysis – Two windows will appear: one to select the region and one to set seeds.
- Select the centre of the samples for each and press FINISH.
- A window will then display a single subset across the pre- and post-images. Use the arrow at the bottom right to verify that the speckle pattern within the circular region matches across all images

- Press Finish.





- Format Displacements – Do not need to change anything, press FINISH.
- Set the value to 5 (not critical for 3D reconstruction).
- Select FINISH.
- Everything should be completed and green on the Ncorr user interface

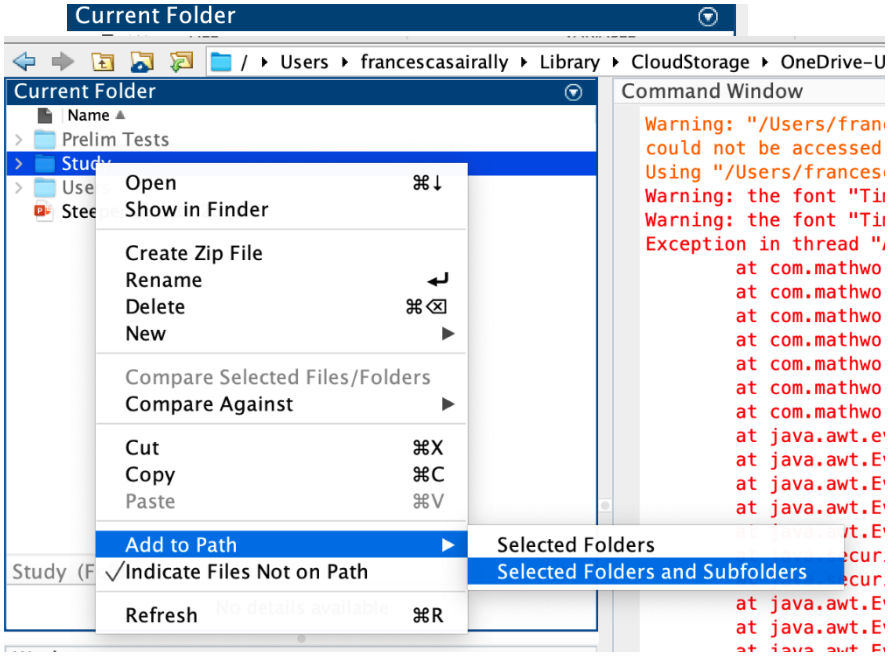


- Return to the MATLAB command window and press any key.
- A confirmation window will appear, select YES and then OK.
- Three figures will open – these can be ignored, as a separate post-processing script will be used.

    - 2D DIC is now complete.
- Step 3 – 3D Reconstruction
    - Run the second function.
    - Select ‘DIC2DpairResults.mat’ when prompted.
    - Then select the calibration file ‘calibrationSession.mat’ and save.
    - Two figures will appear, these can be ignored.
    - 3D reconstruction is now complete.
- Step 4 – Post-processing
    - Run the third function.
    - Select ‘DIC3Dstereo.mat’ and save.
    - A window will ask whether to plot figures. These can be skipped, as a dedicated post-processing script will be used, although preliminary plots may be viewed if desired.
    - Post-processing is now complete.

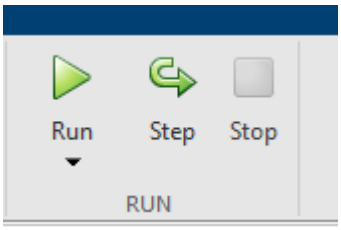
Post-Processing Script

- Before running the post-processing workflow, add the sample data and all post-processing scripts to the MATLAB path. The key components required for processing and masking are listed below. If any are missing from the path, the script will return errors.

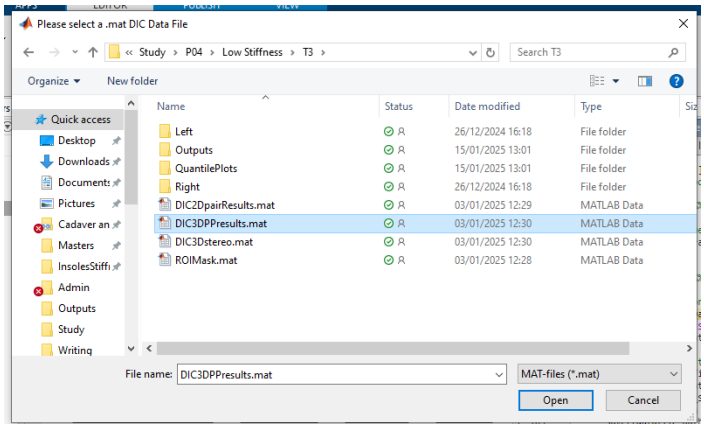


- ‘STAMPoMatic_2_FRAN.m’ – This is the main script for post-processing. It calls the accessory functions stored in the ‘stamps_functions’ folder to load, process, and mask the previously generated DIC data. A description of each function is available within the STAMPS3D directory.

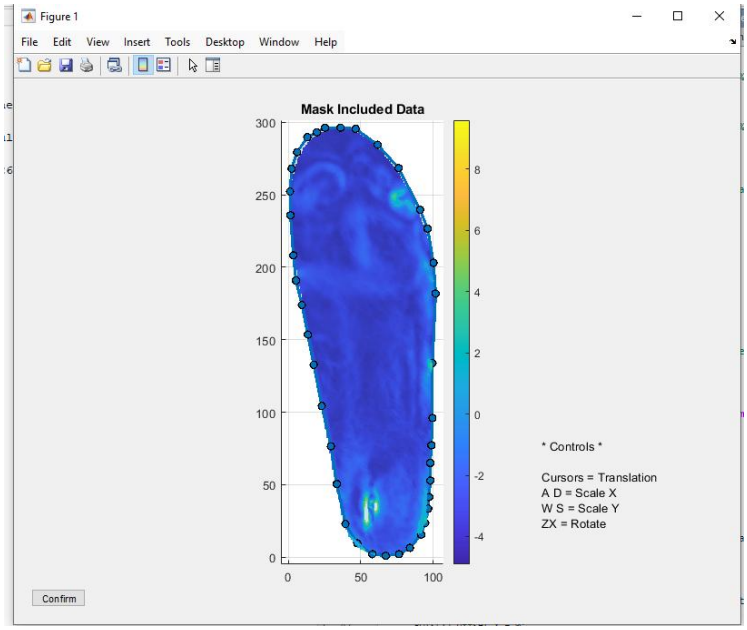
- ‘stamps_functions’ – Contains all functions used by the main script. These can be inspected if troubleshooting is required. The plotting function (‘plot_STAMPS.m’) is located here and can be edited to modify the appearance of the generated figures.
- ‘mask_templates’ – Contains Pedar mask templates for the left and right foot. If processing left-foot samples, adjust the mask selection in the main script (line 45).
- Change lines 55 and 56 for folder corresponding to left or right foot mask – this calls in the correct ROI file.



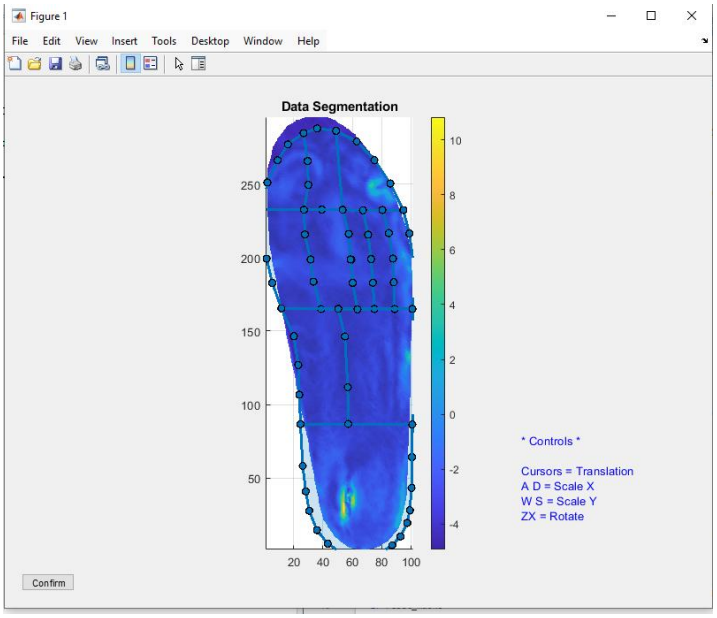
- Select Run (green triangle in the MATLAB toolbar).
- When prompted, select the file ‘DIC3DPPresults.mat’.



- An interactive interface will appear for defining a boundary around the data. This acts as a region of interest for the post-processing stage.
- On-screen key commands allow scaling, rotation and translation of the boundary until it fits the sample appropriately.

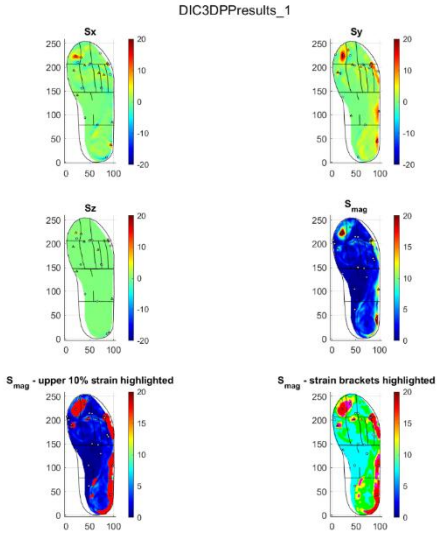


- A second interface will appear to position the anatomical mask.
- Strain maps generated from the raw data typically reveal anatomical landmarks, which can be used to align the mask approximately.



- Once processing is complete, a final figure will display strain maps for the x, y and z components (Sx: medial-lateral, Sy: anterior-posterior, Sz: ‘pressure’), as well as magnitude (Smag) and shear magnitude (Shear Smag).
- Shear Smag is derived only from x and y components and is not typically used.
- The Smag plot includes red highlighted regions representing the upper 10% percentile of strain values. Inclusion of this plot is optional depending on reporting needs.
- Results are saved in the ‘Outputs’ and ‘Quantile Plots’ folders.
- These directories contain .csv, .png, .fig and .mat files.

- .fig and .mat files can be used for further manipulation or additional analysis if required.



B.3 Independent Validation Calculations

Coordinates for the three markers placed on each of the cameras, for repeats 1-3 are reported in Table B.1.

Table B.1: *Marker (A, B, C) coordinates for each camera and repeat.*

	Marker	Repeat 1	Repeat 2	Repeat 3
Camera 1	A	(385.197, -306.77)	(385.132, -306.777)	(59.696, -29.264)
	B	(376.245, -333.134)	(376.215, -333.111)	(52.292, -55.946)
	C	(351.873, -296.007)	(351.802, -295.998)	(26.328, -19.972)
Camera 2	A	(376.72, 0.115)	(376.685, 0.138)	(39.487, 277.763)
	B	(385.676, -25.898)	(385.641, -25.866)	(48.824, 252.534)
	C	(343.988, -9.727)	(343.947, -9.727)	(6.728, 266.517)

Using these coordinates, the centre for each camera was calculated. The corresponding coordinates are reported in Table B.2.

Table B.2: *Centre coordinates calculated for each camera and repeat.*

	Repeat 1	Repeat 2	Repeat 3
Camera 1	(364.335, -314.388)	(364.259, -314.39)	(39.297, -37.969)
Camera 2	(364.518, -18.634)	(364.48, -18.61)	(27.609, 259.027)

Using these coordinates, the distances between markers A and B, and A and C for both cameras, T_X, T_Z, Stereo angle and Baseline were calculated. The corresponding measures are reported in Table B.3.

Table B.3: *Measurements reflecting the relative positioning of the two cameras based on marker positional coordinates.*

		Repeat 1	**Repeat 2**	**Repeat 3**	**Average**	**STD**
Camera 1	Distance between A and B	27.84	27.80	27.69	27.78	0.06
	Distance between A and C	35.20	35.03	34.64	34.96	0.23
Camera 2	Distance between A and B	27.51	27.50	26.90	27.30	0.29
	Distance between A and C	34.18	34.19	34.64	34.34	0.21
	T_X	281.48	281.50	282.98	281.99	0.70
	T_Z	90.76	90.81	90.91	90.83	0.06
	Stereo Angle	34.66	34.70	34.49	34.62	0.09
	Baseline	295.75	295.78	297.23	296.25	0.69

Appendix C

C.1 Discussion Group Questions

Discussion Group 1:

1. How do you typically assess a patient with a DFU in your practice? What key things do you look for? Common scenarios?
2. For assessment, what kind of tools do you use? Do you look at measurements? What kind of things do you look at specifically? Is it in terms of pressure measurements?
3. While you are assessing your patients, how do you communicate what you find? Do you communicate as you go along? Do you show anything?
4. Do you find any frustrations or limitations with your current practices? Do you find what you're doing is effective? Any tools that would be useful?
5. What kind of clinical scenarios or patient groups could you see the STAMPS tool being most useful?
6. Looking at this tool in application in a clinical setting, what do you think would be needed to make it feasible in practice? Can you see any limitations to this being used?
7. Could you see something like this being useful in a home environment?
8. How do you think patients would respond to this from your perspective? How do you think they would feel about something like this being used for their assessments? How would they respond? Do you think they would be open to that?

Discussion Group 2:

1. Can you walk me through how you typically assess a patient in your practice? What are the key things you look for? Common scenarios? What do you tend to do within an appointment slot with patients?
2. How do you go about communicating with the patients during assessments? Does this tend to be afterwards or as you go? Scenarios? Variation between patient cases?
3. Do you show anything? If someone has a DFU, are you able to show them anything to indicate to them either their risk or where they are at?
4. What tools or clinical signs are relied on most? Do you use tools? What are you looking at, numbers? Are you looking for anything in particular?
5. To what extent do you also consider mechanical factors like pressure or shear in your assessment? In what ways?
6. When you notice wear on shoes and you show this to patients, does it help them understand the link?
7. In terms of someone's development, do you take a picture when they're at a low risk and then compare or show them?

8. What are the main limitations or frustrations you have experienced with current risk identification, tools, or methods you use? Do you find your current practice effective in suitable identifying a patient's risk?
9. Do you feel your current assessments provide a complete picture of DFU risk? Are there any areas you think are under assessed?
10. Are there any other tools you think would be really useful? Whether that's for risk or for assessing the wounds that the patients come in with?
11. If you were using a tool in a slot where you have 15 minutes, would it have to fit within that time frame to be appropriate? For example, devices such as Pedar and emed, do you think those would be useful? And if so, are there any other limitations to those being used up than cost?
12. How would you feel about using more advanced tools? Would you feel confident using those to assess your patients? Would you need training to be able to use them?
13. Is it useful having quantitative measures as well or do you prefer working with just visual guides? What kind works better for you, for prevention or management?
14. How do you think patients would respond to STAMPS3D being used as part of their assessments? Do you think they would respond well? Do you think they would be happy to wear them? Or worn at home?
15. Do you think you would be confident to apply STAMPS3D in your practice?
16. What is your response to you having to do the post-processing involved? Would you prefer it was automated and if so, why?
17. Any limitations or things you like about the STAMPS3D tool?

Discussion Group 3:

1. Do you all know what DFUs are or have you heard of them?
2. What do you know that might cause you to develop a foot ulcer or any foot problems.
3. When did you learn about these sort of things? Did your doctor speak to you about it?
4. When you go in for your appointments and they're looking at your foot or ulcer, do they talk about risks? Do they show you anything? What it looks like? Any problems with it? Do they give you any information?
5. Do you feel that time is a problem when it comes to your appointments?
6. For those who have had their feet looked at, how often do they do that?
7. Is it the same when you have a foot ulcer? When they know you have a foot ulcer, do you see them more frequently?
8. Do you feel like things are communicated well in your appointments? Do you feel like you understand your diabetes and your foot health? Do you understand what is going on?
9. Do you prefer it if you can see the same doctor or nurse?

10. Do your doctors ever mention that you might be low, moderate or high risk?
11. How would you feel if your doctor was to use this kind of insole to assess your foot health? Would you feel okay to do that? Would you not want that?
12. Is there any reason you wouldn't want to use it? For example, if it took longer than 15 minutes (or normal appointment length)? Would it be something that would stop you from wanting to do it? Are you bothered about appointments being longer?
13. Would you find it useful if the doctor gave you some like this (the strain maps) so that could visually see what is going on?
14. How would you feel if these were sent home to be worn for a longer period of time?

C.2 PPIE Activity Research Articles

A blog was published to celebrate the work supported by the RRI funding scheme. The article corresponding to this work can be found in Figure C.1. The full blog can be found at the following webpage: https://researchculture.leeds.ac.uk/celebrating-our-rri-award-winners/.

This work was also added to the NIHR Leeds Biomedical Research Centre, PPIE 2025 Winter Newsletter. The corresponding section of work included is shown in Figure C.2.

RRI award: STAMPS3D: Engaging Clinicians and Patients to Prevent Diabetic Foot Ulcers – Francesca Sairally (School of Mechanical Engineering)

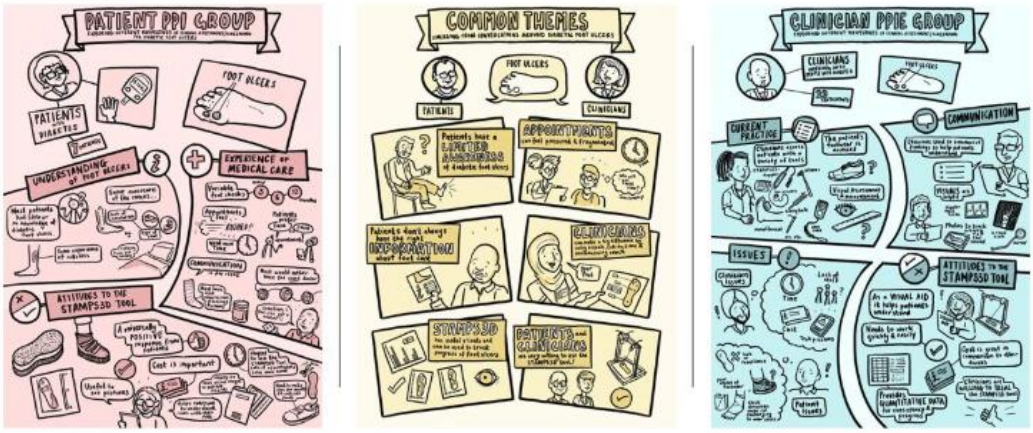
Francesca's research focuses on preventing foot ulcers, a serious complication of diabetes that can lead to infection, amputation and reduced quality of life. Central to this work is **STAMPS3D**, an in-shoe measurement tool that captures both pressure and sideways (shear) forces to assess ulceration risk.

With support from the RRI award, Francesca brought together clinicians and people living with diabetes for three focus groups exploring current assessment methods, the limitations of existing tools, and the usability of STAMPS3D's visual strain maps. Clinicians highlighted its potential for guiding orthotic design, offloading strategies and patient education, while patients found the visual outputs intuitive, empowering and easy to understand.

"The tool's ability to visualise foot strain patterns within just 10 steps was particularly impactful, helping bridge the gap between abstract risk and tangible understanding," Francesca reflected.

Early engagement has shaped STAMPS3D's future development and demonstrated the value of inclusive practices, work Francesca will continue through upcoming proof-of-concept studies.

These visual summaries, illustrated by Tom Bailey, capture the themes of what patients and clinicians said about their experiences of foot ulcer care.



You can check out more of Tom Bailey's work on their Instagram @mrtombailey.

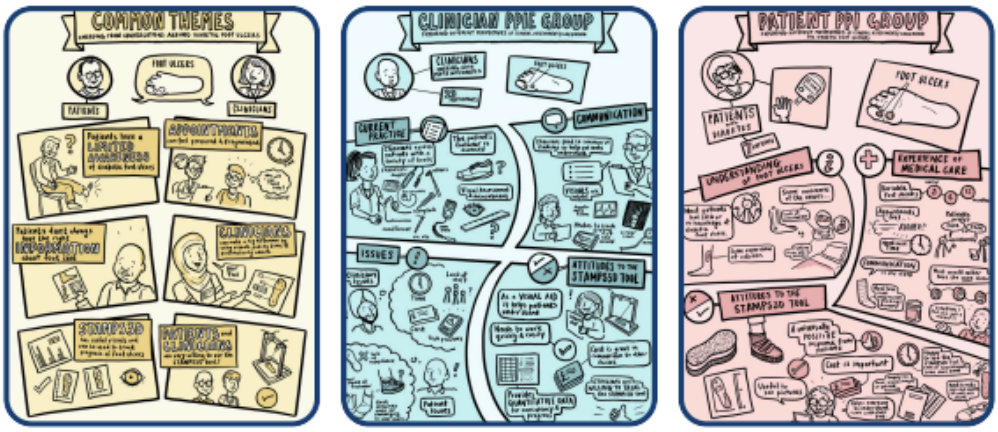
Figure C.1: *Blog article corresponding to PPIE activity work supported by the RRI funding scheme.*

Diabetic Foot Ulcers: Exploring different perspectives of clinical risk assessment/screening

A team of researchers at the NIHR Leeds BRC ran a focus group to look at peoples understandings around diabetic foot ulcers, and to gather patients thoughts on their research method: STAMPS3D. This method uses Digital Image Correlation (DIC) to measure the strain captured by an insole placed in a patients shoe. in particular they were looking at:

- Awareness and knowledge of diabetic foot health and ulceration risk.
- Peoples perceptions of current assessment methods.
- Acceptance and attitudes towards STAMPS3D and potential impacts.

The team heard from both clinicians and Patients, and produced some info graphics to demonstrate their findings. Please contact the PPI team at **PPIBRC@leeds.ac.uk** if you would like full scale copies of these graphics.



Graphics developed as part of the Diabetic Foot Ulcers project

Figure C.2: *Extract from the NIHR Leeds Biomedical Research Centre PPIE 2025 newsletter.*

Appendix D

D.1 Mechanical Tests – 'Piano key' Stiffness Measurements

Table D.1: *Young's Modulus for each piano key sample, calculated between 10-20% strain. Each trial measure, average and standard deviation (STD).*

Sample	T1	T2	T3	Average	STD
1	0.61	0.54	0.50	0.55	0.05
1.1	1.33	1.16	1.25	1.25	0.07
1.2	2.45	2.18	2.08	2.24	0.16
1.3	0.81	0.70	0.77	0.76	0.04
2	1.55	1.43	1.43	1.47	0.06
2.1	2.29	2.24	1.84	2.12	0.20
2.2	3.08	2.69	2.47	2.75	0.25
2.3	1.43	1.29	1.27	1.33	0.07
3	1.54	1.56	1.75	1.62	0.10
3.1	2.05	1.86	1.86	1.92	0.09
3.2	3.18	3.04	2.71	2.97	0.20
3.3	1.98	1.84	1.90	1.91	0.06
4	3.01	2.73	2.76	2.83	0.13
4.1	4.04	3.94	3.69	3.89	0.15
4.2	5.22	4.89	4.57	4.89	0.27
4.3	3.57	3.42	3.16	3.39	0.17
5	4.56	4.23	4.17	4.32	0.17

D.2 Mechanical Tests – Insole Stiffness Measurements

Table D.2: *Young's Modulus measurements for the 3 mm thickness insoles for Low, Medium, High and Medium + Spot insole stiffness types.*

Insole Stiffness Type	Region	T1	T2	T3	Average	STD
Low	Hallux	6.61	6.53	6.16	6.43	0.19
	Forefoot	6.78	6.52	7.16	6.82	0.26
	Mid	1.03	1.17	1.11	1.11	0.06
	Heel	4.27	8.13	7.25	6.55	1.65
Medium	Hallux	6.00	5.68	5.07	5.58	0.39
	Forefoot	4.56	5.48	5.39	5.14	0.41
	Mid	2.56	2.29	2.56	2.47	0.13
	Heel	1.17	1.01	2.41	1.53	0.63
High	Hallux	6.11	5.76	5.48	5.79	0.26
	Forefoot	6.11	5.73	6.20	6.01	0.20
	Mid	4.45	5.31	4.53	4.76	0.39
	Heel	8.03	2.74	6.84	5.87	2.27
Medium + Spot	Hallux	6.40	5.76	5.11	5.76	0.53
	Forefoot	5.33	5.37	5.39	5.36	0.02
	Mid	1.89	1.68	1.74	1.77	0.09
	Heel	4.48	3.21	5.24	4.31	0.84

Table D.3: *Young's Modulus measurements for the 6 mm thickness insoles for Low, Medium, High, Medium + Spot and Medium + Plug insole stiffness types.*

Insole Stiffness Type	Region	T1	T2	T3	Average	STD
Low	Hallux	1.95	1.96	1.68	1.86	0.13
	Forefoot	1.78	1.74	1.55	1.69	0.10
	Mid	1.17	1.14	1.14	1.15	0.01
	Heel	1.74	2.02	1.67	1.81	0.15
Medium	Hallux	2.17	2.21	2.00	2.12	0.09
	Forefoot	1.87	2.01	2.06	1.98	0.08
	Mid	2.46	2.38	2.34	2.39	0.05
	Heel	2.51	3.17	2.83	2.84	0.27
High	Hallux	5.09	4.81	4.74	4.88	0.15
	Forefoot	3.91	3.74	3.77	3.81	0.07
	Mid	5.91	6.03	5.67	5.87	0.15
	Heel	4.94	5.55	4.92	5.14	0.29
Medium + Plug	Hallux	0.85	0.79	1.18	0.94	0.17
	Forefoot	1.98	2.00	2.11	2.03	0.06
	Mid	1.97	2.00	2.04	2.00	0.03
	Heel	2.40	2.84	2.71	2.65	0.19
Medium + Spot	Hallux	1.28	1.47	1.18	1.31	0.12
	Forefoot	2.22	2.17	2.13	2.17	0.03
	Mid	2.36	2.28	2.34	2.33	0.03

	Heel	2.63	2.83	2.80	2.75	0.09

Table D.4: *Young's Modulus measurements for the 3 mm thickness insoles for Low, Medium, High and Medium + Spot insole stiffness types together with plasticine.*

Insole Stiffness Type	Region	T1	T2	T3	Average	STD
Low	Hallux	5.65	4.52	5.37	5.18	0.48
	Forefoot	5.29	4.26	5.55	5.03	0.56
Medium	Hallux	5.40	5.06	5.82	5.43	0.31
	Forefoot	4.70	3.86	5.43	4.67	0.64
High	Hallux	4.88	2.79	5.14	4.27	1.05
	Forefoot	4.98	2.94	4.82	4.25	0.93
Medium + Spot	Hallux	5.24	3.76	4.58	4.53	0.60
	Forefoot	4.9	3.17	4.73	4.29	0.79

Table D.5: *Young's Modulus measurements for the 6 mm thickness insoles for Low, Medium, High, Medium + Spot and Medium + Plug insole stiffness types together with plasticine.*

Insole Stiffness Type	Region	T1	T2	T3	Average	STD
Low	Hallux	3.39	2.71	3.04	3.05	0.27
	Forefoot	3.33	2.68	3.08	3.03	0.27
Medium	Hallux	4.02	2.83	3.23	3.36	0.49
	Forefoot	3.00	2.39	3.17	2.85	0.33

High	Hallux	4.99	3.56	5.09	4.55	0.70
	Forefoot	4.29	3.00	4.45	3.91	0.65
Medium + Plug	Hallux	1.97	1.50	1.86	1.78	0.20
	Forefoot	3.57	2.86	3.38	3.27	0.30
Medium + Spot	Hallux	2.35	2.21	2.41	2.32	0.08
	Forefoot	4.21	2.95	3.48	3.55	0.52